GEOLOGY OF THE 1.33–1.32 Ga BARTH ISLAND RING COMPLEX, NEAR NAIN, LABRADOR

OWEN GASKILL

Geology of the 1.33-1.32 Ga Barth Island Ring Complex, near Nain, Labrador

by

© Owen Gaskill

A thesis submitted to the School of Graduate Studies

in partial fulfilment of the requirements

for the degree of Master of Science in Earth Sciences

Memorial University of Newfoundland

April, 2005

Abstract

The ca. 40 km^2 Barth Island Ring Complex comprises spatially associated, concentric sheets of leucotroctolite, leuconorite, ferrogabbroid, and monzonite. The ring complex is a part of the ca. 1.36 - 1.29 Ga Nain Batholith, a typical Proterozoic massif-type anorthosite complex located in northern Labrador, Canada. Unlike most anorthosites in the Grenville Province to the south, the Nain Batholith (NB) was not involved in regional ductile deformation and therefore offers an excellent opportunity to probe the problem of the formation of Proterozoic massif-type anorthosites. The Barth Island Ring Complex contains, in close proximity, some of the distinctive rock types of massif-type anorthosite complexes. The ring complex therefore provides an ideal opportunity for study of the 'anorthosite problem'.

Previous workers had considered the ring complex to be the result of closed-system differentiation of a single pulse of magma in a single chamber. However, mapping at a scale of 1:20 000 has resulted in a reappraisal of the mechanisms of formation and magmatic history of the Barth Island Ring Complex. Field relationships demonstrate an intrusive relationship between all the major rock types, although there is abundant evidence of the contemporaneity of the ferrogabbroid and monzonite. Based on the presence of well-preserved cumulate textures and modal layering, the leucotroctolite appears to have crystallized more slowly than the other units and to have differentiated *in situ* to some degree. The latter interpretation is supported by an upward transition from

leucotroctolite into more Fe-rich leuconorite. Monzonite is interpreted to have been emplaced before ferrogabbroid, based on the presence of features such as dyke-like bodies of ferrogabbroid within monzonite. Evidence for hybridization of the ferrogabbroid and monzonite is present in many locations. Field evidence suggests the leucotroctolite was emplaced before the ferrogabbroid and monzonite. An outer unit of leuconorite postdates all the other rock types.

U-Pb ages were obtained by Thermal Ionisation Mass Spectrometry (TIMS) from zircon in ferrogabbroid and leuconorite, and from zircon and baddeleyite in leucotroctolite. The ferrogabbroid age of ca. 1317 Ma is within error of previously published values of ca. 1320 Ma for monzonite of the Barth Island Ring Complex, and therefore supports the field evidence of contemporaneity of the ferrogabbroid and monzonite. U-Pb data obtained for zircon and some baddeleyite from the leucotroctolite, and zircon from the leuconorite, gave an age of ca. 1332 Ma. One population of baddeleyite grains gave an age of 1318 ± 10 Ma, in disagreement with zircon from the same sample of leucotroctolite. The petrographic association of zircon with late-stage minerals such as magnetite and biotite strongly suggests that the zircon was not inherited, and it is therefore suggested that the U-Pb system of the ostensibly younger baddeleyite was disturbed during a heating event. This event could be associated with the intrusion of monzonite and ferrogabbroid at ca. 1318 Ma. Petrographic evidence for pervasive recrystallization at the margin of the troctolite may provide corroborating evidence, though it is possible that the observed textures are due instead to auto-annealing.

Trace element geochemical and Nd isotopic data are presented. Good first-order evidence exists for a genetic link between the leucotroctolite and leuconorite, so the leuconorite's overall lower abundances of most incompatible trace elements must be explained by AFC processes or differences in phase proportions. The monzonite and ferrogabbroid have similar trace element abundances. A broad spectrum of negative ϵ_{Nd} values (from -4 for one troctolite to -11.8 for one ferrogabbroid) suggests crustal influence on the major rock types of the ring complex was heterogeneous.

The leucotroctolite and leuconorite of the Barth Island Ring Complex were emplaced at ca. 1332 Ma into massif-type anorthosite; the leucotroctolite is bounded to the west by a shear zone that was active during its emplacement. The leucotroctolite magma may have exploited the adjacent shear zone during its emplacement, because the shear zone would have been a plane of weakness in the crust. It is possible that, for the same reason, the crystal-laden monzonitic and ferrogabbroid magma utilised the same conduit ca. 13 m.y. later.

Table of Contents

Chapter 2 (continued)

List of tables

List of figures

List of figures (continued)

List of figures (continued)

List of figures (continued)

List of plates

List of plates (continued)

List of plates (continued)

List of plates (continued)

List of appendices

Acknowledgments

The research contained in this thesis was supervised by Drs. John Myers and Alison Leitch, and funded through the following grants: National Science and Engineering Research Council (NSERC) CRD grant for collaboration between the Voisey's Bay Nickel Company and Dr. John Myers; additional NSERC funding was provided through Dr. Alison Leitch. Such funding was invaluable, and I greatly appreciate it.

I thank Dr. Myers for providing me with the opportunity to study such a fascinating part of the world's geology, and for furnishing me with advice on mapping and interpretation in the field. I thank Dr. Leitch for providing me with invaluable direction in research and prolonged intellectual support. I thank both Dr. Myers and Dr. Leitch for critical reviews and helpful suggestions on interpretation of data. I would like to thank the many researchers at the Memorial University of Newfoundland's Department of Earth Sciences who provided me with advice and suggestions, particularly Drs. Paul Sylvester, Greg Dunning, and Aphrodite Indares. I would also like to recognize valuable discussions with fellow graduate students Ron Voordouw, Tanya Tettelaar, and Donald Wright, who are also involved in the Nain Batholith research project.

I would like to recognize the invaluable efforts of the technical/analytical staff who conducted chemical and isotopic analyses for this project. The chemical analyses were done by Mr. Mike Tubrett and Ms. Pam King. Dr. Marc Poujol ran U-Pb and Sm-Nd analyses, and also provided valuable advice on possible interpretations of the U-Pb data.

I owe a particular debt of gratitude to my friend Jason Burt, who provided instrumental support both in the field and in the final stages of the writing of this thesis.

Finally, the comments and criticism given by two reviewers, Dr. Toby Rivers and Mr. Bruce Ryan, were very helpful in improving the presentation and clarity of this thesis.

Chapter 1 Introduction

1.1 Background, purpose and methods

1.1.1 Massif-type anorthosite

The processes involved in the formation of Proterozoic massif-type anorthosites and associated rock types are still poorly understood. There is little agreement on a mechanism for producing and concentrating large amounts of plagioclase without complementary volumes of ultramafic rocks (Isachsen, 1969; Morse, 1982; Wiebe, 1992). Most massif-type anorthosites are intimately associated with other distinct rock types, such as rapakivi granite and ferrodiorite. A suitable theory must explain the genesis of these magmas as well. A variety of analytical methods, including isotope and trace element abundances, have been used to constrain the origins of massif-type anorthosites and the associated intrusions (Emslie *et al.*, 1994; Dempster *et al.*, 1999; Bédard, 2001). Different methods generally produced different conclusions.

1.1.2 Nain Batholith

The 1.36-1.29 Ga Nain Batholith (also called the Nain Plutonic Suite, or NPS) of northern Labrador (fig. 1-1), is an excellent example of a Proterozoic massif-type anorthosite batholith. It is well exposed, is very large (exposed over ca. 15 000 km^2), and has not been affected by subsequent ductile deformation. The Nain Batholith (NB) contains the variety of rocks typical of Proterozoic anorthosite terranes. The most

abundant rock types are anorthosite and rapakivi-type granite, with smaller amounts[1] of mafic and intermediate rocks. The NB intrudes Archean and early Proterozoic gneisses. It cuts out the Abloviak Shear Zone (ASZ), the north-south trending, eastward-dipping suture in the core of the Torngat Orogen, between the Churchill and Nain Provinces (Emslie *et al.*, 1994; Funck *et al.*, 2000). The plutonism that produced the NB is considered to be the second and final episode of a period of apparently anorogenic magmatism, from ca. 1460 - 1290 Ma (Emslie, 1978). The preceding tectonic episode was the collision of the North Atlantic and Rae Cratons, from ca. 1870 to ca. 1700 Ma (Scott, 1998), which produced the Torngat Orogen.

At the time of writing, the oldest known component of the NB is the Tessiarsuyungoakh ferrodiorite, marked by the black square labeled 'A' directly west of the box outlining the Barth Island Ring Complex on fig. 1-1. This ferrodiorite has a zircon U-Pb crystallization age of 1364 Ma (T. Tettelaar, pers. comm., 2003). The peralkaline Flowers River granite, located farther south of the map area limit of fig. 1-1, is the youngest NB intrusion yet dated, at ca. 1289 Ma (Miller *et al.*, 1997). There does not appear to be any strict order of intrusion by rock type; that is, anorthositic rocks, granitic rocks, ferrodiorite, and mafic rocks all span the 75 m.y. time frame bracketed by the oldest and youngest dated intrusions in the episode of magmatism that produced the NB.

[1]Ca. 10% by area (Emslie *et al.*, 1994), and probably much less by volume (see Funck *et al.*, 2000).

1.1.3 The Barth Island Ring Complex

The Barth Island Ring Complex consists of spatially associated, concentric sheets of leucotroctolite, ferrogabbroid, monzonite, and leuconorite located immediately northwest of Nain. These sheets crop out over an area of ca. 40 km² (fig. 1-2). The Barth Island Ring Complex is bordered to the north and east by two older massif-type anorthosite intrusions, and to the south by two older massif-type anorthosite intrusions and gabbroic/noritic sheets of unclear relative age. It is bounded to the west by a septum of gneiss, which separates the Barth Island Ring Complex from the Mount Lister anorthosite. The surface trace of the Abloviak Shear Zone (ASZ) is found ca. 30 km to the west of the ring complex (Funck *et al.*, 2000); the ring complex is therefore intruded into the Nain Province.

Results of previous studies of the Barth Island Ring Complex have been reported in the Ph.D. thesis of Rubins (1973), in the M.Sc. theses of Mulhern (1974) and Levendosky (1975), and by de Waard (1976), and de Waard *et al.* (1976). Reconnaissance mapping of the ring complex was performed by Ryan (2000, 2001).

Mulhern (1974) performed detailed petrography and mineral chemistry on samples collected from the northern third of the intrusion. Analyses of rocks from the central and southern parts of the structure were reported by Rubins (1973), Levendosky (1975), de Waard (1976), and de Waard *et al.* (1976). These authors identified the major rock types and included anorthosite immediately surrounding the intrusion as a part of the structure. All contacts between the major rock types of the Barth Island Ring Complex

were interpreted to be gradational; this interpretation was supported by major-element mineral chemistry. Mulhern (1974) suggested that the Barth Island Ring Complex, which she called the Barth Layered Structure, is an example of continuous differentiation of a single body of magma. This was taken as evidence to support a single parent magma for the rock types of the NB, as opposed to the two-parent scheme of Morse (1972).

Ryan (2000) identified the need for a reappraisal of the Barth Island Ring Complex. He suggested that the major rock types of the Barth Island Ring Complex were not the result of continuous differentiation of a single body of magma, and that the anorthosite which surrounds much of the ring complex was unrelated. Ryan (2000) demonstrated the monzonite and ferrogabbroid to be contemporaneous magmas, and interpreted the troctolite to be an older body. Ryan (2001) later revised that interpretation and suggested instead that the troctolite was younger than, but broadly contemporaneous with, the monzonite and ferrogabbroid. The conclusions of Ryan (2000, 2001) were based on field observations and petrography.

1.1.4 Thesis scope and methods

The nature of the relationship between the various magmas associated with massif anorthosites is clearly important. For instance, it is commonly asserted that ferrodiorite magmas are residues from anorthosite genesis (Morse, 1982; Emslie *et al.*, 1994) ; or that the granitic magmas are the result of crustal anatexis associated with anorthosite

formation (Emslie *et al.*, 1994; Bédard, 2001). The Barth Island Ring Complex offers a unique opportunity to gather first-order data about the relationships between some of the rocks typical of anorthosite terranes. Preliminary reports concerning a sequence of similar rock types to the north of the Barth Island Ring Complex indicate that the some of the relationships between rock types found there are similar to those in the Barth Island Ring Complex (Myers, pers. comm., 2002). It is probable that the relationships displayed in the Barth Island Ring Complex contain information on the nature of anorthosite genesis, as suggested by both Mulhern (1974) and de Waard (1976). A summary and review of some recent models of anorthosite formation, within which the Barth Island Ring Complex can be placed in context, is provided in section 1.2.

The thesis describes the rock types present in the field area, characterizes their field relationships, and proposes a suitable emplacement and magma chamber evolution model. Trace element geochemical trends and isotopic values for the rocks of Barth Island Ring Complex are considered. The data and conclusions are then placed alongside relevant information for the Nain Batholith.

To this end, the Barth Island Ring Complex was mapped at a scale of 1:20 000 during the summers of 2000 and 2001 on airphotos obtained from the National Airphoto Library of Natural Resources Canada. Samples were collected, subjected to density determinations, and analysed using thin section petrography and whole rock analyses for both major and trace elements. Thermal ionisation mass spectrometry was used to obtain ages for both troctolite and ferrodiorite.

Most parts of the field area covered in this thesis are readily accessible by boat from the town of Nain within a day. The northwestern areas are at a higher elevation and are more difficult to reach, but can easily be covered on foot from the shore.

1.2 The anorthosite problem

The anorthosite 'problem' is the absence of an obvious mechanism for production of large amounts of plagioclase without producing complementary volumes of ultramafic rocks. Proterozoic (massif-type) anorthosites are distinguished from Archean anorthosites on the basis of modes of occurrence[2]. Archean anorthosites generally occur as thin sills associated with mafic and ultramafic rocks, and are derived from basaltic magma. In contrast, Proterozoic massif-type anorthosites are most commonly found as part of a terrane of contemporaneous acid and intermediate rocks, such as rapakivi-type granite, monzonite, and ferrodiorite. All Archean anorthosites, where primary contact relationships are preserved, are found associated with oceanic volcanics (within greenstone belts: Myers, pers. comm., 2003), whereas massif-type anorthosites are wholly intracratonic. The characteristics of massif-type anorthosites must reflect the physical parameters controlling the formation and emplacement of the batholith: magma sources (such as the type of mantle reservoir or crustal source), melting mechanism (such as

[2]The plagioclase compositions are also different. Proterozoic massif-type anorthosites have plagioclase of composition An_{40-60}, whereas Archean anorthosites have plagioclase of composition An_{80-100}.

decompression melting or plume-related basaltic underplating), and the process by which plagioclase is concentrated.

Theories of massif-type anorthosite genesis begin with this fundamental constraint: a proposed mechanism must be capable of generating all the rocks found in the anorthosite batholith. Constraints are imposed by conclusions from the usual methodologies: field relationships, isotopic and geochemical values, absolute ages, geophysics, etc. These constraints are the keys to a successful solution. The nature of solutions proposed thus far, however, has depended in large part on the respective methodologies used. In the following section, important field and theoretical observations, and some recent theories of anorthosite genesis, are summarized.

1.2.1 Anorthosite emplacement mechanisms

Anorthosite emplacement can be placed within a framework of two plausible ascent mechanisms, which depend on whether the magma (liquid + crystals) functions as a solid or as a liquid. If the crystal-liquid mixture functions as a liquid, conduit ascent, that is, ascent through relatively narrow cracks in the crust, is possible. The other ascent mechanism is diapirism (ascent of a discrete, large balloon-shaped body by viscous deformation of surrounding crust), a type of ascent invoked for bodies that have been thought to be emplaced as solid masses. In the text below, 'magmatic liquid' is used to indicate a magma which functions as a rheological liquid.

A problem of fundamental importance concerning anorthosites has been the plausibility of hyperfeldspathic liquids, defined by Wiebe (1990a) to contain more than ca. 75% normative plagioclase. Strong evidence for the existence of hyperfeldspathic liquids would be of great importance, because it would vindicate the proposition that anorthosite plutons may be emplaced by fracture or conduit ascent. Most objections to proposals of fracture and conduit ascent are raised solely on the basis of an anorthosite's likely high crystallinity upon ascent (discussed below). The yield strength of a highly crystalline magma may be too high for conduit flow to take place (Philpotts and Carroll, 1996); however, there have been no rheological experiments specific to magmas of anorthositic composition. Longhi *et al.* (1993) estimated that a moving magma (a crystal-liquid mixture under shear stresses) of up to 65% crystallinity might behave as a liquid, and show relatively little deformation upon emplacement. This view is supported by the presence of depositional features such as layering, troughs, or scours (Wiebe, 1979; D. Wright, pers. comm., 2003; R. Voordouw, pers. comm., 2003), which indicate that some anorthositic bodies must have been magmatic liquids. Evidence for the ascent of massif-type anorthosites as diapirs has been given by Barnichon *et al.* (1999).

The argument surrounding the existence of hyperfeldspathic liquids has primarily focused on the viability of such liquids existing at crustal temperatures. Bowen (1913) argued that the liquidus temperature of pure plagioclase was too high (fig. 1-3) for such liquids to exist at crustal temperatures. Yoder (1969) proved that the presence of large amounts of water lowers the melting temperature of anorthite substantially (fig. 1-3)

and proposed that anorthositic liquids might be emplaced saturated with water. The NB, however, is characterized by dry assemblages and appears to be essentially unmetamorphosed, so it is unlikely that water could have played a substantial role early in the suite's history and subsequently been driven off.

The discovery of anorthosite dykes in the southern part of the Nain Batholith, first reported by Wiebe (1979), suggested that the prevailing wisdom concerning the viability of anorthositic liquids at crustal temperatures needed substantial revision. Berg (1977a) had estimated the ambient temperature of the mafic granulite into which the dykes had intruded at no more than 300°C. Wiebe (1979) analysed the dykes and a spatially associated leuconorite pluton, and concluded that the dykes are apophyses of the pluton. Substantiating evidence was provided by the leuconorite pluton, which shows no internal differentiation and has a composition nearly identical to that of the dykes. Such evidence seems to require the dyke to represent a primitive, parental liquid.

Wiebe (1990a) provided further evidence for the existence of hyperfeldspathic liquids. He cited the observation of numerous dykes and chilled margins of anorthositic composition throughout the NB. These bodies have textural features (such as the absence of any protoclasis) which suggest their intrusion as liquids with a low crystal content. Further, it was calculated using the method of Ghiorso and Sack (1985) that the liquidus temperature of a particular dyke sample (sample 500B) is 1280°C. Crystallization of plagioclase (alone on the liquidus) would continue until 1175°C, when a cotectic with pyroxene would be reached. At this point, 35% of the original mass would be liquid. It

was concluded that if the dyke had intruded as a cotectic liquid, it would have been at least 65% crystalline. Wiebe postulated that fractionation of mafic minerals from a cotectic, mafic magma had enriched the residual fluid in plagioclase, some of which had remelted (by depressurization) en route to emplacement.

In order to establish the validity of the dykes as liquids, Fram and Longhi (1992) carried out a simple test. They fused and crystallized a sample of one of the anorthositic dykes and compared the mineral assemblage, modal proportions, and major-element composition to the original sample. The authors concluded that the dykes could not represent liquids, because the comparison showed substantial difference between the mineral assemblage and modal proportions of the original and fused samples. In addition, the plagioclase was found to be of a more calcic composition in the fused sample (fig. 1-4, from Longhi *et al.*, 1993). The authors concluded that the plagioclase of intermediate composition found in the original sample must have formed at great depth because, from a magma of a given composition, high pressures favour the formation of more albitic plagioclase[3]. Fram and Longhi (1992) used other evidence to infer that most of the plagioclase crystals in the sample formed at a pressure of 10-11.5 kbar (corresponding to a depth of ca. 35 km) from an aluminous, mafic magma.

Both Wiebe (1990a) and Fram and Longhi (1992) concluded that there was a basaltic precursor to the anorthosites. A corollary of this conclusion is the existence of

[3] It is notable that the authors did not manage to achieve the mineral compositions of the natural dyke by crystallizing fused sample at higher pressure. The resulting plagioclase compositions were more calcic than the original compositions, although the approximation was much better than experiments at the ambient pressure of ca. 5 kbar inferred by Berg (1977a) for the dyke's emplacement.

byproducts (mafic and ultramafic cumulates) of such fractional crystallization. A geophysical survey of the NB (Funck *et al.*, 2000) indicates that the NB extends ca. 10 km into the crust, and that ultramafic cumulates are not present within this block of crust (fig. 1-5). If the assumption of a basaltic precursor is correct, the cumulates must have been left at or near the base of the crust. There are examples of rocks in the lower crust in other parts of the world with P-wave velocities high enough to be considered ultramafic (Rudnick and Fountain, 1995). No decisive data are available for the lower crust below the NB, but the present absence of such bodies would not be proof that they never existed. The existence of the necessary volume of cumulates residual to anorthosite formation in the lower crust remains an untestable hypothesis.

1.2.2 High alumina orthopyroxene megacrysts

One of the most important field observations, around which great debate has centred, is the rare occurrence of high alumina orthopyroxene megacrysts (HAOM) in massif-type anorthosite. These giant (up to more than 1 m) crystals have exsolved lamellae of plagioclase and were estimated by Emslie (1975) to contain up to 9.4 wt% Al_2O_3. Al_2O_3 compatibility in pyroxene is positively correlated with increasing pressure in mafic magmas. The HAOM have therefore been used by some workers (Emslie, 1975; Longhi *et al.*, 1993) to estimate the depth at which at least partial formation of anorthosite took place. Other workers (Xue and Morse, 1994) have interpreted the aluminous nature

of the orthopyroxene megacrysts as a product of rapid growth at the site of emplacement in highly aluminous liquid.

Longhi *et al.* (1993) argued on two fronts for the formation of HAOM at high pressure. First, megacrysts show a threefold increase in alumina content compared to matrix pyroxenes (which presumably grew at the site of emplacement), and if this were not due to pressure effects, it would "...imply physically impossible amounts of Al_2O_3 in the liquid."[4] Second, Longhi *et al.* (1993) assert that analysis of Cr_2O_3 concentrations in megacrysts shows a positive correlation with Al_2O_3 content. This result contrasts with the negative correlation expected for rapid, low pressure growth (fig. 1-6) according to the solute-rejection equations of Smith *et al.* (1955), and can be explained most easily if the HAOM have a high-pressure origin.

This conclusion provides further support for the crystallization of parts of anorthosite bodies at depth. However, Bédard (2001) rejected the notion that the HAOM and most of the plagioclase could have crystallized concurrently from the same magma. Using whole-rock trace element data and partition coefficients, Bédard constructed trace element data sets for magmas parental to both anorthosites and the HAOM[5]. The substantial difference between the trace element compositions of the parent magmas, as calculated by Bédard, refute cocrystallization of HAOM and plagioclase. The data set for

[4]Longhi *et al.* do not quantify how much alumina would be 'physically impossible'. No references support this statement.

[5]Bédard's method and conclusions will be examined in a following subsection.

an HAOM parental magma suggests a liquid more evolved than the ostensible anorthosite parent.

1.2.3 Experimental predictions

A number of theoretical and experimental observations concerning phase relationships have been utilised in the anorthosite debate, an early collection of which may be found in *Origin of Anorthosites and Related Rocks* (Isachsen, 1969). The earliest work on relevant phase equilibria was probably performed by Bowen (1913); his arguments are still of importance. In more recently proposed solutions to the anorthosite problem, two considerations have been important. First, the cotectic boundary between anorthite and an arbitrary mafic phase shifts away from plagioclase with decreasing pressure (fig. 1-7), thereby increasing the range of compositions which will crystallize plagioclase alone. Second, from a magma of a given composition, a positive correlation exists between pressure and the proportion of sodium component in plagioclase (fig. 1-4).

The first observation means that a magma which, at high pressure, had both a mafic mineral and plagioclase on the liquidus will, upon ascent, crystallize only plagioclase until the liquid composition again reaches the cotectic. Some authors (Morse, 1982) envisioned a central role for this process in the creation of massif anorthosites. However, Fram and Longhi (1992) calculated that the decompression of an aluminous, mafic magma from 11.5 kbar to 3 kbar (an ascent of ca. 25 km) would result in a 10%

excess of plagioclase. This is a significant amount, but it does not solve the problem. At 3 kbar, closed-system crystallization of an aluminous basalt will produce plagioclase and mafic minerals in respective proportions of 70:30, so decompression of such magma from great depth to 3 kbar would produce this proportion as a maximum. To create a volume of anorthosite (in proportions of 90:10), mechanical enrichment of plagioclase (separation of mafic minerals from plagioclase crystals by density fractionation, for instance) would have to occur. Morse (1982) suggests that the mechanical enrichment would have taken place during the ascent of the magma.

Increasing pressure has the effect of raising the Na partition coefficient for plagioclase. If massif-type anorthosites are the product of fractional crystallization from otherwise normal basaltic magmas at the depth of emplacement, the Ca content of the plagioclase is lower than expected (Schwartz and McCallum, 1998). A deep origin for most of the plagioclase may make it possible to reconcile the observed intermediate plagioclase with production from a typical basaltic magma. Objections to this reconciliation proceed as follows. Unless all anorthosite plutons in the NB intruded diapirically, with very little interstitial liquid, some crystallization must have occurred at or near the level of emplacement[6]. If partial crystallization of the massif-type anorthosite occurred at 11.5 kbar (ca. 35 km), the depth change to the emplacement level calculated by Berg (1977a, 1977b) for some NB anorthosites would be ca. 25 km. It might therefore

[6]The only constraint on the emplacement crystallinity, as noted in the text above, is the presence of depositional features such as layering, troughs, or scours (e.g. Wiebe, 1979; Wright, pers. comm., 2003; Voordouw, pers. comm., 2003), and such features are not a part of all NB anorthosites.

be expected, as a consequence of the pressure dependence of Na plagioclase-liquid partitioning, that strong reverse and/or oscillatory zoning on plagioclase megacrysts would be ubiquitous, but the absence of zoning in plagioclase megacrysts of the NB is well documented (Emslie, 1980; Longhi *et al.*, 1993).

However, Longhi *et al.* (1993) have shown that, for bodies with a large fraction of plagioclase crystals, decompression produces very little change in the composition that crystallizes. This is illustrated by the ternary Ab-An-mafic diagram in fig. 1-8. Because a given composition will crystallize more albitic plagioclase at higher pressures, the tie-line linking the melt composition to the plagioclase composition at 12 kbar is steeper than comparable 3 kbar tie-lines. The plagioclase 'mush' (crystal-liquid mixture) that ascends to 3 kbar has a hyperfeldspathic bulk composition. Closed-system crystallization requires the tie-lines to rotate about this bulk composition. The change in crystallizing plagioclase composition (from a* to b*) is therefore not very great. If the bulk composition of the 'mush' was much more mafic, the crystals would either develop strong reverse zoning, or be resorbed.

The viability of proposed parental compositions has been tested in a number of melting experiments, performed by various workers. For example, Green (1969) suggested that quartz diorite was a viable candidate for the production of anorthosite. Melting of this type of rock and subsequent crystallization was shown to produce two rock types: initial melting produced granitic liquid, leaving behind a gabbroic anorthosite residuum. These are the two most abundant rock types found in typical anorthosite

terranes. Additionally, the compositional nature of such a source bypasses the 'problem' of the intermediate plagioclase that is commonly observed in Proterozoic anorthosite; the source would likely crystallize intermediate plagioclase at any depth, unlike a typical basaltic magma. However, analyses of major element chemistry for massif-type anorthosites has yielded Mg numbers for both olivine and pyroxene which correspond to more primitive sources. This evidence does not support an intermediate parent magma. Nor have more recent field studies produced evidence for an intermediate parent. For instance, the composition of a proposed chill on the Harp Lake Complex (see below) was a mafic rock.

Longhi *et al.* (1999) performed extensive melting experiments on samples from the Hettasch Intrusion (a leucotroctolitic intrusion in the NB) and some synthetic samples designed to represent the aluminous gabbro (sample HLCA) proposed by Emslie (1980) to be the parent magma for Labrador's Harp Lake anorthosite suite. The paper also includes a summary and discussion of other melting experiments performed on these and other rocks (Vander Auwera and Longhi, 1994; Vander Auwera *et al.*, 1997), including a parent ferrodiorite (sample TJ) from the Norwegian Bjerkreim-Sokndal AMC (anorthosite-mangerite-charnockite) suite. The methods and background theory are too complex to be explored in detail here, but their results are important and deserve discussion.

It was shown that the samples HLCA and TJ lie within a thermal divide, an area on a compositional diagram separating quartz- and nepheline-normative liquid

evolution trends. That is, mantle-derived rocks lie on either one side of the divide or the other, and evolve accordingly. Liquid-evolution trends necessarily do not extend into the compositional area defined by the thermal divide. According to Longhi *et al.* (1999), typical, mantle-derived, mafic magmas would not have the opportunity to bridge this thermal barrier without either the presence of substantial amounts of water, or simultaneous assimilation-fractional crystallization (AFC) of large amounts ($\geq$ 20% of the volume of the magma) of granitic material at pressures no higher than 4 kbar, where the thermal divide is unstable.

Both of these conditions, in the NB and elsewhere, seem to be unsatisfied. There is no evidence for substantial assimilation of country rock in the NB (plutons at the current level of exposure were emplaced between 3 and 5 kbar (Berg, 1977a), and the NB is considered to be broadly anhydrous (Berg, 1977b). Furthermore, Longhi *et al.* (1999) stated that, at depth, no plausible fractional crystallization (FC) or AFC paths, excepting the case of close to 100% (one-to-one) assimilation, will drive the composition of a mantle melt into the thermal divide. Therefore, it was concluded that, because the compositions likely to represent magmas parental or residual to anorthosite lie within the thermal divide, these compositions could not have been mantle-derived.

Instead, the compositions of HLCA and TJ point to wholesale melting exclusively of lower crust to derive the magmas parental to anorthosites. Heat for this process might be provided by a few plausible scenarios. Glazner (1994) suggests that upwelling asthenospheric mantle or underplating bodies might melt foundered mafic

intrusions in the lower crust; Duchesne *et al.* (1999) present a model in which a crustal 'tongue' is melted by being thrust into the asthenosphere. In any case, the result of Longhi *et al.* (1999) contradicts the predominant theoretical basis for massif-type anorthosite production found in the literature: large amounts of mantle-derived basaltic magma ponding at the base of the lower crust undergoing FC or AFC processes to produce volumes of plagioclase (Morse, 1982; Wiebe, 1992; Ashwal, 1993; Emslie *et al.*, 1994). Isotopic and geochemical evidence, which will be discussed below in the context of Emslie *et al.* (1994) and Bédard (2001) respectively, provide good opportunity to independently test the validity of crustal and mantle sources proposed for Proterozoic massif-type anorthosites.

1.2.4 Isotopic evidence

The isotopic ratios of Nd and Sr are widely used to investigate the nature of magmatic sources (Emslie *et al.*, 1994, and references therein). ^{147}Sm decays to form ^{143}Nd, and ^{87}Rb decays to form ^{87}Sr. The important nonradiogenic isotope of Nd is ^{144}Nd. The important nonradiogenic isotope of Sr is ^{86}Sr. In each decay scheme, the ratio of the radiogenic isotope to the nonradiogenic isotope ($^{143}Nd/^{144}Nd$ and $^{87}Sr/^{86}Sr$) is geologically of great value. These decay schemes are particularly useful because Rb and Sm each have a different partition coefficient than their respective decay product. Specifically, Rb is less compatible than Sr, and Sm is more compatible than Nd. Therefore, during partial

melting events in the mantle and elsewhere, Nd will be preferentially concentrated relative to Sm, and Rb relative to Sr, into the melt fraction. The relative concentrations of parent to daughter are therefore altered by partial melting events. Importantly, isotopes of a given heavy element do not fractionate from one another, because they possess essentially identical chemical properties. Partial melting therefore cannot change an isotopic ratio.

There are three different rock types to consider, each with a different parent/daughter ratio, when examining the effect of partial melting on radiogenic isotope systems. The first ratio to consider is the original parent/daughter ratio, that of the unmelted source. The second ratio is the parent/daughter ratio of the the melt, and the third is the parent/daughter ratio of the source after extraction of the melt (the residue). These rocks, immediately after extraction of the partial melt, have identical isotopic signatures. However, the parent/daughter ratio will have been altered. In the case of the Sm-Nd decay scheme, the result of a partial melting event is a higher Nd/Sm ratio in the melt product relative to the unmelted source, and a lower Nd/Sm ratio in the residue. The higher Nd/Sm ratio in the melt product means that less Sm is available in the melt to decay to ^{143}Nd. The ratio $^{143}Nd/^{144}Nd$ will increase more slowly than it would have in the unmelted source. The lower Nd/Sm ratio in the residue means that the ratio $^{143}Nd/^{144}Nd$ will increase more quickly than the unmelted source. So, the isotopic systems of both Nd and Sr will evolve along different trends in the melt product and residue. It is important to

note that different sizes of melt fractions result in different changes in parent/daughter ratios, which will affect the resulting isotopic evolution trend.

Since the crust is essentially composed of melt fractions derived from the mantle, the $^{143}Nd/^{144}Nd$ value of the crust must evolve along a different trend than that of the mantle. This difference in evolution is expressed using 'epsilon notation' (ϵ_{Nd}). Negative ϵ_{Nd} values suggest crustal sources, whereas mantle that has had a partial melt extracted from it should have positive ϵ_{Nd} values. The more negative the value, the longer the crustal residence time. Sr isotopic ratios are similarly expressed as I_{Sr}; the higher this value is, the longer the crustal residence time. A thorough discussion of the specifics of these isotopic systems and their utility in gauging geological processes and sources is found in Dickin (1995).

As has been noted, the north-south trending suture zone of the Churchill (west) and Nain Provinces runs through the NB. In a study of Nd and Sr isotopic data gathered from rocks of the Nain Batholith, Emslie *et al.* (1994) found that the ϵ_{Nd} values of NB anorthosite, granite, and ferrodiorite vary systematically with respect to the suture. In the eastern Nain Province, NB anorthosite ϵ_{Nd} values are most commonly lower ($\epsilon_{Nd} < -10$) than those of the Churchill Province ($\epsilon_{Nd} > -10$) (table 1-1a). Isotopic values of granitic and ferrodioritic rocks can be similarly grouped; the samples with the most negative ϵ_{Nd} were invariably obtained from the eastern Nain Province. As discussed above, the ϵ_{Nd} of a rock is known to decrease with increasing crustal residence time. Given a magma of a particular isotopic composition, it is expected that assimilation of

comparatively older crust will produce comparatively more negative ϵ_{Nd} values. This is apparently the case; Emslie *et al.* (1994) stated that the Nain Province (Nain Batholith $\epsilon_{Nd} < -10$) is of Archean age, whereas the Churchill Province (Nain Batholith $\epsilon_{Nd} > -10$) is predominantly of early Proterozoic age.

Emslie *et al.* (1994) use these data to infer that large amounts of crust were assimilated by the magmas that produced the NB rocks. However, the Churchill Province contains rocks of Archean age, and the Nain Province contains small amounts of early Proterozoic rocks, so any conclusions based on blanket ages for these terrains are suspect (Myers, pers. comm., 2004).

The I_{Sr} values of the NB rocks provide some corroborating evidence. I_{Sr} also varies by geographic location, but shows a stronger correlation by rock type (table 1-1b). For instance, ferrodiorites tend to have I_{Sr} similar to one another, and their range overlaps the upper end of the anorthosite I_{Sr} range. This evidence is consistent with ferrodiorites typically having assimilated as much or more crust than anorthosites. Granitic rocks have, in general, the highest I_{Sr} and most negative ϵ_{Nd}, suggesting that the crust had more influence in the production of NB granites than it did for any other rock type. Similarly, mafic rocks tend to have the opposite attributes: lowest I_{Sr} and highest ϵ_{Nd} (tables 1a and 1b).

Using these and other data, Emslie *et al.* (1994) developed a theory of anorthosite production. Granites, which typically have the highest I_{Sr} and most negative ϵ_{Nd}, were hypothesized to have been formed from lower crustal melts. Specifically, the

granites are inferred to have been derived from up to 90% crustal material. The heat for crustal melting would have been provided by large amounts of underplating and intrusive basaltic material. The extraction of granitic melts from the lower crust would leave an aluminous restite. The subsequent assimilation of this residue by the basaltic, mantle-derived melt, would provide the impetus for the basalt to crystallize plagioclase alone on the liquidus for extended periods of time. After crystallizing large volumes of plagioclase, the mush ascended and expelled its residual interstitial melt: ferrodiorite. Emslie *et al.* (1994) therefore subdivide the rocks of the NB into three categories: mafic and anorthositic, granitic, and ferrodioritic.

1.2.5 Geochemical evidence

If the rocks of the NB are indeed related in the way that Emslie *et al.* (1994) describe, the whole rock chemistry should reflect these links. From whole rock geochemical data, Bédard (2001) employed the equilibrium distribution method (EDM) to obtain elemental concentrations for magmas ostensibly parental to each rock. The EDM functions by assuming that because the trace element concentrations of minerals will reflect those of the magma they crystallized from, the chemical character of the parent magma can be known. The modal abundances and partition coefficients are employed in a set of equations:

$$C^{rock} = (\Phi^{cpx}C^{cpx}) + (\Phi^{opx}C^{opx}) + (\Phi^{plag}C^{plag}) + (\Phi^{tm}C^{tm}) \qquad (1)$$

$$C^{cpx} = C^{plag}(D^{cpx/liquid} / D^{plag/liquid}) = C^{opx}(D^{cpx/liquid} / D^{opx/liquid}) \qquad (2)$$

where C is the concentration of some chemical species, Φ is the modal proportion of the mineral in question, and D is the partition coefficient particular to the mineral and species in question. The superscript 'tm' refers to 'trapped melt'. Equation (2) can be substituted into equation (1) to solve for all minerals present. If a mineral's trace element budget is known, division by the appropriate partition coefficient produces the corresponding abundances of the magma that crystallized the mineral.

Comparison of the data obtained by this method reveal two chemically distinct groups: an anorthositic series, and a mafic series. Bédard (2001) argued that these series must have separate origins, because FC-AFC processes cannot reconcile the chemical trends. Furthermore, because liquids parental to ferrodiorite have higher trace element concentrations than liquids parental to anorthosite, and because these concentrations cannot be derived by fractionation of the anorthosite parent, ferrodiorites are neither parental to, nor derived from, anorthosite. Instead, Bédard (2001) suggested that the ferrodioritic rocks are probably related to the mafic series he defined. By analysis of the likely trace element budgets for various types of lower crust, he concluded that anatexis of garnet granulite would satisfy the anorthosite's geochemical signature.

Finally, Bédard (2001) stated that, though large amounts of basaltic magma might provide the impetus for crustal melting, basaltic magma could not have been a major component of the anorthosites:

> "Model melts calculated for these feldspar-rich products (anorthosites) imply that their incompatible trace element budgets are largely inherited from the crustal source, suggesting that it is not correct to refer to them as the products of crustal contamination of basaltic magma . . . it seems more accurate to invoke contamination of remobilized crust by basalt."[7]

This conclusion is similar to the conclusion of Longhi *et al.* (1999), who argued that Proterozoic massif anorthosites are products of crustal anatexis. Recall that Longhi *et al.* (1999) used some rocks that were considered to be chills in the experiments that led them to this conclusion. Although Bédard (2001) analyzed only rocks from the NB, he disputed some of these and other putative chills, on the basis that their trace element signatures do not match calculated parent liquids. Instead, Bédard (2001) concluded the signatures are suggestive of rocks that have lost a significant part of liquid and are therefore partly cumulate in nature.

1.2.6 Summary of previous theories of massif-type anorthosite formation

The theories of massif-type anorthosite formation presented by Emslie *et al.* (1994), Longhi *et al.* (1999) and Bédard (2001), have some important differences. Emslie *et al.* (1994) suggest that mantle-plume-derived, basaltic melt ponded at the base of the

[7]Quoted from Bédard (2001).

crust. The heat from this process partially melted the lower crust; the partial melts ascended to form the granites of the NB. The anorthosites were formed when the basaltic melt began to assimilate the aluminous residue of the partial melting process. In contrast, Longhi *et al.* (1999) and Bédard (2001) suggest that both the granites and anorthosites of the NB are almost wholly formed from crustal melts.

The origin and nature of the NB mafic rocks, and the mantle melt, is also debated. For instance, the leucotroctolitic Kiglapait Intrusion is described as a fairly direct sample of the mantle component by Emslie *et al.* (1994). Because of the relatively enriched nature of the trace element budgets for the model melts of this and other 'primitive' liquids, as calculated by Bédard (2001), and the negative ε_{Nd} values for the Kiglapait Intrusion reported by Emslie *et al.* (1994), both Bédard (2001) and Emslie *et al.* (1994) agree the mantle melt must have been relatively enriched. However, Bédard (2001) rejects the mantle plume suggestion of Emslie *et al.* (1994), due to the presence of a ubiquitous negative Nb anomaly. Bédard (2001) instead suggests decompression melting of asthenosphere or fertile mantle lithosphere, followed by crustal contamination.

Longhi *et al.* (1999) and Bédard (2001) are in agreement that at least some of the mafic rocks are mantle-derived and heterogeneously contaminated, but they are in disagreement about the origin of ferrodiorites: Bédard (2001) tentatively suggests the ferrodiorites are kin of mafic series rocks (which are mantle-derived), perhaps through fractionation processes, whereas Longhi *et al.* (1999) concluded that sample TJ, a

ferrodiorite chilled margin, must be either a crustal product or the result of one-to-one mixing between crust- and mantle-derived liquids.

Emslie *et al.* (1994) presented I_{Sr} data that suggest ferrodiorites are generally at least as contaminated by crust as the anorthosites (table 1b), and concluded that ferrodiorites are the residual melt of anorthosite. The anorthosites show various amounts of crustal contamination but appear to require, based on the data of Emslie *et al.* (1994), a budget dominated by crustal material. According to these isotopic data, the anorthosites could be described, in accord with Bédard (2001), as remobilized crust contaminated by mantle melt.

1.2.7 Summary of previous work

From the preceding discussion, some general conclusions about Proterozoic massif-type anorthosites may be reached.

1. There is no evidence for anorthositic liquids (that is, hyperfeldspathic liquids with a low degree of crystallinity). Field evidence (Myers, pers. comm., 2004; Voordouw, pers. comm., 2003; Wright, pers. comm., 2003; Wiebe, 1979) does require the operation of magmatic processes in some plutons, indicating that not all anorthosite plutons can have risen as solid-state diapirs. The absence of certain textural features, such as protoclasis, in anorthositic dykes suggests that magmas of anorthositic composition,

which probably have high crystallinity during ascent and upon intrusion, behave as liquids (Fram and Longhi, 1992).

2. If anorthosites are to be formed from basaltic magmas, they must be quite crystalline prior to ascent. This follows from basic principles. If a basaltic magma begins crystallizing mafic minerals, the magma's composition changes until it becomes saturated with plagioclase. In order to produce the high proportion of plagioclase crystals observed, large volumes of mafic minerals must crystallize and be removed, presumably by density-difference-driven fractionation. Ultramafic rocks formed from these fractionated minerals are not found with massif-type anorthosites which were emplaced at mid-crustal levels, so the production of large amounts of the plagioclase must have already occurred at depth. The case (for instance) of superheated magmas dissolving large amounts of plagioclase to become hyperfeldspathic, or of extremely delayed nucleation of plagioclase, is unsupportable at present, because of the lack of evidence for anorthositic liquids as defined by Wiebe (1990a). The results of Longhi *et al.* (1993) also stress the importance of large fractions of crystals formed at depth to explain the observed lack of significant chemical zoning in the plagioclase crystals that constitute Proterozoic massif-type anorthosites.

3. The disagreement about the origin of HAOM (high alumina orthopyroxene megacrysts) is ongoing, and strong arguments have been made connecting them with both deep and *in situ* crystallization. It has been shown that the pressures needed to produce the intermediate plagioclase observed in many anorthosites directly

from a basaltic magma are coincidental with pressures resulting in the incorporation of substantial amounts of Al_2O_3 in the pyroxene structure (Longhi *et al.*, 1993). Even from this evidence, however, it is not necessarily true that the plagioclase and HAOM are cogenetic. One may agree with a deep origin for both while postulating separate sources for each (Bédard, 2001).

4. The most extensive melting experiments performed to date on rocks associated with Proterozoic massif-type anorthosites (Longhi *et al.*, 1999) have resulted in liquid evolution paths and phase relationships that preclude derivation of the massif-type anorthosites and the associated rocks directly from mantle melts. The reasoning is correct if and only if the samples used in the study (Longhi *et al.*, 1999) are actually parental, or are directly related to the suite at depth. If the samples used were (for instance) the result of low pressure AFC processes, the suite might still be a product of mantle-derived melt.

5. The minimum ratio of plagioclase crystals to cotectic melt needed to produce a rock consisting of 90% plagioclase can be calculated from data in Fram and Longhi (1992). Based on their 70 : 30 estimate of plagioclase : pyroxene phase proportions for an aluminous basalt, for any one unit of cotectic melt, two units of plagioclase crystals are required, if the final result of closed-system crystallization is to be an anorthosite. This proportion is at the limiting end of a generally accepted estimate of a maximum crystal-liquid ratio for magmas to behave as rheological fluids. Although experiments specific to plagioclase suspensions are lacking, material with ratios higher

than this are commonly expected to be rheological solids incapable of fluid behaviour (that is, capable of fracture ascent), and must be emplaced diapirically.

6. The isotopic and geochemical evidence is strongly in favour of significant crustal contributions to anorthosite genesis, whatever the exact proportions may be. The isotopic evidence of Emslie *et al.* (1994) could be interpreted to support the assertion of Bédard (2001) that anorthosites are primarily products of anatexis of a depleted mafic lower crustal source region. This hypothesis is similar to that of Longhi *et al.* (1999), although the details of each proposal do not agree in their entirety.

Table 1-1a. Summary of Nd isotopic data for the NB.

	N	Age (Ga)	Crust Age (Ga)	ε_{Nd} @ 1.3 Ga mean	range	CC
Umiakovik (W)	3	1.32	2.7	-8.2	-7.7 to -8.7	-14.6
Makhavinekh (W)	3	1.32	2.7	-8.7	-8.7 to -8.8	-14.6
Notakwanon (W)	3	1.29	2.7	-9.2	-8.3 to -9.7	-14.6
West granitoids	4	1.3	2.7	-5.6	-4.7 to -6.1	-14.6
West anorthosites	15	1.3	2.7	-7.2	-3.7 to -10.2	-14.6
West ferrodiorites	10	1.3	2.7	-7.1	-3.6 to -8.7	-14.6
Churchill Province orthogneiss		2.7	2.7	-14.6	-11.1 to -18.3	-
East and west mafic rocks	7	1.3		-4.9	-3.0 to -6.4	-
East granitoids	10	1.3	3.2	-13.1	-11.5 to -13.4	-21.9
East anorthosites	14	1.3	3.2	-11.8	-8.9 to -17.4	-21.9
East ferrodiorites	12	1.3	3.2	-12	-9.8 to -14.8	-21.9
Nain Province orthogneiss		3.2	3.2	-21.9	-14.2 to -28.1	-

Note. All data from Emslie *et al.* (1994); this is an adaptation of their table 3. N is the number of samples from each pluton. CC is the $_{Nd}$ of the crust thought to have been assimilated (in the case of anorthosites and ferrodiorites) or partially melted (in the case of granites) to yield rocks of the Nain Batholith. The ε_{Nd} values are calculated for 1.3 Ga. Designations of 'West' and 'East' mean that the inferred crustal component is derived from either the Churchill Province (west) or Nain Province (east). The Umiakovik, Makhavinekh, and Notakwanon are granitic bodies with crustal components derived from the Churchill Province. Entries under the heading 'Crust Age' give the age of the inferred crustal component; the ages are based on mean ages for granitoid gneiss samples from the Nain and Churchill provinces.

Table 1-1b. Summary of Sr isotopic data for the NB.

	N	Age (Ga)	Crust Age (Ga)	I_{Sr} @ 1.3 Ga mean	range
Umiakovik (W)	7	1.32	2.7	0.7085	0.7072 - 0.7098
Makhavinekh (W)	2	1.32	2.7	0.7074	0.7070 - 0.7078
Notakwanon (W)	9	1.29	2.7	0.7083	0.7051 - 0.7124
West granitoids	3	1.3	2.7	0.7069	0.7054 - 0.7074
West anorthosites	11	1.3	2.7	0.7047	0.7038 - 0.7059
West ferrodiorites	10	1.3	2.7	0.7072	0.7054 - 0.7090
Churchill Province orthogneiss	12	2.7	2.7	0.7102	0.7040 -0.7203
East and west mafic rocks	7	1.3		0.7040	0.7034 - 0.7046
East granitoids	10	1.3	3.2	0.7076	0.7047 - 0.7104
East anorthosites	12	1.3	3.2	0.7062	0.7043 -0.7118
East ferrodiorites	12	1.3	3.2	0.7064	0.7054 - 0.7086
Nain Province orthogneiss	8	3.2	3.2	0.7110	0.7024 - 0.7232

Note. All data as in table 1a.

Figure 1-1. Simplified geological map of the Nain Batholith and some surrounding rocks. Limits of the main map are shown in the upper right corner on a map of Labrador, Canada. The Barth Island Ring Complex is outlined by the box next to the town of Nain, on the main map. The geological map is modified slightly from Ryan and James (2003); the Labrador outline was digitized by Tettelaar (2003).

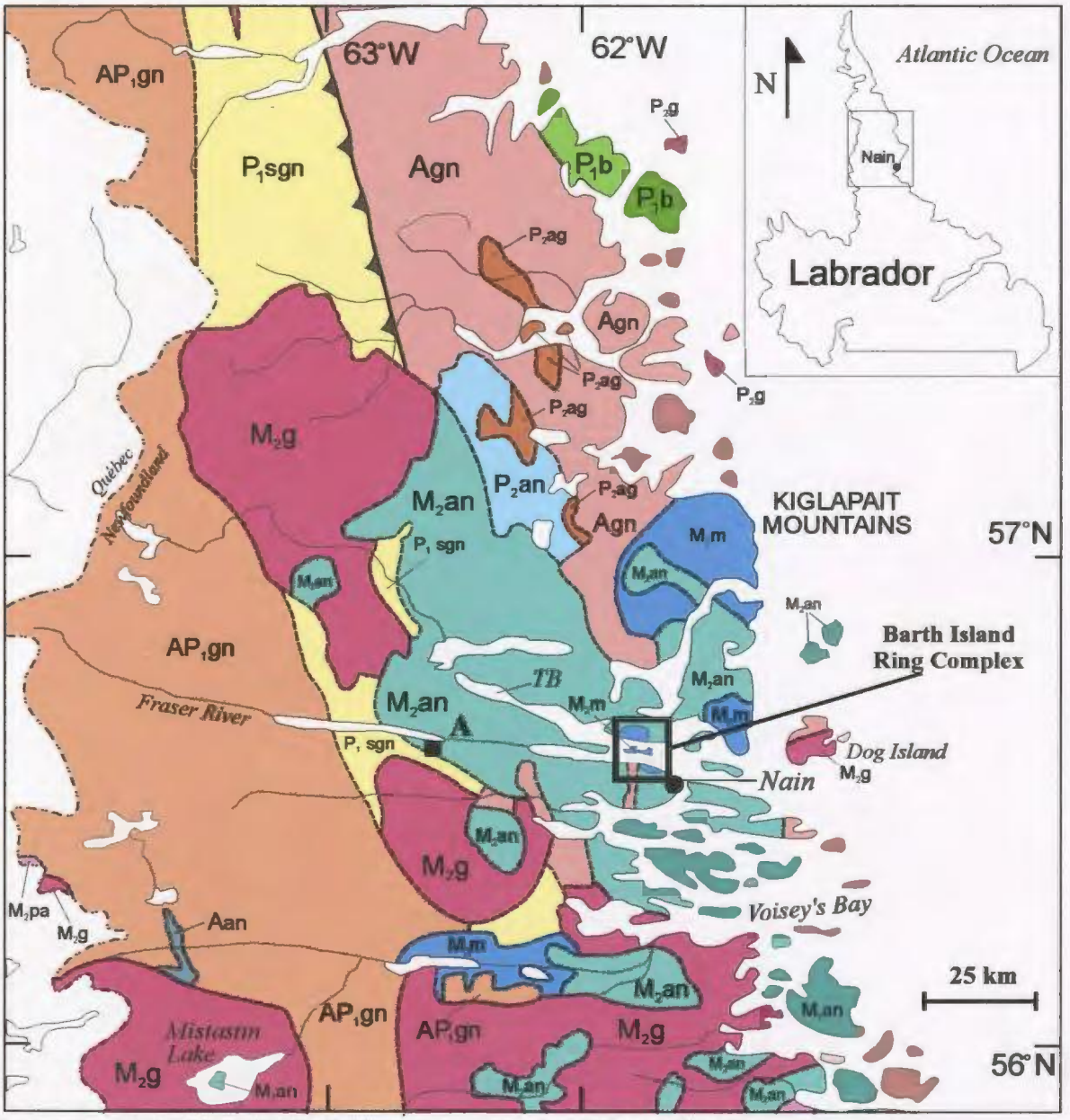

Mesoproterozoic (Nain Batholith)

- M_2pa peralkaline/alkaline intrusion
- M_2g granite plutons
- M_2m gabbro and ferrodiorite plutons
- M_2an anorthosite plutons

Paleoproterozoic

- P_2g granite plutons

Paleoproterozoic (Arnanunat Plutonic Suite)

- P_2ag granitic plutons
- P_2an anorthositic plutons

Archean and/or Paleoproterozoic (Southeastern Churchill Province)

- P_1sgn Tasiuyak (metasedimentary) gneiss
- AP_1gn tonalitic and minor metasedimentary gneiss of predominantly Archean age
- Aan anorthositic rocks
- P_1b mafic volcanic and sedimentary rocks

Archean (Nain Province)

- Agn tonalitic and lesser meta-sedimentary gneiss

thrust fault superimposed on the Abloviak Shear Zone

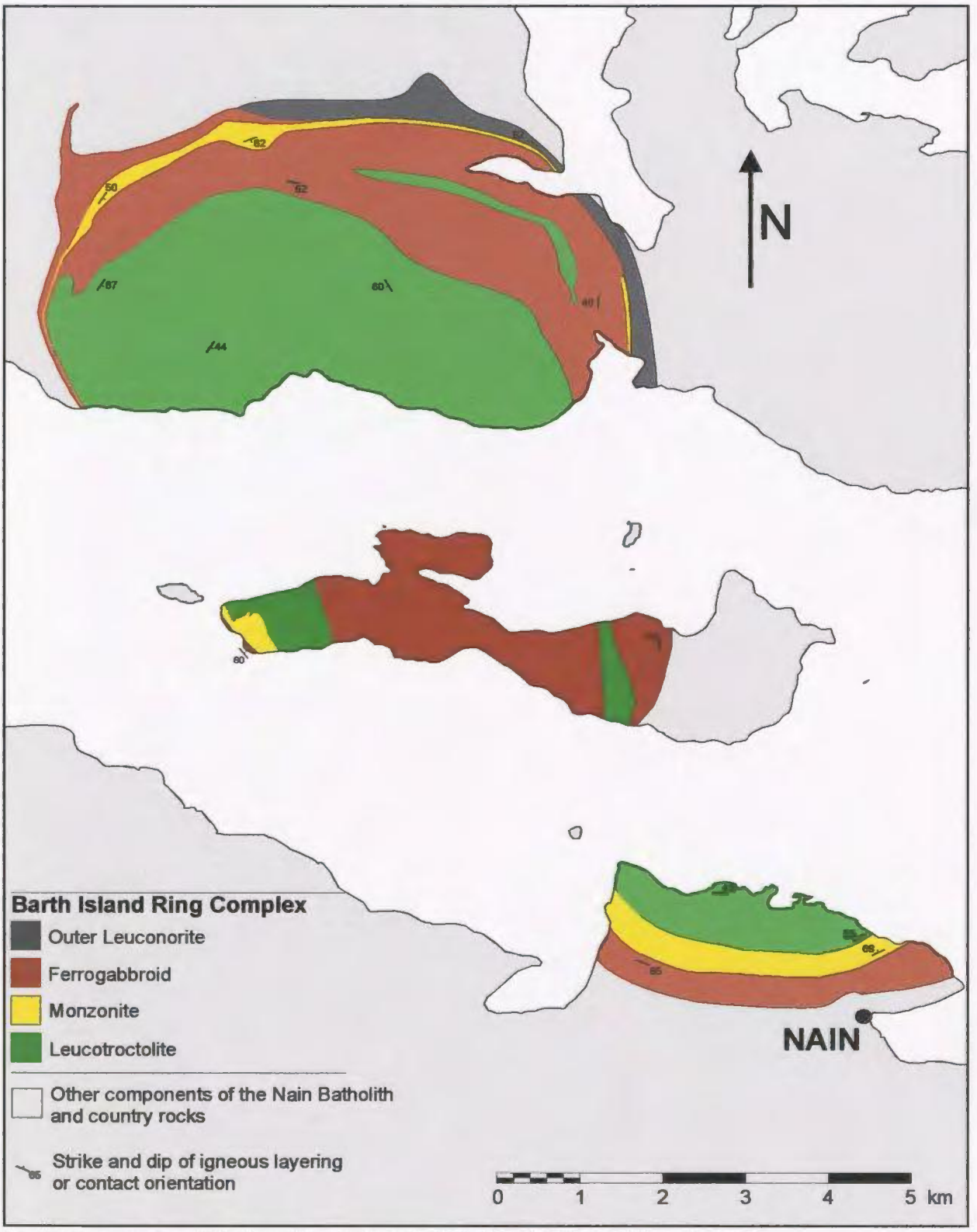

Figure 1-2. A simplified geological map of the Barth Island Ring Complex.

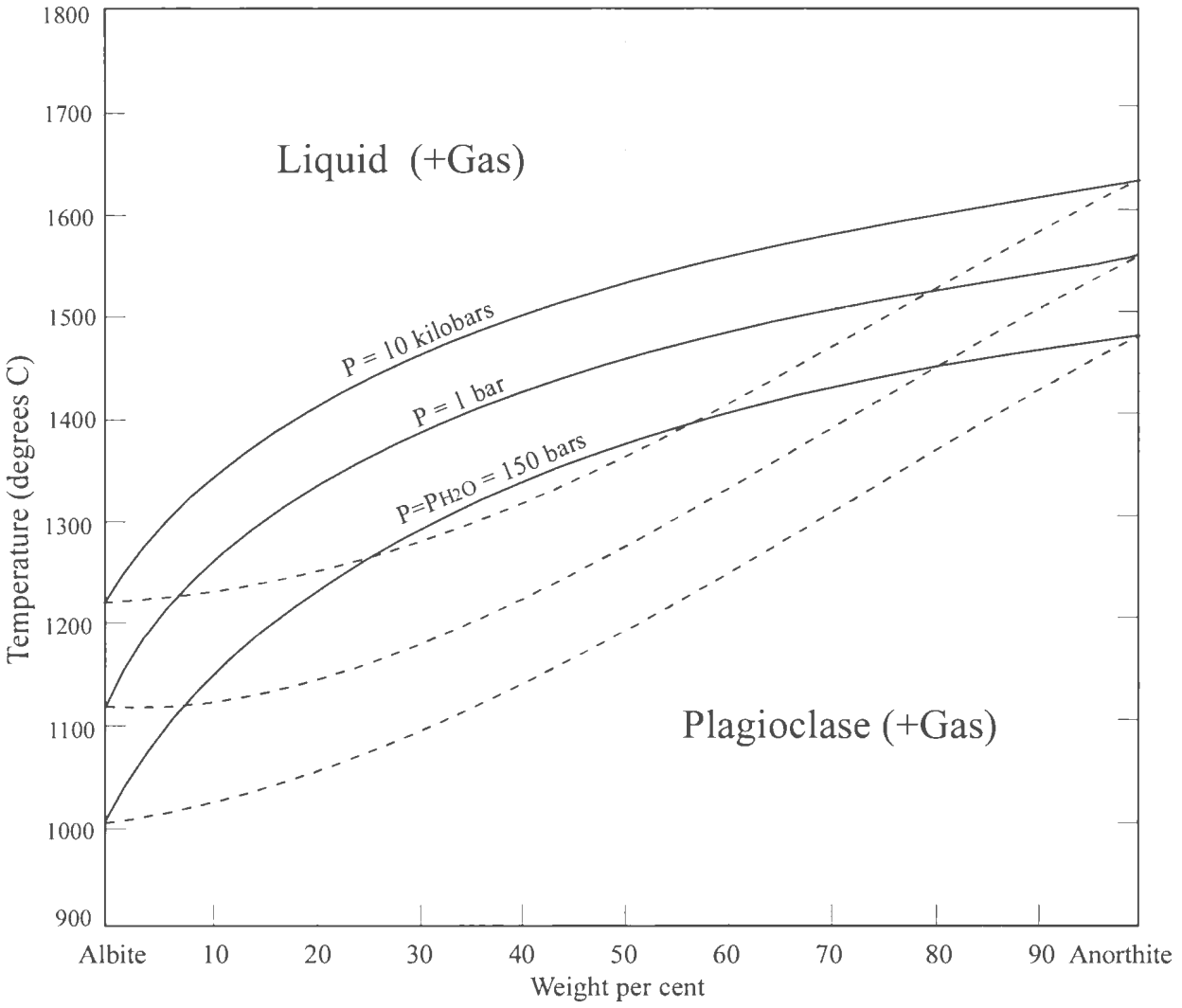

Figure 1-3. Plagioclase phase diagram illustrating the liquidus (solid lines) and solidus (dashed lines) temperatures for plagioclase at compositions which range from pure albite to pure anorthite. Text above each line gives pressure information. Note that two of the given pressures are ambient dry pressures, and one is vapour pressure. The liquidus temperature is significantly lower in the presence of water. Adapted from Yoder (1969).

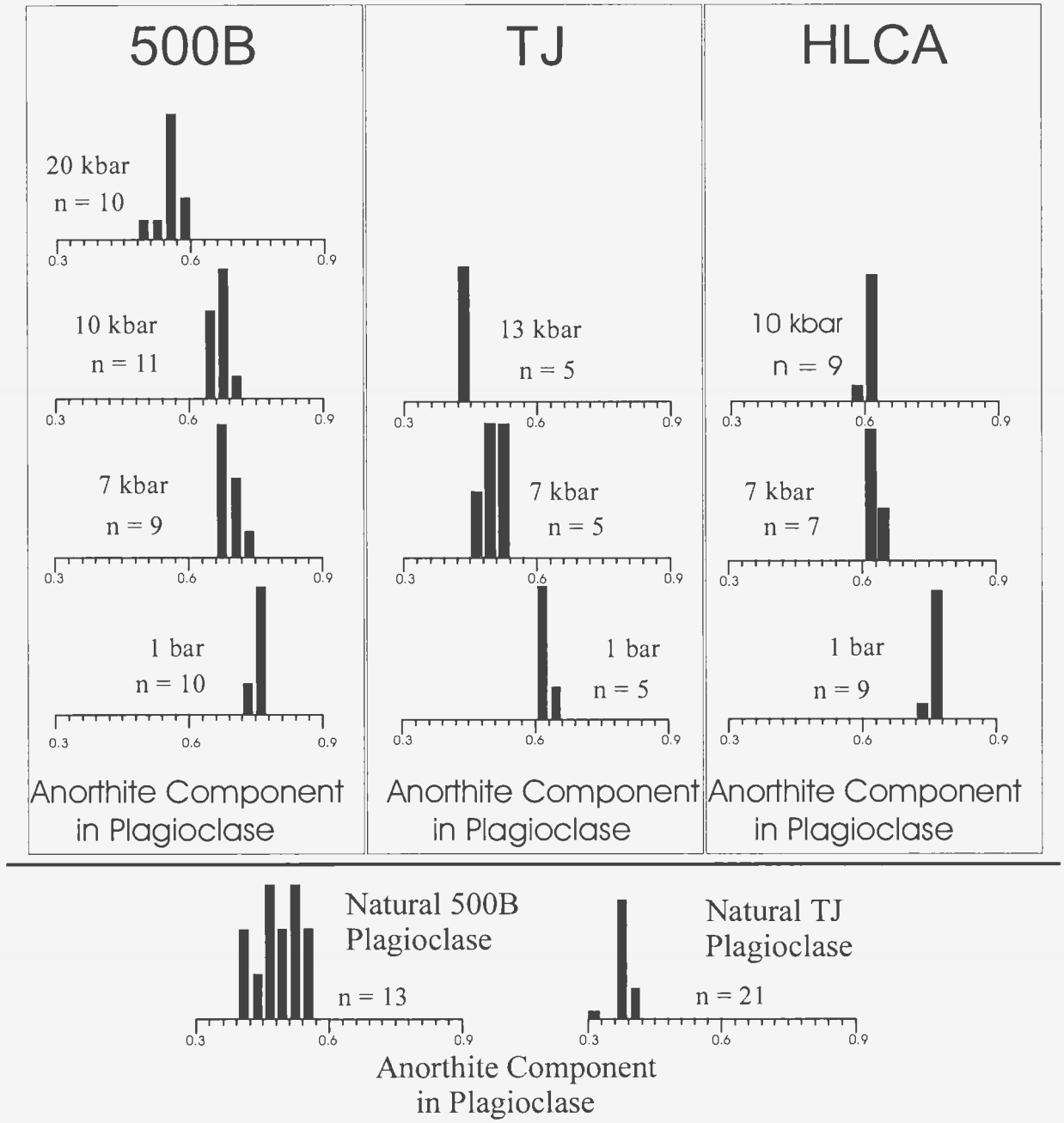

Figure 1-4. Histograms of plagioclase compositions for three rocks, resulting from crystallization at various pressures: an anorthosite dyke from the NPS (500B); a ferrodiorite from Norway (TJ); and one synthetic composition (HLCA, an aluminous mafic composition designed to represent the hypothetical parent for the Harp Lake Complex, as postulated by Emslie, 1980). 'N' gives the number of samples processed. The fusion experiments on the samples show that higher pressures favour the formation of more albitic plagioclase. The natural plagioclase compositions for TJ and 500B are shown at the bottom. Note that no experiment recreated the exact compositions found in the original rock. Diagram taken from Longhi *et al.*, 1993 (their fig. 1).

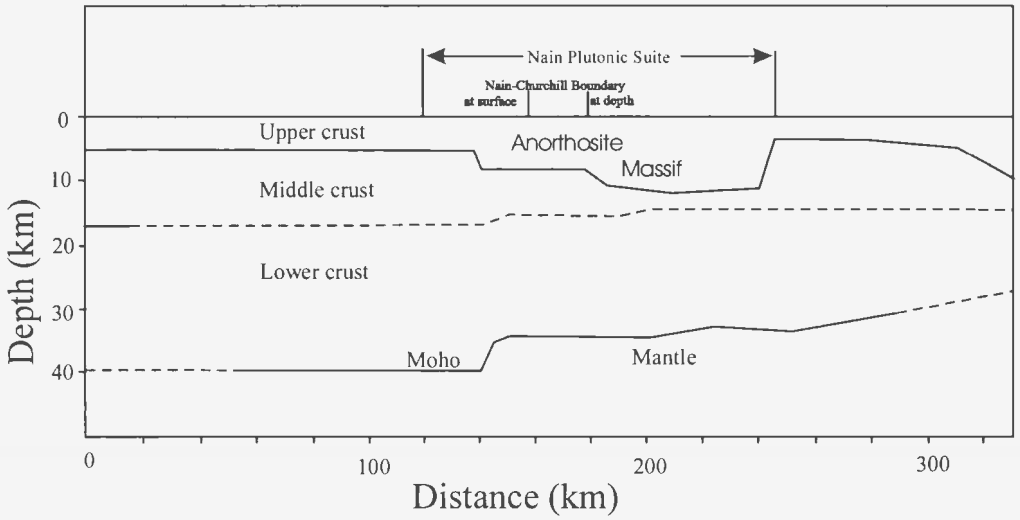

Figure 1-5. Simplified p-wave model of the crust beneath the Nain Batholith, illustrating the presence of a large volume of anorthosite. Corroborating evidence is found in gravity and s-wave data (not shown). Diagram simplified from Funck *et al.*, 2000 (their fig. 3).

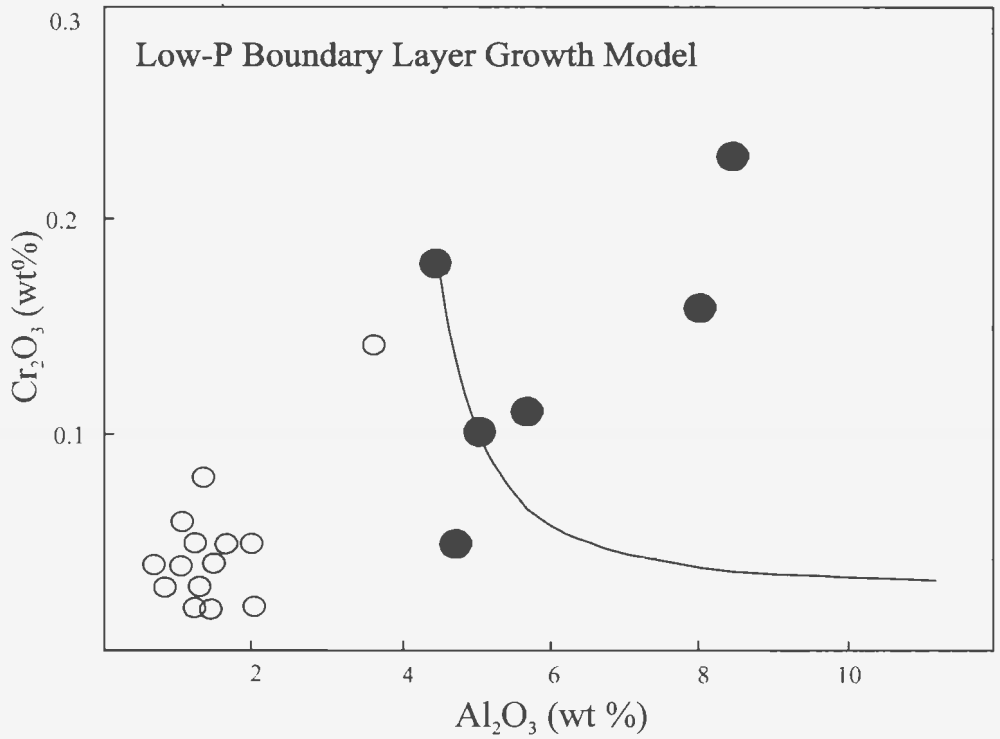

Figure 1-6. Concentration of chromium oxide vs. alumina content (solid curve) calculated from the solute-rejection equations of Smith *et al.* (1955). The solid circles are measured concentrations from aluminous orthopyroxene megacrysts; the empty circles are matrix pyroxenes. Low-P boundary layer growth is expected to produce the negative correlation represented by the solid line, whereas the observed correlation is, according to Longhi *et al.*, positive. Diagram simplified from Longhi *et al.*, 1993 (their fig. 7).

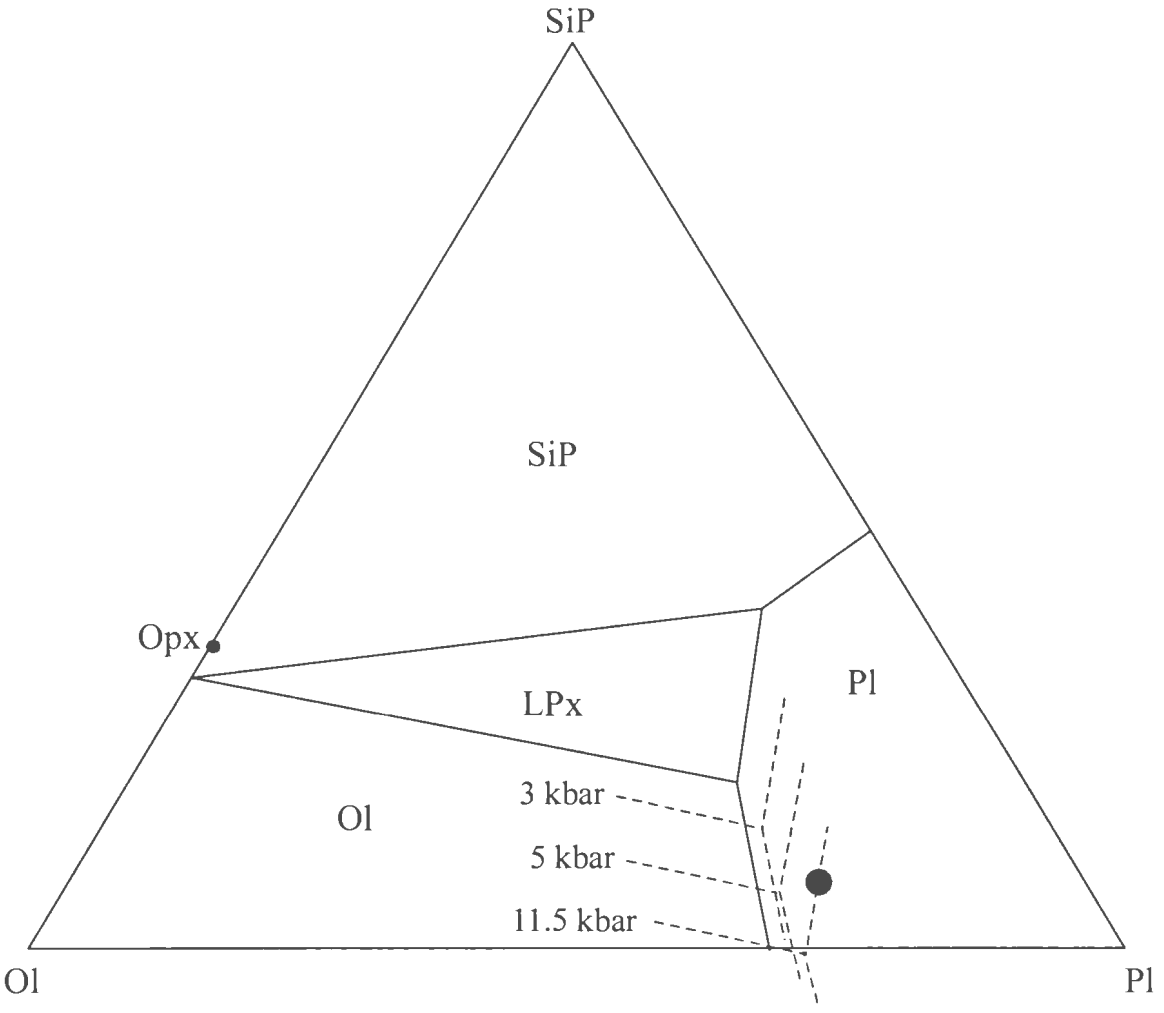

Figure 1-7. Ternary phase diagram illustrating the effect of changing pressure on plagioclase liquidus boundaries. Solid lines in diagram show boundaries at 1 bar. Each of the dashed lines shows the boundary at a different pressure (text next to lines). Observe how decreasing pressure expands the plagioclase field. A magma of the composition represented by the solid circle shares a cotectic with low-calcium pyroxene (LPx) at 11.5 kbar. Decompression of this magma to 3 kbar leaves the composition well inside the plagioclase field. Abbreviations are as follows: SiP = silica polymorph, Pl = plagioclase, Ol =olivine, and Opx = orthopyroxene. Diagram simplified from Fram and Longhi, 1992 (their fig. 7).

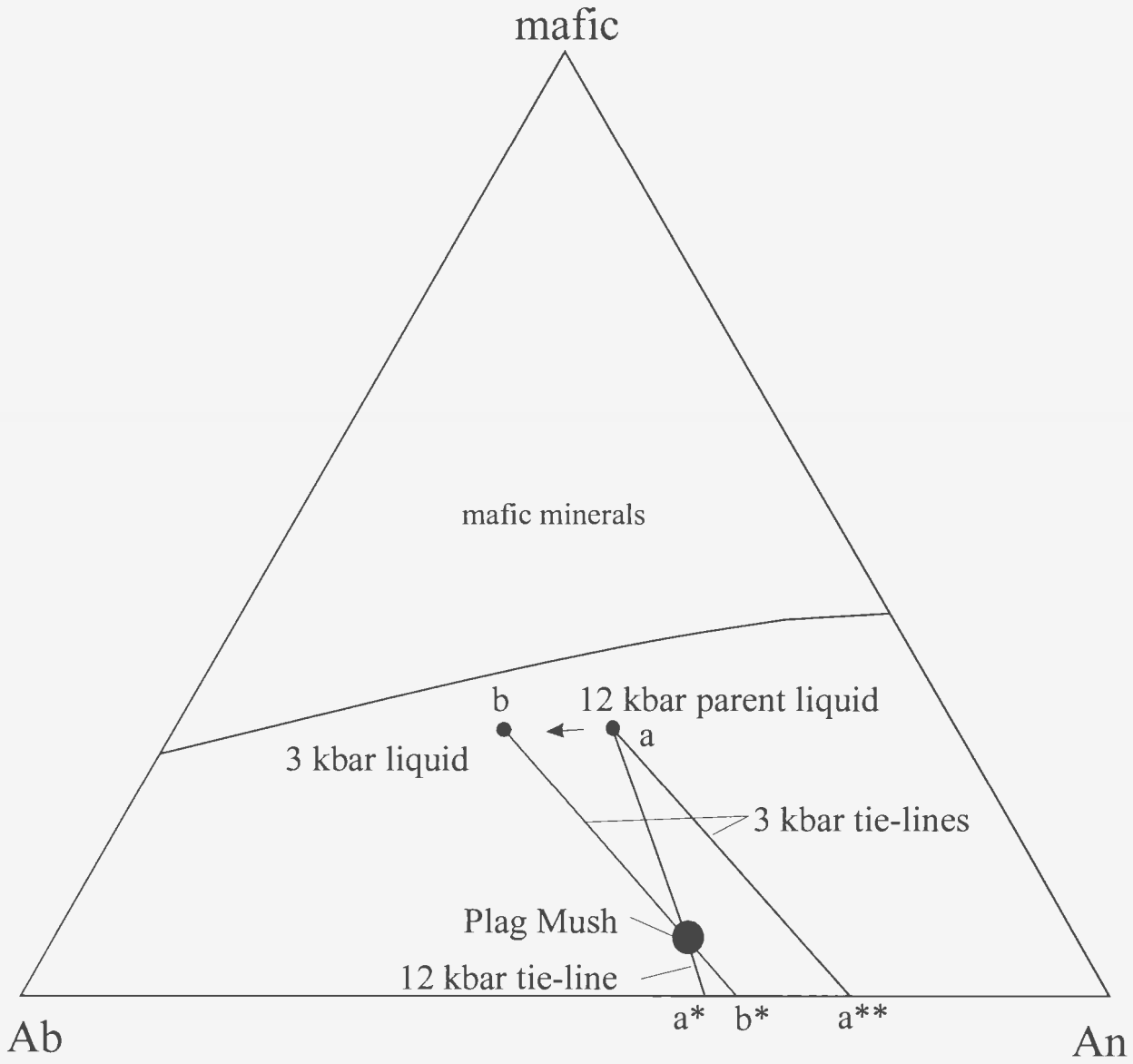

Figure 1-8. Ternary albite-anorthite-mafic diagram illustrating the change in plagioclase composition crystallizing from magma of a given composition as a result of decompression, and the effect bulk composition has on this shift. Since high pressures require crystallization of more Na-rich (albitic) plagioclase, a magma of bulk composition 'a' that crystallizes plagioclase of composition of 'a*' at 12 kbar will crystallize plagioclase of composition 'a**' at 3 kbar. Note that the tie-lines connecting the bulk and crystallizing compositions become more shallow after decompression. If the ascending magma has a large fraction of plagioclase crystals, the bulk composition is changed (shown by large filled circle labeled 'Plag Mush'). Equilibrium requires the tie line to rotate about this composition; decompression makes the tie line more shallow. In the case of magmas carrying a large fraction of plagioclase, the composition of crystallizing plagioclase will not be greatly shifted (from a* to b*). Diagram adapted from Longhi *et al.*, 1993 (their fig. 6).

Chapter 2 The Barth Island Ring Complex

2.1 Introduction

2.1.1 Structure and outcrop pattern

The Barth Island Ring Complex (fig. 2-1, located in the back flap) is an oval body composed of three major rock types: leucotroctolite (hereafter referred to as troctolite), ferrogabbroid, and monzonite. The major bodies of each rock type form concentric rings about the middle of Barth Island. The outer ring of the intrusion is mainly composed of ferrogabbroid, and has an inner contact with monzonite. This contact is well exposed at several locations in both the northern and southern parts of the intrusion. At the northeast margin of the ring complex, the outermost rock type of the Barth Island Ring Complex is leuconorite. On the south side of the ring complex, the body of monzonite has a well-exposed inner contact with the troctolite. On the north side, the monzonite's inner contact is with ferrogabbroid. A thin sheet of troctolite, surrounded by ferrogabbroid or ferrogabbroid-monzonite hybrid rock where contacts are exposed, is found in the northeast section of the intrusion. A second unit of ferrogabbroid, the central ferrogabbroid, which crops out in the centre of Barth Island, does not have any exposed contacts with other members of the Barth Island Ring Complex.

The troctolite forms the bulk of the high topography of the complex; one area of high topography on the south side of Nain Bay also comprises monzonite. These rock types are both composed primarily of feldspar, which is resistant to weathering. The

ferrogabbroid, because of its relatively high proportions of iron oxides and mafic minerals, is more easily eroded than the troctolite and monzonite, and tends to form lowlands. This general rule is illustrated by examining the topography from A to A' in fig. 2-1. At A, the rock is troctolite, which is in contact with a ferrogabbroid. This change in rock type is accompanied by a rapid decrease in elevation. The following rise in elevation, which culminates at A', begins at the ferrogabbroid's contact with monzonite. There are exceptions. For instance, the relief of the central part of Barth Island is formed from ferrogabbroid.

The foliations and layer orientations within and between each of the major rock types are essentially parallel at any given location throughout the ring complex. That is, the broadly oval shape of the ring complex is defined by textural orientations in each rock type, as well as in the large-scale morphology, including contact and layer orientations. The structures are generally steeply dipping (>50°), with various dip angles over short distances. The dip angles near the southern margin of the ring complex dip most steeply, between 70° to 90°. All rock types (excepting the central ferrogabbroid) dip toward the centre of the ring complex. Fig. 2-1 includes strike and dip measurements taken by other workers (de Waard, 1976), as well as those taken during the course of the present study.

Two faults, which run broadly parallel to the length of Barth Island, have been inferred to exist between Barth Island and the mainland to the north and south of Barth Island (de Waard, 1976; Ryan, 2000; Ryan, 2001). These faults (referred to hereafter as the 'northern' and 'southern' faults) are suggested to exist, because the orientations of

layering, contacts, and foliations in the rocks of the Barth Island Ring Complex are broadly N-S along its eastern and western margins. According to the orientation of these structural features, the correlative rocks on Barth Island and either side of Nain Bay are not in alignment. In order to roughly align the structures, movement along the faults has been interpreted to be sinistral (de Waard, 1976). The conclusions of the present study are in accord with the presence of these faults. It is unclear, however, whether the offset should be purely horizontal, purely vertical, or some combination of the two. For instance, Ryan (2001) inferred ca. 400 m of upthrow to the north on the northern fault, and ca. 2 km of upthrow to the north along the southern fault.

The presence of the northern fault is independently corroborated by aeromagnetic data (fig. 2-2, see below). North of the eastern end of Barth Island, the aeromagnetic map shows two thin sheets of highly magnetic rock (which broadly correlate with a ferrogabbroid unit) that terminate abruptly to the north; to the west, two apparently identical sheets terminate abruptly to the south along the trace of Nain Bay. The sheets can be brought together by inferring either ca. 1 km of sinistral horizontal movement, or 1.2 km of vertical upthrow to the north. The actual movement along the fault is probably some combination of vertical and horizontal movement, so these estimates should be considered end-members.

Based on the orientations of the structural features mentioned above, the fault to the south of Barth Island is inferred to have ca. 4 km of sinistral offset; however, detailed aeromagnetic data are not available for parts of this area, so there is no independent

support for this offset. As mentioned above, possible vertical upthrow of 2 km to the north of the southern fault was suggested by Ryan (2001).

The detailed aeromagnetic survey of Barth Island and the surrounding area, cited above, was performed by the Voisey Bay Nickel Company (fig. 2-2). The magnetic map of the Barth Island Ring Complex corresponds well with the geologic map. The red on the aeromagnetic map areas signify ferrogabbroid: for example, the central ferrogabbroid (section 2.5), is distinguished by a magnetic high. The troctolite, monzonite, and surrounding anorthosite generally have low magnetic signatures (green or blue on the aeromagnetic map).

The aeromagnetic data are useful for establishing patterns of rock distribution where no outcrop is present. However, it is obvious that the surface geology cannot be perfectly correlated with the magnetic signatures displayed on the map (fig. 2-2). The northern boundary of the troctolite, for instance, appears farther south by magnetic signature than at the surface. This is because the ferrogabbroid-troctolite contact dips to the south at an angle of ca. 50°, and therefore ferrogabbroid underlies this part of the troctolite near the level of exposure. Also, the leuconorite sheet located along the eastern and northeastern edge of the ring complex appears to have two different magnetic signatures: one positive (red, along the eastern margin), and one negative (blue and green, along the northeastern margin. The leuconorite should be consistently negative, as it is composed primarily of plagioclase feldspar. However, along the eastern contact, the

leuconorite is interlayered with a melanocratic norite which contains a high proportion of magnetite.

As noted above, the monzonite has a negative magnetic signature. However, the observed location of the contact between the monzonite south of Nain Bay and ferrogabbroid to the south of it does not correlate well with the magnetic map, even though contact inclination measurements taken at the southern margin of the monzonite indicate that the ferrogabbroid-monzonite contact dips relatively steeply (fig. 2-1). This may be caused by the relatively high proportion of mafic minerals in the monzonite along the contact, which is probably an artifact of mixing and mingling between the monzonite and ferrogabbroid. In the following sections, I will appeal to the aeromagnetic data to support interpretations of the subsurface geology.

2.1.2 Sample nomenclature

Sample locations are shown in fig. 2-1. Solid lines show suites of samples, which were collected perpendicular to the strike of local structures. Sample numbers preceded by 'BI-' were collected during the 2000 field season; all other samples were collected during the 2001 field season. The samples taken during the 2001 field season are preceded by various prefixes. These prefixes identify the general area from which the samples came. Samples preceded by 'BII' were collected in the northwestern, central, and shoreline parts of the ring complex on the north side of Nain Bay. Also on the north side

of Nain Bay, samples preceded by 'LBE' were taken in the northeastern, central, and northern marginal parts of the ring complex. Samples preceded by 'BIII' were collected on Barth Island, and those preceded by 'BIV' on the small island off the west coast of Barth Island. Samples preceded by 'NBS' were collected from the area on the south side of Nain Bay, as were the sample suites BS 7 - 9. All other sample suites were collected on the north side of Nain Bay.

2.1.3 Terminology and the ferrodiorite question

The terminology used in this work generally follows the most recent guidelines set out by the IUGS (Le Maitre, 2002). I have found it necessary, however, to deviate slightly from this classification scheme in discussing rocks which may be members of a class of rocks known as 'ferrodiorites'. The bulk of recent literature for the NB, and for Proterozoic massif-type anorthosites worldwide, has referred to a class of rocks as 'ferrodiorites'. These rocks are Fe-rich and of diverse composition. Such rocks have previously been called 'jotunites' (de Waard, 1976). The change from 'jotunite' to 'ferrodiorite' has presumably been undertaken to follow the recommendations of the IUGS (Le Maitre, 2002), although the term 'jotunite' has been retained in the IUGS classification scheme for rocks considered to belong to the 'charnockite suite'. It may be that 'ferrodiorite', by not communicating the genetic association with the charnockite suite that 'jotunite' does, avoids any confusion surrounding the term 'charnockite' that exists

between the fields of igneous and metamorphic petrology. The existing terminology describes the rock using simple, standardized roots, which may then be modified to clarify some aspect of the rock's nature: hence the term '*ferro*diorite'. This method avoids any issues of genesis.

Most of the Fe-rich rocks have a mineral assemblage which (according to the IUGS system) constrains the possible root to -gabbro (*sensu lato*) or -diorite (fig. 2-3). The criterion used to distinguish between these two roots is as follows: rocks with plagioclase of composition An_{0-50} are diorites; rocks with plagioclase of composition An_{50-100} are gabbros. Many of the Fe-rich rocks in this study should be called diorites, as the average plagioclase composition is just below An_{50} (Mulhern, 1974). The Fe-rich rocks in this study, however, contain pyroxene as the primary mafic constituent. The IUGS classification system allows the root name of a rock to distinguish between clinopyroxene- and orthopyroxene-bearing types only when using the roots -gabbro and -norite. The root -gabbro indicates a rock that is primarily clinopyroxene-bearing, whereas -norite indicates rocks which are primarily orthopyroxene-bearing.

In this study, the distinction between clinopyroxene- and orthopyroxene-bearing types is a useful one, and I have therefore used the root 'gabbro' and the general term 'ferrogabbroid' for referring to the rocks in general, without regard to the specific mafic mineral they contain. 'Ferrogabbroid' was chosen as the general term to refer to both clino- and orthopyroxene-bearing rocks instead of 'ferrogabbro', because the term

'ferrogabbro' could then be used, free of any confusion, to specifically describe rocks that bear clinopyroxene as the primary mafic mineral.

2.2 Exterior contacts and surrounding rock types

The Barth Island Ring Complex was emplaced into a number of rock types (fig. 2-4). The exterior contacts are generally well exposed, but it is difficult to determine the nature of these contacts because the margins of the ring complex are deformed. Descriptions of the exterior contacts and the outlying rocks follow. The descriptions begin at the eastern edge of the ring complex north of Nain Bay and move counterclockwise.

2.2.1 The eastern-northeastern margin

On the mainland north of Barth Island (B to B'; C to C'), the eastern contact is well exposed. However, the contact between what should be considered the Barth Island Ring Complex and outlying rocks is difficult to define. It is easy to appreciate how Mulhern (1974) and de Waard (1976) came to consider the boundary to be a gradational change between cogenetic rock types. From B to B', monzonite at the eastern edge of the ferrogabbroid unit contains numerous anorthosite xenoliths, two of which are large enough to be shown on the 1:20 000 map (fig. 2-1). East of this location, the monzonite contains moderately abundant deep blue and black xenocrysts of plagioclase, and is in

sharp contact with a coarse leuconoritic rock: the outer leuconorite of the Barth Island Ring Complex. The monzonite appears to crosscut the general trend of the foliation in the latter rock at a low angle. However, this interpretation is suspect, because what appears to be the same unit of outer leuconorite clearly intrudes ferrogabbroid of the Barth Island Ring Complex, described below at F. The interpretation is further discussed following the description of C to C' (below).

The outer leuconorite becomes interspersed to the east with melanocratic layers of gabbronorite. Each leuconorite layer to the east is progressively coarser and more pyroxene-free, until the melanocratic rock layers are interspersed with layers of recrystallized anorthosite, which becomes the dominant rock type. The plagioclase crystals in the anorthosite are strongly aligned, and the structure of some plagioclase megacrysts (10 - 20 cm long) is preserved, despite the predominantly recrystallized texture. Pyroxene in the anorthosite (and to a lesser extent, the leuconorite) appears to be oikocrystic, and forms elongate, podlike structures that define, in conjuction with plagioclase, the broadly N-S foliation. These 'oikocrysts' can be up to 40 or 50 cm long.

Three samples (LBE 35 - 37) were collected along B to B', one of each rock type. Sample LBE 35 is the outer leuconorite, sample LBE 37 is an example of the melanocratic, gabbronoritic layers found within the outer leuconorite, and sample LBE 36 is the anorthosite. Of note in samples LBE 35 and 37 are the coarse anhedral pyroxenes and oxides (plate 2-1). This texture is typical of coarse-grained plagioclase-pyroxene rocks found throughout the Barth Island Ring Complex.

Also of particular interest is the plagioclase grain size apparent in a thin section of sample LBE 36 (plate 2-2). Although megacrystic grains were observed in this rock in the field, the grain size in thin section is on the scale of a few mm. The anorthosite is recrystallized, but the shapes of some original coarse igneous grains are preserved in outcrop. A strong alignment in plagioclase, evident in both thin section and outcrop, must have formed when the anorthosite recrystallized.

From C, along C to C', plagioclase and pyroxene in homogeneous outer ferrogabbroid become progressively more strongly foliated. Petrographic analysis of LBE 14, a sample of this ferrogabbroid, has shown it to be medium to coarse-grained clinopyroxene ferronorite, with orthopyroxene occurring as single grains and grain aggregates, which have coarse exsolution of augite. Small amounts of solitary clinopyroxene grains and subophitic-textured (poikilitic) orthopyroxene also occur. Single plagioclase grains in this sample commonly contain many grains of apatite.

To the east, progressively coarser layers of outer leuconorite, generally less than 1 m thick and strongly foliated parallel to layer contacts, become the dominant rock type. Layer contacts between the outer leuconorite and the clinopyroxene ferronorite are sharp; no crosscutting relationships were observed. A sample of this rock (LBE 13) is very coarse-grained (pyroxene and plagioclase > 1 cm long). Orthopyroxene (inverted pigeonite) is the dominant mafic mineral, with lesser amounts of what may be augite. Most pyroxenes in this rock contain coarse and complex exsolution textures. The orthopyroxene appears to be Fe-rich, as shown by its 2° blue-violet interference colours

(plate 2-3). The outer leuconorite here is generally rusty-weathering, a feature which is caused by heterogeneous, but generally high, proportions of coarse interstitial magnetite.

Toward C', prominent layering becomes developed between the outer leuconorite and melanocratic gabbronorite. The nature and origin of the layering, and the transition into anorthosite, are discussed below. The characteristics of the layering are the same as described above along B to B', with anorthosite becoming the dominant rock type to the east.

The orientations of structures in the rocks and contacts of the area of B to B' and C to C' are vertical, or steeply dipping toward the west. Contacts between the various layers are sharp and parallel, and it is difficult to tell whether these layers are the result of intrusion of one body into the other, or are the products of differentiation. However, the grain size of the leuconoritic and melanocratic layers is larger than that of the anorthosite, and igneous features, such as subophitic-textured pyroxene and coarse pyroxene exsolution textures, are well-preserved. Because these rocks are not recrystallized, the recrystallization of the anorthosite must have taken place before the leuconoritic and melanocratic layers were in place. The transition into anorthosite described from C to C' is similar, and is interpreted in the same way: the leuconorite was emplaced as sheets into the anorthosite.

The xenoliths of anorthosite found within the monzonite strongly suggest that the monzonite and contemporaneous outer ferrogabbroid (sections 2.4, 2.4.1, and 2.6) postdate the anorthosite. However, it is unclear whether the monzonite and outer

ferrogabbroid antedate or postdate the outer leuconorite and melanocratic gabbronorite. Relationships around point F, described below, clearly require a leuconoritic rock of similar composition and texture to that described from B-B' and C-C' to have intruded the outer ferrogabbroid of the Barth Island Ring Complex. A conclusion regarding the relative intrusive timing of the outer leuconorite unit with respect to the monzonite and outer ferrogabbroid is given below.

Along transect D-D', monzonite which displays a weak foliation defined by feldspars, is in contact with a body of leuconorite (-gabbro?), which becomes coarser to the northwest. Mafic minerals in this latter rock type are weakly aligned parallel to the contact, as is the foliation in the monzonite. Toward D', the mafic index of the rock increases; there are a few xenoliths of anorthosite. This body (at D') is in contact with undeformed, coarse grained leuconorite to anorthosite, which has an oikocrystic pyroxene texture similar to the outer leuconorite and anorthosite described from localities B' and C'. It is unclear from the contact relationships which is the older body. However, the xenoliths of anorthosite noted above are most likely derived from the oikocrystic-textured anorthosite, suggesting the outer leuconorite is the younger body.

Farther west, at E, undeformed leuconorite (-gabbro?), the field appearance of which is similar to that found at locations farther east (D-D') and slightly farther west (sample LBE 6, along G-G'; see below), is well exposed.

From F to F' (and west to the finger of ferrogabbroid found at I), no contacts between ferrogabbroid at the edge of the ring complex and outlying anorthosite are

exposed. This seriate-textured anorthosite (hereafter referred to as the 'northern anorthosite') is massive and grades to leuconorite in some areas; orthopyroxene is coarse and interstitial. Dark, square plagioclase crystals up to 15 cm across are abundant. North of F, a thin, elongate, dyke of foliated monzonite, which contains both small, fine-grained inclusions of ferrogabbroid, and small areas of mingled ferrogabbroid and monzonite, is well exposed. This body intrudes the northern anorthosite and pinches out along strike to the east. Unconsolidated material hides the body to the west.

Toward the point F', a substantial body of deformed, fine-grained ferrogabbroid is in sharp contact with the surrounding northern anorthosite. This was mapped as a xenolith of ferrogabbroid during the 2001 field season, but further mapping by Myers (pers. comm., 2002) suggests that it is actually a dyke. If this dyke is related to outer ferrogabbroid of the Barth Island Ring Complex, the northern anorthosite must be older than outer ferrogabbroid of the Barth Island Ring Complex.

Mapping in the area around the point F during the 2001 season revealed that the outer ferrogabbroid here is layered and has a distinct layer-parallel foliation defined by mafic minerals, trending ca. 050, whereas the outer leuconorite along strike (along G-G') is unlayered, like that at point E. Petrographic analysis of one sample of the outer leuconorite (sample LBE 6) has shown mineral assemblage and texture similar to the leuconoritic rock described near B (LBE 13). Thin-section petrography of samples collected in the area of F (sample suite BS 10, and the samples LBE 2 - 4), has shown that the very coarse plagioclase-rich character and textures of LBE 6, are not replicated in any

of the rocks in question. These samples generally contain subophitic-textured Bushveld-type (Nesse, 1991, p. 205) orthopyroxene, which is lacking in the outer leuconorite.

Mapping by Myers (pers. comm., 2002) has revealed that the outer leuconorite and outer ferrogabbroid are interfingered. It appears that the outer leuconorite intruded the outer ferrogabbroid, because the strike of the layers and the foliation indicate that the outer ferrogabbroid is truncated by the outer leuconorite.

To the north along G to G', rafts of oikocrystic anorthosite are found within the outer leuconorite. The exposure of the contact zone is poor, and it is difficult to map out the ultimate contact between these two rocks. The oikocrystic anorthosite is virtually identical to the oikocrystic anorthosite found in the description of D to D', and differs only in being whiter.

The relationship between outer leuconorite and the outlying oikocrystic anorthosite, described along B to B', C to C', D to D', and along G to G', consistently yields the same relative timing. In each case, the outer leuconorite appears to intrude the oikocrystic anorthosite. This fact, and the petrographic similarity between the leuconoritic rocks described along B to B', C to C', and G to G', along with the similarities in field appearance with these rocks and leuconorite described at point E and from D to D', indicate that these rocks should be considered one unit. In addition, field relationships at and around point F indicate that this leuconorite clearly postdates outer ferrogabbroid and monzonite of the Barth Island Ring Complex. This interpretation is represented on the map (fig. 2-4). However, this interpretation calls into question a field observation noted in

the description of rocks at B (see above), in which it was stated that monzonite of the Barth Island Ring Complex was observed to crosscut the apparent trend of the leuconorite. It is possible that two separate leuconorite intrusions are present; however, the similar appearance, structure, and petrography suggest that they are the same. Therefore, on the weight of the evidence presented above, the original interpretation of this observation is discarded. The leuconorite is presumed to be one unit, and is interpreted to be younger than adjacent rocks of the Barth Island Ring Complex.

At point H, a contact between the northern anorthosite and the oikocrystic anorthosite is exposed. The best defined parts of the contact are interlobate; the northern anorthosite has a slightly higher abundance of pyroxene along the contact. The curved nature of the contact is suggestive of a magma-mingling relationship, but a concrete conclusion cannot be made on the sole basis of this observation.

2.2.2 The northwestern and western margins

As mentioned above, the E-W trending contact between the Barth Island Ring Complex and the northern anorthosite is not exposed. The anorthosite grades to the west into a leuconorite of similar texture, which is intruded at I by ferrogabbroid similar in field appearance to the ferrogabbroid of the Barth Island Ring Complex. This ferrogabbroid contains numerous inclusions of gneiss. One sample (LBE 7) of the ferrogabbroid was examined in thin section; the rock contains plagioclase, orthopyroxene,

abundant apatite as inclusions in plagioclase, and ca. 10% opaque minerals. A few plagioclase grains are antiperthitic.

No contacts or continuity between this ferrogabbroid and the rocks of the Barth Island Ring Complex are exposed; the relationship of the unit to rocks of the ring complex is unclear. This ferrogabbroid has nevertheless been included as a part of the Barth Island Ring Complex, based on the both textural and mineralogical similarities to the outer ferrogabbroid of the Barth Island Ring Complex, and the continuity of the positive magnetic anomaly observed on the aeromagnetics map (fig. 2-2).

South of this area (west of J), no contact between the Barth Island rocks and outlying gneiss is exposed. The fine-grained, equigranular polygonal-textured troctolite at J is in contact with a layer (several m thick) of gabbroic rock. In the latter rock, thin section examination has shown that relict pyroxene is preserved within large, poikilitic hornblende crystals, whereas plagioclase is fine-grained and granular. This rock becomes more strongly foliated toward a contact with a thin layer (a few m wide) of deformed monzonite of the Barth Island Ring Complex to the west. The monzonite layer has a strong foliation parallel to the layer contacts. This layer disappears under unconsolidated material to the west.

Farther to the west, only scattered outcrop is present along J-J' until the first outcrops of the well-exposed anorthosite of the Mount Lister Intrusion at J'. The intervening rock is composed of a poorly exposed, highly deformed biotite-bearing pyroxene-plagioclase rock, followed by an orthopyroxene leucogabbro. Thin section

analyses of a sample of each of these rocks (BE 4 and 3, respectively; see fig. 2-1 for locations) have shown that the rocks are mineralogically similar and may be the same rock type, but have undergone different degrees of deformation. BE 3, obtained near the margin of the Mt. Lister anorthosite, is partly recrystallized, but retains much of its igneous texture. BE 4, obtained farther east than BE 3, is more strongly recrystallized; the mafic minerals are concentrated in bands, and pyroxene is rimmed by hornblende. No contacts among these strongly foliated rocks, or between these rocks and the Mt. Lister Intrusion, are exposed.

The Mt. Lister Intrusion is constrained to be older than ca. 1332 Ma, by a U-Pb zircon age obtained from the Apkaume diorite (Hamilton, 1997), which crosscuts the Mt. Lister anorthosite to the west of Barth Island (Voordouw, pers. comm., 2003). It is likely that anorthosite of the Mt. Lister Intrusion is older than the rocks of the Barth Island Ring Complex, from U-Pb zircon ages obtained for troctolite and ferrogabbroid of the ring complex (chapter 4).

A small island at the west end of Barth Island is accessible by foot from Barth Island, during low tide. At the east end of this island (point K, fig. 2-4), a sharp contact between foliated, fine-grained ferronorite of the Barth Island Ring Complex and the gneissic rocks which compose the rest of the island is exposed. The contact is concordant with the attitudes of both the foliation of the gneiss, and the foliation in the ferronorite. During the 2001 field season, two broad categories of gneiss were established on the

island: one of quartzofeldspathic-mafic/ultramafic gneiss, and a separate sequence of mafic rocks.

The gneiss in contact with ferronorite of the Barth Island Ring Complex appears to be primarily quartzofeldspathic, with many fragments of isoclinally folded ultramafic layers of various sizes. These latter fragments are elongate parallel to the contacts, and include both pyroxenite and pyroxene-bearing hornblendite; substantial amounts of olivine (ca. 50% in thin section) are present in one sample.

The quartzofeldspathic parts of this gneiss do not appear, in thin section, to have a texture indicative of complete recrystallization. The edges of feldspar grains are partially recrystallized, as demonstrated by grain bulging and grain boundary migration (plate 2-4); undulatory extinction was noted in quartz. Partial sericite and sausserite alteration of feldspars, and secondary carbonate, is commonly seen. All samples of quartzofeldspathic material show similar features. Although commonly intercalated and seemingly deformed with the ultramafic gneiss, the quartzofeldspathic units are interconnected by a series of veins and dykelets, which surround angular blocks of ultramafic gneiss. The ultramafic parts of the gneiss show evidence of more pervasive recrystallization. For example, BIV 4 (plate 2-5), is composed primarily of hornblende and pyroxene, has a moderate foliation, and an equigranular fabric. Sample BIV 6 represents a body that appears to be a dyke which crosscuts the other units, but is also highly deformed.

The evidence presented above suggests the ultramafic gneiss was deformed and recrystallized before intrusion of the quartzofeldspathic rock; the two rock types must then have been deformed together.

The second category of gneiss identified in the field was a sequence of mafic rock, with small amounts of ultramafic rock. These rocks are mainly two-pyroxene, plagioclase rocks with a significant proportion of opaque minerals; one sample contains substantial accessory apatite (BIV 8, plate 2-6). These rocks appear to be mineralogically similar to fine-grained outer ferrogabbroid of the Barth Island Ring Complex (section 2.4). One felsic sample, presumed in the field to be anorthositic, contains igneous-textured plagioclase with exsolved potassium feldspar similar to that found in the monzonite of the Barth Island Ring Complex (section 2.6). Relict megacrysts of dark blue plagioclase, surrounded by rotational shear structures, are present in a few layers. Some layers appear to be undeformed; for instance, a partially serpentinized dunite sample (BIV 2) has cores of fresh olivine, although these olivine could be the products of prolonged metamorphic growth.

Field observations of the mafic sequence at one locality (near sample BIV 7) seems to imply these rocks intruded into the quartzofeldspathic gneissose rocks. It may be that magmas associated with the Barth Island Ring Complex intruded in sheets concordant with the planes of foliation of the deformed rocks; however, even the most olivine-rich layers in the troctolite of the Barth Island Ring Complex are not dunitic.

Observations by Myers (pers. comm., 2004) suggest that the sequence of rocks described above is older than the quartzofeldspathic unit.

2.2.3 The southern and eastern margins

One large composite anorthosite pluton, the Hosenbein Composite Pluton, mapped by Voordouw (2000 - 2002 field seasons), is present along the southern margin of the Barth Island Ring Complex. A complete geological map and description of this composite pluton is found in Voordouw (2004). It is likely that emplacement of this anorthosite spanned at least several m.y. My work will briefly cover the nature of the few exposed contacts.

To the north of L (fig. 2-4), there is limited exposure of a medium to coarse-grained, moderately foliated ferrogabbroic rock, containing multiple, apparently deformed, m-scale xenoliths of anorthosite. The xenoliths become more abundant toward the contact with the Hosenbein Composite Pluton (at L), which is intruded by dykes of ferrogabbroid. Thin, localized layers of oxide in the ferrogabbroic rock are spatially associated with the xenoliths, and with leucocratic patches of plagioclase-rich ferrogabbro dm to a few m along strike from the xenoliths. The oxide layers are concentrated at the edges of the leucocratic patches. These patches appear to have a gradational relationship with the ferrogabbroic rock, and range from coarse to very coarse-grained (grains up to a

few cm). It is possible that the xenoliths and leucocratic patches are derived from or are the result of interaction with the Hosenbein Composite Pluton.

The Hosenbein Composite Pluton is crosscut, near location L, by ferrogabbroic dykes which appear to emanate from the Barth Island Ring Complex (Voordouw, pers. comm., 2003); however, the Nain Hill intrusion, a large system of oxide and sulphide-rich ferrogabbroic dykes which crosscut the Hosenbein Composite Pluton, is also present in the area (Hinchey *et al.*, 1999). It may be that the dykes are related to the Nain Hill dykes rather than the Barth Island Ring Complex; it is also possible that there is a genetic relationship between the Nain Hill dykes and outer ferrogabbroid of the Barth Island Ring Complex. Much of the Hosenbein Composite Pluton was probably emplaced ca. 1317 Ma (Voordouw, pers. comm., 2004). However, see below for an important exception to this age.

To the east of point L, outer ferrogabbroid of the Barth Island Ring Complex is in sharp contact with the northern margin of the Hosenbein Composite Pluton. The foliation of the outer ferrogabbroid, and the foliation of the Hosenbein Composite Pluton, are parallel to the contact.

From N to N', foliation in the outer ferrogabbroid of the Barth Island Ring Complex becomes progressively more pronounced, toward the contact with leuconorite of the anorthositic Hosenbein Composite Pluton. The outer ferrogabbroid here is intercalated with the leuconoritic margin of the Hosenbein Composite Pluton, which becomes the

dominant rock type. It appears that the outer ferrogabbroid was intruded as concordant sheets into the foliated margin of the composite pluton.

This area of the Hosenbein Composite Pluton is more deformed than much of the other parts of this composite pluton. It is structurally similar to, and is thought to be the same age as, another part of the composite pluton farther south (beyond fig. 2-1 map area), which has an age of ca. 1328 Ma (Voordouw, pers. comm., 2004). Geochronological work in the present study, described in chapter 4, requires the outer ferrogabbroid of the Barth Island Ring Complex to be younger than this part of the Hosenbein Composite Pluton, in accord with the field relationships described above.

On Barth Island, the eastern contact of the ring complex (point P on fig. 2-4) is exposed. A heterogeneously-textured, fine to medium grained, weakly foliated ferrogabbroid contains small, podlike patches of monzonite which are elongate parallel to the contact. Small patches of pegmatitic gabbro or norite of uncertain origin are also present. This outer ferrogabbroid has a sharp contact with weakly foliated, massive anorthosite. This contact is presumed to be intrusive, because of the distinct difference in grain size and composition between the ferrogabbroid and anorthosite. The anorthosite is generally grey and white, and contains megacrystic (crystals up to 25 cm long) black plagioclase in a coarse-grained, recrystallized matrix. Near the contact with the outer ferrogabbroid, this anorthosite has interstitial, anhedral pyroxene grains of similar scale to the megacrystic plagioclase. The anorthosite is presumed to be older than rocks of the Barth Island Ring Complex, because the emplacement of such a massive body of

anorthosite would most likely cause significant contact metamorphism in the surrounding rocks, which was not observed.

2.2.4 Satorsoakulluk Dyke

The Satorsoakulluk Dyke was included on an early geological map of the area constructed by Wheeler (1942), was the focus of a study by de Waard and Hancock (1974), and has been mapped in its entirety by Ryan (2001). A comprehensive study of the Satorsoakulluk Dyke was carried out by Furlong (2004) and Goddard (2004). The part of this dyke exposed on Barth Island was mapped and sampled during the 2001 field season, as a part of the present study.

The Satorsoakulluk Dyke has morphology similar to the central ferrogabbroid (2.5). It weathers red-beige in colour and is massive. In some locations, a weak alignment of feldspar grains, parallel to the dyke's long axis, is evident. Plagioclase and pyroxene are the major mineral constituents. Like the ferrogabbroids described in sections 2.4 and 2.5, in a few localities the Satorsoakulluk Dyke contains ovoid mesoperthite crystals like those described in the monzonite (section 2.6). The Satorsoakulluk Dyke locally contains buff-coloured, subangular inclusions like those described from the monzonite and central ferrogabbroid. The contact with the surrounding anorthosite is sharp, and the dyke does not show a decrease in grain size near the contact. In one seaside outcrop, on the southern end of Barth Island, the dyke contains a large number of angular xenoliths. A few of the

xenoliths are foliated anorthosite, but most are layered ferrogabbro (Myers, pers. comm., 2004). One sample of the Satorsoakulluk Dyke was analyzed for major and trace elements; the results are reported in chapter 3.

2.2.5 Summary of the relative ages of surrounding rock types

The outer ferrogabbroid, monzonite, and outer leuconorite of the Barth Island Ring Complex are younger than most of the surrounding anorthosite intrusions. The exception is the Hosenbein Composite Pluton to the south, which is composed of anorthosite of various ages (Voordouw, pers. comm., 2004). However, field relationships indicate the outer ferrogabbroid of the Barth Island Ring Complex is younger than at least some of this composite anorthosite pluton, and this is confirmed by a radiometric age (Voordouw, pers. comm., 2004).

The septum of gneissose rocks at the Barth Island Ring Complex's western margin must antedate the rocks of the ring complex, because there appear to have been multiple episodes of intense deformation, which created isoclinal folding in some of the gneissose rocks. Such intense deformation is unlikely to have left the rocks of the ring complex unaffected.

2.3 Leucotroctolite and leuconorite

2.3.1 Leucotroctolite

In outcrop, the leucotroctolite (hereafter referred to as troctolite) (plate 2-7) is massive and leucocratic, buff to brown weathering, with reddish stains where olivine is abundant. Plagioclase has greater modal abundance than olivine (generally ca. 70-30 to 75-25 proportions). Modal layering is defined by various proportions of olivine. Olivine-rich layers are marked by an increase in the proportion of deep red lichen on the rock surface (plate 2-8). These layers are discontinuous, and are one cm to dm (rarely up to 1 m) thick. The olivine-rich layers display various amounts of ductile deformation, marked by z- and s-shaped structures and folds (plates 2-9 and 2-10), whereas shear deformation in plagioclase-rich layers is marked by layer displacement. Because of the general lack in the troctolite of dynamic recrystallization or other deformation textures, these features are interpreted to be late stage, pre-solidification structures.

The troctolite commonly displays a weak magmatic foliation parallel to layer contacts, defined by alignment of the long axes of plagioclase crystals. The foliation and layering parallel the outer contact of the troctolite, such that these features define a circular pattern (fig. 2-1). The dip angle of layering becomes less steep toward the centre of the troctolite body. The steepest average dip angles occur at the southern margin of the troctolite.

Plagioclase, olivine, and (where present) biotite and magnetite, are identifiable in hand specimen. Olivine is commonly found as pristine single grains or small (less than 5 mm) aggregates. Some outcrops show preferential weathering of this mineral, a process which has left behind a brown gravel comprising stained plagioclase. Typical troctolite is coarse: average plagioclase crystals range from a few to several mm long, and olivine grains range up to 5 mm in diameter. A decrease in grain size is evident in some areas, particularly near the northwestern margin. This is discussed below in section 2.3.3.

A number of samples of troctolite were measured to determine their densities. The method and results are reported in full in appendix 4. The average density of the measured samples is 2.94 g/cm^3.

In thin section, typical troctolite (plate 2-11) shows somewhat aligned, coarse sub- to euhedral cumulus plagioclase, which generally comprises ca. 70-75% of the section. In some cases, particularly in samples taken near the northwestern contact (for example BS 5d, plate 2-12), the plagioclase lamination is highly developed. Deformation twins and kinked grains are a common feature; plagioclase crystals in many thin sections have granulated margins and subgrain development, suggesting incipient recrystallization (for example plate 2-12). Plagioclase crystals are generally unzoned; however, in most thin sections a few to many average- to large-sized, multiply- or patchily-zoned grains are present (plate 2-13). The zoning is generally normal or oscillatory. According to de Waard (1976), plagioclase in samples taken near the troctolite's exterior contact has

composition ca. An_{62}, and plagioclase farther toward the interior of the ring complex has composition ca. An_{58}.

Olivine is anhedral to subhedral, and occurs as both small and large isolated grains, and as coarse aggregates. Olivine has an average composition of about Fo_{65}, but ranges as low as Fo_{50} (de Waard, 1976). This change is not systematic toward the inner part of the ring complex. In some samples, olivine is mantled by orthopyroxene. Clinopyroxene occurs as small to moderate-size interstitial, anhedral grains.

Both clinopyroxene and orthopyroxene grains in the troctolite almost invariably have exsolution of opaque minerals that may be ilmenite or an opaque form of rutile. Some troctolitic pyroxene are almost completely black because of the high abundance of these minerals. A similar occurrence of exsolution in orthopyroxene is described below in the description of the leuconorite. The inclusions in troctolitic pyroxenes are dominantly opaque, whereas those found in orthopyroxene of the leuconorite are more commonly a mix of rutile and opaque minerals. Exsolution in troctolitic orthopyroxene is confined to lamellae parallel to the (001) direction, indicating that the orthopyroxene is probably not inverted pigeonite.

Biotite and amphibole (probably hornblende) grains occur on a scale of < 1 mm to several mm, and are generally associated with magnetite. Both the biotite and amphibole have strong, reddish-brown pleochroism, indicating high Ti contents. Amphibole was observed mantling pristine cumulus olivine in one thin section (plate 2-14). At the contact between these two minerals, the olivine is completely unaltered, and is subhedral.

The occurrence of biotite and amphibole is also associated with accessory epidote-group minerals. Magnetite (?) may occur as anhedral grains, or as wormlike intergrowths in pyroxene (plate 2-15). Small amounts of pyrite and chalcopyrite are associated with a few magnetite grains. A few elongate, euhedral apatite grains are located in the interstices or as inclusions at the edge of plagioclase crystals. Zircon and baddeleyite are also present, but were not observed in thin section. Grains of these minerals were found in two samples that were crushed for geochronology.

Needles of an unidentified opaque mineral and a more abundant deep red mineral (rutile?) are present as exsolution lamellae in some plagioclase grains. The abundance and size of these needles is different from grain to grain. Furthermore, in a given thin section, the needle-bearing grains may be absent, highly abundant, or of some moderate level of abundance. In some grains, the needles were observed to be associated with chemical variations in the plagioclase crystal (plate 2-16). In the large, compositionally zoned crystal displayed in plate 2-13, the needles appear to be associated with a particular composition. Biotite-magnetite associations are present as inclusions in some of the needle-bearing grains. In one particular grain, these latter minerals were found only in sections which do not have needles. This suggests that the inner parts of the crystals had more Ti or Fe than did the outer parts.

In the northeastern corner of the ring complex, there is a sheet-like body of troctolite which is isolated from the main part of troctolite by ferrogabbroid. This troctolite is morphologically and mineralogically identical to the troctolite described

above. Aeromagnetic data suggest that the body is not contiguous with the main body of troctolite at the present level of exposure. Two isolated lenses of troctolite crop out along strike west from the large body described above. The petrographic appearance of these isolated troctolite lenses, represented by samples BII 65 and 66, is like the appearance of troctolite found at the northwest margin of the ring complex; both this margin and the isolated lenses are described below in section 2.3.3. The aeromagnetic data suggest that the isolated bodies of troctolite described above are actually a single body connected in the third dimension (fig. 2-2), because a magnetic low correlatable with both bodies can be traced along strike.

2.3.2 Leuconorite

In the northwestern part of the troctolite, the troctolite passes upward into medium- to coarse-grained leuconorite (fig. 2-1). The phase change, from olivine to orthopyroxene, is abrupt and marked by a faint red stain on the rock's surface. The leuconorite (hereafter referred to as norite) and troctolite have virtually identical grain size and appearance in outcrop; the distinct difference between these rocks is the lack, in the norite, of olivine and presence of coarse, sub- to euhedral orthopyroxene (plates 2-17a, 2-17b). Anhedral to subhedral clinopyroxene is less abundant, but the rock's composition does range to gabbronorite. Orthopyroxene-rich layers may be composed of up to 70% of that mineral. Monomineralic plagioclase layers are not present. Layers may

be curved into z- and s-shaped structures, like those described above in the troctolite. The rock becomes medium-grained toward the centre of the ring complex.

Petrographic examination of coarse norite samples taken near its contact with troctolite (typical sample shown in plate 2-18) reveals other features similar to features in the troctolite. Plagioclase is large, subhedral to euhedral, and is of composition An_{55} (de Waard, 1976). A weak alignment of plagioclase crystals was noted in one thin section. Needles of an unidentified mineral, as described above in the troctolite (see plate 2-16), are present in some plagioclase, though needle-bearing grains are not as common, nor are needles as abundant in such grains. Plagioclase may also have inclusions of a platy, wine red mineral (rutile?) which may be the same as the needle-like mineral. In samples taken of the medium-grained norite toward the centre of the ring complex, plagioclase is generally subhedral (plate 2-19). Many plagioclase grains are slightly antiperthitic.

Orthopyroxene grains range in size from small to large (1 - 8 mm), and show 1° gray to 2° blue interference colours. Lamellar exsolution of clinopyroxene(?) parallel to the (100) plane is ubiquitous, as are tiny, triangular deep red to brown crystals found along planes of exsolution (see plate 2-17b). These crystals are probably rutile or ilmenite; this interpretation is supported by trace element geochemistry described in chapter 3. Because exsolution, where present, appears to be confined to planes parallel to the (100) direction, the pyroxene is not inverted pigeonite (Nesse, 1991, p. 205). This conclusion was also noted for orthopyroxene found in the troctolite. Clinopyroxene (1 - 2

mm) is generally interstitial and anhedral, or may occur as overgrowths on orthopyroxene.

Biotite appears as described in the troctolite, generally associated with magnetite. Myrmekitic textures at the edges of plagioclase grains were observed in several thin sections (plate 2-20). Apatite was found as elongate euhedral grains in the interstices. Also, a few grains of interstitial quartz were observed in one thin section, associated with an epidote-group mineral. Both baddeleyite and zircon were found in mineral separates from one norite sample. Zircon was observed in thin section as anhedral grains in the interstices, associated with magnetite (see chapter four). Baddeleyite was not observed in thin section.

2.3.3 Marginal features and contact relationships

In some locations along its northern contact, the troctolite grades out into more fine-grained rock composed of plagioclase, olivine, and coarse-grained biotite. Samples of troctolite taken within ca. 100 m of the troctolite's exterior contact share a particular textural feature: coarse euhedral plagioclase and coarse olivine are accompanied, in thin section, by domains several mm wide of polygonal, equigranular plagioclase and medium and fine-grained olivine (plate 2-21). The isolated body of troctolite in the northeastern section of the suite is typified by this kind of texture.

The troctolite becomes most fine-grained at the northwestern corner of the intrusion. The contact between outlying ferrogabbroid and the troctolite is difficult to place in this location (B on fig. 2-1), because the field appearance of the granular, fine-grained troctolite precisely resembles that of the granular, fine-grained ferrogabbroid. Petrographic analysis of samples from location B (fig. 2-1) shows that this troctolite is equigranular and fine-grained, and the plagioclase has a polygonal texture (plate 2-22). Grain boundaries in samples from this location are triple junctions with 120° boundaries (plate 2-23). Samples BII 65 and 66, which were sampled from small, isolated bodies of troctolite within the ferrogabbroid, (fig. 2-1) have a similar petrographic appearance to sample BII 81. These bodies are located along strike from the isolated sheet-like body of troctolite found in the northeastern section of the ring complex.

Plates 2-24a and 2-24b are photomicrographs of sample BII 82, a troctolite located slightly farther from the northern contact than BII 81. It is mineralogically identical and texturally similar to BII 81, but contains more subhedral plagioclase crystals. The remnant igneous lamination is marked by the alignment of feldspar crystals, parallel to layer contacts. Furthermore, under plane polarized light (plate 2-24a), the original plagioclase grain size and shape is delineated by olivine grains. Under crossed polars (plate 2-24b), the outlined plagioclase 'grain' comprises multiple, polygonal grains. Sample BS 2a, which is farther from the northern contact than BII 82, has a higher proportion of subhedral plagioclase and is slightly more coarse-grained (plate 2-25).

Sample BS 2d is still farther from the contact, is quite coarse-grained, and contains subhedral to euhedral plagioclase which display an igneous lamination (plate 2-26).

The boundaries exhibited by plagioclase in samples BII 81 and 82 are a feature typical of the end result of the annealing process (see for example Shelley, 1993, pp. 266-272; Passchier and Trouw, 1996, pp. 45-47), in which built-up strain energies are reduced by grain boundary migration, creating smaller, strain-free grains. Evidence of strain imposed on crystals is eradicated through grain boundary migration. The resultant grain junctions are typically the intersection of three grains (a triple point), and the dihedral angle tends to be 120°. Plate 2-23 illustrates a typical triple point in sample BII 42a.

The texture and fine grain size of the troctolite at the northwest corner of the intrusion are clearly the result of annealing, not the result of a chill against the outlying ferrogabbroid.

It is not clear what process caused these textures. The addition of energy to a crystalline system is the impetus for annealing. The energy can be provided in the form of heat, or in the form of stress. However, it is implausible that the stressor event which caused dynamic deformation of the rocks adjacent to the annealed troctolite (see description J to J' in section 2.2.3), was also responsible for the annealing of the troctolite. There is no evidence of subsolidus dynamic deformation in the troctolite, and though the most deformed of the belt of deformed rocks show evidence of shearing and subsolidus deformation, they are not significantly annealed.

In the case of heat-related annealing, there are two possible sources for the energy input. First, the energy might have been provided by the pluton itself. That is, the exterior of the troctolite pluton would have crystallized more rapidly than the interior. The interior of the pluton cooled slowly, subjecting the crystalline margin to prolonged high temperatures, which may have been coupled with compaction stresses. Second, the addition of a heat source at the margin of the already crystalline troctolite: the intrusion of the ferrogabbroid and monzonite along the troctolite's margin might have provided sufficient energy to anneal the troctolite at the margin.

Unfortunately, it is not clear what kind of test would be able to distinguish between these two possibilities, and the origin of these textures is left unknown.

The appearance of other parts of the troctolite's northern contact with ferrogabbroid is diverse. In many locations, typical marginal ferrogabbroid is easily distinguished from typical troctolite by obvious differences in texture or colour. Small, thin bodies of monzonite or monzonite-ferrogabbroid hybrids may lie in between the troctolite and ferrogabbroid. In the well-exposed contact zone between samples BII 78 and 79 (between A and B on fig. 2-1), at the northwestern exterior margin of the troctolite, small amounts of fine-grained, yellow-white to white rock (morphologically similar to the net-textured dykes, discussed in section 2.8) are present and can be traced from the contact into the troctolite. These dykes were not observed in the ferrogabbroid.

The troctolite, at its southern contact on the south side of Nain Bay and at its eastern contact on Barth Island, does not show the features recognized at the northwestern

part of the contact. Toward these contacts, the troctolite becomes slightly more fine-grained, and may have a slightly higher abundance of biotite. Near the troctolite's southern contact with monzonite, the occurrence of olivine-rich layers decreases and the layers appear to be absent within <100 m of the contact, which is sharp and well exposed. The contact area was not systematically sampled, so it is unclear whether the troctolite at this contact shows the pervasive textural changes that occur at the northernwestern contact.

The western contact on Barth Island is substantially different from any of the above contacts. The troctolite there possesses no layering or foliation, and weathers a grey colour. The contact with monzonite is undulose, and does not parallel the oval shape of the intrusion, as it does elsewhere. A small part of troctolite is completely surrounded by monzonite (fig. 2-1). The nature of this contact is discussed below in section 2.6.1, after the monzonite has been sufficiently described.

2.4 Outer ferrogabbroid

The occurrence of outer ferrogabbroid is shown in fig. 2-1. In outcrop, the rock weathers beige to red-beige in colour. The grain size and texture of ferrogabbroid are diverse (plate 2-27). Grain size ranges from 0.1 mm to 5 mm. Layers are cm to tens of m thick, and are generally defined by changes in grain size, which may be accompanied by textural changes noticeable in thin section. Contacts between layers may be sharp or

gradational. Both straight and lobate contacts between laterally discontinuous layers, defined by grain size, were observed near sample location LBE 15 (see fig. 2-1). Layers may pinch out laterally over meters or tens of meters, or be truncated by other ferrogabbroid layers. Way-up structures are absent, although layer boundaries may be marked or defined by the presence of high concentrations of magnetite. Ferrogabbroid subunits ('coarse ferrogabbroid' and 'xenocrystic ferrogabbroid' layers) in fig. 2-1 are thick enough to form mappable units at 1:20 000 scale.

Ferrogabbroid may have a foliation, which ranges in strength from mild to moderate (plate 2-28). At the scale of an outcrop, the foliation is defined by aligned, elongate pyroxene grains. The orientation of the foliation and strike of layers at any particular location in the outer ferrogabbroid parallels both its interior and exterior contacts. The dip angles of layer contacts are heterogeneous, but are on average steeper at the southern margin of the ring complex. The exterior contacts of the outer ferrogabbroid parallel the structures in the adjoining rock types in all cases.

Ferrogabbroid mainly consists of plagioclase, pyroxene, and magnetite. There may also be large white oblong crystals of either mesoperthite or plagioclase rimmed by potassium feldspar, which are particularly abundant near contacts with monzonite (plate 2-29, 2-30).

Density measurements were performed on a number of marginal ferrogabbroid samples; the method and results are reported in appendix 4. The average density of the measured samples is 3.01 g/cm^3.

The ferrogabbroid samples that were examined in thin section are not consistently defined by a precise texture. The rock ranges from orthopyroxene ferrogabbro to ferronorite, and may be either melanocratic or leucocratic. Plagioclase and pyroxenes generally constitute the bulk of the thin sections examined; their combined abundance normally ranges between 75 and 90 modal percent. Plagioclase is generally more abundant than pyroxene. The weak or moderate foliation mentioned above can be observed in thin section, defined by the alignment of slightly elongate anhedral plagioclase crystals. The foliation may also be partly defined by the orientation of the long dimensions of orthopyroxene oikocrysts (plate 2-31).

Plagioclase is generally anhedral or subhedral, and plagioclase twinning is ubiquitous. A few plagioclase, or in more coarse-grained samples, most plagioclase, may be zoned. A few antiperthitic plagioclase grains were observed in most thin sections (plate 2-32). Plagioclase compositions range from An_{39} to An_{51} (de Waard, 1976); the average composition of plagioclase is An_{45} (Mulhern, 1974). Some grains have dark red or opaque needles of an unidentified mineral, probably rutile. The morphology and occurrence of these needle-bearing grains are similar to that described in the troctolite (section 2.3.1). However, the needles are more commonly found at the centre or in an isolated section of a zoned grain (plate 2-33).

Orthopyroxene and clinopyroxene are the primary mafic minerals; the former mineral is more abundant. Orthopyroxene grains generally have blebby exsolution of augite, which may be elongate at an angle to the cleavage directions in inverted pigeonite,

but lamellar exsolution may also occur along cleavage planes. The most abundant type of exsolution is shown in plate 2-34. Grains in some ferrogabbroid (see below) may be spatially separate but optically continuous (poikilitic), which results in a subophitic or ophitic texture. Clinopyroxene may also show coarse exsolution. Small grains of unidentified opaque minerals and rutile occur in both clino- and orthopyroxene. The morphology of the occurrences is different from the occurrences described in the troctolite. The generally more regular orientation of the occurrences in the troctolitic pyroxene suggest the rutile is an exsolution product, whereas occurrences in ferrogabbroid pyroxene are amorphous and randomly oriented, suggesting that they are inclusions (plate 2-35, compare with plate 2-17b).

Orthopyroxene compositions as reported by Mulhern (1974) and de Waard (1976) are diverse, ranging from En_{30} to En_{55}. Magnetite is ubiquitous, and generally constitutes between 5 and 15 modal percent of a typical rock.

A few modal percent or less biotite is generally present, in association with magnetite. Both olivine and hornblende are uncommon. Olivine occurs as small, isolated grains or in grain aggregates with pyroxene, and hornblende crystals are found as subhedral crystals adjoining pyroxenes, or as rims on pyroxenes. Apatite may be present as randomly oriented elongate, euhedral inclusions within plagioclase and as small grains in the matrix (plate 2-36). A few relatively large grains of apatite, up to several tenths of a millimeter long, were observed. Zircon may also be present as subhedral grains. A red

mineral, probably an iron oxide, is present as rims on virtually all the grains in ferrogabbroid (plate 2-37).

The textural variety of the ferrogabbroid is diverse. Fine-grained samples (grain size 0.1 mm to several tenths of 1 mm) are equigranular and allotriomorphic, with anhedral plagioclase, evenly distributed anhedral Fe-oxide, and pyroxene as discrete, anhedral grains (plate 2-38). A few grains of plagioclase are antiperthitic. Both pyroxenes may have coarse or lamellar exsolution. A few grains of biotite are generally present, associated with magnetite. Accessory apatite may be abundant as inclusions in plagioclase.

Medium-grained ferrogabbroid (grains generally 0.5 mm to 1 mm, with orthopyroxene oikocrysts up to several mm) is generally also equigranular (plate 2-39). However, these samples differ from the fine-grained ferrogabbroid by containing poikilitic orthopyroxene (plate 2-40) and, less commonly, poikilitic clinopyroxene; the resultant texture is generally subophitic, but may be ophitic. Orthopyroxene is generally inverted pigeonite which may have complex, coarse exsolution, likely of augite, at an angle to cleavage. Lamellar exsolution parallel to cleavage is also abundant, as are droplike or irregular patches of exsolution. Lamellar exsolution in orthopyroxene is shown in plate 2-41. Clinopyroxene is generally present as discrete, anhedral to subhedral grains that have third-order birefringence. Fe-oxides are abundant and anhedral. Apatite is abundant, and is texturally similar to that in the fine-grained ferrogabbroid. Biotite grains

may be present and are associated with magnetite (for example, see plate 2-39). The medium-grained ferrogabbroid is commonly gradational with fine-grained ferrogabbroid.

In a few samples, coarse-grained domains (or large single grains of anti- or mesoperthitic plagioclase) were observed within medium-grained ferrogabbroid. These domains generally contain meso- or antiperthite, and/or coarse, subhedral to euhedral plagioclase. The pyroxene in such domains is coarsely-exsolved Fe-rich inverted pigeonite, which may occur as large single grains, oikocrystic grains, or grain aggregates. Very large (up to 1 cm) antiperthitic plagioclase has been found in a few samples.

Two types of coarse-grained ferrogabbroid have been identified. The first, most common type, is texturally similar to the medium-grained ferrogabbroid, and as such is also dominated by equigranular, anhedral plagioclase, though many subhedral grains are common, and zoning may be abundant. As in the medium-grained ferrogabbroid, some plagioclase may be antiperthitic. Orthopyroxene in these coarse-grained ferrogabbroids may be oikocrystic, or may be found as coarsely-exsolved grains or grain aggregates of inverted pigeonite. Clinoyroxene appears to be more abundant, and may also be found as grain aggregates (plate 2-42). This type of coarse-grained rock appears to have much in common, mineralogically and texturally, with leuconorite described in section 2.2.1[1].

The other type of coarse-grained ferrogabbroid is represented by few samples, and is dominated by more sialic assemblages. Patchy antiperthite or mesoperthite grains are abundant. Feldspar crystals in a few sections were observed to have plagioclase cores and

1 See the description of rocks from B to B' and C to C', and especially description of sample LBE 13 and sample LBE 35.

antiperthite, mesoperthite or K-feldspar rims; poikilitic K-feldspar and quartz were observed in one thin section. Some samples have a bimodal grain size distribution. Hydrous minerals are more abundant; this is usually biotite, but amphibole is present in a few samples. In a couple of samples, pyroxene cores were noticed to be surrounded by a strongly-coloured red mineral having high relief. This unidentified mineral is abundant in samples of monzonite.

Of note is a sample (sample BS 6a; for location see fig. 2-1) of medium-grained ferrogabbroid, collected on the south side of Nain Bay, next to the monzonite's southeastern contact. Although the petrology of this sample appears to be identical to other medium-grained ferrogabbroid (plate 2-43), a bulk chemical analysis (XRF) of the sample revealed that it has a silica content higher than other analysed ferrogabbroids (see Chapter 3), and is classified as a monzonite. The layer from which this sample was obtained weathers a more grey colour than typical ferrogabbroid.

In several localities, the outer ferrogabbroid contains various amounts of plagioclase crystals between 1 and 15 cm long. The larger crystals have deep blue or dark grey to black centres and whiten toward their edges. In one location, dispersed large crystals are more tightly concentrated toward a particular point. At this point, large fragments of megacrystic anorthosite up to a few meters in diameter are partially broken apart and surrounded by plagioclase crystals of various sizes. It appears that the feldspar crystals are derived from a process of component dispersal of anorthosite xenoliths, and

other, similar, plagioclase-crystal-rich layers are interpreted to have formed in the same way. Plate 2-44 shows one such xenocryst-rich ferrogabbroid.

In another location, coarse-grained patches of leuconorite or leucogabbro were observed along strike from anorthosite xenoliths (L, fig. 2-4). However, anorthosite xenoliths are not present everywhere along strike from identical irregular coarse-grained leucocratic patches, which were observed to have gradational contacts with the surrounding rock in many other locations within the outer ferrogabbroid.

2.5 Central ferrogabbroid

The ferrogabbroid at the centre of the Barth Island Ring Complex (fig. 2-1) is more homogeneous than the outer ferrogabbroid described above. Substantial exposure shows these rocks to be massive and generally unlayered. The outcrops weather to red or red-beige colour. The rock mainly consists of plagioclase, pyroxene and Fe-oxides, and the average grain size is 2 - 4 mm. A weak foliation, broadly trending N-S, is observable in a few localities. The foliation is generally defined by various amounts of oblong feldspar phenocrysts; however, in one location mafic minerals define the foliation. The phenocrysts resemble those commonly found in the monzonite, and rocks which contain high concentrations of the phenocrysts invariably have lobate and cuspate contacts with surrounding ferrogabbroid, a feature which suggests magma mingling (Ryan, 2000). This phenomenon is described in sections 2.6.1.

The densities of several central ferrogabbroid samples were determined. The method and complete data set are given in appendix four. The average measured density of central ferrogabbroid samples is 2.97 g/cm^3.

The peninsula on the north side of Barth Island is partly composed of two large bodies of melanocratic rock, which appear to be gabbroic. This rock is massive, red-brown weathering, and generally medium-grained (1 - 3 mm). It is referred to hereafter as melanogabbro. Some areas of outcrop are pegmatitic and have plagioclase and pyroxene crystals of up to 2 cm. Contact relationships, though diverse, suggest the melanogabbro bodies are large xenoliths. At two locations along the contact between the ferrogabbroid and melanogabbro, the ferrogabbroid was observed to surround fragments of the melanogabbro. At one of these locations, the ferrogabbroid's grain size decreases sharply; at the other there is no reduction in grain size. The grain size of the ferrogabbroid is smaller at its eastern limit, near sample BIII 10 (fig. 2-1). At the location of this sample, the ferrogabbroid is fine-grained.

Fine-grained, buff-coloured ferrogabbroid xenoliths, cm-dm long, are abundant within the central ferrogabbroid. The long axes of these xenoliths are invariably oriented N-S. Identical xenoliths of ferrogabbroid composition are found in the monzonite, and are described in section 2.6.

As can be seen in fig. 2-1, no contacts between the central ferrogabbroid and surrounding rocks of the Barth Island Ring Complex are exposed; the contact locations are inferred using the aeromagnetic map (fig. 2-2). It will be noticed that the small

patches of ferrogabbroid found on the mainland north of Nain Bay have been nominally included as a part of the central ferrogabbroid, and at one of these locations a contact between the ferrogabbroid and troctolite is exposed. Structures in the troctolite are crosscut by the ferrogabbroid, so the ferrogabbroid is younger. However, the limited extent of the outcrop does not allow any conclusions to be drawn about the actual relationship between this ferrogabbroid and the main body of central ferrogabbroid on Barth Island. The relationship of the central ferrogabbroid to the rest of the Barth Island Ring Complex is therefore unknown.

2.6 Monzonite

In outcrop, the monzonite (plate 2-45) weathers white to grey, with various amounts of red and brown that signify the presence of mafic minerals. Most (ca. 80%) of the monzonite consists of 1 - 2 cm long ovoid mesoperthite (Ryan, 2000). Pyroxene and magnetite are also identifiable in hand sample, however, these grains are much smaller than the mesoperthite grains. The monzonite generally contains subangular xenoliths of a buff-coloured, fine-grained ferrogabbroid, and some of these xenoliths contain oblong white phenocrysts (see below for description). The monzonite generally has a weak foliation defined by aligned elongate phenocrysts of feldspar. Thin layers of monzonite, and monzonite near some contacts with ferrogabbroid, generally have a stronger foliation, in which the mafic minerals appear as granular reddish-brown to black-brown streaks,

which outline the much larger feldspar phenocrysts (plate 2-46). The monzonite foliations are parallel to both its inner and outer contacts, which are parallel to structures in the adjacent rocks.

Densities of several monzonite samples were determined and are reported in appendix four. The average density of the measured monzonite samples is 2.73 g/cm^3.

In thin section, the monzonite was found to be composed of 1 - 2 cm long anhedral mesoperthite crystals (the 'ovoids' are anhedral in detail) or K-feldspar crystals, in a matrix primarily composed of clinopyroxene and feldspar (plate 2-47), although amphibole, orthopyroxene, quartz, and olivine may be present. Some large quartz grains, up nearly 1 cm, were observed. The bimodal size distribution, however, is not a ubiquitous feature. Patches up to 1 cm wide in a few thin sections were found to consist of more equigranular, medium grained grains (plate 2-48). These domains have a lesser proportion of mafic minerals.

Some mesoperthite crystals, particularly near contacts with ferrogabbroid, were found to have undulatory extinction (plate 2-49) and incipient subgrain development. Many of the mesoperthite grains in the monzonite samples collected at the west end of Barth Island have strongly zoned plagioclase cores; in these samples, plagioclase is abundant, and is nearly always rimmed by mesoperthite. All the mafic minerals are generally found as isolated grains of a millimeter or less, but a few clinopyroxene grains were found to be poikilitic and therefore substantially larger (the largest was ca. 3 mm) than the isolated grains. Amphibole also occurs as slightly larger grains (for example, see

plate 2-47). Plagioclase is present as anhedral to subhedral grains of various sizes. Quartz occurs in the matrix and as coarse crystals; the rock's composition ranges through quartz monzonite to monzogranite, though this latter composition is uncommonly seen. Many of the largest quartz crystals have undulatory extinction. A few to several percent Fe-oxides are commonly present.

An unidentified, strongly coloured, non-pleochroic deep red mineral having high relief was observed (plate 2-50) between grain boundaries, and appears in some cases to be a pseudomorph of the anhedral clinopyroxene grains. It resembles the orange to red coloured mineral found between grain boundaries in ferrogabbroid.

Olivine, orthopyroxene and plagioclase compositions have been determined for the monzonite by Mulhern (1974) and Levendosky (1975). The average plagioclase composition is ca. An_{33}. Orthopyroxene compositions are of greater range, from ca. En_{25} to ca. En_{50}. Olivine was found to be fayalitic.

At the west end of Barth Island, a medium-grained rock of similar composition to the monzonite shares gradational contacts with the typical monzonite. This rock is more sialic, having very small amounts of mafic minerals (plate 2-51). It is also more equigranular, similar to sialic patches in the monzonite, described above (compare plate 2-51 with plate 2-48), with many oval quartz grains. The composition appears to range from quartz syenite to syenogranite. It is referred to as syenogranite hereafter. The petrographic appearance of the syenogranite is similar to domains present within net-textured dykes found in the northwestern section of the troctolite (see section 2.8).

Two large xenoliths of buff-coloured, fine to medium-grained rock were observed in the monzonite on the south side of Nain Bay (fig. 2-1). The mineral assemblage and texture of these occurrences (plate 2-52) is similar to that of the fine and medium-grained ferrogabbroid: plagioclase and pyroxene in ca. 70:30 proportions, a somewhat granular texture, poikilitic orthopyroxene, discrete clinopyroxene grains, and several modal percent of magnetite, associated with biotite. A few differences were observed: first, the ubiquitous presence of antiperthite and second, abundant zoned plagioclase crystals. A sample of the buff-coloured, fine-grained subangular xenoliths, mentioned at the beginning of this section, is texturally and mineralogically similar to these xenoliths, and has large (ca. 1 cm) crystals of mesoperthite. Outwardly identical subangular inclusions are present in the central ferrogabbroid (section 2.5).

2.6.1 Contact relationships

Monzonite widely occurs as layers within ferrogabbroid; these layers range from less than one meter to a few hundred meters wide. Small bodies of monzonite or ferrogabbroid-monzonite hybrid rocks are also abundant along the troctolite's northern contact. The most substantial body of monzonite is present in the southern part of the ring complex (fig. 2-1), and is bounded to the north by troctolite, and to the south by ferrogabbroid.

The proportion of mafic minerals in the latter body of monzonite gradually decreases from the contact with the ferrogabbroid to the contact with the troctolite. Sample BS 6b, obtained near the monzonite's southern contact with ferrogabbroid on the south side of Nain Bay (fig. 2-1), has 20 - 25% mafic minerals. Sample BS 6e, ca. 80 m from the contact, has a lower mafic proportion; BS 6f, obtained ca. 150 m from the contact, contains 10 - 15% mafic minerals. Near this contact, thin layers of ferrogabbroid occur within the monzonite; these layers appear to have gradational contacts with mafic domains in the monzonite.

Near its contact with troctolite, the monzonite has a weak foliation, defined by feldspar phenocrysts, parallel to the contact orientation. Normal to strike, to the south, the strength of the foliation gradually increases, and is strongest at the contact with ferrogabbroid unit. Sample BS 6b, collected near this contact, has a large mesoperthite crystal which shows undulatory extinction, a feature suggestive of near-solidus or subsolidus deformation. Other monzonite units also show such features. For instance, the thin body of monzonite described in section 2.2.2 (location J to J') appears to have undergone some deformation, indicated in the field by a strong foliation. Petrographic analysis of a sample of this rock shows the development of deformation in mafic minerals (plate 2-54), but evidence for pervasive recrystallization of the matrix is absent.

These deformation features are ubiquitous around thin monzonite layers, and are also present in many other monzonite-ferrogabbroid contact zones. Within such zones, the monzonite and ferrogabbroid may be interlayered and are commonly partially

hybridized. The hybridization is indicated by high concentrations of large mesoperthite crystals within a matrix of fine-grained, granular ferrogabbroid.

At undeformed contacts between the monzonite and outer ferrogabbroid, magma mingling textures, such as cuspate and lobate contacts (plate 2-55), are well developed. Synplutonic dykes of ferrogabbroid are found within the monzonite (plate 2-56). In some locations, the synplutonic dykes have partially disaggregated into globules, probably by motion within the monzonitic magma (plate 2-30). Crystals of mesoperthite are commonly distributed irregularly within ferrogabbroid near contacts with monzonite.

The magma-mingling textures, partial hybridization, and disaggregation into globules of ferrogabbroid dykes all indicate the monzonite and outer ferrogabbroid were contemporaneous magmas.

The greatest length of exposed contact between the troctolite and monzonite occurs on the south side of Nain Bay. The contact is generally sharp and may be gently undulose. In a few locations, buff, granular, fine-grained ferrogabbroid is present in the contact, and closely resembles the adjacent troctolite. A few straight-walled dykes of medium- to coarse-grained monzonite were observed within 10 m of the southern troctolite-monzonite contact; these dykes are oriented normal to the the contact. The longest of these dykes is approximately 10 m. Some smaller (< 20 cm wide), anastamosing fine- to medium-grained monzonite dykes are also found near this locality.

On the west end of Barth Island, the monzonite has an irregular contact with the troctolite (plates 2-57a and b). Here, the monzonite grades into thin layers and zones of

syenogranite (section 2.6); one such zone of syenogranite completely surrounds a part of the troctolite.

On the basis of this evidence, the syenogranite and monzonite appear to have been emplaced after the troctolite. In order to test this conclusion, a sample of troctolite from the west end of Barth Island, which has a vein of monzonite within it, was cut for petrographic analysis. Plates 2-58a and 2-58b show the texture of the troctolite, and the texture of the vein and its immediate surroundings. The vein is surrounded by vermicular orthopyroxene and feldspar (symplectite). The symplectite indicates reaction between the vein and the surrounding rock. The troctolite, which is generally hydrous and contains primary biotite and amphibole (section 2.3.1), shows formation of secondary biotite and hornblende. The biotite is interpreted to be secondary because, unlike all other biotite observed in the troctolite, it presents as grain aggregates rather than pristine single grains. The hornblende is interpreted to be secondary because it was observed to pseudomorph olivine: other examples of amphibole co-existing with olivine in the troctolite have been documented herein (2.3.1), and in these cases there is no evidence of replacement or reaction.

There is also considerable evidence of fluid circulation in the rock, including sericite and chlorite alteration; there also appears to be small amounts of a carbonate mineral. The vein itself, however, is completely devoid of hydrous minerals, as is the area surrounding the vein.

These features can be accounted for by granulitization. Heat from the monzonite could have driven the dehydration reaction

biotite + quartz = orthopyroxene + potassium feldspar + water (Harley, 1989)

The fluids liberated from biotite would have both enhanced the reaction rates and enabled the alteration of olivine to amphibole. Secondary biotite would have formed by both fluid alteration processes and by recrystallization due to the high temperatures.

The interpretation of the evidence as presented above suggests that the monzonite is younger than the troctolite. This is discussed further in section 2.9.3.

2.7 Outer leuconorite

The outer leuconorite was described in detail in section 2.2.1. The nature of the contact relationships between the outer leuconorite and anorthosite required close examination, which necessitated the description of the outer leuconorite.

2.8 Dykes and veins

Some outcrops in the northwestern section of the troctolite are intruded by anastamosing, interconnected (net-textured) fine-grained monzonite dykes and veinlets (plates 2-59, 2-60, and 2-61), which are limited in extent. In one outcrop, however, the

dykes make up 10 to 15% of the exposure. In the field, these dykes appear similar to the syenogranite, and, petrographically, have textural similarities to both the monzonite (although this is difficult to observe on the scale of a photomicrograph) and syenogranite (compare plate 2-51 to plate-61). The margin of one of these dykes has distinctly smaller grain size than its interior (plate 2-62), indicating that the surrounding troctolite was relatively cool when the dykes were emplaced. These dykes also resemble dykes which emanate from the northwestern contact between troctolite with outer ferrogabbroid (section 2.3.3) into the troctolite. On the basis of similar appearance and petrographic features, the dykes are interpreted to be derived from the magma which produced the monzonite and syenogranite.

A small body of fine-grained rock, cropping out over a few m^2, is found in the northwestern section of the troctolite. It has a well-exposed, intrusive contact with the surrounding troctolite, and appears to have been fed by the net-textured veins. This rock is mineralogically and texturally similar to the monzonite.

Small, coarse-grained, leuconoritic dykes, generally spatially associated with fine-grained, buff to red-buff ferrodiorite dykes, are present in a few locations near the troctolite's exterior contact. These two dyke morphologies are commonly found side by side, and are subparallel. These dykes are also found in the troctolite immediately north of point A on fig. 2-1.

Sets of parallel, sub-mm to mm scale glassy black veins are present in several locations. These veins do not appear to have any preferred orientation. In one location,

green-black veins contain crystals of a unidentified dark mineral up to a few mm in size, and have an alteration envelope up to 1 cm wide on either side.

A body of medium-grained anorthosite, which contains oikocrystic pyroxene, was found in one location within the norite. This body crops out over approximately 50 m^2; it is not clear what its relationship to the norite is.

A few dm-scale basalt dykes were observed to cut the outer ferrogabbroid and central ferrogabbroid.

Many dm-scale dykes of pegmatitic leucogranite were observed within both the monzonite, and outer and central ferrogabbroid. In the central ferrogabbroid, these dykes are gently dipping and extensive; one dyke was observed to be present in two separate outcrops, many dac apart.

2.9 Discussion

The following discussion elaborates the magmatic evolution of the Barth Island Ring Complex from the observations in the previous sections. The field relationships, mineral assemblage, and textures, as well as the major-element mineral data of Mulhern (1974) and de Waard (1976) are used to constrain the possible history and mode of evolution of the Barth Island Ring Complex.

2.9.1 Magma evolution

Some review of cumulate theory and basic magma evolution trends is necessary for an interpretation of the textures of troctolite and norite of the Barth Island Ring Complex. Cumulus crystallization is the process by which crystals accumulate in a magma chamber (Cox *et al.*, 1979, pp. 286-96). The following is an outline of the process.

The process begins with the emplacement of magma (liquid or liquid + crystals) at some depth in the crust, which creates a chamber. As the magma cools, it becomes saturated in certain minerals which begin to crystallize, or existing crystals grow. Because these minerals form early in the crystallization history, their physical growth is not constrained. This process results in large, euhedral crystals.

The growing crystals accumulate as a pile or mat at the edges of the chamber, where heat is being lost rapidly. The pile or mat consists of a framework of crystals which define an interconnected system of pore spaces filled with intercumulus liquid. The intercumulus liquid is the magma residual from formation of the cumulus minerals (depleted now in certain components, because the crystals have used up some of the primary constituents). If this depleted liquid is expelled from the pile and replaced with fresh, primitive magma, subsequent crystallization of the fresh magma results in what are termed adcumulus textures. The euhedral crystal forms, however, cannot be preserved because the mineral is now crystallizing in a confined space. Furthermore, efficient supply of undepleted magma to the growing crystals results in a lack of chemical zoning

in the grains. Adcumulate textures are therefore typified by subhedral or anhedral mineral forms and unzoned grains: the primitive intercumulus liquid is saturated in the cumulus mineral, which continues to grow without sufficient space to maintain its euhedral form.

The opposite end of the cumulate spectrum is orthocumulus crystallization, in which the residual liquids crystallize *in situ*. The mineral assemblage of the pockets of residual liquid will be evolved, because the liquid is enriched in components excluded from the early-formed crystals. In this situation, the euhedral forms of the cumulus minerals may be preserved, because the intercumulus liquid crystallizes a different assemblage. Chemical zoning of the cumulus minerals will occur, because the components removed from the primitive magma by the cumulus minerals are in large part not replaced. No further growth of the cumulus minerals occurs. Mesocumulate textures describe a history of cumulus crystallization somewhere between the end-members of ortho- and adcumulus growth.

A common byproduct of cumulate crystallization is the development of modal and rhythmic modal layering. Modal layers may form as the result of gravity settling of minerals which are more dense than the surrounding magma; for example, olivine-rich layers may form this way. Rhythmic modal layering, in which layer types are repeated, has been shown to develop as a result of many processes, such as repeated pulses of magma into a crystallizing magma chamber (Cox *et al.*, 1979, pp. 322-323; McBirney, 1984, p. 195) or oscillatory chemical and thermal gradient shifts (McBirney, 1984, pp.

219-221). With sufficient time between pulses, the magma has time to evolve modal layering, which may become rhythmic modal layering upon the input of fresh magma.

A magma with a certain minimum amount of silica from which extensive crystallization of cumulus minerals has occurred becomes more evolved, that is, the residual liquid becomes more silica-rich. The first mafic mineral to crystallize from a silica-deficient, primitive basic magma is olivine: $(Mg,Fe)_2SiO_4$. As the magma evolves, the mafic mineral changes as a result of the magma's trend toward silica saturation. The primary mafic mineral thus becomes orthopyroxene: $(Mg,Fe)_2Si_2O_6$. Further liquid evolution results in crystallization of quartz-bearing compositions (Bowen, 1928; McBirney, 1984, pp. 228-230; Blatt and Tracy, 1996, pp. 126-28).

The evolution of magma in a magma chamber crystallizing a cumulus assemblage will also be manifested in progressive evolution of mineral compositions. Ca-rich plagioclase will crystallize first, followed by grains with lower Ca content. Mafic minerals crystallize Mg-rich compositions first, followed by more Fe-rich phases. This latter trend (Fe-enrichment) is called the tholeiitic trend, and is a typical result of evolution of basaltic magmas. Certain textural and mineralogical features are typical of tholeiitic rocks. The presence of myrmekitic intergrowths at the edge of plagioclase grains, for instance, is a commonly seen feature in evolved tholeiitic magmas. Pyroxene in tholeiitic rocks is typically Ca-poor (Shelley, 1993, pp. 51, 138).

2.9.2 Troctolite and norite

The crystallization history of the interior of the troctolite and norite of the Barth Island Ring Complex is well preserved in pristine igneous textures and mineral assemblages. In most troctolite samples, subhedral or anhedral olivine crystals conform to the shape of euhedral plagioclase grains (plate 2-63). Plagioclase, in many places in the stratigraphy of the intrusion, must have crystallized before olivine. In one olivine-rich layer, plagioclase grains were observed to both partially surround euhedral olivine grains, and have euhedral terminations against anhedral olivine grains (plate 2-64). This evidence indicates co-crystallization, at least in olivine-rich layers. In the case of both the troctolite and norite, the forms of euhedral plagioclase grains are not preserved at plagioclase-plagioclase boundaries. In other cases, euhedral plagioclase and olivine forms are well preserved against amphibole, biotite, and magnetite (plates 2-14 and 2-15). In the troctolite, anhedral clino- and orthopyroxene also enclose euhedral plagioclase and olivine. These observations provide strong evidence that plagioclase and olivine were cumulus minerals.

The general lack of zoning in plagioclase of the troctolite implicates some adcumulus processes in their formation. However, amphibole, biotite, magnetite, and some pyroxene formed late, because their forms are controlled by euhedral and subhedral plagioclase and olivine. Therefore, these late-forming minerals crystallized from intercumulus liquid. The association of these latter minerals, epidote group minerals and,

in the norite, quartz, is typical of crystallization from evolved magma. The troctolite must have resulted from a mixture of adcumulus and orthocumulus processes.

Evidence for the final stages of evolution of the troctolitic magma is preserved in the stratigraphy of the troctolitic intrusion. The troctolite-norite contact does not appear to be an intrusive contact, and is defined by the abrupt replacement of olivine, as the primary mafic mineral, with orthopyroxene. The troctolite and norite are similar in appearance, grain size, texture, and colour index. An abrupt shift from the crystallization of olivine to orthopyroxene is typical of basic magma bodies evolving along a silica-saturation trend (Blatt and Tracy, 1996, p. 125). The common presence in the norite of myrmekite at grain boundaries, and the dominant pyroxene being Ca-poor, are also consistent with the norite being a product of tholeiitic differentiation.

Further evidence for the differentiation of the troctolitic magma body to produce the two rock types is given by the progressive shift in mineral compositions from the outer rim of the troctolite through to the norite (Mulhern, 1974; de Waard, 1976). Plagioclase generally becomes more sodic, and olivine and orthopyroxene generally more Fe-rich, upwards toward the centre of the intrusion. Major-element geochemical data obtained in this study also provide evidence for a tholeiitic differentiation trend. The Mg number, given by the formula Mg / (Mg + Fe), is lower in noritic samples than it is in troctolitic samples. This evidence is detailed in Chapter 3.

There is no evidence to suggest the troctolite and norite are linked to the ferrogabbroid-monzonite, at the level of intrusion, via a 'parental' magma, as suggested by

de Waard (1976). Consider the following line of reasoning. The first crystallization products of the magma which produced the troctolite would not have been rocks of ferrogabbroic and monzonitic composition: these rock types would crystallize from a magma of more evolved composition than that which produced the troctolite. However, the ferrogabbroid and monzonite are stratigraphically below the troctolite. If the ferrogabbroid and monzonite are related to the troctolite as concluded by de Waard (1976), the observed stratigraphy could only be achieved if the Barth Island Ring Complex was overturned, or strongly folded, with overturned folds at the margins. Previous workers (Mulhern, 1974; de Waard, 1976) proposed that the ring complex was strongly folded during ascent to its present level of emplacement, which is the sole reason for addressing the possibility of a genetic link between the rock types in the present study.

2.9.3 The relative age of the troctolite

Although the field evidence related in section 2.6.1 has been interpreted to suggest the troctolite is older than the monzonite, it is possible to interpret some of this evidence to suggest the troctolite is slightly younger than, but broadly contemporaneous with, the monzonite. For instance, if the troctolite intruded into the centre of mostly-crystalline monzonite and ferrogabbroid magmas, still-magmatic monzonite might have been forced as dykes into the troctolite, thus explaining their presence in the troctolite's margin. However, supporting evidence for this theory, such as magma mingling textures, which

might be expected to develop at the contact between two magmatic bodies of different temperature and composition, is notably absent. The weight of evidence indicates that the troctolite was present at the level of intrusion before the monzonite.

2.9.4 Outer ferrogabbroid and monzonite

The outer ferrogabbroid and monzonite of the Barth Island Ring Complex present a different story than the troctolite and norite. There is good reason to propose that the outer ferrogabbroid and monzonite are not linked by *in situ* differentiation of a single magma: magma-mingling textures, the presence of synplutonic dykes of ferrogabbroid within monzonite, and the presence of dispersed mesoperthite xenocrysts of the monzonite within the outer ferrogabbroid, indicate an intrusive relationship. In some coarse-grained varieties of outer ferrogabbroid, the mineral assemblage is indicative of hybridization between outer ferrogabbroid and monzonite. Hybridization and magma-mingling/mixing between ferrodioritic magma and more sialic magma has been documented in other areas of the Nain Batholith (Wiebe, 1990b; Tettelaar, 2004, pers. comm.).

The presence of synplutonic ferrogabbroid dykes within the monzonite (plate 2-56) suggest that at least some of the monzonite was emplaced before the outer ferrogabbroid. These morphologies, and the local presence of large mesoperthite crystals within the ferrogabbroid, indicate that the monzonite must have been partially crystalline

when it was intruded by the outer ferrogabbroid; therefore, the monzonite was relatively cool. This inference is independently supported by the fine grain size of outer ferrogabbroid near contacts with monzonite.

A generalized chamber evolution hypothesis proposed by other authors (Shelley, 1993, p. 242) fits well with the monzonite-ferrogabbroid chamber evolution model and intrusion chronology already inferred from the field evidence. In this generalized model, dense mafic magma (corresponding to the outer ferrogabbroid of the Barth Island Ring Complex) intrudes underneath a cooler, sialic, crystal-rich magma. A zone of mingling develops, which is then disaggregated into globules by magma movement. Excellent evidence of similar processes is well-preserved in the Barth Island Ring Complex (plate 2-30). Similar mingling processes between mafic and sialic magma have also been well documented elsewhere in the world (Wiebe, 1994; Wiebe *et al.*, 2002).

It must be emphasized that this is a generalized chamber hypothesis, and is too simplistic to explain the whole pattern of monzonite and outer ferrogabbroid distribution (fig. 2-1). For instance, monzonite is present at many different stratigraphic levels in the ring complex, including one relatively thick layer near the base of the ring complex at the northeastern margin. This does not contradict the general model (the emplacement of the ferrogabbroid need not have been solely underneath the monzonite), but points to complicated processes, including multiple, perhaps alternating pulses of each monzonite and outer ferrogabbroid. For instance, the fine-grained, subangular and large xenoliths of ferrogabbroid in the monzonite could be explained if the monzonite followed

ferrogabbroid into the chamber through the same conduit. Evidence that could be interpreted to support multiple pulses of ferrogabbroid, such as crosscutting and curvilinear interlayer contacts between layers of different grain size, is present in many locations.

The cumulate textures of the troctolite and norite are not present in the outer ferrogabbroid. The primary textural feature of the outer ferrogabbroid is the equigranular, anhedral nature of the major mineral constituents: magnetite, pyroxenes and plagioclase. Clearly, the minerals in fine-grained outer ferrogabbroid did not have much time to grow, particularly where the ratio of ferrogabbroid magma to monzonitic magma was low; this interpretation is supported by the fine grain size of ferrogabbroid at contacts with relatively thick (ca. > 5 m) sequences of monzonite. The equigranular, anhedral texture of the fine-grained ferrogabbroid therefore probably resulted from rapid cooling, but also from the simultaneous appearance, on the ferrogabbroid magma's liquidus, of plagioclase and pyroxene. The minerals therefore might have restricted each other's growth.

The medium-grained ferrogabbroid shares the equigranular textural features of the fine-grained ferrogabbroid, but does have some much larger orthopyroxene grains, which are generally oikocrysts: optically continuous but spatially separate grains. Few euhedral grains are present. In the case of the medium-grained ferrogabbroid, the anhedral nature and even distribution of the grains might be explained, as in the fine-grained ferrogabbroid, as the result of a system in which crystals did not have much room or time to grow. In this case, the ferrogabbroid would have been supercooled: plagioclase

nucleated and grew rapidly, but was speedily followed on the liquidus by pyroxene, which had little space available to it, necessitating the formation of the oikocrystic (skeletal) orthopyroxene. The orthopyroxene would have had to appear on the liquidus soon enough after plagioclase to impede the development of euhedral plagioclase.

An alternative explanation for the textural characteristics of the medium-grained ferrogabbroid might be that it experienced some directed stress during solidification, equivalent to a 'densification' processes (Hunter, 1996). In this case, the ferrogabbroid magma would have crystallized a substantial amount of plagioclase prior to the appearance, on the liquidus, of pyroxene. Directed stress of unknown origin on the crystallizing magma might have compacted the existing plagioclase grains, such that when pyroxene began to crystallize, it developed as oikocrysts in the limited space available to it. Where oikocrysts are not present, sufficient space must have been available to the nucleating pyroxene.

Many of the various textural and mineralogical features that constitute the erratic layering in the outer ferrogabbroid (for example, abrupt differences in grain size over a few cm and laterally discontinuous layering) have been documented elsewhere in the Nain Batholith (Wiebe and Wild, 1983; Wiebe, 1990b). In the Tigalak Intrusion, irregular, laterally discontinuous layering in ferrodiorite may be defined by abrupt changes in grain size or various abundances of fine-grained dioritic inclusions; and alternate coarse- and fine-grained layers of ferrodiorite have both sharp and gradational boundaries, and are mixed on a scale of a few cm to a few m. Elsewhere in the Tigalak

Intrusion, ferrodiorite occurs within granodiorite as fine-grained pillows and chilled lenses (Wiebe and Wild, 1983).

The explanation for some of the changes in grain size, which appear to define erratic layering in some locations, has been hybridization of granodiorite with ferrodiorite. This explanation is substantiated by excellent first-order evidence. For instance, the granitic rock of the Tigalak Intrusion bears hydrous minerals such as biotite and hornblende. In the Tigalak diorite, abrupt changes in grain size occur on cm- and mm-scale and are associated with changes in the mineral assemblage, for example from pyroxene to hornblende; xenocrysts of K-feldspar, rimmed with sodic plagioclase, are abundant in areas of increased grain size. Major-element geochemical evidence is also in favour of hybridization (Wiebe, 1990b).

Field relationships throughout the Barth Island Ring Complex suggests that similar hybridization may also have occurred between ferrogabbroid and monzonite, and may explain some features of the ferrogabbroid's erratic layering. Mesoperthitic ovoids, typical of monzonite of the Barth Island Ring Complex, are found in various abundances as intermittent layers within the ferrogabbroid in several locations. This feature is especially notable in the northwestern section of the ring complex, where a precipitous slope exposes a cross-section of the outer ferrogabbroid. The abundance of these ovoids may be associated with local changes in grain size, which in part define layer boundaries.

Some support to this theory is given by petrographic features. For instance, a mineral commonly found in the monzonite (the deep red mineral pictured in plate 2-50),

is present in some ferrogabbroid samples where hybridization is suspected. This conclusion is supported in part by the presence of antiperthite xenocrysts in coarse-grained ferrogabbroid (plate 2-65).

Hybridization is probably not the sole cause of all erratic layering. For instance, multiple pulses of ferrogabbroid could have caused lobate, pillow-like textures between fine- and medium-grained ferrogabbroid, observed near sample location LBE 15, in the northeastern section of the ring complex. If a late pulse of fresh ferrogabbroid magma had intruded into an area of partially crystallized ferrogabbroid, the fresh, hot magma might have been partly chilled, resulting in the lobate structures. Changes in grain size may also be spatially associated with anorthosite inclusions or the appearance of layers of leuconorite, as near location L (fig. 2-4). Some coarse-grained ferrogabbroid are mineralogically and texturally similar to leuconorite found at the northeastern margin of the ring complex (see descriptions associated with locations B and C, section 2.2.1).

The monzonite may be a cumulate rock, because it is primarily composed of mesoperthite grains which are much larger than the other constituent minerals of the rock, and some supporting geochemical evidence for this conclusion is given in chapter three. However, there is no supporting petrographic evidence of cumulus crystallization processes. Euhedral grains, for instance, are not generally present, and most grains, both coarse and fine, are intergrown with each other. The monzonite is a typical sialic rock in this regard: the coarse mesoperthite grains, intergrown minerals, lack of layering, wispy streaks defining concentrations of mafic minerals, preferred alignment of coarse feldspars

paralleling intrusive contacts, and even the minor dynamic recrystallization evident in thin section, are characteristic of rocks of monzonitic composition (McBirney, 1984, pp. 346-348; Shelley, 1993, pp. 29-31, 228-238). However, these features do not reveal much about the monzonite's magmatic history.

In comparison with the ferrogabbroid, the monzonite is relatively homogeneous. Its texture and grain size are similar throughout the ring complex, and deviations from the standard features, such as increases in the proportions of mafic minerals, can be explained by a spatial link to ferrogabbroid occurrences.

2.10 Summary

The combined weight of field and petrographic evidence suggests the troctolite is older than the monzonite and outer ferrogabbroid. A brief summary of this evidence is as follows.

1. Dykes of monzonite appear to emanate from the southernmost troctolite-monzonite contact, and net-textured dykes of monzonitic composition within the northwestern part of the troctolite, discussed in section 2.8, have similar textures to monzonite of the Barth Island Ring Complex. A sample of the margin of one of these net-textured dykes is more fine-grained than the middle, suggesting that it chilled against the troctolite; this indicates the troctolite was cool when the dykes intruded. However, despite these similarities, the link between these net-textured dykes and the monzonite is not

conclusive, because they cannot be seen to emanate from the contact between the troctolite and ferrogabbroid-monzonite. Notably, these dykes are not found in either the monzonite or ferrogabbroid at any location throughout the Barth Island Ring Complex, as would be expected if the dykes were part of a phase of magmatism later than all the rocks of the ring complex.

2. The monzonite appears to crosscut the troctolite at an outcrop on the west end of Barth Island. A part of troctolite in this location is completely surrounded by syenogranite, which is related to the monzonite.

3. Veins of monzonitic rock crosscut a sample of troctolite, obtained within a few m of a contact with monzonite at the west end of Barth Island. The troctolite is generally coarse-grained, indicating that it did not cool quickly. It must have been completely solid upon the intrusion of the monzonite vein, because intrusion of the vein caused granulitization of the troctolite immediately surrounding it, liberating fluid from biotite and recrystallizing the surroundings. Biotite has been identified as one of the final minerals to crystallize from the magma that gave rise to troctolite.

Further evidence supporting this interpretation of the relative timing of the magmas is given in chapter four, which details the results of U-Pb age determinations on troctolite and ferrogabbroid of the Barth Island Ring Complex.

The field observations and petrography provide evidence from which a partial magmatic history of the Barth Island Ring Complex can be constructed. A magma parental to both the troctolite and norite was emplaced in a setting of massif-type

anorthosite, adjacent to a shear zone, and cooled slowly. The slow cooling aided the operation of processes which gave rise to the formation of modal layering and cumulate textures. In some layers, plagioclase was on the magma's liquidus before olivine, indicating that the parental magma may have been rather aluminous; however, co-crystallization of these two minerals was observed in other layers. Differentiation of the magma followed a tholeiitic trend, leading to silica enrichment and the formation of the norite.

Petrographic textural evidence from the troctolite's margin indicates that some annealing took place, suggesting a history of prolonged high temperatures. The annealing is extreme at the northwestern margin, where the troctolite is progressively more recrystallized toward its exterior contact; similar textures were observed in samples from isolated bodies of troctolite in the central northern and northeastern sections of the ring complex (fig. 2-1). These recrystallization textures occurred either during the cooling of the pluton, or upon the emplacement of the monzonite and ferrogabbroid.

Field relationships clearly demonstrate that the ferrogabbroid and monzonite were contemporaneous magmas. Furthermore, the monzonite was likely present at the site of emplacement and was partially crystalline before the intrusion of at least some of the ferrogabbroid magma. However, some of the erratic layering of the ferrogabbroid was probably caused by multiple pulses, and the evidence is consistent with alternate pulses of ferrogabbroid and monzonite. Partial hybridization of these two magmas occurred at many stratigraphic levels.

The outer leuconorite is younger than the outer ferrogabbroid and monzonite of the ring complex. It appears to have been emplaced as a series of sheets into older anorthosite and outer ferrogabbroid along the eastern margin of the suite, whereas it crosscuts outer ferrogabbroid along the northern margin of the suite.

The central ferrogabbroid has no exposed contacts with any other members of the Barth Island Ring Complex, and its relationship to these other members is therefore unclear.

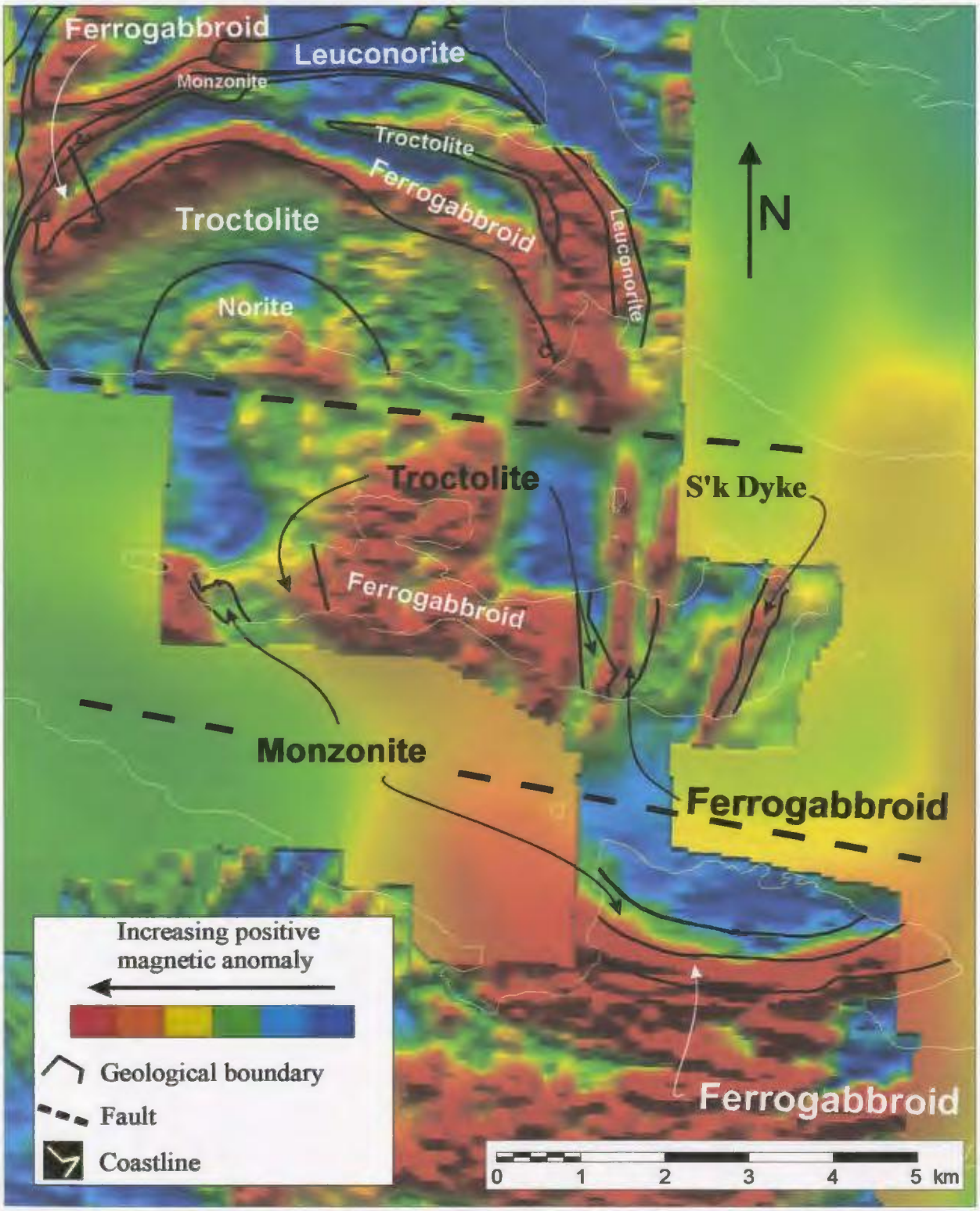

Figure 2-2. Aeromagnetic map of Barth Island and surrounding area. Rock types are labeled according to observed surficial geology; black lines are observed or inferred boundaries. S'k Dyke is the Satorsoakulluk Dyke, a ferrogabbroid body. See text for details. Aeromagnetic image from Kilfoil (2002).

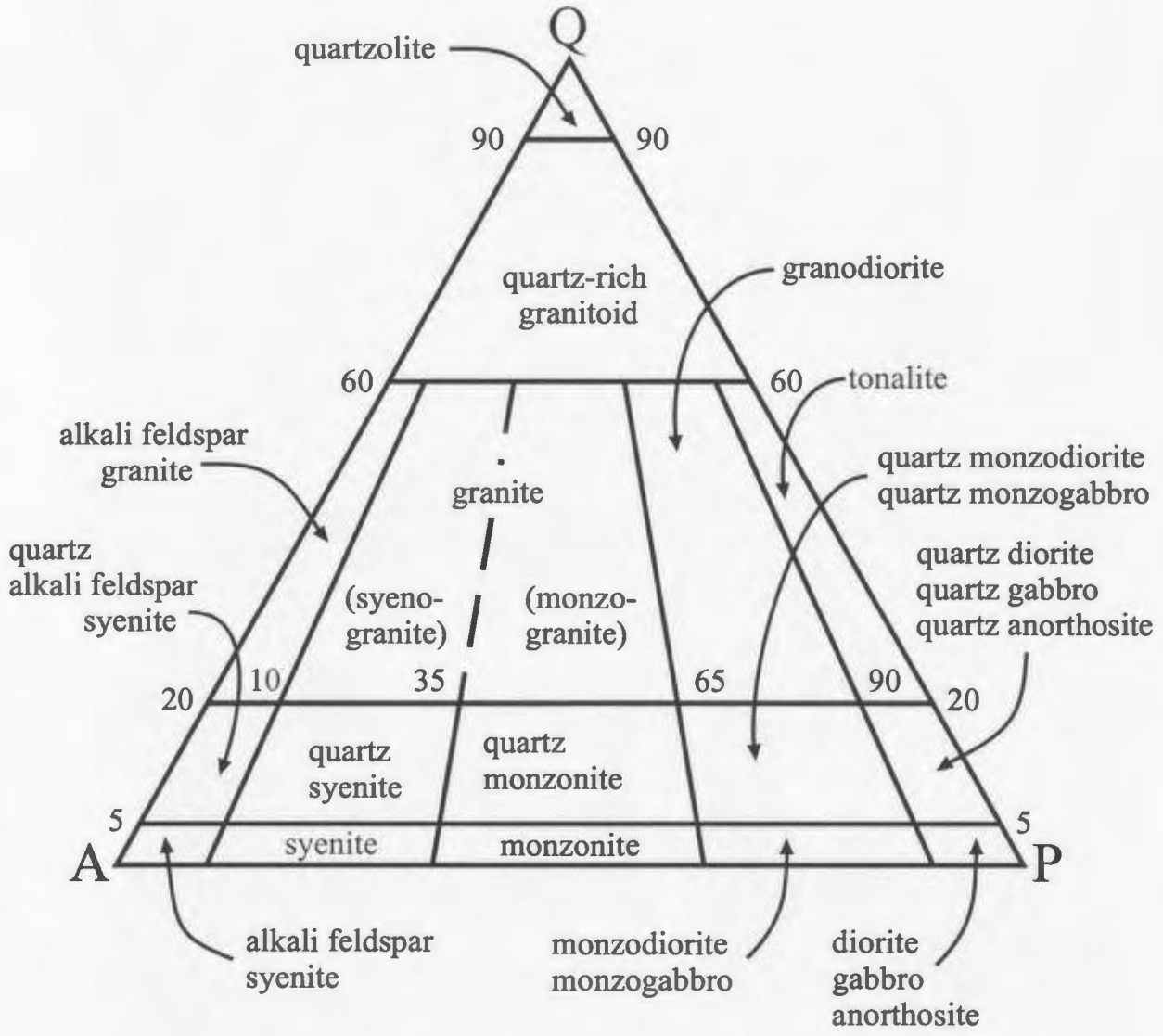

Figure 2-3. QAP triangle modal classification of plutonic rocks. The corners of the triangle are Q = quartz, A = alkali feldspar, and P = plagioclase feldspar. Diorite and gabbro are in the same field for the compositional range expressed in this diagram. Adapted from Le Maitre (2002), his fig. 2.4.

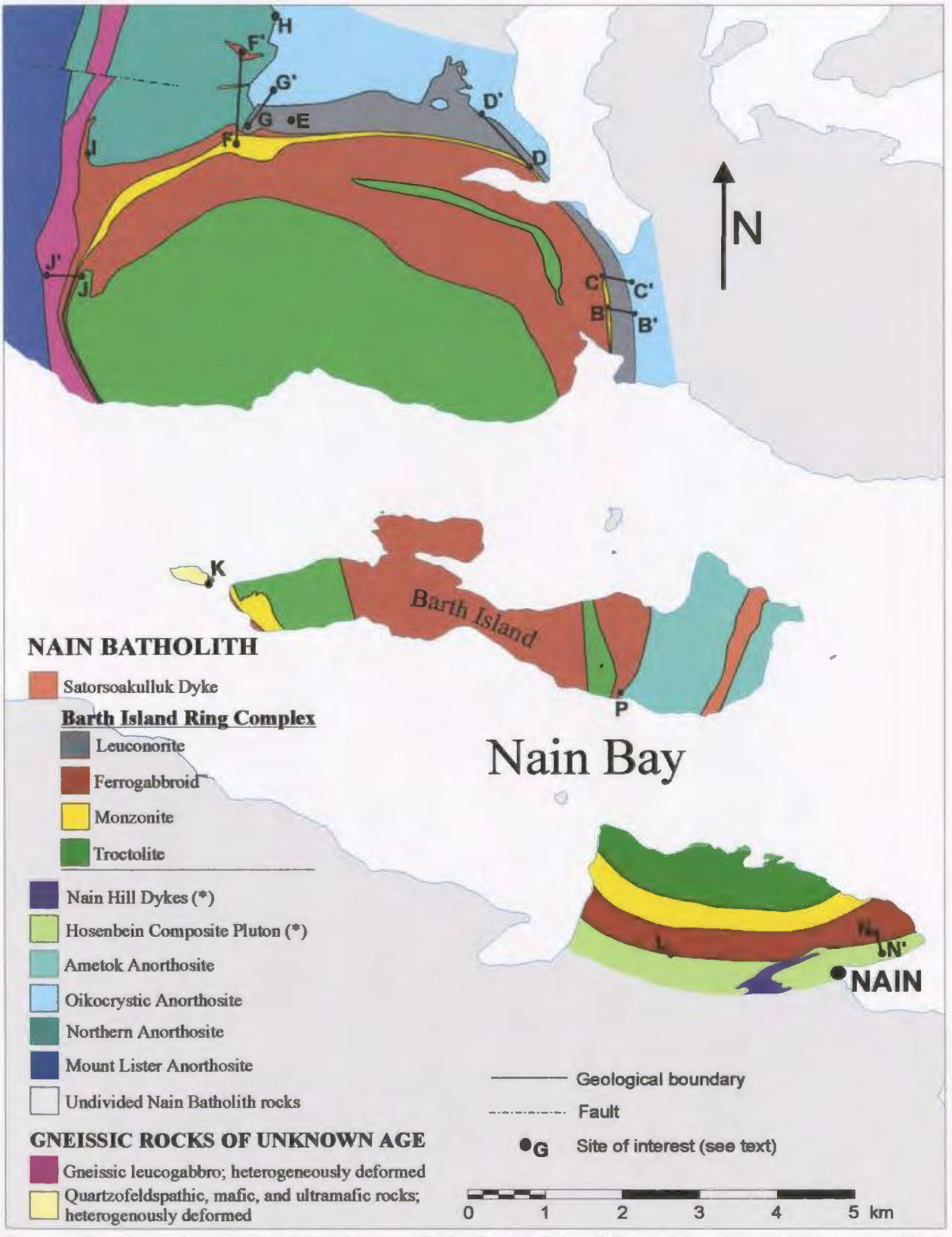

Figure 2-4. Simplified geological map of the Barth Island Ring Complex and surrounding area. All units mapped by the author except (*) mapped by R. Voordouw.

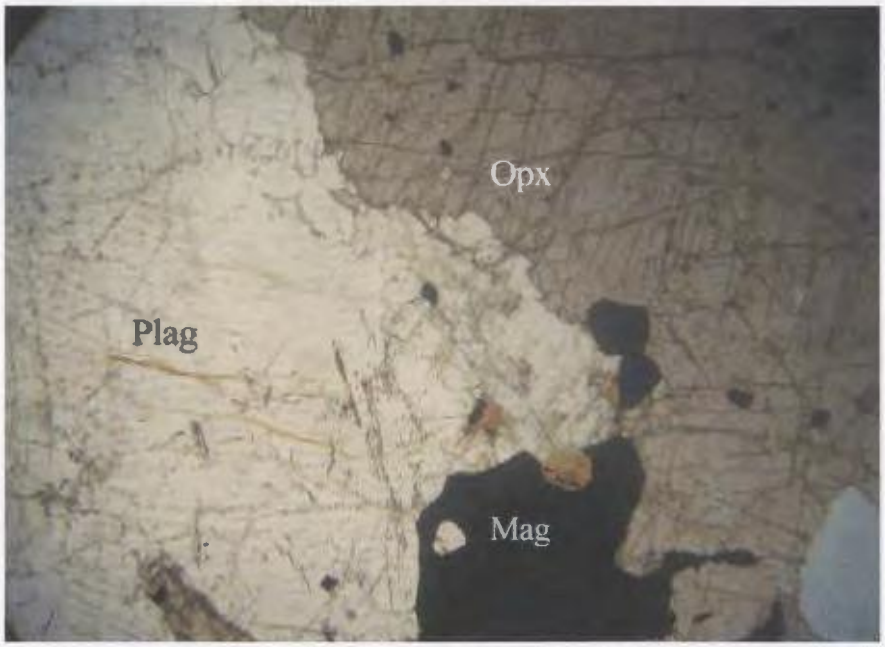

Plate 2-1. Photomicrograph of sample LBE 35, a leuconorite at the eastern margin. Plane polarized light. Note the anhedral nature of the plagioclase (Plag), magnetite (Mag) and orthopyroxene (Opx). Horizontal field of view ca. 5.5 mm. In the following plates, 'field of view' refers to the horizontal length.

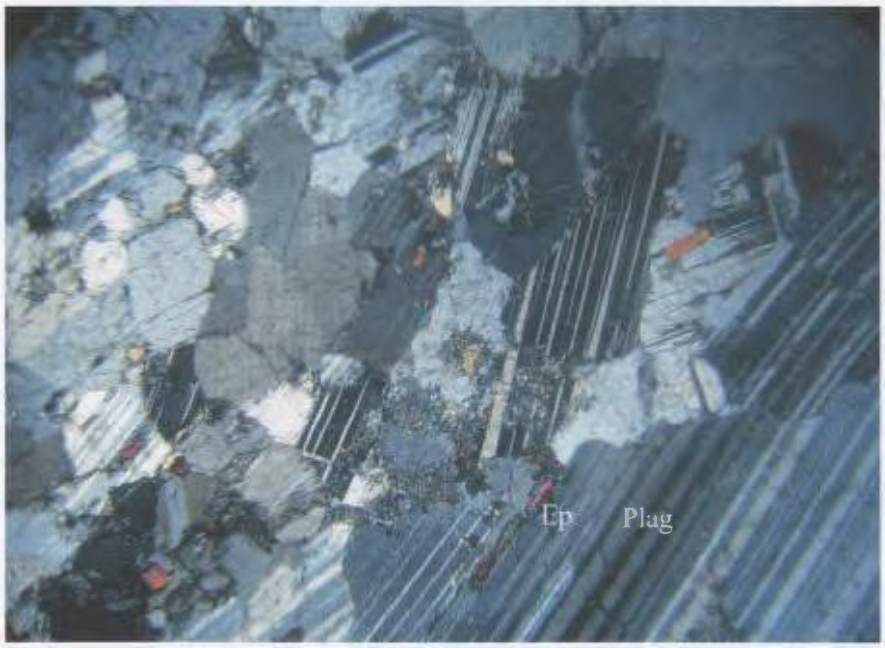

Plate 2-2. Photomicrograph of sample LBE 36, an anorthosite east of the outer leuconorite in plate 2-1. Crossed polars. The average grain size of this anorthosite is not as coarse as it appeared to be in the field. The brightly coloured mineral is epidote (Ep). Plag = plagioclase. Field of view ca. 5.5 mm.

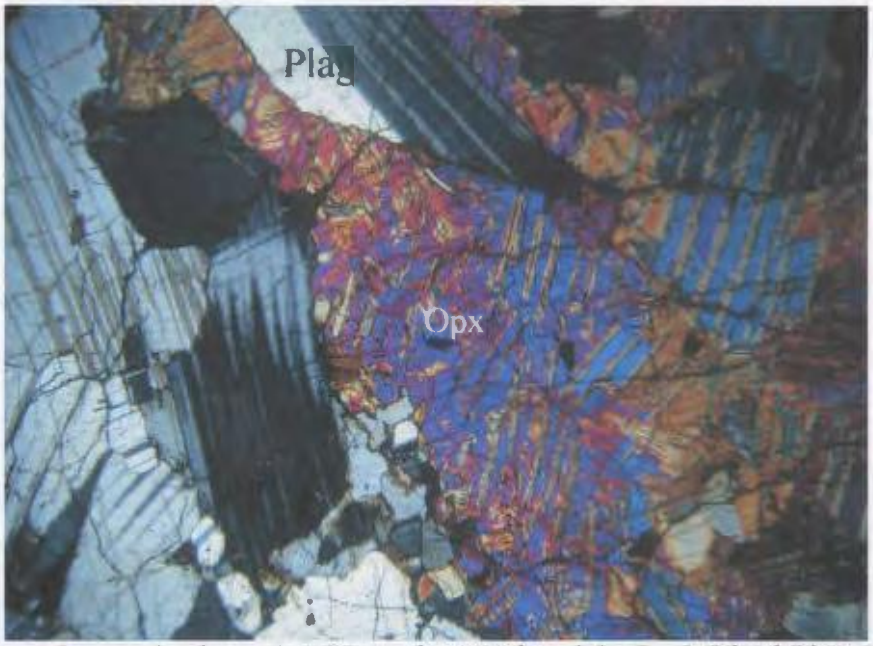

Plate 2-3. Photomicrograph of sample LBE 13, leuconorite of the Barth Island Ring Complex at the northeastern margin. Crossed polars. The blue-purple, coarsely-exsolved orthopyroxene (Opx) is inverted pigeonite. Note also the deformation in the plagioclase crystal (Plag), indicated by the warped twins. Field of view ca. 5.5 mm.

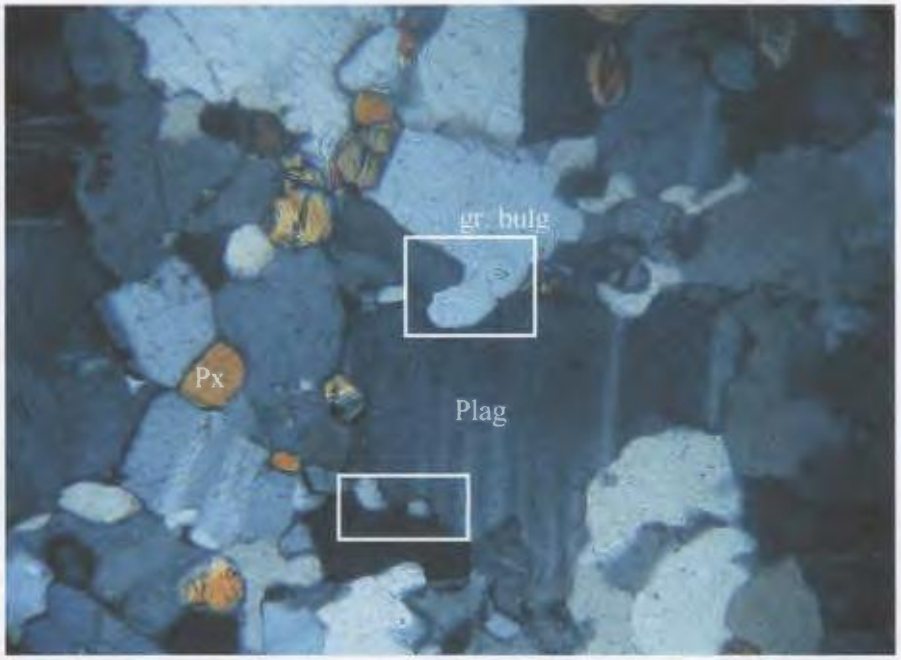

Plate 2-4. Photomicrograph of sample BIV 12. A partially recrystallized tonalitic rock from the small island west of Barth Island. Crossed polars. The central box outlines an example of grain bulging (gr. bulg), while the lower box surrounds grains that have formed through grain boundary migration. Plag = plagioclase; Px = pyroxene. Field of view ca. 1.5 mm.

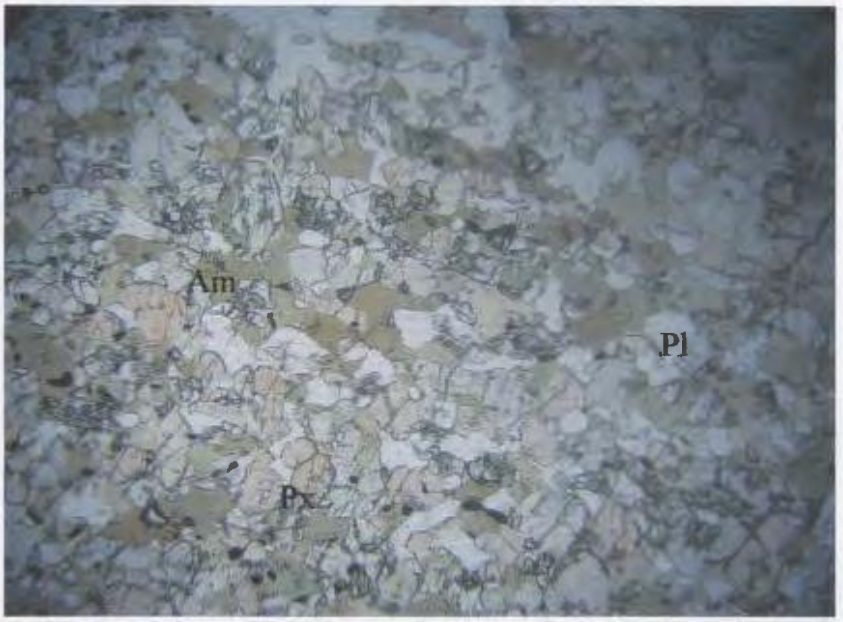

Plate 2-5. Photomicrograph of sample BIV 4, mafic-ultramafic gneiss from the small island west of Barth Island. Plane polarized light. This plagioclase-bearing 2-pyroxene amphibolite gneiss is probably at a higher metamorphic grade than the felsic rock it is intercalated with. Note the equigranular texture and moderate fabric. Pl = plagioclase; Px = pyroxene; Am = amphibole. Field of view ca. 5.5 mm.

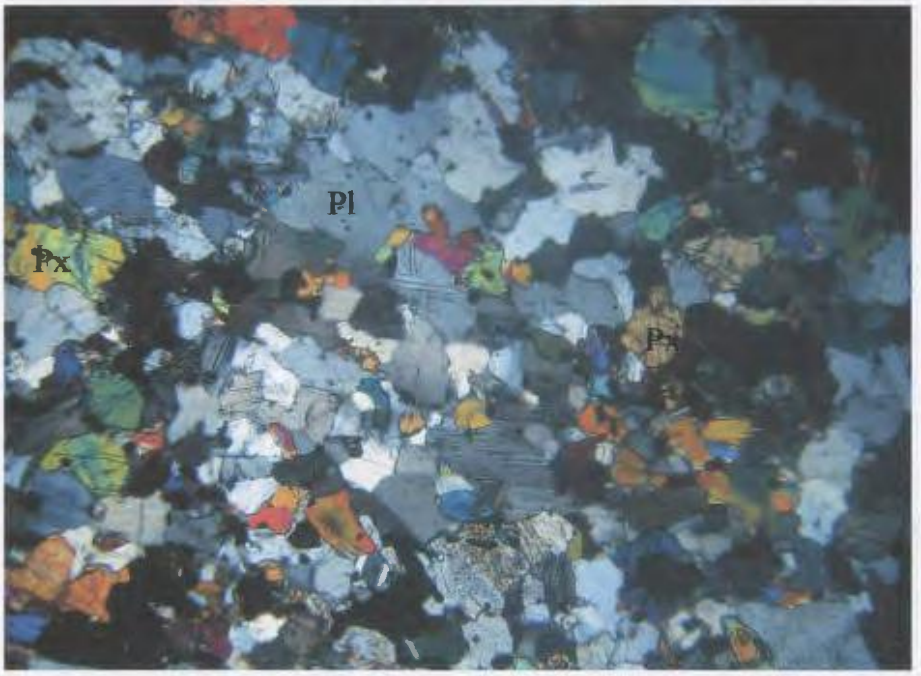

Plate 2-6. Photomicrograph of sample BIV 8, a mafic rock from the small island west of Barth Island. Crossed polars. This mafic rock is similar in both composition and texture to ferrogabbroid of the Barth Island Ring Complex. Pl = plagioclase; Px = pyroxene. Field of view ca. 5.5 mm.

Plate 2-7. Photograph of leucotroctolite, taken north of Nain Bay. Rock hammer is ca. 0.5 m.

Plate 2-8. Photograph of olivine-rich layer (deep red) in troctolite (white), taken north of Nain Bay. The layer is truncated by a dyke of monzonite. Pencil is ca. 0.1 m.

Plate 2-9. Photograph of z-structure in troctolite, taken on the north side of Nain Bay. The black line is placed above the structure and is drawn parallel to it. Pen is ca. 0.1 m.

Plate 2-10. Photograph of folded layers in troctolite, taken on the north side of Nain Bay. The black line is placed inside one of the fold hinges. Notebook cover circle diameter is 7 cm.

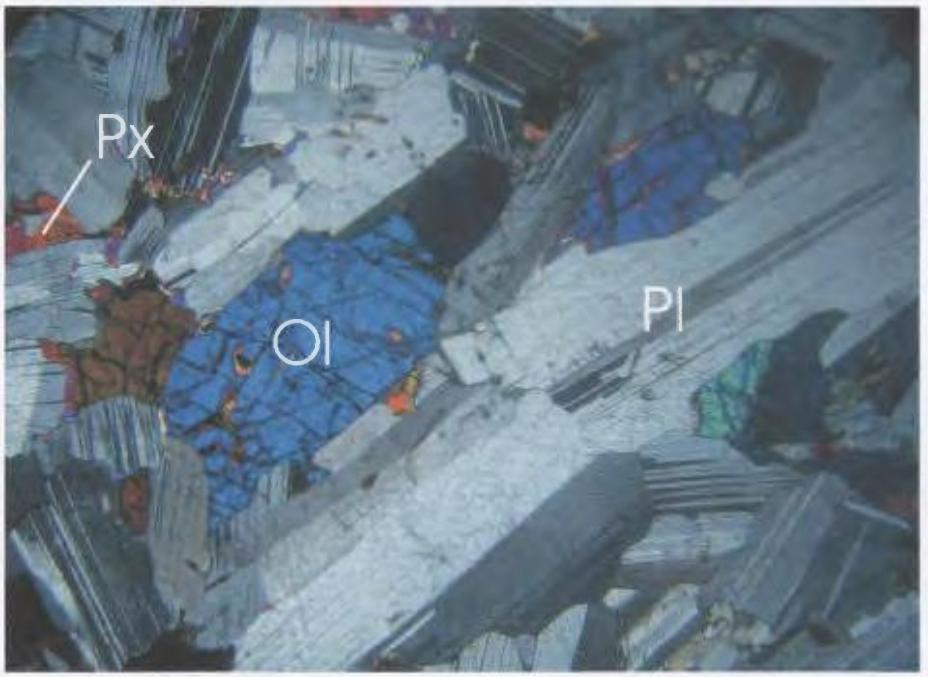

Plate 2-11. Photomicrograph of troctolite sample BII 12a, north of Nain Bay. Crossed polars. Typical troctolite. Note the coarse, euhedral plagioclase (Pl), subhedral olivine (Ol), and interstitial, anhedral pyroxene (Px). Field of view ca. 5.5 mm.

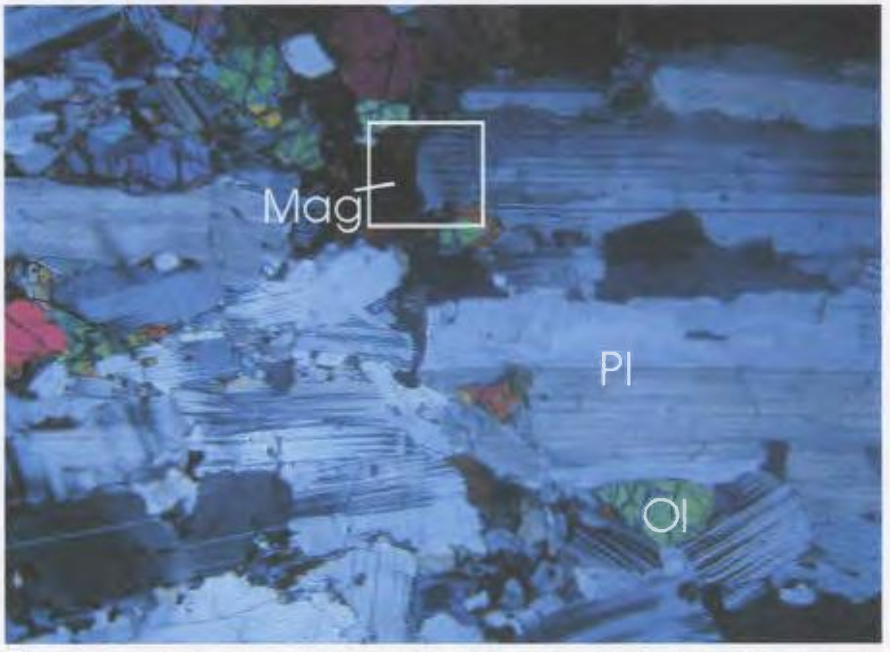

Plate 2-12. Photomicrograph of troctolite sample BS 5d, near the northwest contact with ferrogabbroid. Crossed polars. Note the alignment of the long direction of plagioclase (Pl) grains. Also note incipient granulation (subgrain formation) along the edges of the large plagioclase. The box surrounds the euhedral terminus of a plagioclase against magnetite (Mag). Ol = olivine. Field of view ca. 5.5 mm.

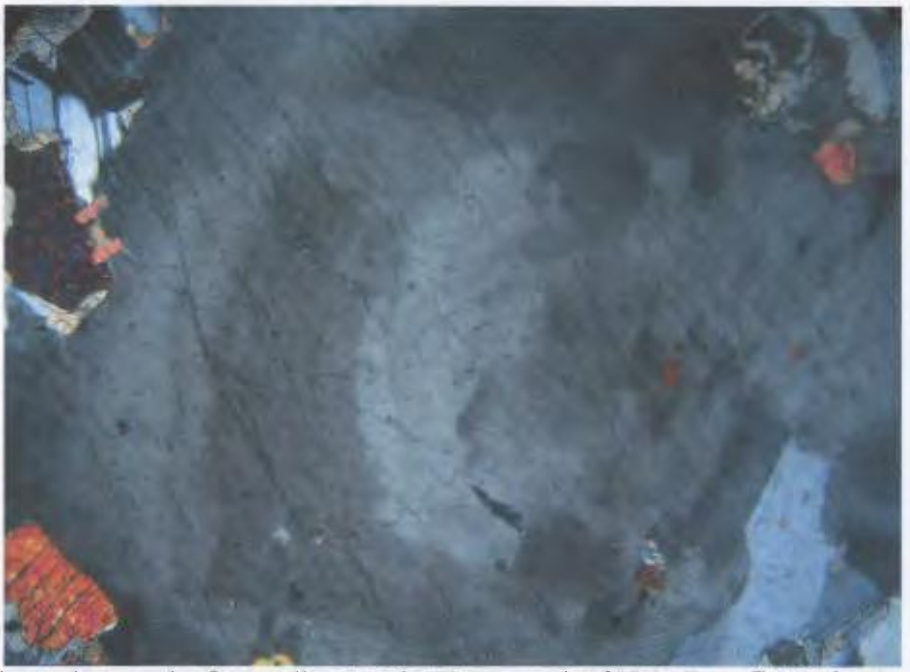

Plate 2-13. Photomicrograph of troctolite sample BI 32, north of Nain Bay. Crossed polars. A coarse plagioclase crystal. Chemical zoning is manifested in the different shades gray. Field of view ca. 5.5 mm.

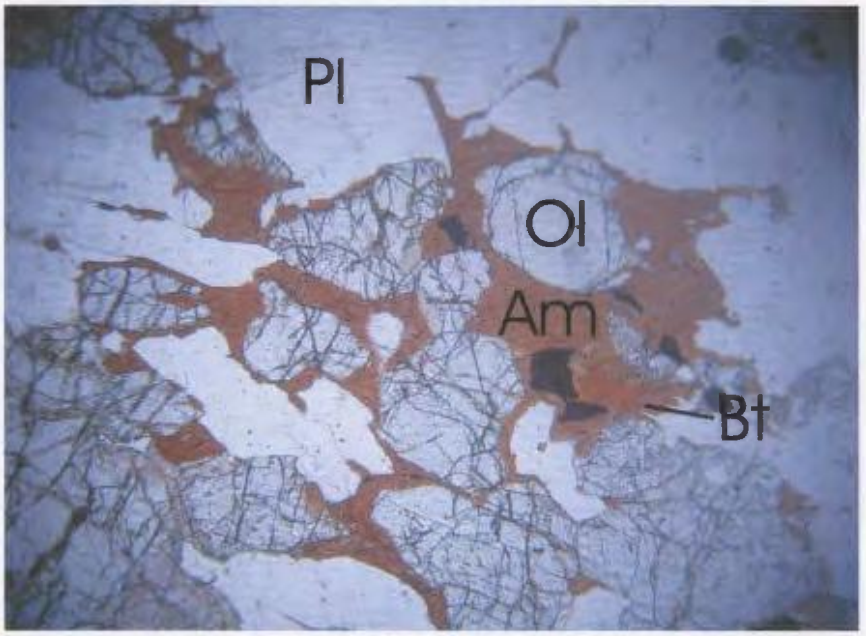

Plate 2-14. Photomicrograph of troctolite sample BI 16, north of Nain Bay. Plane polarized light. Coarse subhedral and euhedral olivine (Ol) mantled by amphibole (Am). Note the strong red-brown colour of the latter mineral. Also observe the lack of any alteration and euhedral terminations of olivine against amphibole. The amphibole is completely anhedral; its form is controlled by olivine and plagioclase. A small biotite (Bt) crystal, also deep red-brown, is associated with the amphibole. Pl = plagioclase. Field of view ca. 5.5 mm.

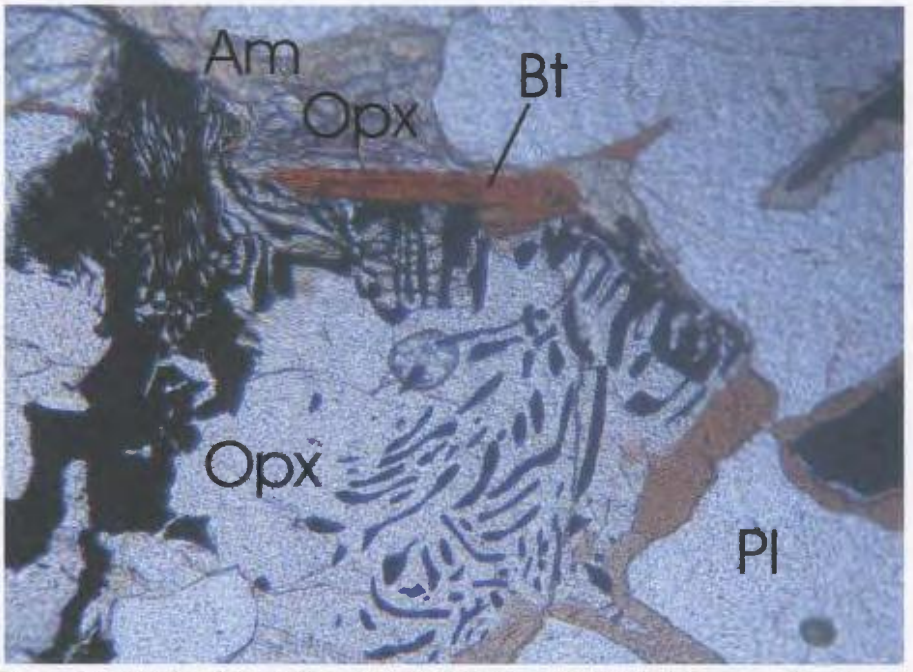

Plate 2-15. Photomicrograph of troctolite sample BII 12a, north of Nain Bay. Plane polarized light. Magnetite (black mineral) at the edges of, and as wormlike intergrowths with orthopyroxene (Opx). The pyroxene is rimmed by amphibole (Am); the small, deep red-brown bladelike crystal at top is biotite (Bt). Pl = plagioclase. Field of view ca. 1.5 mm.

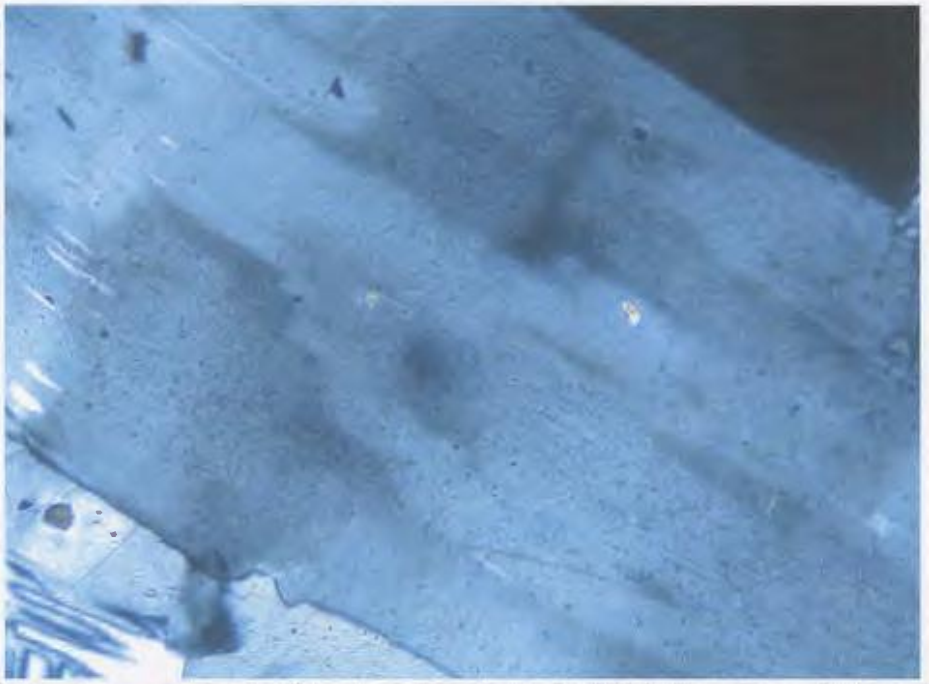

Plate 2-16. Photomicrograph of troctolite sample BS 5d, north of Nain Bay. Crossed polars. Tiny, dark needlelike inclusions in plagioclase. The abundance of the needles is associated with chemical zoning in the grain. Chemical zoning is demarcated by grain darkness. Field of view ca. 1.5 mm.

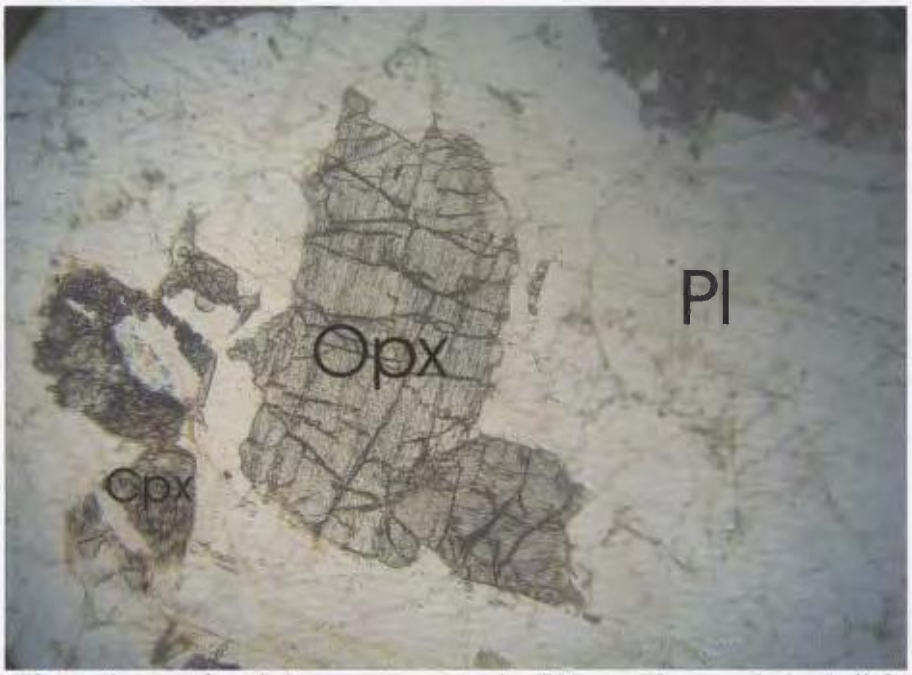

Plate 2-17a. Photomicrograph of leuconorite sample BII 4. Plane polarized light. Euhedral orthopyroxene crystal (Opx) surrounded by plagioclase (Pl); some interstitial, anhedral cpx (Cpx) is also present. The darkness of the crystals, especially noticeable in the clinopyroxene grains, is caused in large part by inclusions of opaque minerals and rutile. Field of view ca. 5.5 mm.

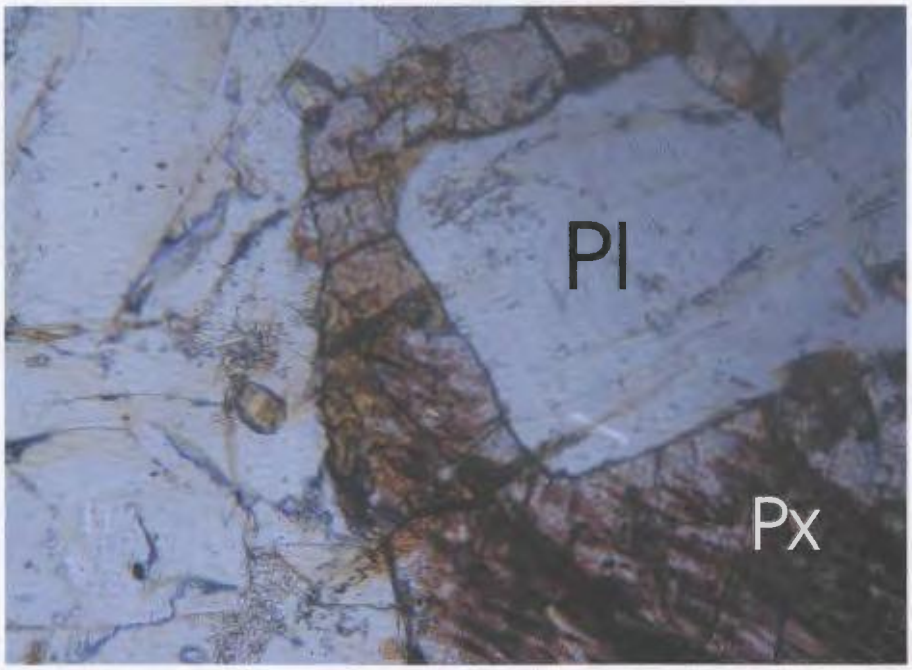

Plate 2-17b. Photomicrograph of leuconorite sample BS 4d. Plane polarized light. Exsolution of rutile (small red crystals) in an interstitial pyroxene grain (Px). Note also the euhedral terminus of the plagioclase crystal (Pl) it is contact with. Field of view ca. 1.5 mm.

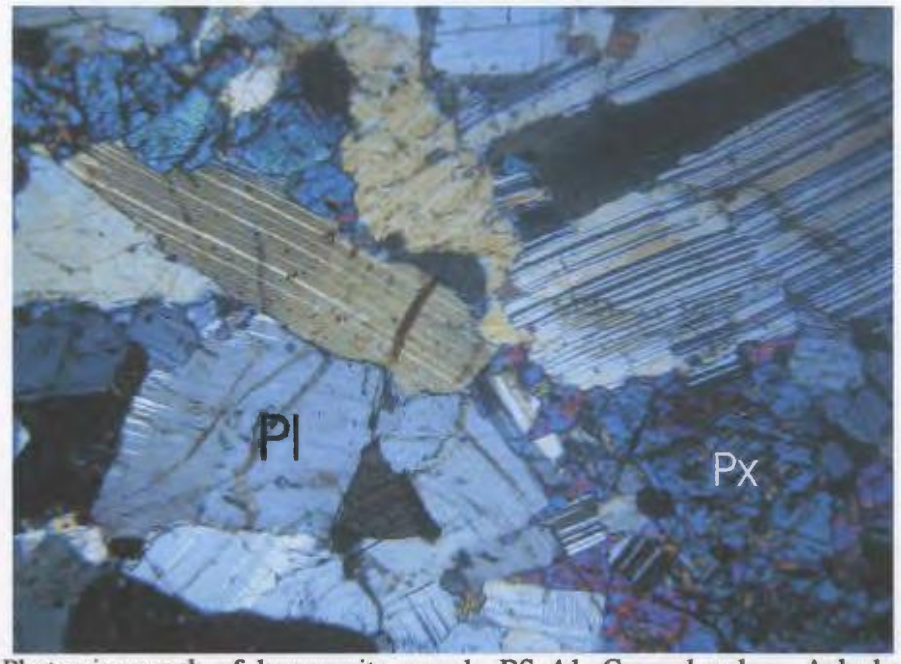

Plate 2-18. Photomicrograph of leuconorite sample BS 4d. Crossed polars. Anhedral and minor subhedral pyroxenes (Px) surrounded by subhedral and euhedral plagioclase (Pl). Dark spots on the pyroxene crystals are inclusions of opaque minerals and rutile. Field of view ca. 5.5 mm.

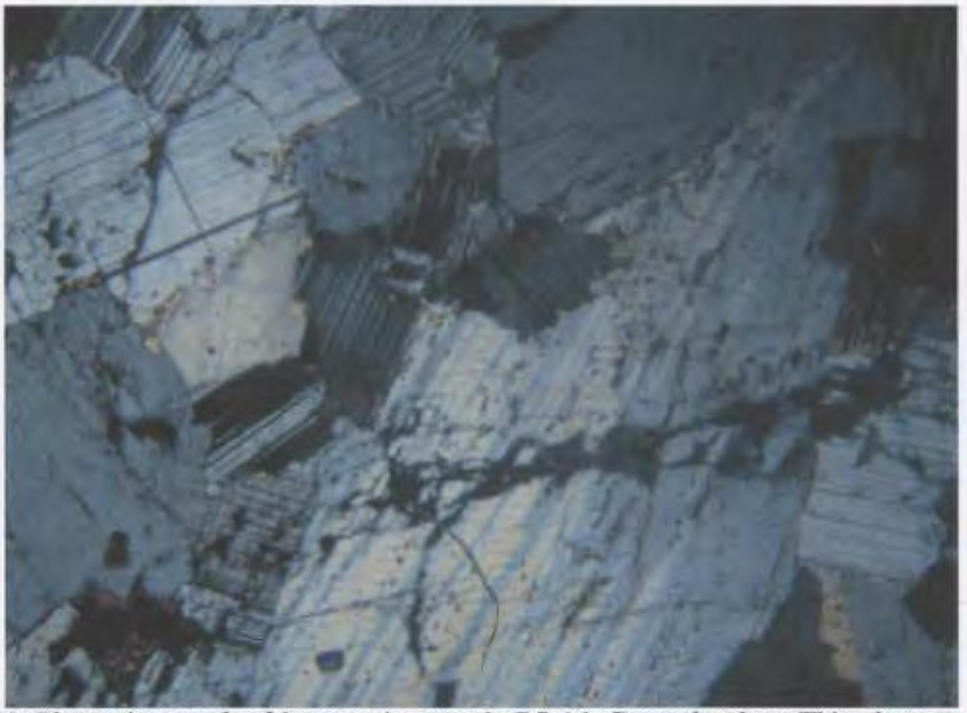

Plate 2-19. Photomicrograph of leuconorite sample BS 1d. Crossed polars. This photo illustrates the primarily subhedral plagioclase typical of much of the leuconorite. Field of view ca. 5.5 mm.

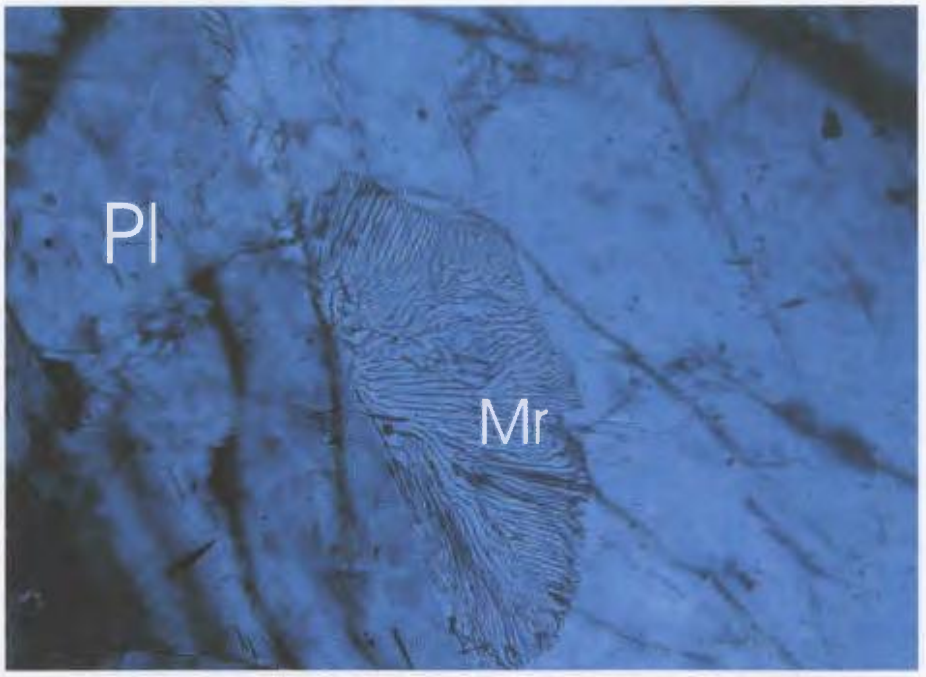

Plate 2-20. Photomicrograph of leuconorite sample BS 4d. Crossed polars. Myrmekitic (Mr) textures caused by exsolution. It is not clear what minerals are involved in the exsolution; it is most likely alkali feldspar and quartz. Field of view ca. 1.5 mm.

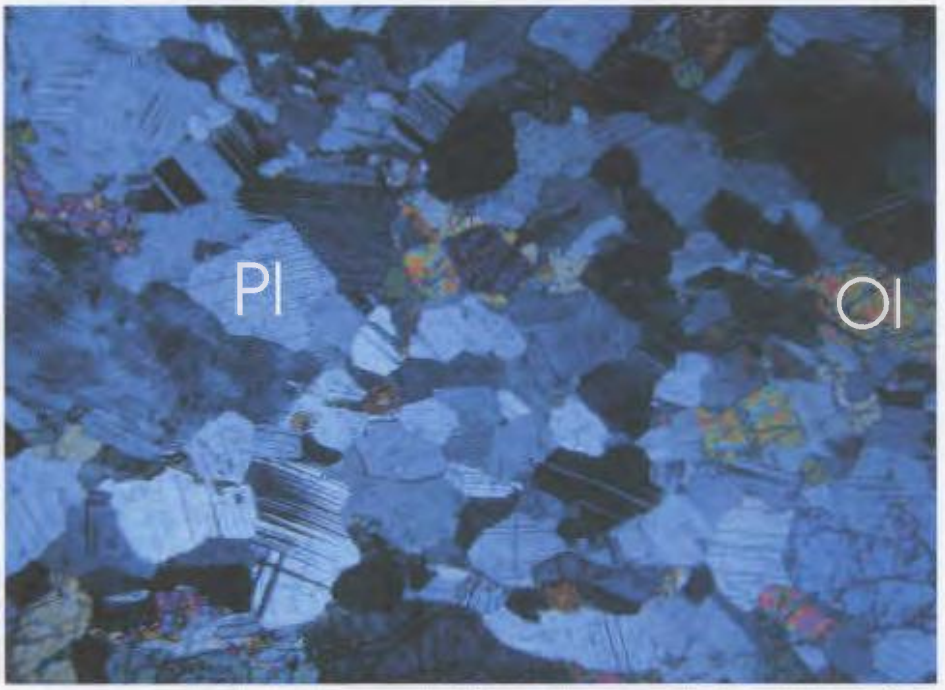

Plate 2-21. Photomicrograph of troctolite sample BI 37, taken from the isolated body in the northeast corner of the complex. Crossed polars. Typical texture of the marginal troctolite. Notice the equigranular domain of plagioclase (Pl) and olivine (Ol) at center, compared to the more coarse plagioclase and olivine at the sides and bottom of the photo. Field of view ca. 5.5 mm.

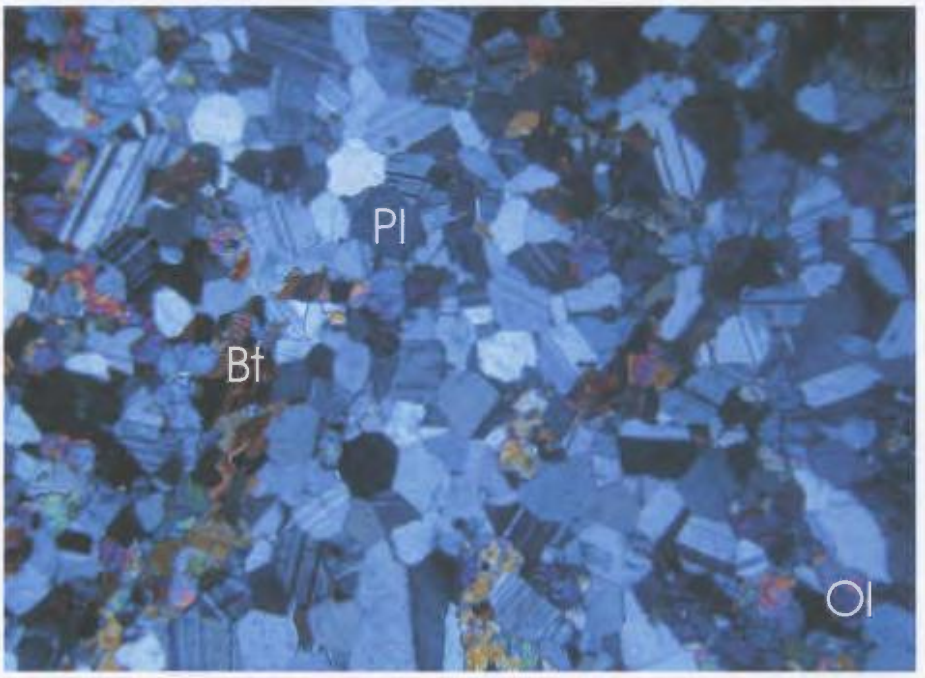

Plate 2-22. Photomicrograph of troctolite sample BII 81. Crossed polars. This texture is typical of samples collected near location B (fig. 2-1). Plagioclase (Pl) is equigranular and polygonal; intergrain junctions are commonly at or near 120 degrees. Ol = olivine; Bt = biotite. Field of view ca. 5.5 mm.

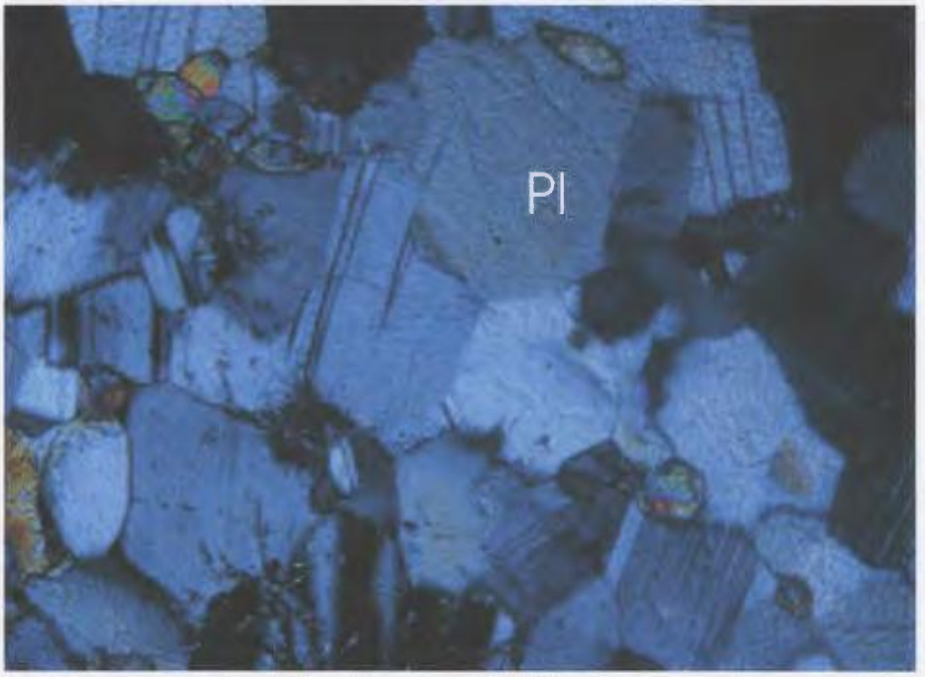

Plate 2-23. Photomicrograph of troctolite sample BII 42a. Crossed polars. Plagioclase grain boundaries at center are the intersection of three polygonal grains; the dihedral angle is 120 degrees. Pl = plagioclase. Field of view ca. 1.5 mm.

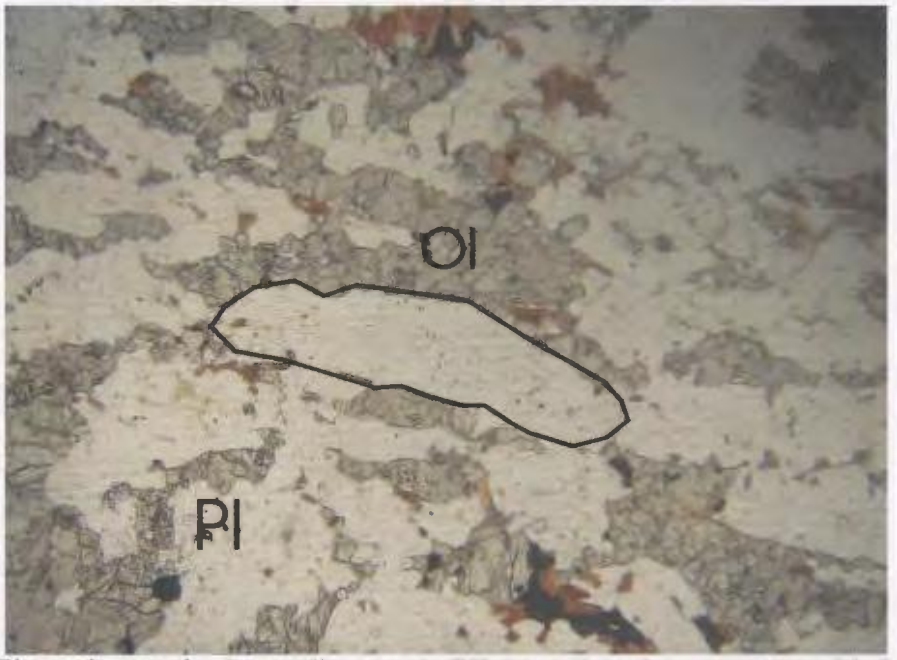

Plate 2-24a. Photomicrograph of troctolite sample BII 82, collected near contact with ferrogabbroid. Plane polarized light. The shape of original igneous plagioclase grains are delineated by olivine grains. The black line outlines what appears to have been a single plagioclase crystal. Ol = olivine; Pl = plagioclase. Field of view ca. 5 mm.

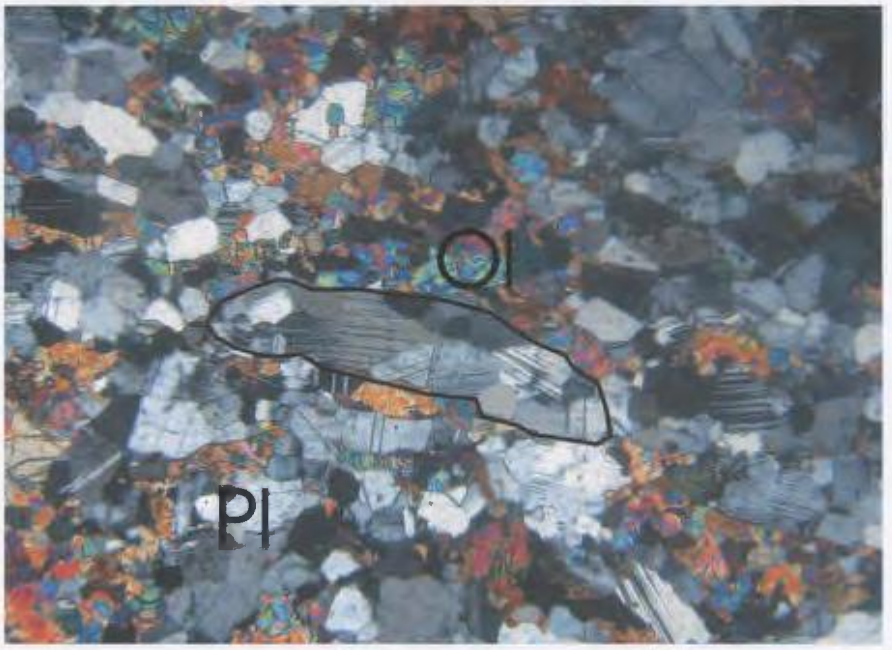

Plate 2-24b. Photomicrograph of sample BII 82. Crossed polars. With the polars crossed, the area that appeared to be a single euhedral, plagioclase grain in plane polarized light can be seen to be multiple grains, some of which have a polygonal texture. Ol = olivine; pl = plagioclase. Field of view ca. 5 mm.

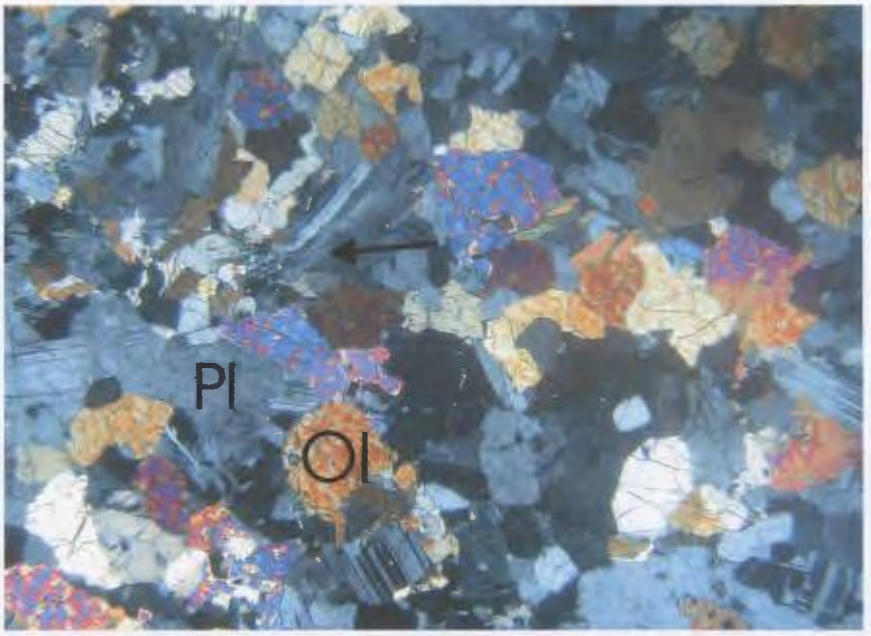

Plate 2-25. Photomicrograph of troctolite sample BS 2a. Crossed polars. This sample has a mixture of polygonal-textured domains and subhedral grains. The arrow points to plagioclase deformation manifested in bent twin planes. The section is slightly thinner than is normal, so olivine appears less strongly coloured. Pl = plagioclase; Ol = olivine. Field of view ca. 5.5 mm.

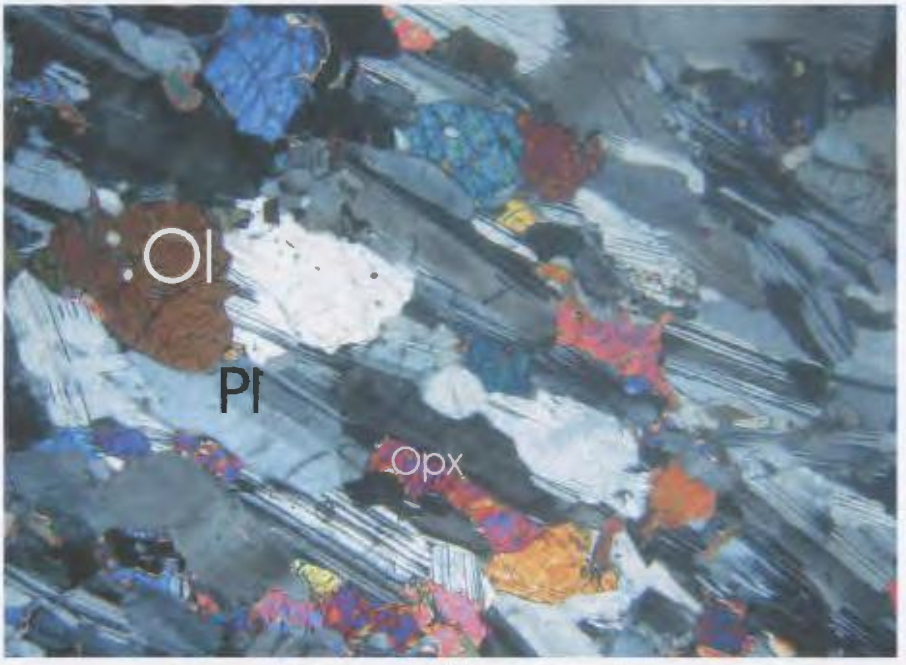

Plate 2-26. Photomicrograph of troctolite sample BS 2d. Crossed polars. Primarily igneous-textured coarse-grained troctolite displaying strong alignment of plagioclase. Pl = plagioclase; Ol = olivine; Opx = orthopyroxene. Field of view ca. 5.5 mm.

Plate 2-27. Photograph of average ferrogabbroid, taken on north side of Nain Bay. Notice the variation in grain size over small distances, and diffuse layering defined by grain size. Lens cap is 6 cm.

Plate 2-28. Photograph of fabric in ferrogabbroid, defined by elongate minerals. Photo taken on south side of Nain Bay. Also note diffuse grey layers; these are slightly more felsic areas. Camera case is ca. 12 cm.

Plate 2-29. Photograph of ferrogabbroid (Fg) mingled with monzonite-ferrogabbroid (Fg-mz) hybrid, taken north of Nain Bay. The contact is delineated by the black line. Notice the ferrogabbroid contains a few scattered white mesoperthite crystals. The monzonite-ferrogabbroid hybrid has a strong mineral alignment. Field notebook for scale.

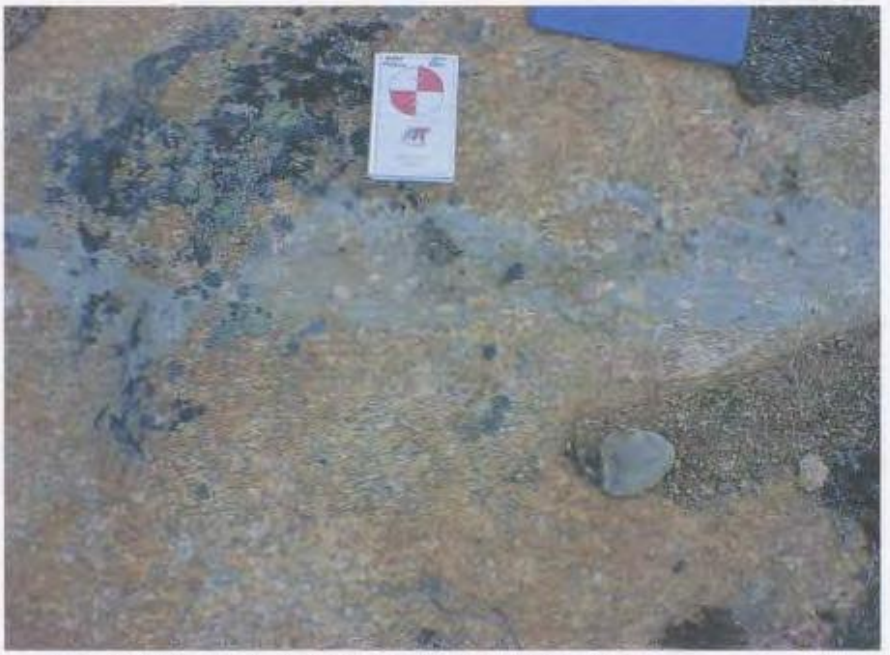

Plate 2-30. Photograph of interconnected ferrogabbroid globules (fine-grained, tan-brown areas) in monzonite, taken in the northeastern corner of the ring complex. Note the large white phenocrysts of mesoperthite inside the fine-grained globules. Also observe the distinct alignment of mesoperthite in monzonite. The elongate direction of the globules parallels this alignment. Field notebook for scale.

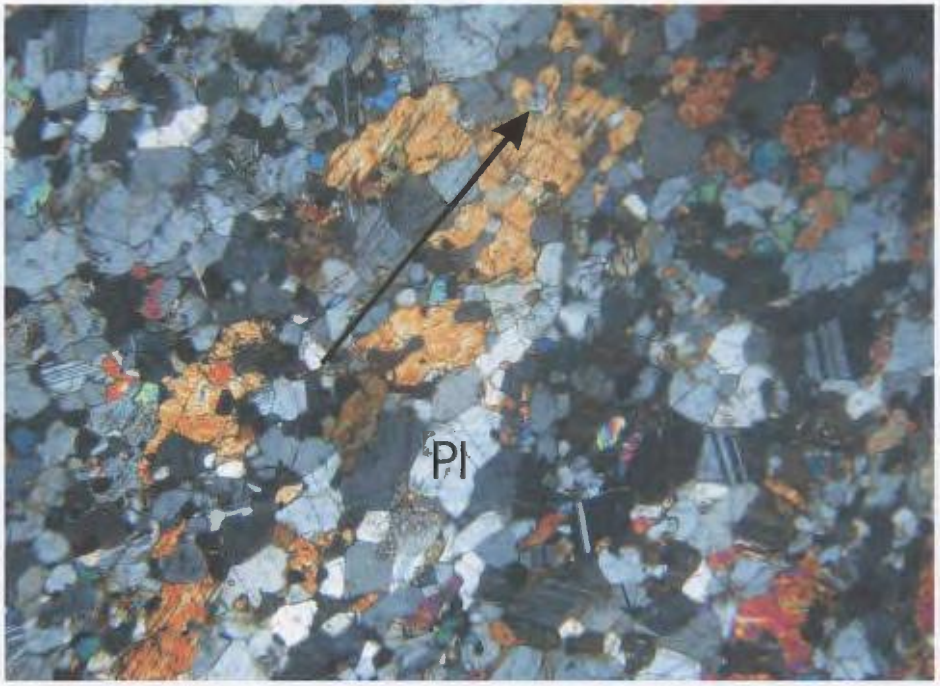

Plate 2-31. Long direction of orange subophitic orthopyroxene aligned with the orientation of the long direction of anhedral plagioclase in ferrogabbroid sample BS 7c (south of Nain Bay). Arrow shows direction of elongation. Plagioclase = Pl. Field of view ca. 5.5 mm.

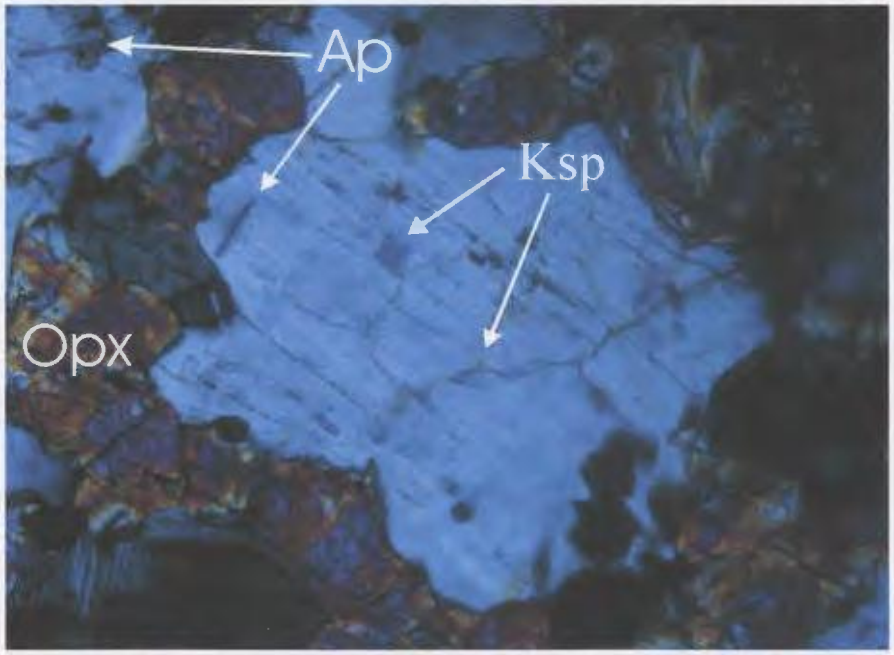

Plate 2-32. Photomicrograph of ferrogabbroid sample BII 62, north of Nain Bay. Crossed polars. Anhedral plagioclase with dark areas which are exsolution of potassium feldspar (Ksp). The antiperthite grain is surrounded by an optically continuous orthopyroxene (Opx) (see text). Also note small, euhedral apatite (Ap) as inclusions in plagioclase. Field of view ca. 1.5 mm.

Plate 2-33. Photomicrograph of ferrogabbroid sample LBE 9a, north of Nain Bay. Plane polarized light. Needles of an opaque mineral in plagioclase. The grain boundary is given by the black outline. The needles are partly surrounded by a needle-free zone. Field of view ca. 1.5 mm.

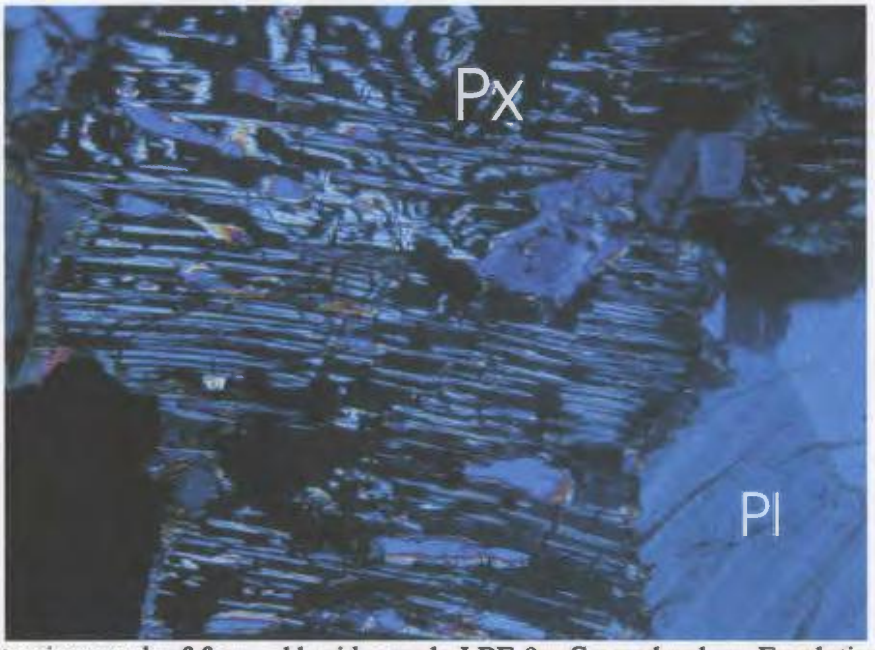

Plate 2-34. Photomicrograph of ferrogabbroid sample LBE 9a. Crossed polars. Exsolution textures in orthopyroxene. The orthopyroxene (Px) grain is in extinction and is therefore black. The brighter and blue colours within the black areas are exsolved clinopyroxene. Note the presence of both lamellar and blebby, irregular exsolution. Pl = plagioclase. Field of view ca. 1.5 mm.

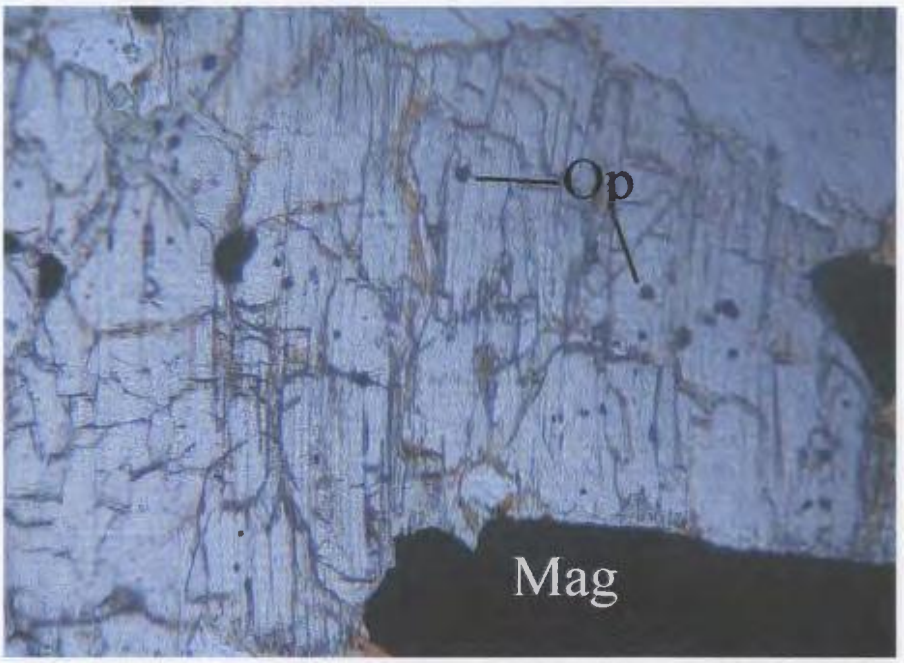

Plate 2-35. Photomicrograph of ferrogabbroid sample LBE 9a. Plane polarized light. Morphology of opaque inclusions in pyroxene in ferrogabbroid. Compare with plate 2-17b, which shows morphology of inclusions in noritic pyroxene. Magnetite = Mag; opaque = Op. Field of view ca. 1.5 mm.

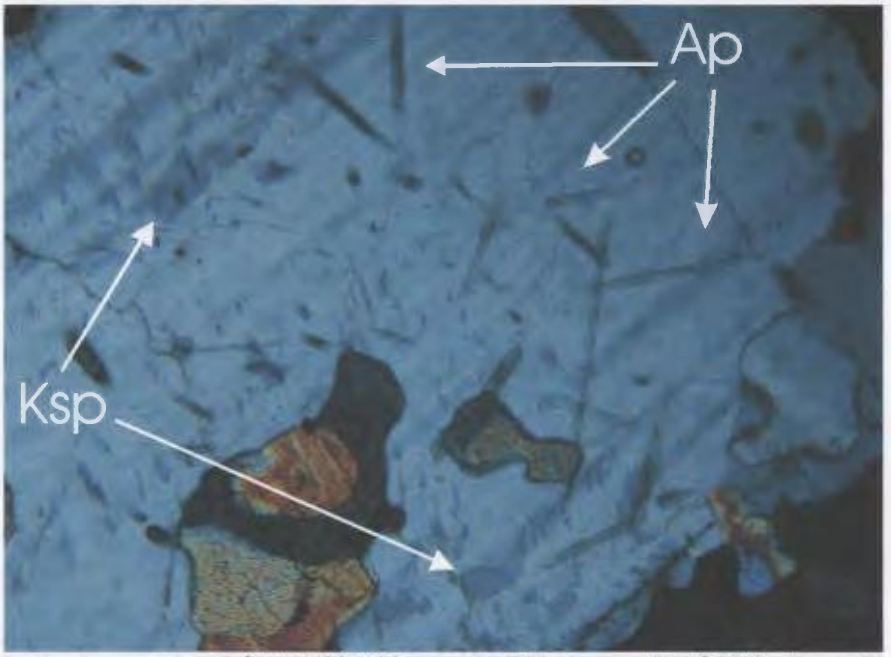

Plate 2-36. Photomicrograph of ferrogabbroid sample BII 62, north of Nain Bay. Crossed polars. Multiple apatite (Ap) inclusions in antiperthite. Note the random orientations of the euhedral apatite crystals. Dark patches in the antiperthite are exsolved K-feldspar (Ksp). Field of view ca. 1.5 mm.

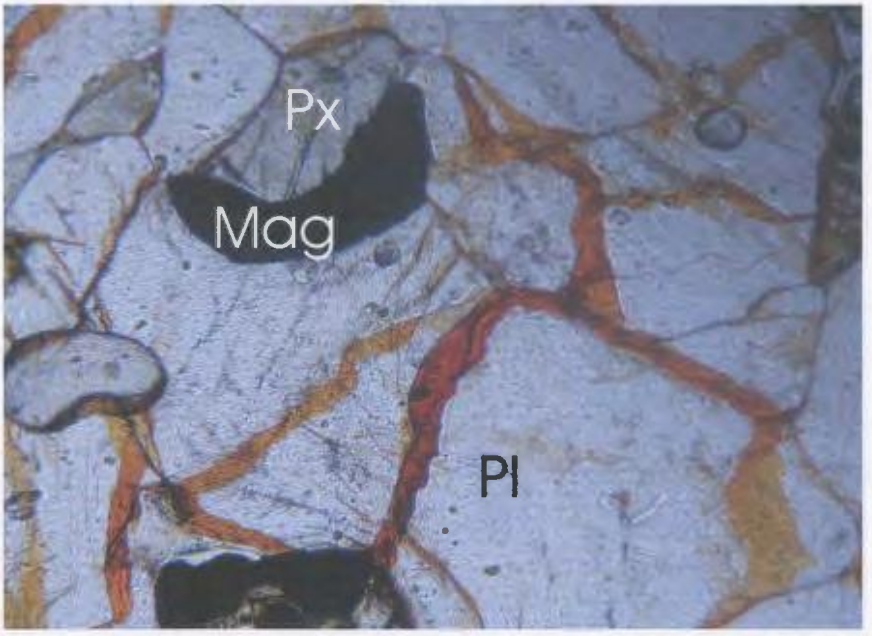

Plate 2-37. Photomicrograph of ferrogabbroid sample LBE 9a. Plane polarized light. An orange - red rim outlines nearly all grain boundaries in ferrogabbroids. This rim is also present in space created by fractures through minerals, and is probably an Fe-oxide. Pl = plagioclase; Px = pyroxene; Mag = magnetite. Field of view ca. 1.5 mm.

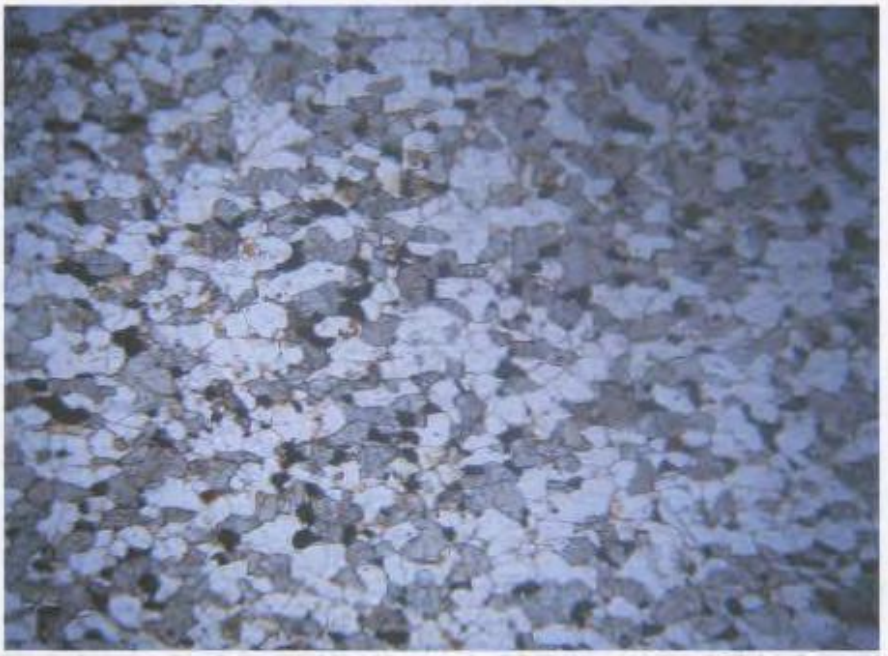

Plate 2-38. Photomicrograph of ferrogabbroid sample LBE 42, north of Nain Bay. Plane polarized light. The anhedral, equigranular texture of the fine-grained ferrogabbroids is well-illustrated. Note the distinct alignment of both plagioclase (white mineral) and pyroxene (darker mineral). The opaque mineral is magnetite. Field of view ca. 5.5 mm.

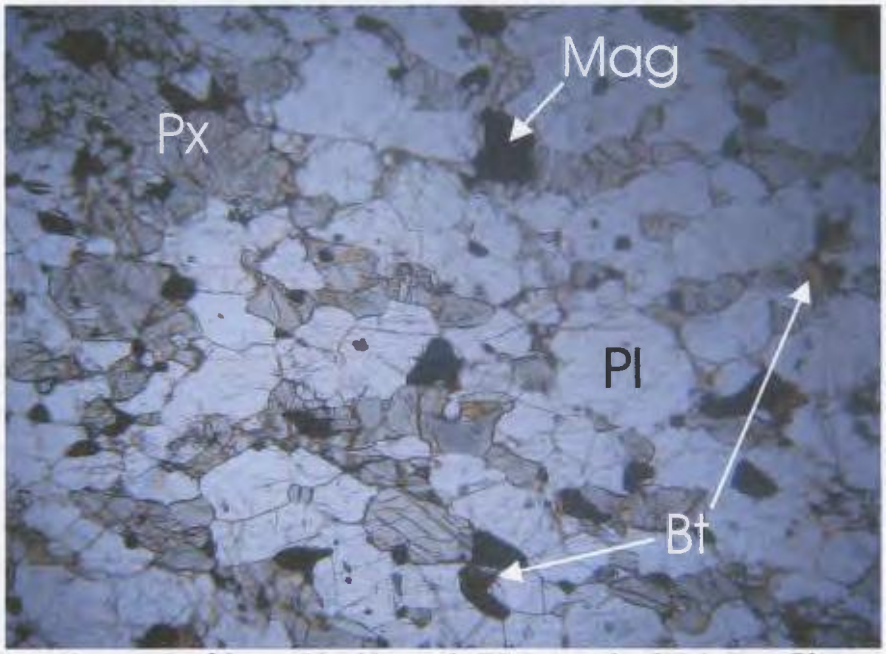

Plate 2-39. Photomicrograph of ferrogabbroid sample BS 9c, south of Nain Bay. Plane polarized light. The equigranular nature and slight alignment of minerals in a medium-grained ferrogabbroid. Note the few, scattered biotite grains (Bt). Pl = plagioclase; Px = pyroxene; Mag = magnetite. Field of view ca. 5.5 mm.

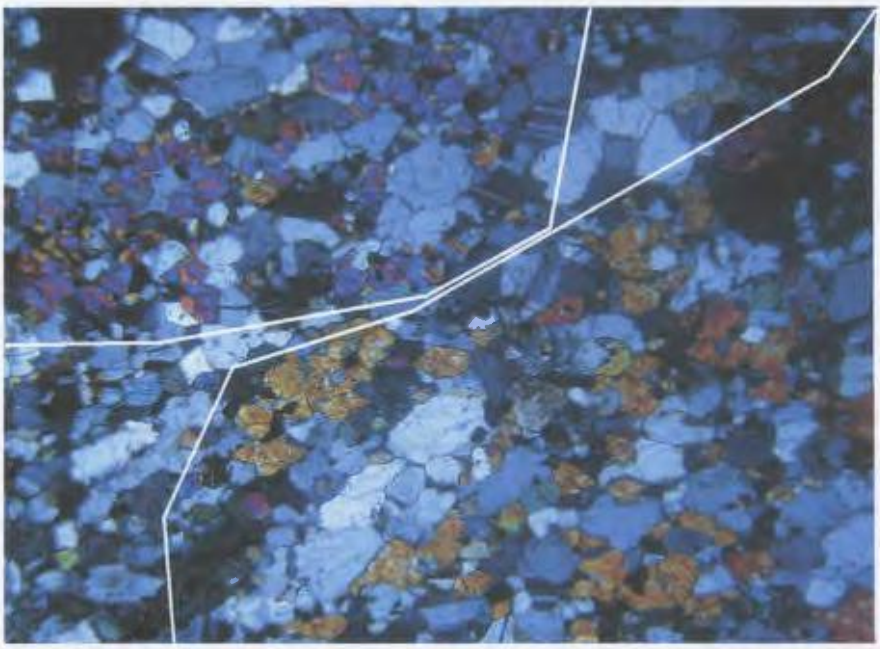

Plate 2-40. Photomicrograph of ferrogabbroid sample BS 7c. Crossed polars. Two optically continuous but spatially separate (oikocrystic) grains of orthopyroxene, both of which span the length of the field of view and are outlined by white boxes. The grain in the bottom half of the photo has first-order orange birefringence, and the upper grain shows second-order colours of blue and purple. Note that the overall texture of the section is equigranular with anhedral grains. Field of view ca. 5.5 mm.

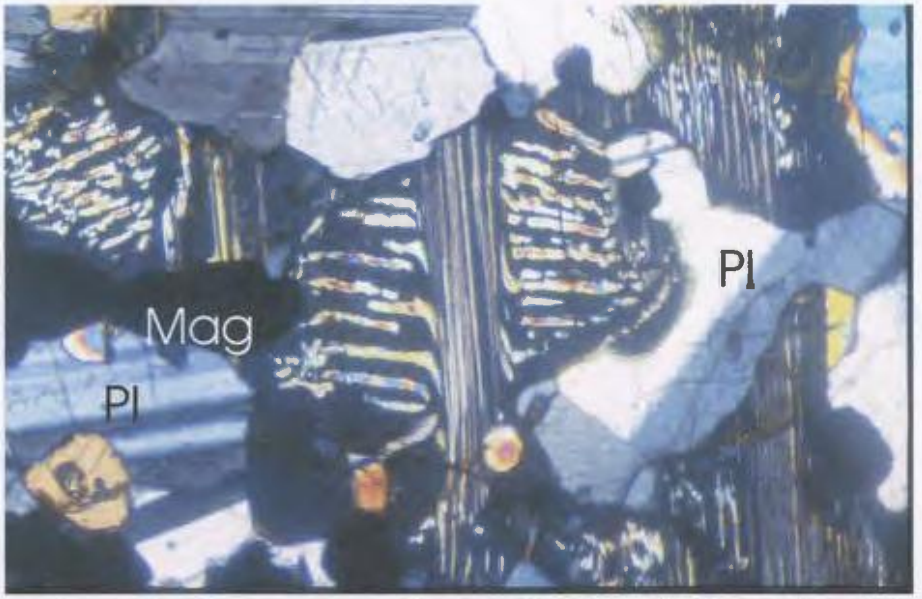

Plate 2-41. Photomicrograph, in orthopyroxene in ferrogabbroid sample BS 7b (south of Nain Bay), of possible shear movement along planes of exsolution. The orthopyroxene grain is in extinction; the bright or brightly coloured areas within it are exsolved clinopyroxene. Pl = plagioclase. Crossed polars. Field of view ca. 0.8 mm.

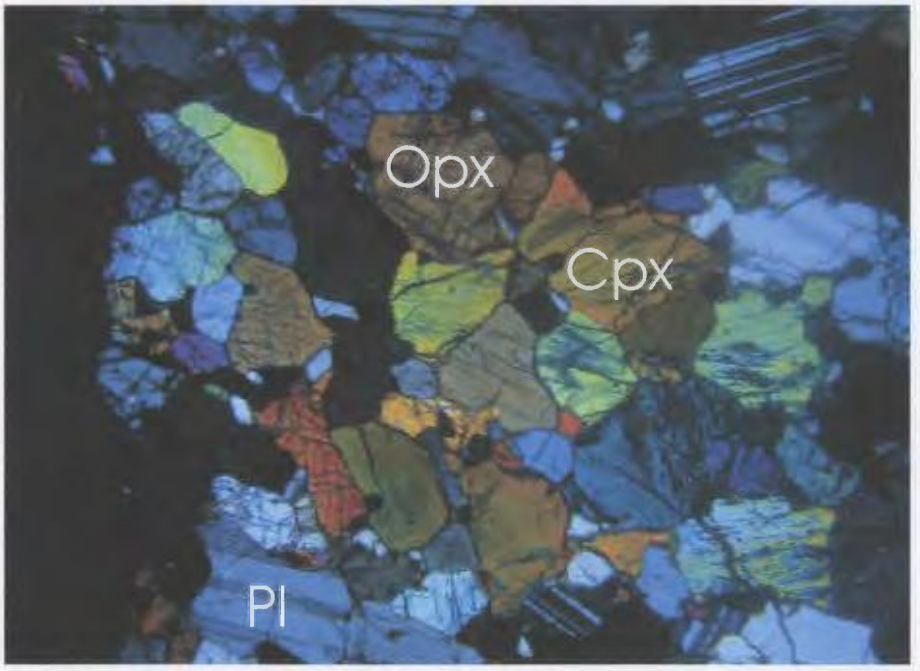

Plate 2-42. Photomicrograph of coarse-grained ferrogabbroid sample BS 7g, south of Nain Bay. Crossed polars. Most of the pyroxene in the aggregate is clinopyroxene (Cpx) although there is some orthopyroxene (Opx). Pl = plagioclase. Field of view ca. 5.5 mm.

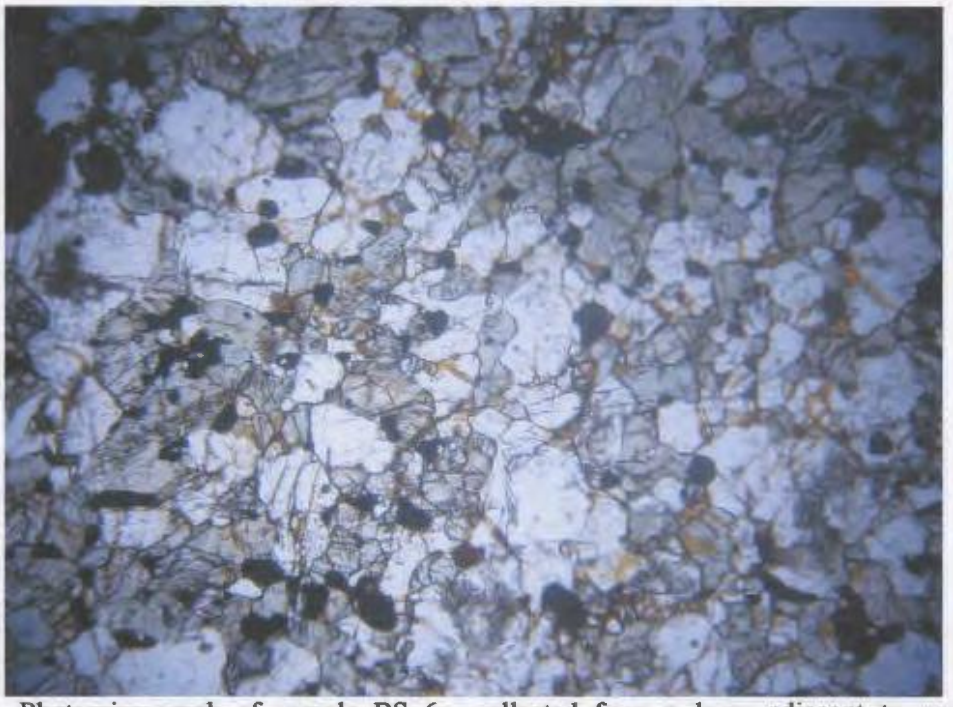

Plate 2-43. Photomicrograph of sample BS 6a, collected from a layer adjacent to contact with monzonite on the south side of Nain Bay. Plane polarized light. The texture of this rock is identical to medium-grained ferrogabbroid, but it has silica content much higher than typical ferrogabbroid. Field of view ca. 5.5 mm.

Plate 2-44. Photograph of densely packed xenocrystic plagioclase in ferrogabbroid, located on the south side of Nain Bay. Lens cap diameter 6 cm.

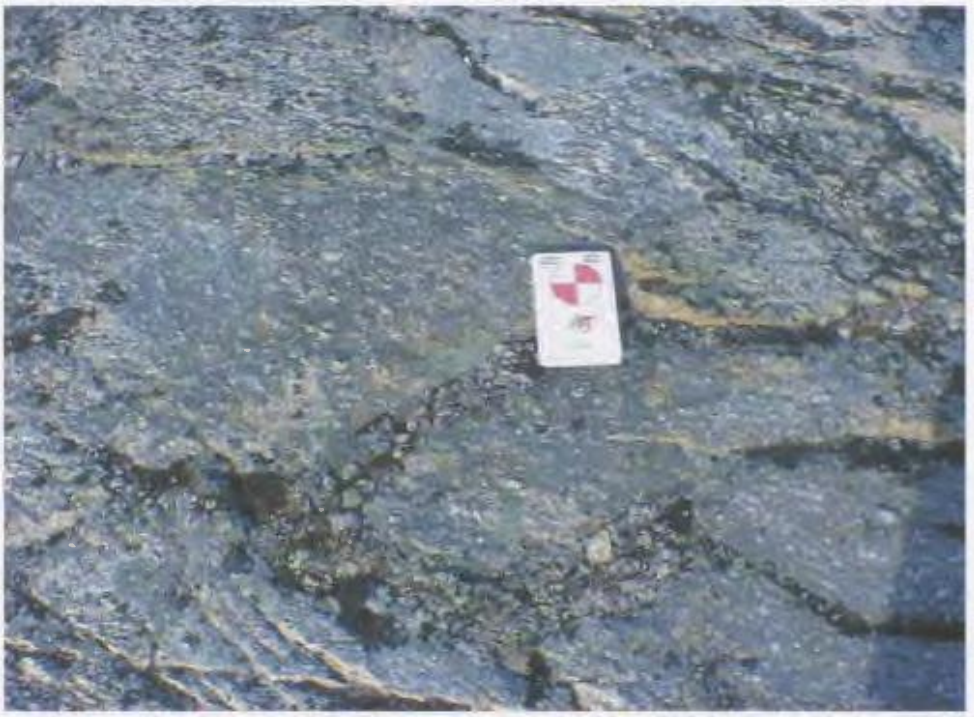

Plate 2-45. Photograph of monzonite, taken on the south side of Nain Bay. Circle on field notebook cover is 7 cm in diameter.

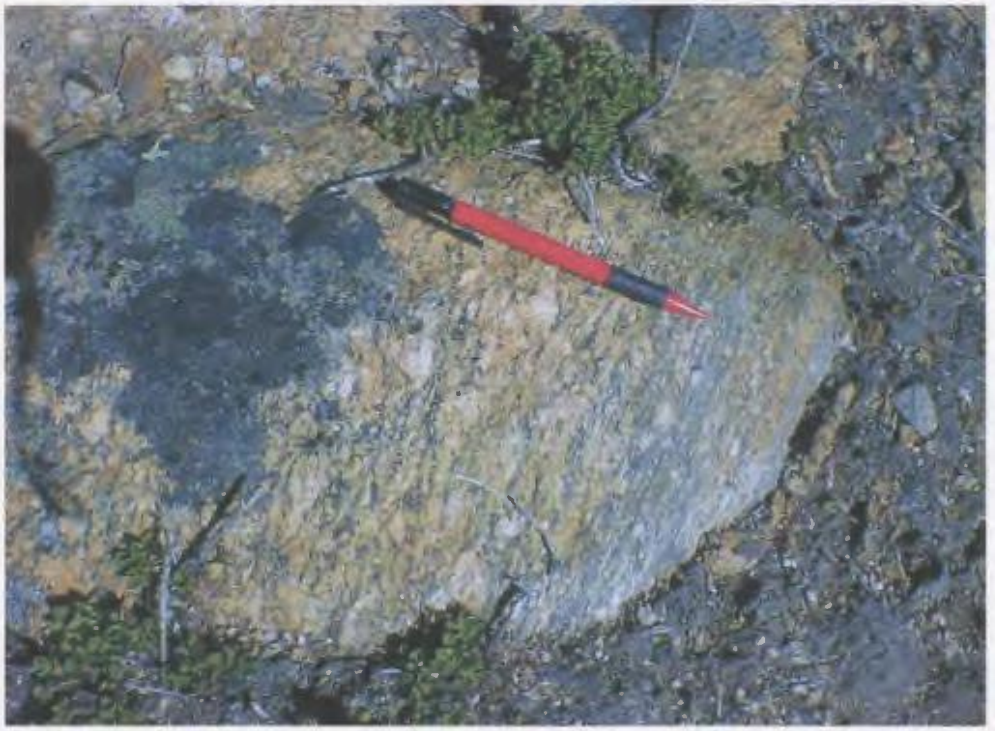

Plate 2-46. Photograph of monzonite showing strong foliation, and high modal proportion of mafic minerals compared to typical monzonite. Taken on the south side of Nain Bay. Pencil is ca. 1 dm.

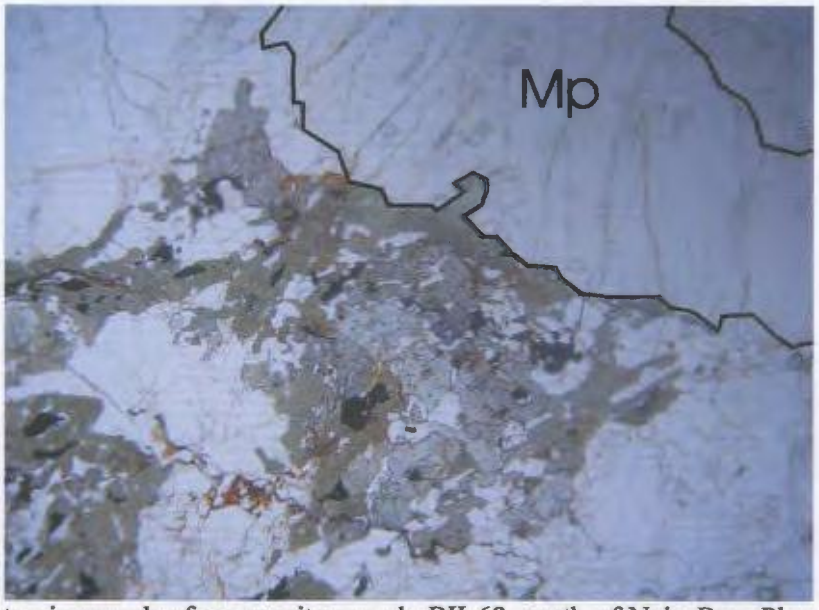

Plate 2-47. Photomicrograph of monzonite sample BII 68, north of Nain Bay. Plane polarized light. Typical monzonite. Mafic minerals (dark and coloured grains) are concentrated together as a medium-grained matrix which surrounds much coarser mesoperthite (Mp) crystals. The black outline delineates the edges of one such coarse crystal. The green mineral is amphibole; the grayish minerals are clinopyroxene. Field of view ca. 5.5 mm.

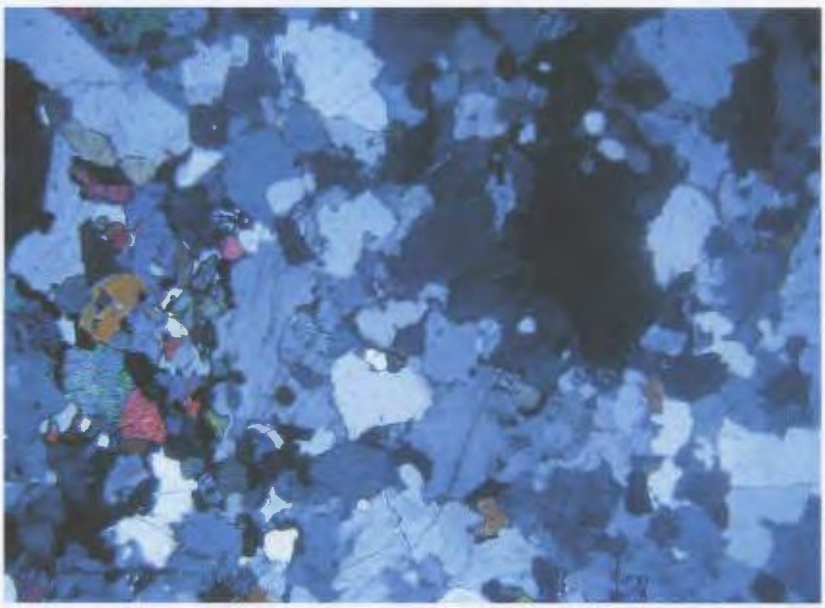

Plate 2-48. Photomicrograph of monzonitic sample BIII 20, west end of Barth Island. Crossed polars. This section has a more even grain size distribution than typical monzonite, but occurs as a domain in a thin section that also displays typical monzonite texture (not shown). The brightly coloured minerals are clinopyroxene and fayalitic olivine. Other minerals in the thin section are plagioclase, potassium feldspar, and quartz. Field of view ca. 5.5 mm.

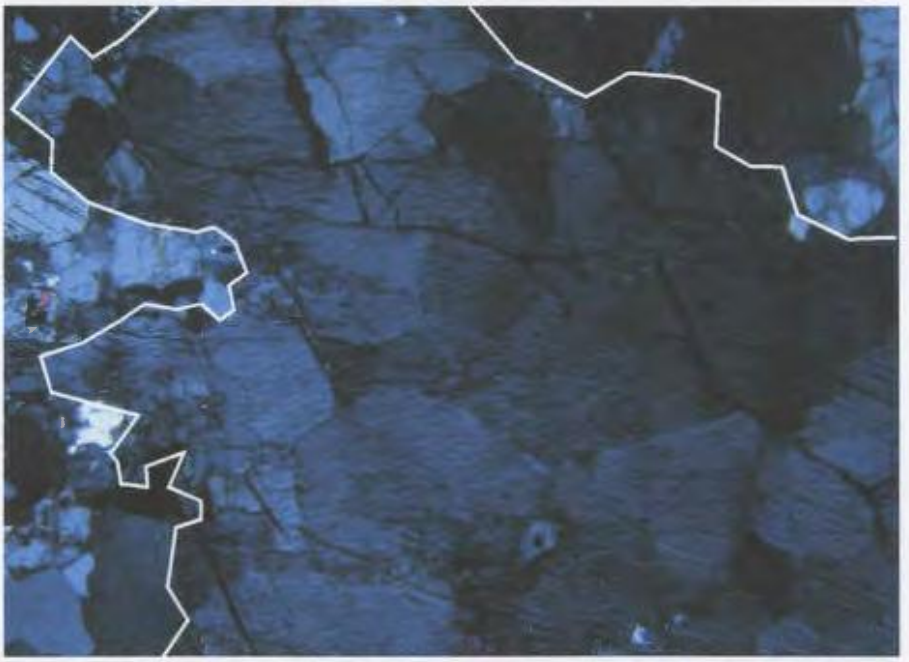

Plate 2-49. Photomicrograph of monzonite sample BS 6b. Crossed polars. Photo of undulatory extinction in a large mesoperthite grain, which signifies the development of subgrains. White outline marks the grain boundary, subgrains are delineated by the different brightnesses in the grain. Field of view ca. 5.5 mm.

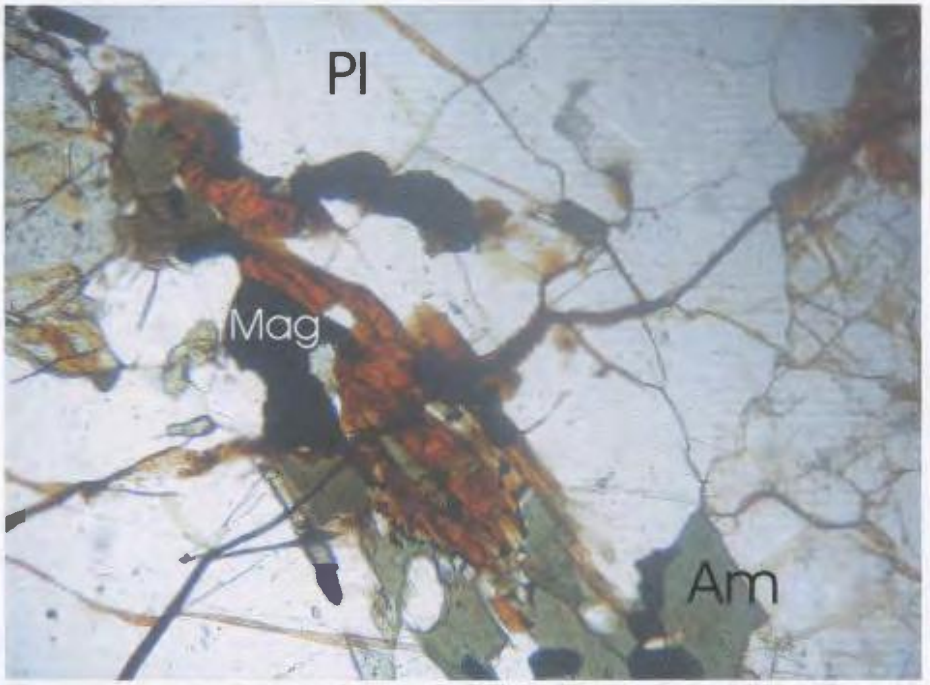

Plate 2-50. Photomicrograph of monzonite sample BII 68. Plane polarized light. The unidentified deep red mineral is a typical minor component of the monzonite and monzonite-ferrogabbroid hybrid rocks. Am = amphibole; pl = Plagioclase; Mag = magnetite. Field of view ca. 1.0 mm.

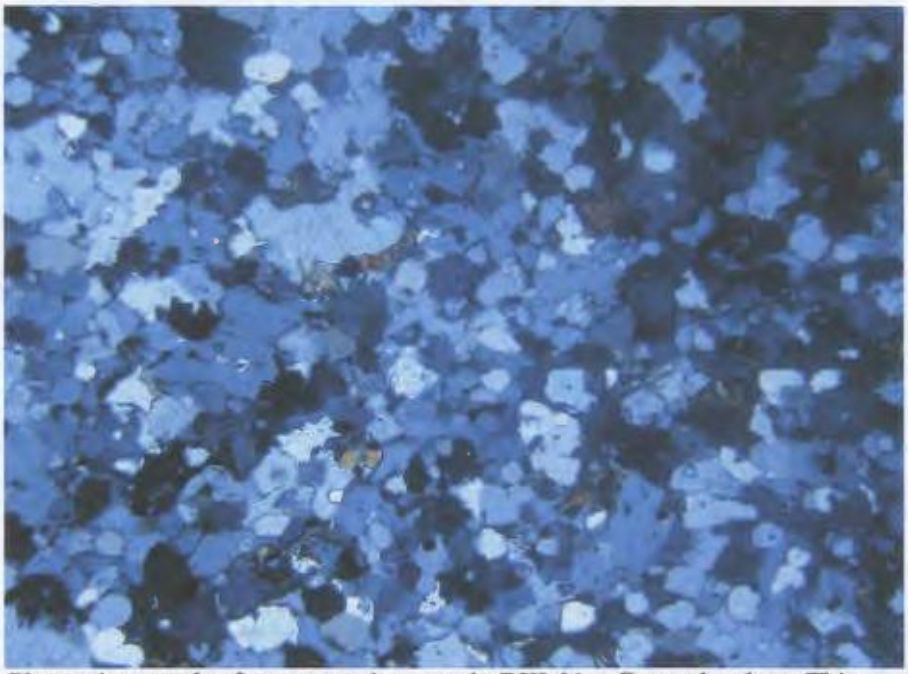

Plate 2-51. Photomicrograph of syenogranite sample BIII 21a. Crossed polars. This section has more equigranular texture and is more felsic than typical monzonite. Other minerals in the thin section are plagioclase, potassium feldspar, quartz, and minor pyroxene. Field of view ca. 5.5 mm.

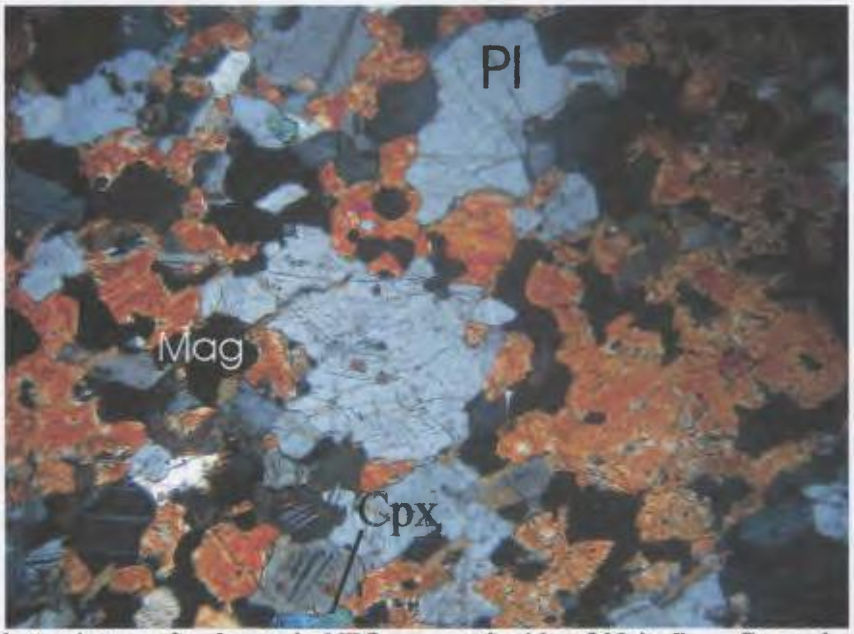

Plate 2-52. Photomicrograph of sample NBS 25, south side of Nain Bay. Crossed polars. This shot illustrates the texture and mineral assemblage of the fine-grained inclusions in monzonite. The orange mineral is a single orthopyroxene grain. The section is composed primarily of plagioclase and two pyroxenes, with a significant proportion of magnetite. Mag = magnetite; Pl = plagioclase, Cpx = clinopyroxene. Field of view ca. 5 mm.

Plate 2-54. Photomicrograph of monzonite sample BII 68. Plane polarized light. Apparent deformation of ductile mafic material around a large mesoperthite crystal in monzonite. Field of view ca. 5.5 mm.

Plate 2-55. Photograph of ferrogabbroid (dark) and monzonite pale), taken near the isolated body of troctolite in the northeastern corner of the complex. Note that the ferrogabbroid along the contact contains a few large crystals of mesoperthite. Also, note the curved boundaries between the two rocks. Pencil for scale.

Plate 2-56. Photograph of ferrogabbroid (rock under lens cap) and monzonite, taken on the west end of Barth Island. Note the lobate contacts; this appears to be a synplutonic dyke. Lens cap for scale.

Plate 2-57a. Photograph of troctolite-monzonite contact at the west end of Barth Island. Troctolite is darker rock at left; the arrow points to the contact. Hammer is ca. 0.5 m.

Plate 2-57b. Photograph of troctolite-monzonite contact at the west end of Barth Island. Monzonite is the light-coloured rock at top.

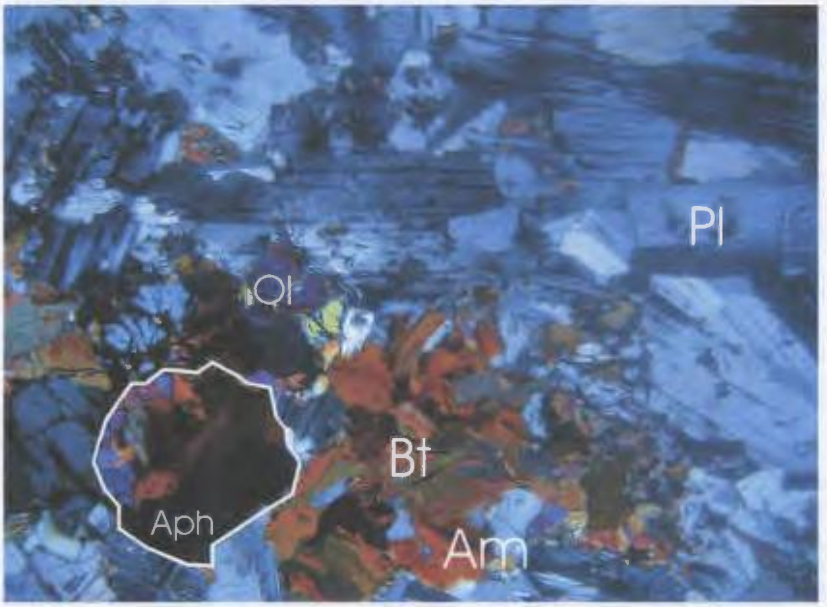

Plate 2-58a. Photomicrograph of sample BIII 19. Crossed polars. Troctolite near its contact with monzonite on the west end of Barth Island. Notice the coarse plagioclase (Pl). The white outline delineates amphibole as a pseudomorph (Aph) of olivine (Ol). A piece of the original olivine crystal is preserved at the left side of the amphibole crystal. Much of the biotite (Bt) and amphibole (Am) is secondary. Field of view ca. 5.5 mm.

Plate 2-58b. Photomicrograph of sample BIII 19. Plane polarized light. Photomicrograph of a monzonite vein (Mv) in troctolite host. The vein is surrounded by feldspar-pyroxene symplectite, which consists of elongate crystals (see text for discussion). Field of view ca. 5.5 mm.

Plate 2-59. Photograph of net-textured (interconnected) monzonitic dykes (white) intruding troctolite (reddish), taken in the northwestern corner of the ring complex. Field notebook for scale.

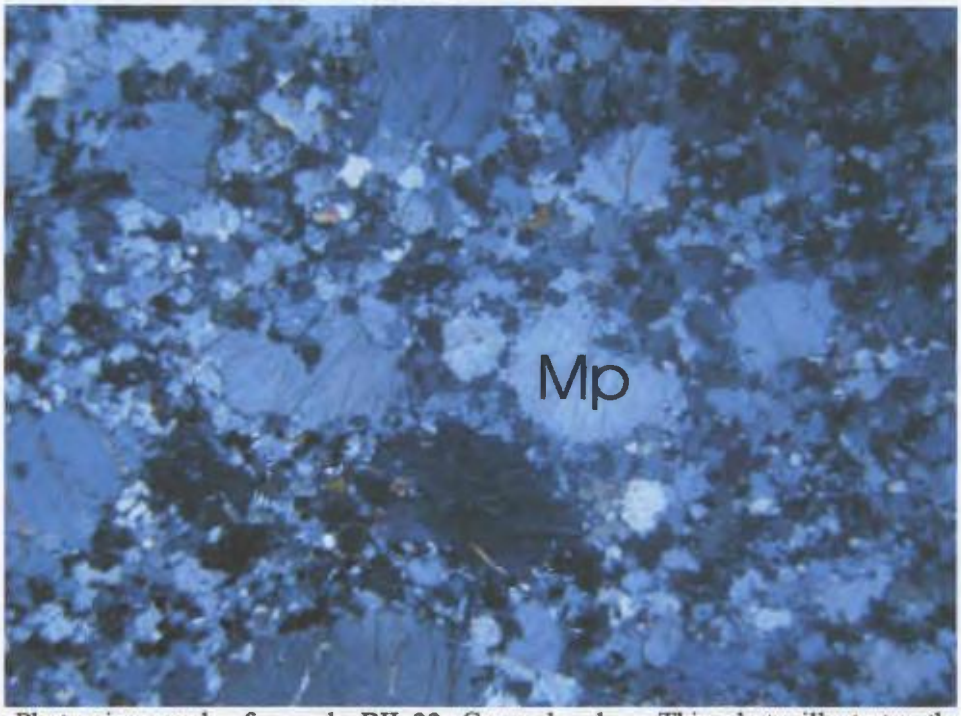

Plate 2-60. Photomicrograph of sample BII 22. Crossed polars. This photo illustrates the mineral assemblage and texture of one of the net-textured dykes. Though less coarse, the dykes are texturally similar to the monzonite. Mp = mesoperthite. Field of view ca. 5.5 mm.

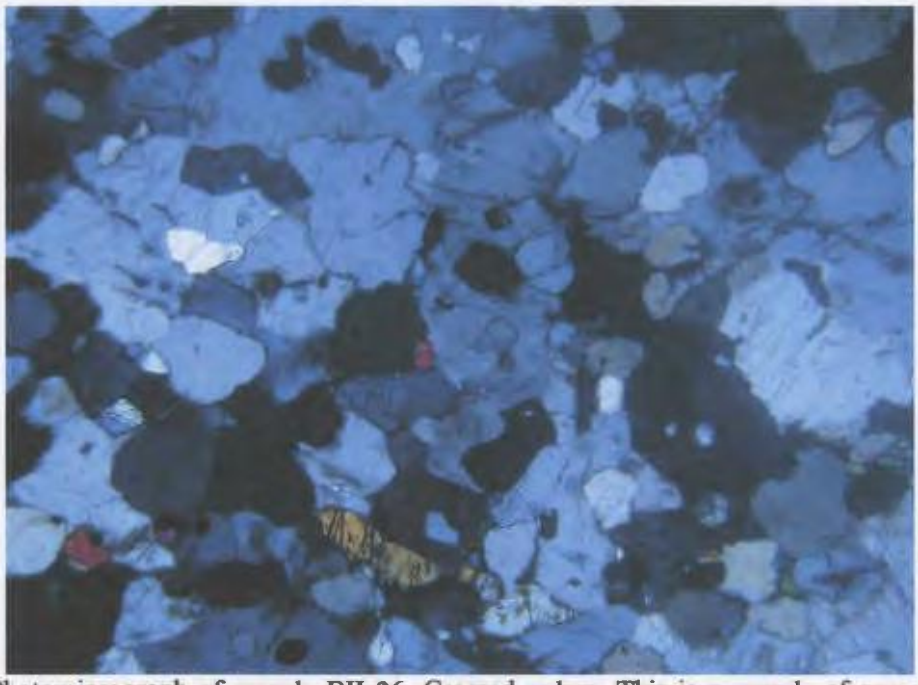

Plate 2-61. Photomicrograph of sample BII 26. Crossed polars. This is a sample of one of the net-textured dykes in the troctolite. Notice the subequigranular texture and felsic composition, which is similar to the syenogranite (plate 2-51). Field of view ca. 5.5 mm.

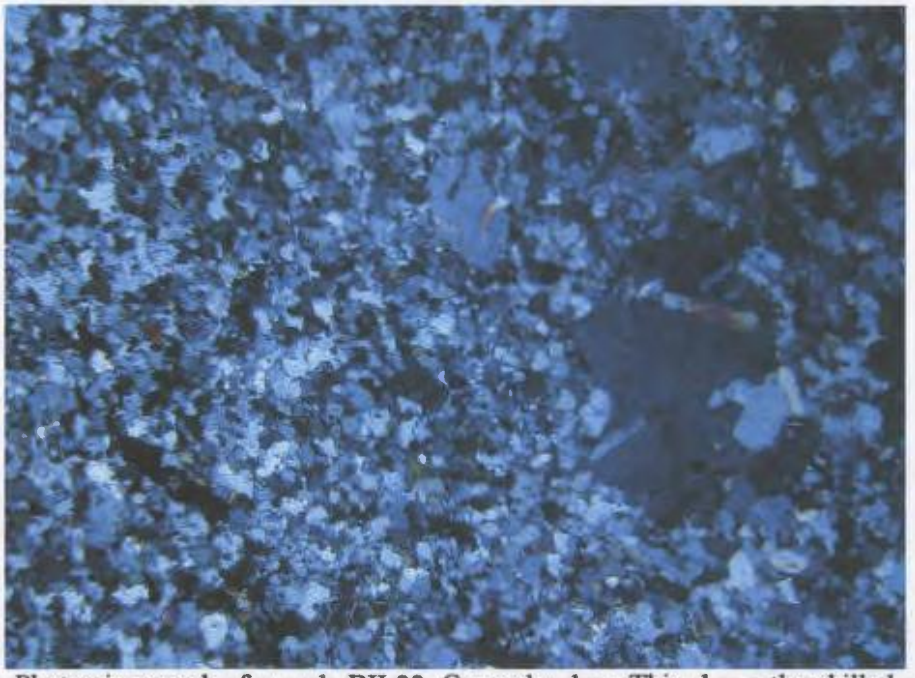

Plate 2-62. Photomicrograph of sample BII 22. Crossed polars. This shows the chilled margin of one of the felsic dykes in the troctolite. Note the fine-grained texture in the left side of the photo. The right side of the photo shows the bimodal grain size distribution typical of the monzonite. Field of view ca. 5.5 mm.

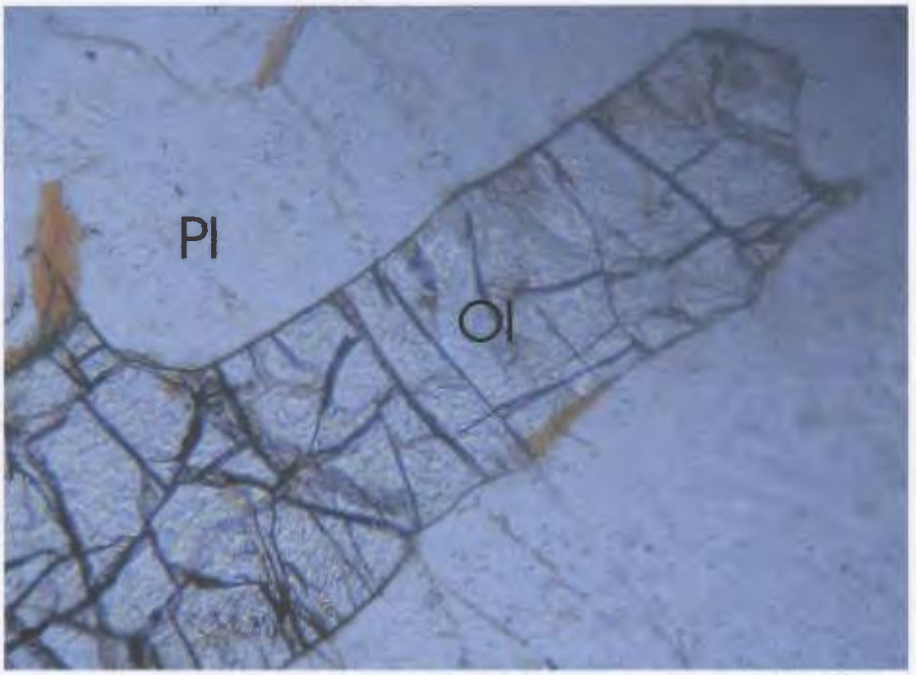

Plate 2-63. Photomicrograph of troctolite sample BI 16. Plane polarized light. The shape of these olivine (Ol) grains is dictated by the euhedral plagioclase (Pl) they are in contact with. Field of view ca. 1.5 mm.

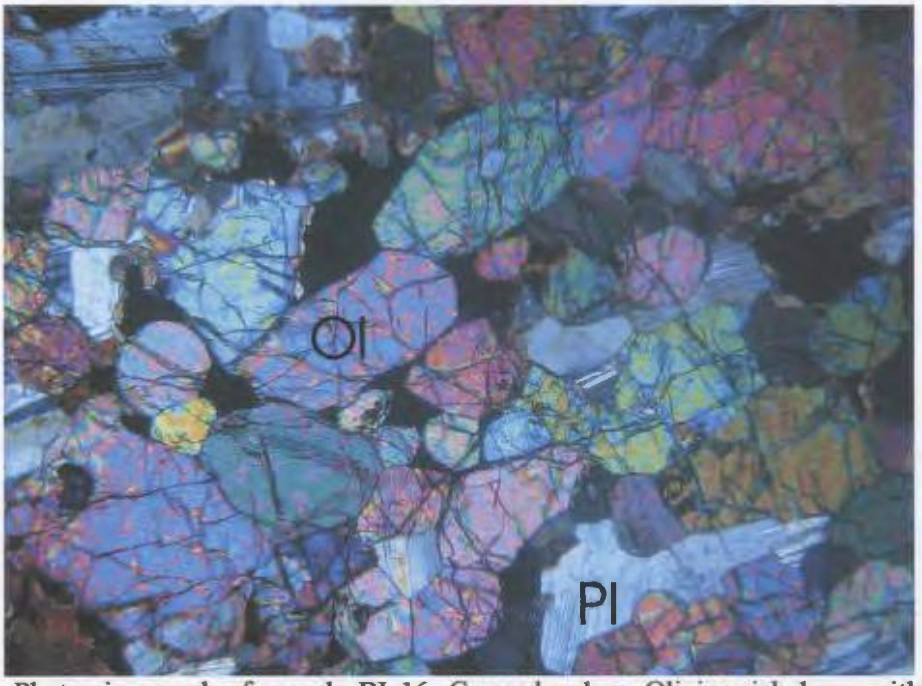

Plate 2-64. Photomicrograph of sample BI 16. Crossed polars. Olivine-rich layer within troctolite. Notice some anhedral plagioclase (Pl) grains in contact with euhedral olivine (Ol). Field of view ca. 5.5 mm.

Figure 2-65. Photomicrograph of medium-grained ferrogabbroid sample BII 63, north of Nain Bay. This is a large (ca. 1 cm) xenocrystic antiperthite grain; it is accompanied by coarse-grained pyroxene aggregates (not shown). Field of view ca. 5.5 mm.

Chapter 3 Geochemical and Isotopic Analysis

3.1 Introduction

The major rock types of the Barth Island Ring Complex have been previously interpreted to be the result of closed-system differentiation of a single pulse of mafic magma, a conclusion based on both field relationships and major element chemical trends (Mulhern, 1974; de Waard, 1976; de Waard *et al.*, 1976). A primary conclusion of the present study is that the field relationships between troctolite, ferrogabbroid, and monzonite of the Barth Island Ring Complex suggest intrusive relationships among all these rock types. The major rock types thus do not appear to share a simple cogenetic relationship in the manner postulated by previous workers.

Geochemical modeling provides an opportunity to independently test the previous theories of formation of the Barth Island Ring Complex, as well as provide further insight into the nature of possible sources and history of evolution of the Barth Island Ring Complex. This chapter is focused primarily on reporting and describing the results of inductively-coupled plasma mass spectrometry (ICP-MS) and x-ray fluorescence (XRF) geochemical analyses, in order to accurately characterize the major rock types of the Barth Island Ring Complex. All preparation and analytical procedures were performed at Memorial University, Newfoundland.

3.1.1 Previous work

The previous interpretation of the Barth Island Ring Complex as the result of a single pulse of magma was based in part on a study of the changes in major element mineral compositions across the structure. Rubins (1973), Mulhern (1974), and Levendosky (1975) each examined different parts of the Barth Island structure, and found that the ratio Mg / (Mg + Fe) in pyroxene and olivine, and the ratio Ca / (Ca + Na) in plagioclase[1], change systematically across the contacts between the various rock types. For instance, Mg content in olivine decreases from the troctolite's outer contact toward its centre; orthopyroxene content shows similar variation. The apparently gradational nature of the changes in mineral composition across the contacts between the rock types constitutes the main line of geochemical evidence for their cogenetic nature. An example of the major element geochemical evidence of the previous workers is presented, along with an interpretive cross-section, in chapter 5.

3.1.2 Sample types and locations

The locations of most samples used for geochemistry are shown on a simplified map of the Barth Island Ring Complex in fig. 3-1. Four troctolite samples (BS 2d, BS 8g, BS 8c, BI 32), two leuconorite samples (BII 1, BII 3), three outer ferrogabbroid samples (BS 7c, BS 7i, LBE 42), two central ferrogabbroid samples (BII 56, BIII 10), and two monzonite samples (BS 6a, BS 6c) were analysed. Four other

[1]Expressed hereafter as $En_{0\text{-}100}$, $Fo_{0\text{-}100}$, and $An_{0\text{-}100}$, respectively.

samples were also analysed: NA 3, a ferrogabbroid sheet intruded into the northern anorthosite, NA 6, a ferrogabbroid-monzonite hybrid sheet intruded into the northern anorthosite, NA 8, a ferrogabbroid dyke also found in the northern anorthosite, and BIII 30, a sample of the Satorsoakulluk Dyke. The location of sample NA 8 is farther north than the map limit. Appendix 1 gives the approximate mineral assemblages, modal proportions, and textures of selected analysed samples.

3.2 Preparation and analytical procedures

3.2.1 XRF and ICP-MS Preparation

Identical preparation procedures were employed for XRF, ICP-MS, and isotopic analyses. Weathered surfaces were removed with a rock saw. Samples were then cut into slices and wrapped separately in clean plastic bags. Crushing was carried out using either a jaw crusher or a hammer and iron plate. A tungsten carbide puck mill was used to pulverize the sample. Sample powders were stored in clean plastic vials. The crushing and powdering equipment were cleaned with water, air, and alcohol between samples.

3.2.2 Loss on ignition (LOI)

Loss on ignition (LOI), a measure of the volatile content of the samples, was determined by the following method. Two g of rock powder was placed in a ceramic

crucible. The crucible and powder were then weighed and placed in an oven at 450°C. The samples were then reweighed. The LOI values are given as percent total sample weight in table 3-1. Weight decreases (positive values) were attributed to loss of volatiles. Weight increases (negative values), probably due to oxidation, were noted in most samples. The totals given for each sample in table 3-1 do not include LOI results.

3.2.3 Disc and pellet preparation

The preparative procedures and analyses in the following sections were performed by the staff of the ICP-MS and XRF facilities at Memorial University, excepting the Sm-Nd isotopic preparation and analysis, which was performed by Dr. Marc Poujol.

Rock powder (5 g) was homogenized with 0.7 g of BRP Bakelite phenolic resin for ten minutes in a roller mixer. The mixed powder-resin was then pressed in a pellet-press for 5 seconds; the pellets were then baked in an oven for 15 minutes. Trace elements were analysed using the pellets.

Fused beads were used to analyse major elements. Fused beads were prepared by mixing 1.5 g of dried rock powder with a flux of 6.0 g lithium metaborate and 1.5 g of lithium tetraborate. The powder was then mixed in a dry platinum crucible with 0.02 g solution of lithium bromide. Fused beads were then heated to 1500° C over 12 minutes in a LECO FX 200 burner.

3.2.4 XRF analyses

Major and trace elements were analysed using a Fisons/ARL 8420+ sequential wavelength-dispersive X-ray spectrometer. The instrument has a simple goniometer, which is capable of holding six analyzing crystals. Trace-element analysis for this study was performed using five analyzing crystals, including one LiF200H crystal specially treated for heavy element sensitivity. The rhodium anode end-window was operated at 3 kW with either a scintillation or argon flow-proportion detector.

The following limits of detection (LOD) values are the averages for the facility at Memorial University, where the analyses were performed, and are given as they stand at the time of writing. For further information, see Longerich (1993; 1995). The LOD for the major elements are: SiO_2, 0.02%; TiO_2, 0.01%; Al_2O_3, 0.06%; Fe (total oxide), 0.01%, MnO, 0.002%; CaO, 0.01%; Na_2O, 0.04%; K_2O, 0.01%; P_2O_5, 0.01%. The LOD for trace elements for which data are presented are, in parts per million: Rb, 0.7; Ba, 23; Nb, 0.7; Pb, 4; Sr, 1.2; Zr, 1.2; Y, 0.7. The precision and accuracy of the analysis is below 1% for each of the reported trace elements.

3.2.5 ICP-MS powder preparation

ICP-MS analyses were performed using Na_2O_2 sinter sample dissolution. A mixture of 0.2 g rock powder and 0.8 g Na_2O_2 was placed in a Ni crucible and sintered in a muffle furnace at 480°C for 1.5 hours. The crucible was cooled, and distilled water was

added in 10 mL proportions to stop the reaction. The resulting mixture was centrifuged after being diluted with water. 8N HNO_3 and oxalic acid were used to dissolve the mixture before further dilution with water.

3.2.6 ICP-MS analysis

Data were acquired with an HP4500+ ICP-MS. Each run cycle contained (in addition to samples) 4 standards and one calibration blank. Samples were spiked with a Rb-Cs-Tl-U solution standard. The blank was used to make a background correction. The standard ratio UO/U was used to correct oxide interference. Matrix effects were corrected for by using interpolation between spike signal intensity of samples and standards. The limits of detection (LOD) are below ten parts per billion (ppb) for all elements measured by ICP-MS; these values are the averages for the equipment at Memorial University, where the analyses were performed, and are given as they stand at the time of writing. The precision for most reported elements is between 3% and 10%. Hf (precision 10%-15%) and Ta (precision >20%) are reported, but the results for these elements are not used in detailed interpretation because of the poor precision.

ICP-MS procedures can be found in greater detail in Longerich *et al.* (1990).

3.2.7 Nd isotopic analysis powder preparation

Approximately 0.1 g of powder of each sample was immersed in a mixture

of concentrated HF and HNO_3 acid in Savilex containers, then spiked with a mixed $^{150}Nd/^{149}Sm$ solution. The spiked samples were then allowed to dissolve over a five day period. At the end of the dissolution period, the samples were allowed to evaporate volatiles until dry. The samples were then immersed in 6 N HCl, and allowed to dissolve for two days. At the end of the two day period, the liquid fraction was allowed to evaporate, the samples were dissolved in 2.5 N HCl, and were then loaded on a cationic exchange chromatograph, using AG50W - X8 resin. The rare-earth element (REE) fraction was then purified, and Sm and Nd were isolated using a secondary column loaded with Eichrom Ln resin. All reagents were distilled to ensure a low level of contamination.

3.2.8 Analytical procedures

Sm and Nd contents, and Nd isotopic composition were analysed using a Finnegan MAT 262 mass spectrometer, in static mode. The Nd isotopic ratios were normalized to $^{146}Nd/^{144}Nd = 0.7219$. The reported values were adjusted to La Jolla Nd standard ($^{143}Nd/^{144}Nd = 0.511860$). During data acquisition, standard replicates gave a mean value of $^{143}Nd/^{144}Nd = 0.511885 \pm 15$ (error is 2 ; the number of runs is 22). In-run precision for Nd isotopic data is given at a 95% confidence level. The errors on Nd isotopic compositions are <0.002%, and error on the $^{147}Sm/^{144}Nd$ ratio is estimated to be <0.1%.

Epsilon-Nd (ϵ_{Nd}) values were calculated using chondritic uniform reservoir

(CHUR) values of $^{147}Sm/^{144}Nd = 0.1967$ and $^{143}Nd/^{144}Nd = 0.512638$. The decay constant for ^{147}Sm is 6.54 10^{-12}/y. Model ages (T_{DM}) were calculated with respect to a depleted mantle (DM) that has $\epsilon_{Nd} = 10$. Model ages were also calculated with respect to the De Paolo (1981) mantle model (T_{DM} DeP).

3.3 Major and minor element geochemistry

3.3.1 Principles

Major element geochemical results are commonly interpreted as being indicative of more, or less, 'evolved' or 'differentiated' rocks. This terminology uses as a reference point a hypothetical average magmatic composition that would be the result of a partial melting event in the mantle. That is, a mafic magma, formed from partial melting of the mantle[2], which has not undergone any fractional crystallization, has some arbitrary 'primitive' composition. In a set of major element compositional values, the most 'primitive' or 'least evolved' composition is typically understood to be the composition that is most Mg-rich, because the first (high-temperature) mafic minerals to crystallize from a mafic magma will be the most Mg-rich (Bowen, 1928; Philpotts, 1990, pp. 235-236). Mg partitions into mafic minerals, relative to melt, at a higher rate than Fe. The progressive depletion of Mg from the magma relative to Fe via such crystallization results in progressively lower magnesium numbers (expressed here as $MgO/[MgO+FeO^T]$, where

[2] The mantle is of heterogeneous composition, but can, for the purposes of this discussion, be considered to be spinel lherzolite, because this probably the most common composition (Hall, 1996, pp. 288-294; Condie, 1989, p. 56).

FeO^T = [FeO + Fe_2O_3]). When comparing Mg numbers of different samples, the lowest of these numbers are therefore said to represent the most 'evolved' or 'differentiated' rocks (Rollinson, 1993, p.74).

The differentiation of a primitive magma also results in the enrichment of incompatible elements (those that have relatively low partition coefficients, such as P, K, Ti, and Na) in the residual ('evolved') magma. The enrichment of each element continues until the magma becomes saturated in, and begins to crystallize, a mineral which incorporates that element, effectively reducing the concentration of that particular element in the magma. For instance, the concentration of P in a differentiating mafic magma will increase until apatite [$Ca_5(PO_4)_3$ (OH,F,Cl)] becomes saturated and begins to crystallize, thus halting the magma's P-enrichment trend.

Indices of differentiation, such as the Mg number, do not necessarily establish genetic links between rock types. Granites typically have low Mg numbers, diorites typically have intermediate Mg numbers and basalts typically have high Mg numbers; this does not mean that all granite is the final product of a differentiation sequence from basalt through diorite.

Preferential local accumulation of a particular phase, referred to as the 'cumulate process' (see section 2.9.1), may result in whole-rock geochemical values which reflect the partition coefficients specific to the cumulus mineral. For instance, an olivine cumulate would have high relative proportions of Mg and Fe compared to Al, which olivine does not incorporate. Minor and trace element values in a rock may also

reflect the effects of the cumulate process. For instance, elevated values of Ni may indicate the presence of cumulus olivine, whereas plagioclase cumulates commonly have elevated values of Eu. Note, however, that the dominance of a particular cumulus phase will not alter indicators of differentiation (such as the Mg number), because this value reflects the composition of the melt (with respect to a particular phase) from which the minerals crystallized, rather than the cumulus assemblage.

3.3.2 Major and minor element results

Major and minor element geochemical results (XRF) and corresponding CIPW normative mineralogies of the analysed rocks are presented in table 3-1. The rocks of the Barth Island Ring Complex, excluding the central ferrogabbroid samples, are addressed first; discussion of other analysed rocks follows. The rock types of the Barth Island Ring Complex are divided into four groups based on the major and minor element results, illustrated in figs. 3-2 to 3-4: the monzonite, norite, troctolite, and outer ferrogabbroid.

The two rock types which constitute the bulk of the Barth Island Ring Complex, troctolite and outer ferrogabbroid, have distinctly different compositions. The troctolites have high alumina (> 20 wt%) in contrast to the ferrogabbroids, which all have alumina contents of less than 13.5 wt% (fig. 3-2). A large difference is also evident between the two groups in total iron content: ferrogabbroids have an average of 20 wt%,

whereas troctolites have ($FeO + Fe_2O_3$) less than 10 wt%. The Mg number of the samples is plotted against silica content in fig. 3-3. The Mg number of troctolites averages 0.47; the ferrogabbroids have average Mg number of 0.18. The two groups have similar average silica content. The ferrogabbroids range between 45 and 50 wt% silica; the troctolite samples have 46 – 49 wt% silica (fig. 3-3). The troctolites have much lower P_2O_5 and TiO_2 than the ferrogabbroids (figs. 3-4a and 3-4b).

The norite and monzonite each form distinct groups. The monzonites have low P_2O_5 and TiO_2, and have the lowest Mg numbers and highest silica of all the samples (fig. 3-3). The norite samples have slightly higher silica and TiO_2 than the troctolite samples (fig. 3-4a), while having lower Mg number and P_2O_5 (fig. 3-4b).

The troctolite samples show little internal variation; the outer ferrogabbroid samples show slightly more internal variation, particularly in P_2O_5 and TiO_2 (figs. 3-4a and 3-4b); sample BS 7c also has higher silica and K_2O than the other outer ferrogabbroid samples. Noritic samples have strikingly different silica, alumina, MgO and ($FeO + Fe_2O_3$), ($CaO + Na_2O$), and Ti (table 3-2) from each other, but virtually identical Mg numbers: 0.31 (BII 3) and 0.32 (fig. 3-3). Both norite samples have lower P_2O_5 than the troctolitic samples (fig. 3-4b).

The two monzonite samples have low totals (table 3-1). The analyses were repeated three times; the values shown are the best results. It is not clear why the analyses gave such low totals. Their alumina contents are slightly higher than the ferrogabbroids (fig. 3-2), but are still well below the troctolitic alumina contents. The monzonites have

similar P_2O_5 and TiO_2 to the troctolites (figs. 3-4a and 3-4b) and much higher K_2O (fig. 3-4c) than most of the other samples.

Data for samples of the central ferrogabbroid, and for samples of dykes and sheets outside the Barth Island Ring Complex, are given in fig. 3-5. These samples show broad variations in major element values with no apparent correlations. However, for most of the major and minor elements, the samples fall within a range defined by the values of the monzonite and outer ferrogabbroid of the Barth Island Ring Complex.

The central ferrogabbroid samples BIII 10 and BII 56 (crosses in fig. 3-5) have silica contents similar to each other, which are within the range defined by the outer ferrogabbroid samples. These samples also have P_2O_5 contents within the range defined by the outer ferrogabbroid samples. However, whereas one (BII 56) has Mg number similar to the outer ferrogabbroid samples, the other (BIII 10) has Mg number closer to that of the monzonite samples. The TiO_2 content of sample BII 56 is also within the range of the outer ferrogabbroid samples, whereas sample BIII 10 has TiO_2 midway between values of the monzonite and outer ferrogabbroid samples. The alumina content of BII 56 is slightly less than the alumina contents of the outer ferrogabbroid samples; the alumina content of sample BIII 10 is within the range defined by the monzonite samples.

The sample of the Satorsoakulluk Dyke (S on fig. 3-5), sample BIII 30, has major and minor element composition comparable to the outer ferrogabbroid samples, with the exception of its much higher P_2O_5 content.

The samples NA 3 and NA 6 are sheets within the oikocrystic anorthosite to

the north of the Barth Island Ring Complex. NA 3 is a ferrogabbroid sheet, and NA 6 appears to be a monzonite-ferrogabbroid hybrid. Sample NA 6 has slightly higher silica than the outer and central ferrogabbroids, and has Mg number similar to sample BIII 10 and the monzonite samples. Sample NA 6 has TiO_2 and P_2O_5 contents closer to the values of the monzonite samples than to other analysed ferrogabbroid samples. This sample also has notably elevated alumina. Sample NA 3 is a typical ferrogabbroid, except that it has a much higher P_2O_5 content than the other ferrogabbroid samples. The P_2O_5 value of sample NA 3 is similar to that of the Satorsoakulluk Dyke sample, BIII 30.

Sample NA 8 is a ferrogabbroid dyke within the western margin of the northern anorthosite. This sample has notably elevated alumina, similar to that of sample NA 6, Mg number of 0.20, P_2O_5 content at the upper end of the range defined by the outer ferrogabbroid samples, and TiO_2 slightly below the range of the outer ferrogabbroid samples.

3.3.3 Discussion

The disparate major-element values of the two norite samples, which were collected in close proximity to one another, are attributable to phase proportions. Sample BII 3 is plagioclase-rich and therefore has very high alumina and higher silica than sample BII 1, which has substantial amounts of orthopyroxene. The high Ti content of sample BII 1 is attributable to large amounts of rutile in orthopyroxene. These two

samples have identical Mg numbers, indicating the same degree of differentiation. These values are more evolved than those of the troctolite, which has the most primitive values of all the analysed rock types. The norites, however, have slightly lower P_2O_5 than the troctolite samples. This is unexpected, because field relationships suggest the norite is genetically related to the troctolite by *in situ* differentiation of a common parent magma; P is generally incompatible in mafic rocks, and it should therefore have been more enriched in the magma when the norite crystallized than it was when the troctolite crystallized. The abundances of most other trace elements are also lower in the norites than the troctolites (section 3.4.1), and this feature is disussed further in section 3.6.

From the petrography (2.2.1), it is clear that all the troctolite and norite samples are cumulates, and their bulk compositions therefore cannot represent the composition of a parental magma. In the absence of any fine-grained marginal rocks that might be considered chilled parental magma, it is difficult to infer much about the parent. Both the norite and troctolite have high alumina values (fig. 3-2) compared to tholeiitic basalts, which average 14-16 wt% alumina (McBirney, 1984, p. 233). The samples obtained closest to the troctolite's margin are recrystallized, but have similar proportions of plagioclase and olivine to the analysed samples; the rest of the intrusion is also plagioclase-rich. Although the lack of any 'chilled' samples requires that any inference about the bulk chemistry of the troctolite's parent magma be met with skepticism, it is possible that the parent was relatively aluminous.

The highest of the troctolite Mg numbers is near 0.50, from sample BS 2d,

which was collected close to the margin of the troctolite. The Mg number is similar to average normal mid-ocean ridge basalt (NMORB) and somewhat higher than that of average ocean island tholeiites and continental flood basalts (Blatt and Tracy, 1996, p. 157). The troctolite samples are therefore not overly primitive or evolved compared to common mafic rocks.

The fine-grained ferrogabbroid samples do not have cumulate features, and it is therefore possible that the bulk major-element compositions approximate a parental magma composition. In a few locations, the ferrogabbroid was observed to be chilled against monzonite, which lends some support to this view.

The high iron content of the ferrogabbroid is typical of liquids residual from fractional crystallization of tholeiitic magmas. The ferrogabbroid samples have Mg numbers that are relatively evolved, but have on average lower silica values than the troctolite. The ferrogabbroid samples have many other hallmarks of evolved tholeiitic liquid, such as high P_2O_5 and TiO_2.

It might be expected that the ferrogabbroid samples should have more silica than the troctolitic rocks, because they are more evolved. Much of the discussion of liquid evolution trends in this work has emphasized that the compositional trend followed by residual liquid, during fractional crystallization of mafic magmas, is towards silica enrichment (as well as iron enrichment). However, the relatively low silica contents of ferrogabbroid samples of the Barth Island Ring Complex are typical of some liquids thought to have evolved by differentiation of mafic magma. For instance, in the

Skaergaard Intrusion, the composition of the evolved liquids calculated by Wager and Deer (1939) (as reported in Mueller and Saxena, 1977, p. 303), and reported by McBirney and Naslund (1990) have (Fe_2O_3 + FeO) > 20%, Mg numbers as low or lower than those of ferrogabbroid of the Barth Island Ring Complex, and silica contents between 45 and 50 wt%. The conclusion of Wager and Deer (1939) is still supported today, albeit in modified form (Jang *et al.*, 2001; McBirney and Naslund, 1990). Fine-grained rocks of the Skaergaard Intrusion's margin thought to be 'chills' have mafic or 'primitive' compositions. It should therefore be considered possible that the compositions of the ferrogabbroids could be produced by fractional crystallization processes in a mafic magma of typical composition, such as mid-ocean ridge basalt (MORB).

Another theory, which might explain the origin of both the ferrogabbroid and monzonite, is presented following the discussion of trace element data.

3.4 Trace element geochemistry

Trace element data (ICP-MS and XRF) are presented in table 3-2. The following report of the results and discussion is divided into three sections: the first covering troctolitic and noritic samples, the second for outer ferrogabbroid and monzonite samples, and third for central ferrogabbroid and samples not considered to be part of the Barth Island Ring Complex. A variety of spidergrams (or, multi-element plots) and rare-earth element (REE) plots are presented (figs. 3-6 through 3-14, excluding fig. 3-10). The

trace element abundances of the analysed samples were plotted after normalization[3] to a set of standard reference values.

3.4.1 Principles

A particular set of standard reference values essentially denotes the elemental abundances of some hypothetical reservoir, or the average composition of a rock type from a particular geological environment. There are many such sets of standard reference values. Two of the most commonly used points of reference are the primitive (primordial) mantle, which is thought to be the composition of the silicate earth before extraction of the crust; and the composition of MORB. The particular set of reference values used in the present study is the primitive mantle values of McDonough and Sun (1995). The mantle reference point was chosen arbitrarily, because it is unclear what source or variety of sources might be inferred to have produced the rocks of the Barth Island Ring Complex. Each diagram is labeled according to the normalizing values used. In order to be consistent, the same set of spidergrams and REE plots is presented in each of the two sections.

For elemental abundances normalized to primitive mantle, the elements are listed, from left to right, in order of increasing compatibility. In this context, compatibility is a measure of the size of an element's bulk mantle-liquid partition coefficient with

[3] Normalization is accomplished by dividing the elemental abundances of the samples by the corresponding elemental abundances given in the set of reference values.

respect to a small proportion of partial melting in the mantle (Rollinson, 1993, p. 142). The order in which the elements are plotted on spider diagrams is important, because the plotting order can emphasize or downplay variations in trace-element abundances. Because the elements are plotted in order of increasing compatibility, a rock whose composition approximates an undifferentiated mantle partial melt would have a smooth curve, with the slope decreasing to the right. The result of fractional crystallization, however, is to alter the relative abundances of elements, as mentioned in section 3.3.1. The relative abundances of the rare earth elements (REE) provide a simple specific example.

Subgroups within the REE are distinguished on the basis of atomic weight and referred to in the following terminology. The light rare earth elements (LREE) refer to La through Nd (La-Nd), the heavy rare earth elements (HREE) refer to Er-Lu. The middle rare earth elements, or MREE, include Sm-Ho and sometimes Y, because this latter element, although not a REE, has identical charge and similar ionic radius to Ho. Because the REE typically exist in the same state of ionization (3+), each increase in atomic weight is correlated with a decrease in ionic radius, and the decrements are small. Ionic radius and charge provide a reliable measure of relative partition coefficients for a given melt composition.

The LREE are more compatible in a mantle partial melt than the HREE, which are more compatible in the restite. The slope of the curve defined by the abundances of the REE in a mantle-derived partial melt, normalized to primitive mantle,

would be negative. The grade of the slope would be gentle because each REE, having only slightly smaller or larger radius than its neighbour, is respectively only slightly more or less compatible than its neighbour. The actual slope can be measured by taking the ratio of one LREE to one HREE, for instance La/Yb. Under the right circumstances, such a ratio can provide an index of the amount of partial melting of a rock's source.

This simple system is complicated by crystal fractionation. For example, the three common igneous minerals plagioclase, amphibole, and pyroxene each preferentially incorporate a different set of REE. Plagioclase prefers to incorporate La and Ce, amphibole prefers MREE, and pyroxene HREE. Fractionation of any these phases will therefore result in appropriately modified REE patterns in both the cumulate and the residual magma. However, because the increment of compatibility between each REE is relatively small, the REE operate as a relatively coherent group.

One exception to this rule is the REE Eu. Under the reducing conditions typical of many magmatic environments, this element forms a divalent ion in addition to the trivalent ion typical of the REE. The radius of Eu^{2+} is such that it is highly compatible in plagioclase, so the abundance pattern of a plagioclase cumulate will have an anomalous positive spike at Eu. The relative enrichment of Eu is calculated by dividing the normalized Eu value by the geometric mean of the normalized values of the two REE surrounding Eu, Sm and Gd ($Eu/[Sm \cdot Gd]^{½} = Eu/Eu^{M}$, where Eu^{M} is the geometric mean of Sm and Gd). Values that are less than unity indicate a negative anomaly, and positive anomalies are indicated by values greater than unity. Relative enrichment for any element

can be calculated in the same way (appendix 3).

The REE are the best elements to use for interpolating in this manner because of their low propensity to fractionate from one another. Interpolating in the same way between non-REE elements that are controlled by specific mineral phases can be made meaningless by the effects of fractional crystallization, and in any case it is the relative abundance of these very elements that one typically wishes to obtain.

The point of the Eu example is that the ordering of the elements with respect to compatibility enables the recognition of crystal fractionation processes. Positive or negative anomalies in spidergram or REE plot patterns may represent preferential accumulation or removal of a particular phase. In cases where it is known that no phase can cause fractionation of one element from another (that is, the partition coefficients of those two elements with respect to the possible phases are essentially identical), it is possible the ratio of those elements is the same as in the magma's source. However, the issue of sourcing is complicated by the possibility of magmatic contamination through assimilation, and the possibility of multiple sources.

Furthermore, it is clear that, with respect to spidergram patterns, 'anomalous' values can be created for any element simply by placing it out of the correct order of compatibility. For example, if the heavy rare-earth element Yb were placed between, say, the light rare-earth elements La and Ce, a prominent negative Yb anomaly would appear.

Though there is overall general agreement for the order of the elements in

multi-element plots, when normalizing to primitive mantle, the location of some elements may vary by one or two places between sources (Hofmann, 1988; Sun and McDonough, 1989; Rollinson, 1993, pp. 142-146, and references therein). In the spidergrams presented below, the order of included elements is, for the most part (see below), that recommended by Sun and McDonough (1989). The following discussion is meant to elucidate certain points on the location of the elements P and Hf-Zr in the spidergrams presented below.

The compatibility of P is roughly equal to that of Nd. In the present work P is placed to the right of Nd. This placement was chosen because Sr and P are elements whose abundances may be largely controlled by certain mineral phases (Sr is highly compatible in plagioclase, and P may be controlled by apatite). Neighbouring REE, however, are not typically highly fractionated from one another. The placement of P to the right of Nd serves to emphasize relative depletion or enrichment of a sample in Sr without the variability of P affecting the visual demonstration of strontium's relative abundance. There is no actual change as to strontium's relative compatibility; Sr^M is calculated using the elements Pr and Nd regardless of the position of P. Calculation of possible P anomalies proceeds as though P has the same compatibility as Nd, according to Sun and McDonough (1989). The value of P^M is calculated using the normalized abundances of Pr and Sm.

The compatibility of Sm is roughly equal to that of Hf and Zr. Sm has been placed to the left of Hf and Zr, and serves as one-half of a bracket for P following the same reasoning as given above for P and Nd. For the calculation of Zr^M, the normalized

abundances of Nd and Dy are used.

The calculation of Ti anomalies proceeds using the normalized abundances of Sm and Dy.

It is unclear what level of anomaly should be considered significant. The levels of precision and accuracy during measurement of the elemental abundances must be accounted for. For Pb, Sr, and Zr, the level of precision and accuracy is below 1% (section 3.2.4). However, anomalies are calculated using the REE of comparable compatibility, which cannot be measured as precisely (section 3.2.6). Assuming the maximum possible imprecision, the measured elemental abundance can be incorrect by a factor of 1.1. For the purposes of the present study, only values that are anomalous by a factor of ≥ 1.1 are considered significant.

Partition coefficients used in the interpretations were either obtained from various sources and are appropriately referenced, or were calculated. Partition coefficients were calculated for the elements Ca, Sr, Pb, Ba, Sc, the rare earth elements (REE), and for Rb (plagioclase only). The coefficients for these elements were calculated for olivine using the method of Beattie (1994), for plagioclase and orthopyroxene using the method of Blundy and Wood (1994), and clinopyroxene using the method of Wood and Blundy (1997).

3.4.2 Troctolite and norite

A spidergram of the results for troctolite and norite samples is presented in fig. 3-6. Fig. 3-7 shows the troctolite and norite REE abundances. The average ferrogabbroid and monzonite are plotted on fig. 3-7 for comparison. The trace element data for these rocks are presented below. A discussion of these data follows the presentation.

The four troctolite samples are relatively homogeneous. The trace element abundances and patterns are similar in three of the four samples. The most striking features of the plots are the low Rb and Nb, large positive Pb and Sr anomalies (average $Pb/Pb^M = 2.8$; $Sr/Sr^M = 3.2$), and low P ($P/P^M = 0.7$). The troctolite samples have subequal La/Yb.

Sample BI 32 has higher abundances of all the elements, but its abundance pattern is nearly identical to the other samples; the two main differences are weaker Pb and Sr anomalies. Sample BS 2d does not have a P anomaly; this sample also has enriched Sm-Gd (fig. 3-7) compared to the other troctolite samples, and has Yb/Lu less than unity. All the troctolite samples have positive Eu anomalies. The troctolite average is $Eu/Eu^M = 1.57$. Weak positive Zr anomalies are present in three of the four troctolite samples; sample BS 8c does not have a Zr anomaly.

The norite samples (squares in figs. 3-6, 3-7) have a pattern similar to the troctolite, but with lower abundances of most plotted elements. The obvious differences between the patterns of the norite and troctolite are the norite's relative enrichment in K

(indicated by higher K/La), Sr (average $Sr/Sr^M = 6.9$), Eu (average $Eu/Eu^M = 2.4$), and Ti (average $Ti/Ti^M = 4.1$). Both norite samples are more strongly depleted in P ($P/P^M = 0.6$). There appears to be a depletion of Nb in sample BII 3, relative to the troctolite samples and the other norite sample. However, the value is below the LOD for this element, and so is not considered.

The Eu, Sr and Pb anomalies in the troctolite provide good evidence supporting the conclusion that these rocks are plagioclase cumulates, because all of these elements are preferentially partitioned into plagioclase relative to elements of comparable compatibility.

The differences between the trace element abundances and patterns of the two norite samples provide a further example (in addition to the XRF major-element results) of the effect of modal mineralogical proportions on the trace element signatures. The plagioclase-rich sample, BII 3, has higher La through Tb (La-Tb) and lower Er-Lu (fig. 3-7), probably a result of the fact that mineral/melt partition coefficients of LREE are higher for plagioclase than they are for orthopyroxene. The extreme positive Ti anomaly ($Ti/Ti^M = 6.5$) of sample BII 1 is likewise associated with the samples's abundant cumulus orthopyroxene, which contains large amounts of rutile (see plate 2-15b). The significant but smaller Ti anomaly ($Ti/Ti^M = 2.1$) of sample BII 3 is notable because this sample also contains rutile-bearing orthopyroxene, but in lower abundance. The positive Pb, Sr, and Eu anomalies, however, are larger in BII 1, the sample with less plagioclase. This is the opposite of what is expected.

The norite, despite having crystallized from a more fractionated, evolved magma than the troctolite, has lower trace element abundances. This might be explained by digestion of anorthosite, which has lower trace element abundances than either the norite or troctolite (Voordouw, 2005). Assimilation of a plagioclase feldspar cumulate would be consistent with the large positive Pb, Sr and Eu anomalies in the norite. However, anorthosite would be resistant to assimilation, due to the refractory nature of plagioclase.

Alternatively, the norite's lower trace element abundances and larger Eu, Pb, and Sr anomalies might be explained by phase proportions. Because the sample modes were not determined by the precise method of point counting, it is possible that the norite samples, compared to the troctolite samples, had lower proportions of accessory minerals, which contain the bulk of the rock's trace element budget.

3.4.3 Outer ferrogabbroid and monzonite

A spidergram illustrating the trace-element abundances of the ferrogabbroid and monzonite is shown in fig. 3-8. Fig. 3-9 is a plot of the REE only. The data are presented first; discussion of the data follows.

The monzonite and ferrogabbroid have several features in common. The overall trace element abundances of all samples are similar, with the monzonites having in general slightly lower abundances. The two rock types have subequal Nb/La and have

strong depletions in Sr ($Sr/Sr^M < 0.60$). All samples also have somewhat depleted Rb and Nb.

The monzonite samples have high K and Ba (K/La = 2-3; Ba/La = 11-14), enrichment in Zr (average $Zr/Zr^M = 5.4$) and Hf, and strongly depleted Ti ($Ti/Ti^M = 0.3$). The REE pattern of the monzonitic samples indicates enrichment in Eu (average $Eu/Eu^M = 1.7$) and Pb (average $Pb/Pb^M = 2.2$). The monzonite samples also have sharply upturned Yb-Lu segments.

In contrast to the monzonite samples, all of the ferrogabbroid samples have K/La below unity and Ba/La <4. Considerable heterogeneity is evident with respect to other elements. Relative to the other ferrogabbroid samples, sample BS 7c has higher K/La. BS 7c also has a positive Zr anomaly and a weak negative P anomaly. The other two ferrogabbroid samples, LBE 42 and BS 7i, have negative Zr anomalies. BS 7i has a weak positive P anomaly. BS 7c and LBE 42 have positive Pb anomalies, whereas BS 7i has a sharp negative Pb anomaly. LBE 42 and BS 7c appear to have slightly depleted Sm-Eu-Gd. Samples BS 7c and BS 7i have weakly negative Ti anomalies, whereas LBE 42 has a weak positive Ti anomaly.

The mineral assemblage of the monzonite serves to explain some of its trace element variations. The high Zr/Zr^M is explained by the presence of large zircon crystals in the rock, and the presence of K-feldspar (in mesoperthite) as a cumulus phase may be sufficient to explain the high K/La and Ba/La. The positive Eu anomaly in the monzonite samples support the interpretation of mesoperthite as a cumulus phase, because Eu is

strongly partitioned into both plagioclase and K-feldspar (Larsen, 1979; Stix and Gorton, 1990). The positive Pb anomaly can be similarly explained because the plagioclase partition coefficient of Pb is nearly an order of magnitude greater than that of Ce and Pr.

As a corollary of the presence of cumulus mesoperthite, it might be expected that the Sr values would also be anomalously positive to some degree, because Eu and Sr have essentially the same plagioclase/melt and K-feldspar/melt partition coefficients. For instance, the plagioclase-cumulate troctolite and norite have positive anomalies in both Eu and Sr, and the Eu/Sr ratio of these rocks is far less than unity. However, both monzonite samples have a negative Sr anomaly, and the average Eu/Sr ratio of these samples is 1.9.

The simplest explanation for these observations is that the monzonite crystallized from a magma which was highly depleted in Sr. The most direct way for a magma to become depleted in Sr would be to fractionate large amounts of plagioclase; however, the monzonite samples are not depleted in Eu or Pb. The ultimate source of the Sr anomaly is therefore uncertain, but the monzonite's mesoperthite must have fractionated from a Sr-poor magma.

The large negative P and Ti anomalies suggest that the monzonite's parent magma crystallized substantial amounts of apatite and rutile/ilmenite. However, an alternative explanation for the depletion is given below.

The ferrogabbroid is not considered a cumulate rock (section 2.9.4). It is therefore possible that the trace-element values reflect those of its parent. However, the

obvious mineralogical and textural heterogeneities of the ferrogabbroid observed in the field, and similar features in thin section, indicate that the ferrogabbroid is a complex rock. In particular, the obvious mingling and incomplete mixing between ferrogabbroid and monzonite, which was directly observed or suspected in a substantial proportion of ferrogabbroid outcrops, militates against considering the composition of any ferrogabbroid as representative of its parent magma.

The lack of consistency between the ferrogabbroid trace element patterns cast further doubt on the proposition that the ferrogabbroid samples might generally represent magma compositions. It is possible that some differences (such as the positive Zr anomaly of BS 7c) can be explained by phase proportions, but the fact that the monzonite and ferrogabbroid have similar trace element abundances makes it difficult to determine whether the differences in phase proportions are due merely to some heterogeneity in the ferrogabbroid magma, or are due to mixing with the monzonite. The considerable scatter in ferrogabbroid La/Yb values, which are commonly considered to be a sort of index of fractionation, away from the homogeneous La/Yb value of the monzonites is suggestive of complexities beyond the scope of simple heterogeneity of phase proportions and mixing.

All ferrogabbroid samples are depleted in Sr. This suggests that the ferrogabbroid crystallized from a magma that was depleted in Sr, perhaps as the result of extensive crystallization of plagioclase. The negative Pb anomaly of sample BS 7i supports this interpretation, but BS 7c and LBE 42 actually have large positive Pb

anomalies, and none of the samples show correlative negative Eu anomalies. This case is similar to the monzonite, which also shows depletion in Sr, but enrichment in Pb and Eu. The monzonite and outer ferrogabbroid were contemporaneous, so their parent magmas must have been produced at similar times. These similarities seem to indicate a close magmatic relationship.

One explanation of the origin of the ferrogabbroid (and monzonite) is silicate liquid immiscibility, which has been explored by several authors (Eby, 1983; Naslund, 1983; Philpotts, 1990, pp. 252-256, 307), and is thought to occur during extreme iron-enrichment of a magma. The process is summarized as follows: a magma follows a tholeiitic differentiation trend to produce an iron-rich magma, which separates into two liquids, one iron-rich and the other silica-rich; these are referred to as conjugate liquids.

On the basis of their major-element chemistry, the ferrogabbroid and monzonite might be candidates for such conjugate liquids. This possibility has been suggested, for ferrogabbroid and monzonite of the NB, by Philpotts (1990, p. 307); certainly this association would help explain their ubiquitous field association throughout the NB (section 2.9.4).

The process of immiscibility requires that, during liquid separation, certain elements partition strongly into the iron-rich liquid, and others into the silica-rich liquid. Naslund (1983) stated that immiscible liquid pairs should have some or all of the following characteristics. Of the major elements, the Fe-rich liquid can be expected to retain most of the original magma's P_2O_5, TiO_2, MgO, and MnO, whereas the silica-rich

liquid is expected to retain more K_2O, Na_2O, and Al_2O_3. The Fe-rich liquid should have higher Na/K and Al/(Na + K) than the silica-rich liquid. Both liquids should have similar Fe/Mg and Mn/Fe. The ferrogabbroid and monzonite meet most of these conditions (table 3-1); the one exception are the Fe/Mg values of the monzonite and ferrogabbroid, which are different from one another. The average monzonite Fe/Mg ratio is ca. 18, whereas the average ferrogabbroid has an Fe/Mg ratio of ca. 5.

The ferrogabbroid and monzonite also plot at opposite edges of the two-liquid field of Roedder (1951) (fig. 3-10), as is typical of immiscible liquid pairs (Philpotts, 1990, p. 253, his fig. 14-22). Furthermore, the apparent evolutionary trend of the troctolite is toward the average summed composition of the ferrogabbroid and monzonite (fig. 3-10).

This summed composition assumes that the ferrogabbroid and monzonite exist in one-to-one proportions, and is unlikely to replicate the proportions of silica-rich and iron-rich magma produced by silicate immiscibility processes. However, the point is that a magma of similar composition to the troctolitic magma could have undergone differentiation to produce a composition near the average composition of the ferrogabbroid and monzonite, and could then have formed a pair of immiscible liquids.

Incompatible trace element abundances may also reflect the immiscibility process. During immiscibility, these elements will preferentially partition into the less polymerized liquid, which is, in most cases, the Fe-rich liquid (Eby, 1983; Philpotts, 1990, p. 253). A measure of melt polymerization in a given melt system can be calculated

using the ratio of non-bridging oxygen (NBO) to tetrahedrally-coordinated elements (T); an equation for this calculation, using whole-rock major-element chemical data, is given by Eby (1983). The influence of melt polymerization on partitioning between two immiscible silicate liquids is a linear function of the ratio R of the degrees of polymerization of the conjugate melts ($R = (NBO/T)_A/(NBO/T)_B$, where the subscripts A and B denote the siliceous and Fe-rich liquids, respectively). However, the influence is pronounced only for moderate or large polymerization contrasts, where $(NBO/T)_A/(NBO/T)_B \leq 0.5$. For all small melt polymerization contrasts ($(NBO/T)_A/(NBO/T)_B > 0.5$) preferential partitioning is either not significant, or incompatible elements preferentially partition into the siliceous melt.

The calculation results and procedure for monzonite ($(NBO/T)_{Mz}$) and outer ferrogabbroid ($(NBO/T)_{Fg}$) of the Barth Island Ring Complex are given in Appendix 2. The ratio $(NBO/T)_{Mz}/(NBO/T)_{Fg}$ for rocks of the Barth Island Ring Complex is ca. 0.76. According to this result, the polymerization difference between the two magmas would not have been high enough to cause noticeable preferential partitioning of incompatible elements into the ferrogabbroid. This is consistent with the observed abundances (fig. 3-8), but cannot unequivocally establish the rocks having formed from conjugate liquids.

Although some of the evidence is consistent with an immiscible origin, the rocks have features that weigh against an immiscible-origin hypothesis. There is no systematic complementary distribution of elements which should have shown preferential partitioning independent of the polymerization ratio. The monzonite samples show

depletions in Ti and P and enrichment in K, expected of the silica-rich member of an immiscible pair. But, although the ferrogabbroid samples show greater relative abundances of these elements, they do not invariably show corresponding enrichments. Also, the trace element patterns of granitoid rocks in the NB (Emslie and Stirling, 1993) have some of the same features as monzonite of the Barth Island Ring Complex, such as Sr, P, and Ti depletions.

It must be concluded that, though the monzonite and ferrogabbroid have many features that are consistent with derivation from a magma that became immiscible, there is no compelling reason to prefer this explanation of their origins. However, if the monzonite and ferrogabbroid are conjugate liquids, the parent magma could not have become immiscible at the level of emplacement. The field relationships are more compatible with at least some of the monzonite being at the level of emplacement before the ferrogabbroid (section 2.6). Furthermore, the parent magma was probably depleted in Sr, P and Ti.

3.4.4 Central ferrogabbroid and ferrogabbroid sheets and dykes

The remaining analysed samples are plotted on fig. 3-11. Fig. 3-12 is a plot of the REE only. The data are presented first, and followed by a discussion.

The central ferrogabbroid samples BII 56 and BIII 10, have some similarities, but also some distinct differences. These samples both have a positive Pb

anomaly, and negative Ti and Sr anomalies. However, BII 56 has lower K/La, negative Eu and Zr anomalies, and no P anomaly. BIII 10 has no Eu anomaly, a negative P anomaly, and a positive Zr anomaly.

The sample of the Satorsoakulluk Dyke, BIII 30, has negative Pb, Sr, and Ti anomalies, no P or Eu anomalies, and a positive Zr anomaly.

The sheets within the anorthosite to the north of the Barth Island Ring Complex (the oikocrystic anorthosite), represented by samples NA 3 and NA 6, both have negative Sr and Ti anomalies, and upturned Y-Yb-Lu segments. However, sample NA 6 has positive Pb, Eu, and Zr anomalies, and a negative P anomaly. In contrast, sample NA 3 has negative Pb, Eu, and Zr anomalies, and a positive P anomaly. NA 3 also has lower K/La than does sample NA 6.

Sample NA 8 has negative Sr, Zr, and Ti anomalies, and a positive P anomaly. This sample also has a much higher La/Yb ratio than any of the samples analysed.

There are distinct similarities between the trace element values of the central ferrogabbroid samples presented above and outer ferrogabbroid samples of the Barth Island Ring Complex; for instance, the overall trace-element abundances and negative Sr anomalies. However, the lack of a consistent pattern among the outer ferrogabbroid samples is also observed in the central ferrogabbroid samples and the ferrogabbroid sheets and dykes. The ferrogabbroid-monzonite hybrid, sample NA 6, shares most of the characteristics of the monzonite samples, but has lower K/La.

3.5 Nd isotopic results

A brief background of the Sm-Nd isotopic system and some Nd results for the Nain Batholith are presented in section 1.2.4. The results provide a useful framework for comparison and evaluation of the data presented here. The Nd isotopic results from the present study are presented in table 3-3, along with model ages and the ϵ_{Nd} results calculated for the present day, and for the ages of the respective rock types. Sm dissolution problems prevented the measurement of this element in samples NS 7c and BII 56 , and therefore ϵ_{Nd} values at ca. 1.3 Ga are not calculated for these.

The norite and troctolite ϵ_{Nd} values were calculated using an age of 1330 Ma. The ϵ_{Nd} values of ferrogabbroid and monzonite of the Barth Island Ring Complex were calculated using an age of 1320 Ma. The ϵ_{Nd} of the Satorsoakulluk Dyke was calculated using an age of 1300 Ma (Hamilton, 1997).

The ϵ_{Nd} values, given at ca. 1.3 Ga, fit well with published values for rock types of the Nain Batholith (Emslie *et al.*, 1994; table 1-1a). The troctolite values are the least negative, and the norite value is slightly more negative. The outer and central ferrogabbroid show a range of values, with BS 7i being the most negative of these. The Satorsoakulluk Dyke is slightly more negative than BS 7i. The highest ϵ_{Nd} value of the ferrogabbroids is that of BIII 10, the central ferrogabbroid. The monzonite sample, BS 6c, has ϵ_{Nd} intermediate between most of the ferrogabbroids and sample BS 7i.

For the sake of argument, each rock in the Barth Island Ring Complex can be assumed to be the product of a two-component system, where each component is approximated by either a mantle and crustal source. If the ϵ_{Nd} value particular to each component is assumed, the proportion of Nd in the sample derived from the crust can be calculated, using the Neodymium Crustal Index (NCI) of DePaolo *et al.* (1992). This equation might be considered of use in constraining the mechanisms of formation of Proterozoic anorthosites and associated components, because the crust is thought to play a significant but unquantified role in their production (Emslie *et al.*, 1994; Longhi *et al.*, 1999). The NCI can be modified to correct for the abundances of Nd in each component, such that it yields the mass proportion of crust in each rock. Estimates of the approximate ϵ_{Nd} values of the two components have been given by Emslie *et al.* (1994).

It is clear from the data presented here and by Emslie *et al.* (1994) that the negative ϵ_{Nd} results for many rocks of the NB results from the influence of a relatively old crustal component with highly negative ϵ_{Nd}. However, the data presented here can be interpreted to agree with the conclusions of either Emslie *et al.* (1994), Longhi *et al.* (1999), or Bédard (2001). The latter two publications endorse the bulk of anorthosite derivation from the crust, whereas Emslie *et al.* (1994) are nonspecific, but in favour of mafic magma providing a large proportion of the material required to produce anorthosites.

The Nd isotopic data are so malleable because it is difficult to know the composition and ϵ_{Nd} of the crustal component. Furthermore, other factors, such as the

choice of a crustal melting model[4], the choice of partition coefficients, phase proportions of the crust to be melted, and the choice of some physical parameters for producing the large volumes of plagioclase necessary for massif-type anorthosite formation (the parameters which are in question), result in additional difficulties which limit the utility of isotopic data for understanding the origin of massif-type anorthosites.

3.6 Summary

Negative Zr/Zr^M, Sr/Sr^M, and P/P^M are characteristic of Nain Batholith (NB) ferrodiorites (Emslie *et al.*, 1994; Bédard, 2001). The ferrogabbroid samples of the Barth Island Ring Complex have trace element patterns and ratios which have some features in common with ferrodiorites of the NB. However, within-group variations are significant. This may be due to mixing with monzonite, or to heterogeneities within the ferrogabbroid magma.

The monzonite samples have some characteristics of the average NB granite, such as negative Ti/Ti^M, negative Sr/Sr^M, and P/P^M. However, the monzonite of the Barth Island Ring Complex is distinct from the average NB granite (Emslie and Stirling, 1993) in having low Rb and very high Zr/Zr^M.

Field relationships require the troctolite and norite to be comagmatic. However, on this basis the expectation is that the norite would have overall higher trace

[4]For example, the choice of modal v. fractional melting, and the many different formulations of each of these equations.

element abundances than the troctolite, because it should have crystallized from a magma more enriched in incompatible elements. One hypothesis is that the norite samples had lower proportions of accessory minerals (that is, it is more of an adcumulate), which might have stored a significant amount of the trace element budget of the rock, than the troctolite samples.

An alternative explanation for the observed lower trace element abundances of the norite is assimilation of some depleted country rock. Anorthosite is one possible assimilant. The higher Sr/Sr^M, Eu/Eu^M, and Pb/Pb^M of the norite compared to the troctolite supports this hypothesis, although a systematic evaluation of trace element patterns using appropriate AFC (assimilation-fractional crystallization) modeling tools has not been performed. This hypothesis therefore remains untested. It must also be noted that anorthosite probably would not be readily assimilated, due to its refractory nature.

Still another possibility is that the field and petrographic links between the troctolite and norite are misleading. The data may be indicative of a more complex, less intimate relationship between these two rock types. However, the overwhelming similarity of their trace element patterns does indicate a close relationship.

Fig. 3-13 is a primitive-mantle normalized plot of the average trace element values for each group of the Barth Island Ring Complex, and fig. 3-14 shows group averages for the REE only. The ferrogabbroid average is misleading, because there are broad variations within this group. Furthermore, the lack of a large sample population in all groups means that the averages should be treated with caution; but some limited

comparisons can be made. The most prominent similarities between each group are the low Rb/Ba and Nb/Ba ratios. The REE plots also reveal some similarities between each group. Excepting the monzonite, each group has somewhat depleted Sm-Tb (excluding Eu). All groups have nearly identical slope of Dy-Tm segments. These similarities may reflect the influence of common variables of formation, such as a common source region, at depth.

The isotopic data for each rock type of the Barth Island Ring Complex are in agreement with published values for similar rock types elsewhere in the Nain Batholith (Emslie *et al.*, 1994). In the context of the data of Emslie *et al.* (1994), the ferrogabbroid and monzonite reflect similar, significant amounts of crustal involvement in their formation, whereas the troctolite and norite show relatively little contamination from a crustal component. The slightly more negative ϵ_{Nd} of the norite, compared to the troctolite, supports that rock having either been contaminated by a source with relatively more negative ϵ_{Nd}, or not being a simple differentiate of the magma parental to the troctolite.

Table 3-1. Major-element geochemical analyses and corresponding normative mineralogy.

	BS 8g (Tr)	BS2d (Tr)	BS8c (Tr)	BI 32 (Tr)	BII 3 (N)	BII 1 (N)
	Wt%	Wt%	Wt%	Wt%	Wt%	Wt%
SiO2	46.51	46.06	47.69	48.20	52.29	49.00
TiO2	0.74	0.69	0.54	0.84	0.74	1.94
Al2O3	20.09	20.66	21.75	20.98	23.61	17.19
Fe2O3	3.82	3.62	3.20	3.51	2.46	5.60
FeO	5.97	5.66	4.81	5.26	3.13	8.06
MnO	0.11	0.10	0.09	0.10	0.06	0.17
MgO	8.91	9.27	7.84	6.92	2.55	6.37
CaO	9.57	9.93	9.95	9.62	10.05	7.85
Na2O	2.49	2.28	2.69	2.88	3.74	2.74
K2O	0.30	0.27	0.29	0.45	0.43	0.32
P2O5	0.09	0.11	0.07	0.12	0.04	0.02
LOI	-0.25	-0.31	-0.07	-0.15	0.15	-0.14
Total	98.60	98.65	98.91	98.88	99.11	99.26
	CIPW Norm	CIPW Norm	CIPW Norm	CIPW Norm	CIPW Norm	CIPW Norm
Qz	-	-	-	-	3.20	3.40
Or	1.77	1.59	1.74	2.66	2.56	1.89
Ab	21.05	19.27	22.71	24.34	31.62	23.16
An	42.74	45.32	46.40	42.97	46.34	33.65
Di	3.31	2.56	1.95	3.16	2.57	4.16
Hy	10.28	9.81	10.65	12.32	7.71	21.09
Ol	12.29	13.26	9.59	6.43	-	-
Mt	5.55	5.26	4.65	5.10	3.57	8.14
Il	1.41	1.31	1.03	1.60	1.41	3.69
Ap	0.20	0.24	0.16	0.26	0.10	-

Note. The normative mineralogies were calculated using the program Magma (Wohletz, 2003), which specifies an FeO : Fe2O3 ratio, according to the silica content of the sample. LOI is loss on ignition (see text for explanation). Tr is troctolite; N is norite; OFg is outer ferrogabbroid; CFg is central ferrogabbroid; Mz is monzonite; SD is Satorsoakulluk Dyke; FgSh is ferrogabbroid sheet; F/MSh is ferrogabbroid-monzonite hybrid sheet; FgD is ferrogabbroid dyke. The limits of detection are: SiO_2, 0.02%; TiO_2, 0.01%; Al_2O_3, 0.06%; Fe (total oxide), 0.01%, MnO, 0.00%; CaO, 0.01%; Na_2O, 0.04%; K_2O, 0.01%; P_2O_5, 0.01%.

Table 3-1 (cont.). Major-element geochemical analyses and corresponding normative mineralogy.

	LBE42 (OFg)	NS7c (OFg)	NS7i (OFg)	BS6a (Mz)	BS6c (Mz)	BIII 10 (CFg)
	Wt%	Wt%	Wt%	Wt%	Wt%	Wt%
SiO2	45.87	49.67	44.85	65.83	60.75	48.77
TiO2	4.04	2.93	3.67	0.70	0.99	2.18
Al2O3	11.81	12.85	12.78	13.16	14.48	13.39
Fe2O3	8.14	7.23	7.39	3.47	4.60	8.04
FeO	12.73	9.98	12.06	2.95	4.60	11.57
MnO	0.27	0.22	0.26	0.08	0.13	0.27
MgO	3.89	3.85	4.91	0.43	0.57	1.57
CaO	7.59	6.82	9.02	2.73	3.56	6.63
Na2O	2.63	3.08	2.79	3.25	3.73	3.62
K2O	0.50	1.13	0.32	3.51	3.49	1.31
P2O5	0.66	0.53	0.98	0.13	0.17	0.62
LOI	-0.52	-0.44	-0.31	0.20	-0.03	-0.78
Total	98.12	98.29	99.03	96.24	97.07	97.97
	CIPW Norm	CIPW Norm	CIPW Norm	CIPW Norm	CIPW Norm	CIPW Norm
Qz	6.82	7.68	2.42	27.08	17.14	5.37
Or	2.95	6.67	1.89	20.72	20.60	7.73
Ab	22.23	26.04	23.58	27.47	31.53	30.60
An	18.94	17.90	21.40	10.95	12.46	16.42
Di	11.98	10.29	14.01	1.46	3.48	10.67
Hy	14.19	12.44	15.77	1.89	2.90	9.94
Ol	-	-	-	-	-	-
Mt	11.82	10.50	10.74	5.04	6.68	11.68
Il	7.69	5.57	6.98	1.33	1.88	4.15
Ap	1.44	1.16	2.14	0.28	0.37	1.35

Table 3-1 (cont.). Major-element geochemical analyses and corresponding normative mineralogy.

	BII 56 (CFg)	BIII 30 (SD)	NA3 (FgSh)	NA6 (F/MSh)	NA8 (FgD)
	Wt%	Wt%	Wt%	Wt%	Wt%
SiO2	48.22	47.01	45.66	52.68	47.82
TiO2	3.04	3.33	3.62	1.68	2.74
Al2O3	11.56	12.72	11.65	15.79	15.62
Fe2O3	8.04	7.35	8.31	6.29	5.96
FeO	11.56	11.03	13.00	8.01	8.94
MnO	0.28	0.31	0.40	0.22	0.20
MgO	3.51	3.12	3.54	1.24	3.63
CaO	7.72	7.86	8.83	5.83	7.88
Na2O	2.90	3.40	2.57	4.32	3.67
K2O	0.75	0.73	0.34	1.74	0.50
P2O5	0.97	1.30	1.45	0.41	0.88
LOI	-0.68	-0.57	-0.74	0.23	0.05
Total	98.55	97.59	99.37	98.20	97.84
	CIPW Norm	CIPW Norm	CIPW Norm	CIPW Norm	CIPW Norm
Qz	8.24	5.26	7.21	6.12	3.29
Or	4.43	4.31	2.01	10.27	2.95
Ab	24.51	28.74	21.72	36.55	31.02
An	16.31	17.29	19.24	18.54	24.66
Di	13.07	11.07	12.69	6.60	7.17
Hy	12.32	11.50	14.23	6.86	12.83
Ol	-	-	-	-	-
Mt	11.67	10.68	12.07	9.14	8.66
Il	5.78	6.33	6.89	3.19	5.21
Ap	2.12	2.84	3.17	0.89	1.92

Table 3-2. Trace-element analyses by XRF and ICP-MS (ppm).

	Tr	Tr	Tr	Tr	N	N	OFg
	BS 8g	BS 2d	BS 8c	BI 32	BII 3	BII 1	LBE 42
Rb (XRF)	3.71	3.53	3.82	6.84	3.65	2.86	1.1
Ba	259	213	222	319	305	203	1281
Th	0.38	0.37	0.36	0.72	0.22	0.18	0.15
Nb (XRF)	2.14	2.1	1.71	4.21	0.51	1.27	24.94
Ta	0.2	0.23	0.13	0.31	0.11	0.12	1.17
K (XRF)	4045	3572	4019	6043	6205	4049	3647
La	6.95	5.9	6.3	10.99	4.39	3.15	37.81
Ce	14.86	12.72	12.97	22.91	8.53	6.22	82.59
Pb (XRF)	3.24	3.09	5.16	3.18	6.33	6	9.8
Pr	1.93	1.66	1.65	2.91	1.05	0.76	11.06
Sr (XRF)	476.18	464.04	495.86	461.78	502.41	391.01	417.17
P (XRF)	393	480	310	524	192	87	2880
Nd	8.4	7.25	6.92	12.29	4.32	3.11	48.76
Hf	1.48	1.43	0.92	1.73	0.6	0.58	3.6
Zr (XRF)	57.3	51.74	40.01	77.91	20.93	19.06	165.63
Sm	1.72	2.06	1.39	2.44	0.94	0.73	9.25
Eu	0.91	1.04	0.84	1.07	0.74	0.62	2.95
Ti (XRF)	4436	4136	3231	5035	4448	11628	24216
Gd	1.73	1.99	1.33	2.39	0.95	0.78	8.67
Tb	0.32	0.3	0.25	0.44	0.14	0.12	1.52
Dy	2.03	1.87	1.49	2.78	0.89	0.83	9.25
Ho	0.37	0.32	0.27	0.5	0.16	0.15	1.67
Y (XRF)	8.44	8.05	6.55	11.67	4.04	4.17	47.98
Er	1.07	0.9	0.77	1.41	0.45	0.46	4.67
Tm	0.15	0.13	0.11	0.2	0.06	0.07	0.66
Yb	0.97	0.84	0.69	1.29	0.43	0.48	4.33
Lu	0.14	0.16	0.1	0.18	0.07	0.08	0.62

Note. Elements analysed via ICP-MS unless otherwise noted. Rock name abbreviations as in table 3-1. Ferrogabbroid-monzonite averages were calculated using inner ferrogabbroid and monzonite samples only. The limits of detection for elements determined by XRF were: Rb, 0.7; Ba, 23; Nb, 0.7; Pb, 4; Sr, 1.2; Zr, 1.2; Y, 0.7. The limits of detection for elements determined by ICP-MS were below ten parts per billion (ppb) in all cases.

Table 3-2 (cont.). Results of trace-element analyses by XRF and ICP-MS (ppm).

OFg BS 7c	OFg BS 7i	Mz BS 6a	Mz BS 6c	CFg BIII 10	CFg BII 56	SD BIII 30	FgSh NA 3
12.95	1.27	20.11	20.69	2.56	3.82	9.97	
1123	801	3686	4488	2248	971	1852	708
1.58	0.34	0.28	0.52	0.88	0.69	0.29	0.17
15.8	21.59	18.89	23.29	35.84	32.87	47.03	65.9
0.93	1.18	0.68	1.1	1.83	2.01	1.92	2.75
8654	3808	29138	28972	15201	5624	13512	2823
40.38	51.17	26	39.51	70.38	47.55	70.67	49.89
84.94	116.44	48.96	78.55	154.98	104.84	163.09	117.28
12.5	4.01	11.38	11.87	16.83	13.67	7.6	5.78
10.83	15.8	6.5	10.44	20.78	13.86	22.26	16.61
410.17	623.75	292.26	360.84	781.63	342.24	436.96	571.63
2313	4277	567	742	2706	4233	5673	6328
45.83	69.4	29.29	46.71	91.1	59.93	97.35	77.85
7.28	4.64	18.77	30.09	27.66	3.28	12.57	5.91
255.68	122.42	654.33	862.82	754.59	108.25	478.48	227.45
8.54	12.02	7.1	11.54	19.37	15.58	18.69	19.69
2.45	3.78	4.1	5.74	6.2	3.99	6.29	5.32
17562	21998	4196	5934	13067	18222	19960	21698
7.83	10.23	6.05	9.84	20.27	14.41	17.7	17.32
1.38	1.67	0.8	1.34	2.88	2.03	2.31	2.26
8.47	9.58	4.72	7.79	16.94	12.21	12.95	13.01
1.51	1.65	0.78	1.29	2.93	2.03	2.17	2.09
39.99	41.21	23.42	31.68	75.23	62.77	65.93	64.08
4.26	4.38	2.15	3.62	8.14	5.58	5.81	5.57
0.6	0.57	0.31	0.52	1.11	0.79	0.77	0.75
3.89	3.54	2.07	3.42	7.31	5.03	4.85	4.85
0.56	0.49	0.43	0.71	1.18	0.96	0.76	0.97

Table 3-2 (continued). Trace-element analyses by XRF and ICP-MS (ppm).

F/MSh NA 6	FgD NA 8	Avg Tr	Avg Ln	Avg Fg	Avg Mz	Avg Fg/Mz
5.59	0.03	4.48	3.26	5.11	20.4	12.75
4574	1743	253	254	1068	4087	2578
0.58	0.03	0.46	0.2	0.69	0.4	0.55
22.09	8.46	2.54	0.89	20.78	21.09	20.93
0.85	0.46	0.22	0.12	1.09	0.89	0.99
6212	8573	4420	5127	5370	29055	17212
44.66	48.57	7.54	3.77	43.12	32.75	37.94
97.42	110.8	15.86	7.37	94.66	63.75	79.2
9.7	8.29	3.67	6.17	8.77	11.62	10.2
13.49	14.5	2.04	0.9	12.56	8.47	10.52
632.52	882.22	474.47	446.71	483.69	326.55	405.12
1776	3840	427	140	3156	655	1906
61.39	60.22	8.71	3.72	54.66	38	46.33
25.82	4.48	1.39	0.59	5.17	24.43	14.8
1137.91	181.25	56.74	20	181.24	758.57	469.91
12.78	10.34	1.9	0.84	9.94	9.32	9.63
6.34	3.15	0.97	0.68	3.06	4.92	3.99
10040	16424	4209	8038	21259	5065	13162
12.93	9.13	1.86	0.86	8.91	7.95	8.43
1.74	1.18	0.33	0.13	1.52	1.07	1.3
9.95	6.37	2.04	0.86	9.1	6.25	7.68
1.69	1.06	0.36	0.16	1.61	1.04	1.32
46.96	32.39	8.68	4.11	43.06	27.55	35.31
4.65	2.8	1.04	0.45	4.44	2.88	3.66
0.64	0.36	0.15	0.07	0.61	0.41	0.51
4.24	2.19	0.95	0.46	3.92	2.74	3.33
0.73	0.33	0.14	0.08	0.56	0.57	0.56

Table 3-3. Nd isotopic data for rocks of the Barth Island Ring Complex.

		Nd (ppm)	Sm (ppm)	147Sm/144Nd	143Nd/144Nd	2 sigma	Epsilon Nd (0)
BS 8c	Tr	7.01	1.488	0.1284	0.51184	0.00004	-15.6
BI 32	Tr	11.90	2.529	0.1285	0.51180	0.00003	-16.4
BII 1	N	3.51	0.743	0.1279	0.51169	0.00007	-18.4
LBE 42	OFg	54.76	11.302	0.1247	0.51157	0.00003	-20.9
BS 7c	OFg	43.36	-	-	0.51156	0.00004	-21.0
BS 7i	OFg	70.50	13.334	0.1143	0.51132	0.00009	-25.6
BS 6c	Mz	51.07	10.337	0.1223	0.51144	0.00009	-23.4
BIII 10	CFg	89.85	18.675	0.1256	0.51162	0.00003	-19.9
BII 56	CFg	71.91	-	-	0.51157	0.00003	-20.8
BIII 30	SD	114.42	21.253	0.1123	0.51130	0.00004	-26.1

		T(DM) DeP	T(DM)2	Epsilon Nd (t)	t
BS 8c	Tr	2155	2248	-4.0	1330
BI 32	Tr	2229	2319	-4.8	1330
BII 1	N	2408	2490	-6.7	1330
LBE 42	OFg	2542	2614	-8.7	1320
BS 7c	OFg	-	-	-	-
BS 7i	OFg	2655	2712	-11.8	1320
BS 6c	Mz	2699	2760	-10.9	1320
BIII 10	CFg	2480	2557	-7.9	1320
BII 56	CFg	-	-	-	-
BIII 30	SD	2637	2694	-12.1	1300

Note. T(DM) DeP is the Nd isochron age of the sample, calculated using the method of DePaolo (1981; 1988). T(DM)2 is calculated using a linear evolution for a mantle separated from the CHUR at 4.55Ga and having a present day Epsilon value of +10. The ε_{Nd} (t) of samples for which Sm data are unavailable cannot be calculated. Rock name abbreviations as in table 3-1.

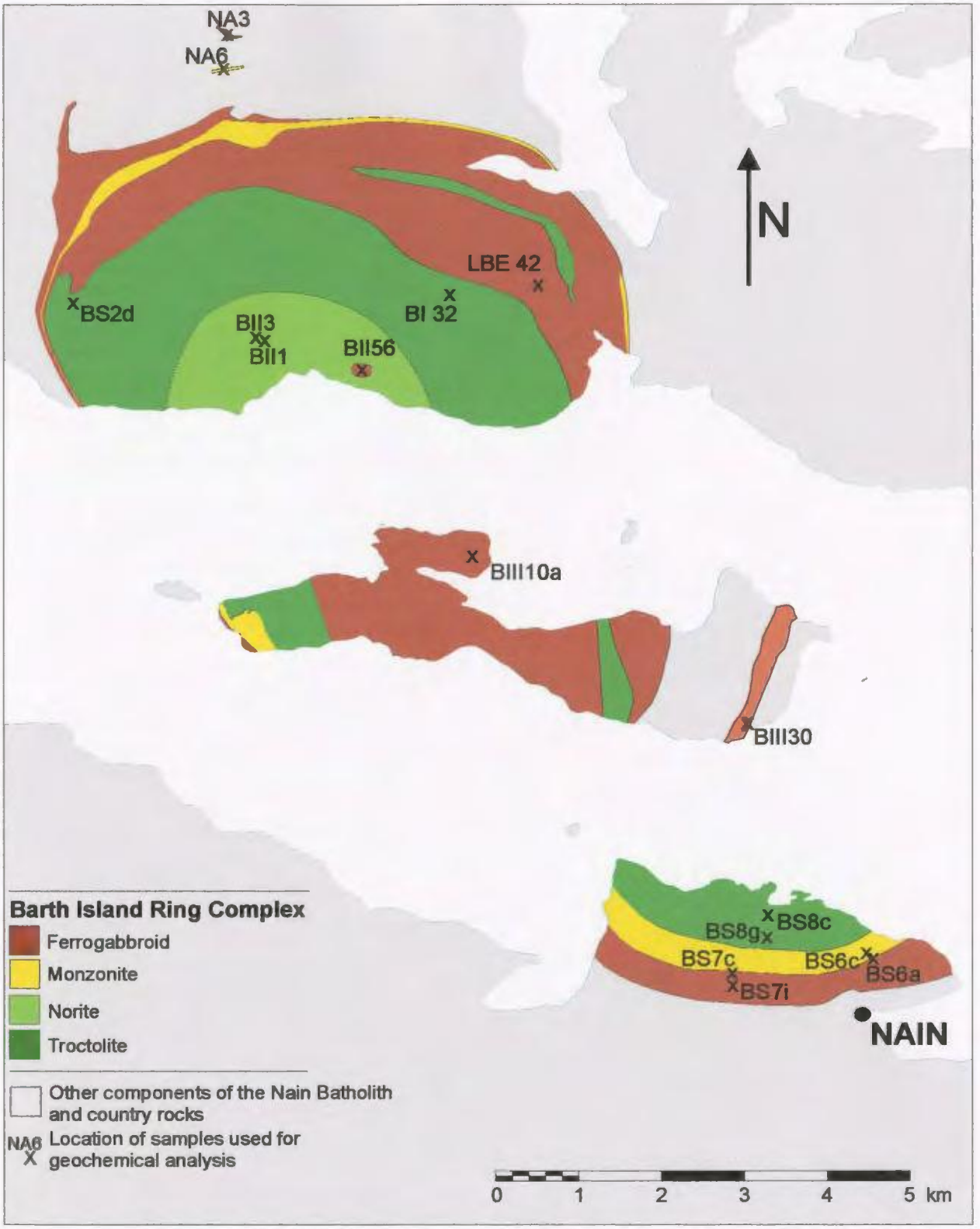

Figure 3-1. Simplified geological map of the Barth Island Ring Complex showing the locations of samples used for geochemical analyses. Sample NA8 is not shown; it is located farther north. Outer Leuconorite unit not shown.

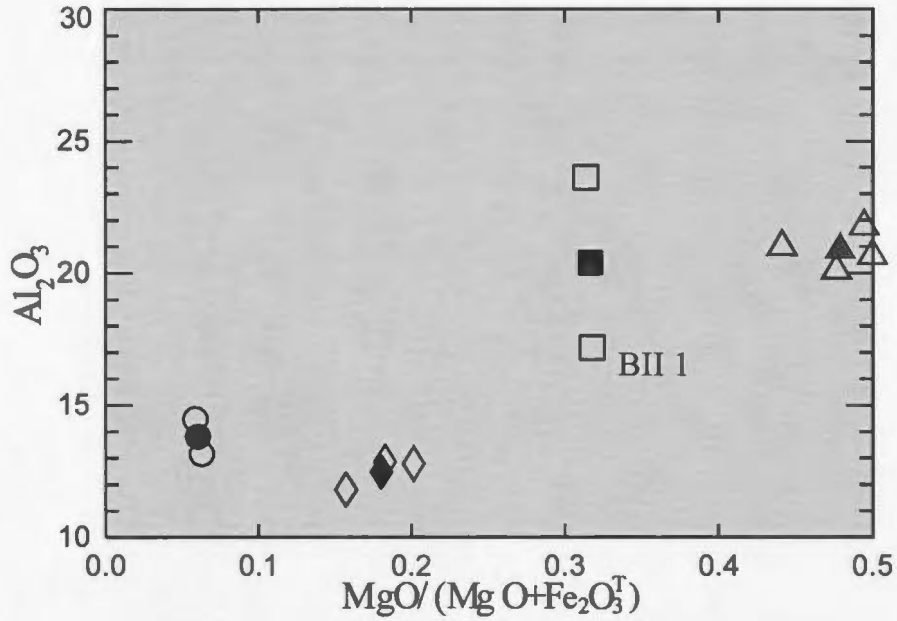

Figure 3-2. Plot of wt. % Al_2O_3 against Mg number for samples of the Barth Island Ring Complex. Explanation of symbols: triangles are troctolite; squares are leuconorite; diamonds are outer ferrogabbroid; circles are monzonite. Averages for the troctolite, leuconorite, outer ferrogabbroid, and monzonite are represented by filled symbols of the same respective type.

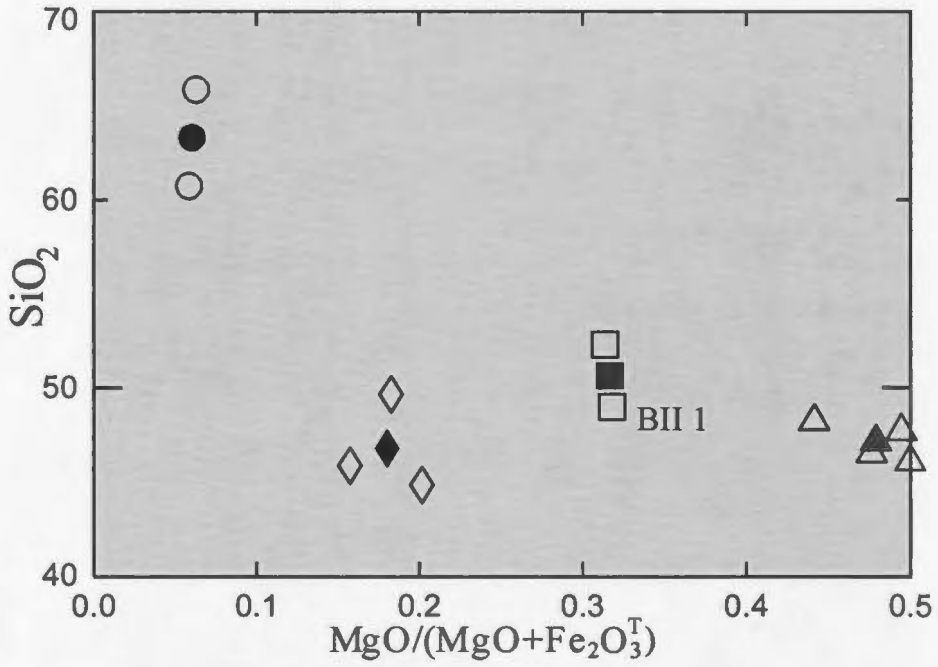

Figure 3-3. Plot of wt. % SiO_2 against Mg number for samples of the Barth Island Ring Complex. Total silica values for ferrogabbroid samples and troctolite samples are similar, but the Mg numbers of the ferrogabbroid samples are much lower than the troctolite samples. Symbols as in fig. 3-2.

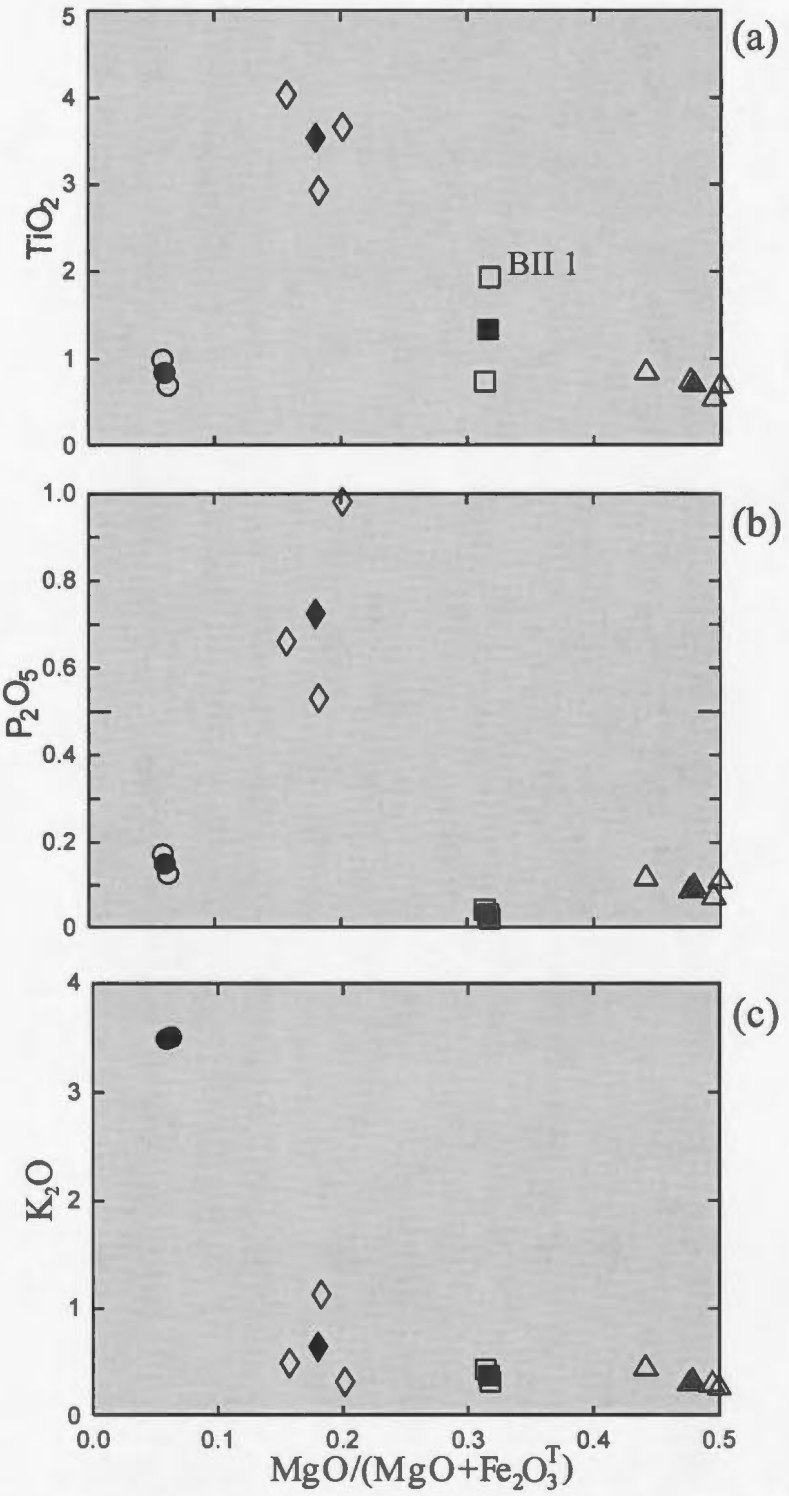

Figure 3-4. Plots of (a) TiO_2, (b) P_2O_5 and (c) K_2O against Mg number for samples of the Barth Island Ring Complex. Symbols as in fig. 3-2. The ferrogabbroid samples have higher TiO_2, P_2O_5 and lower K_2O than the monzonite samples. Troctolitic and noritic samples have low P_2O_5 and K_2O.

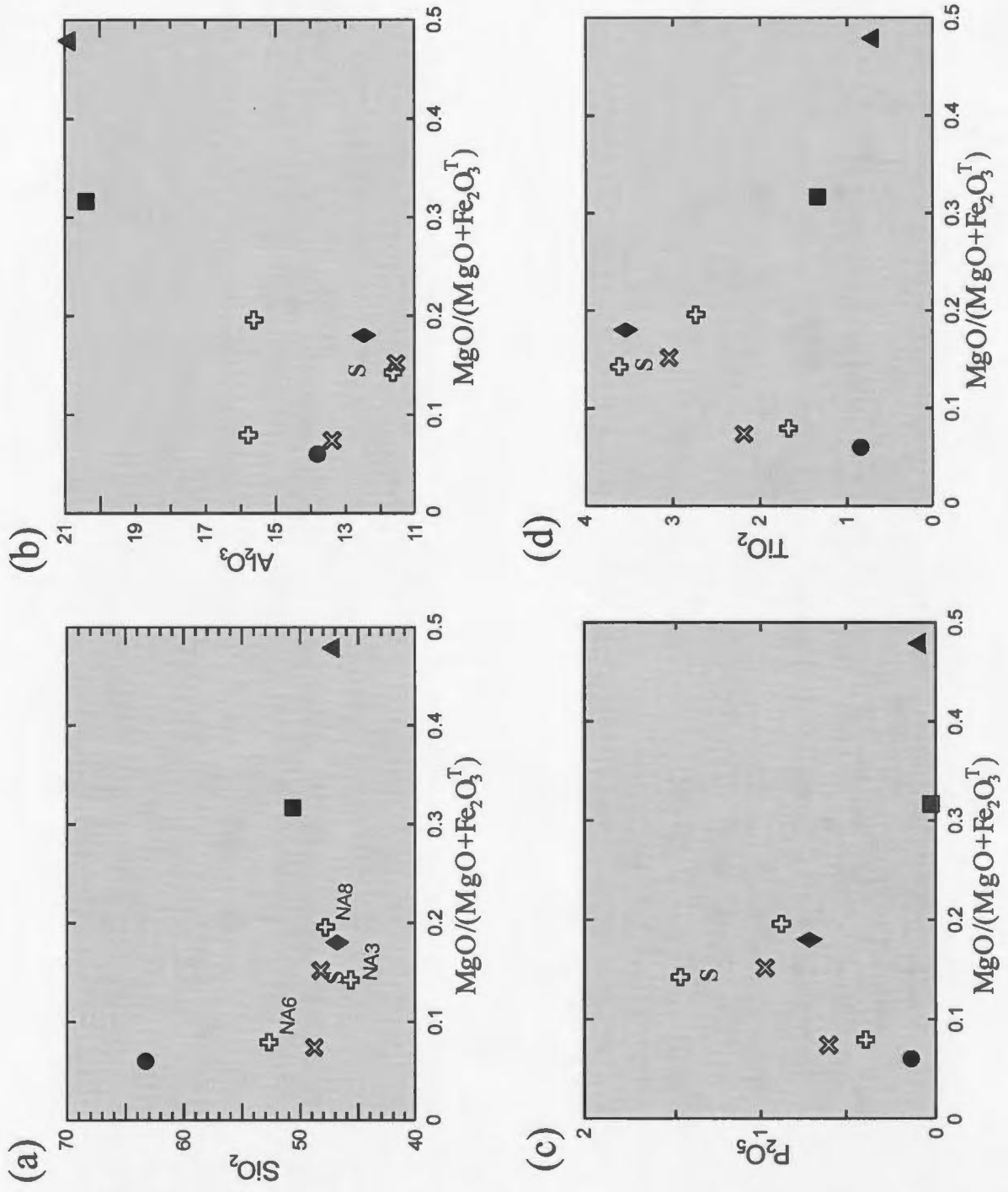

Figure 3-5. Plots of (a) SiO_2, (b) Al_2O_3, (c) P_2O_5, and (d) TiO_2 against Mg number for the central ferrogabbroid and samples other than those of the Barth Island Ring Complex. The data show large spread in values and no obvious correlations; see text for details. Upright crosses represent sheets or dykes intruded into anorthosite to the north of the Barth Island Ring Complex, diagonal crosses denote central ferrogabbroid of the Barth Island Ring Complex, and the 'S' denotes the Satorsoakulluk Dyke. All other symbols as in fig. 3-2.

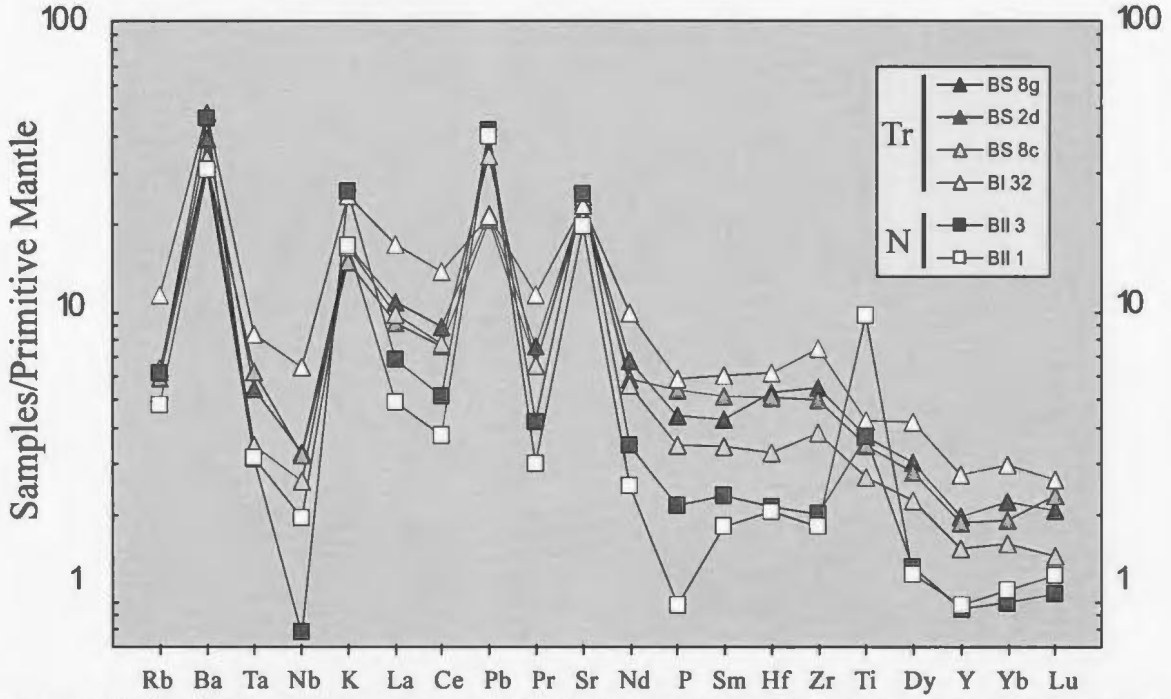

Figure 3-6. Multi-element plot illustrating trace-element variations in troctolite and norite of the Barth Island Ring Complex. Values on this and all other multi-element plots are normalized to the primitive mantle values of McDonough and Sun (1995).

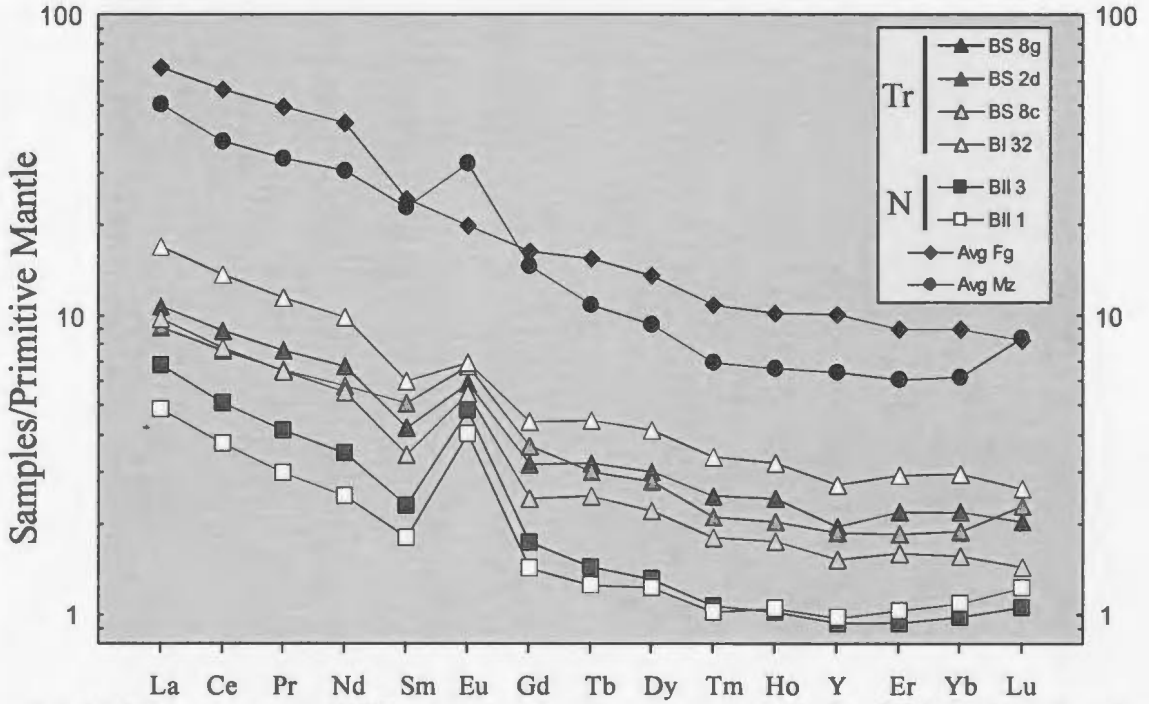

Figure 3-7. Multi-element plot of REE values for troctolite and norite of the Barth Island Ring Complex.

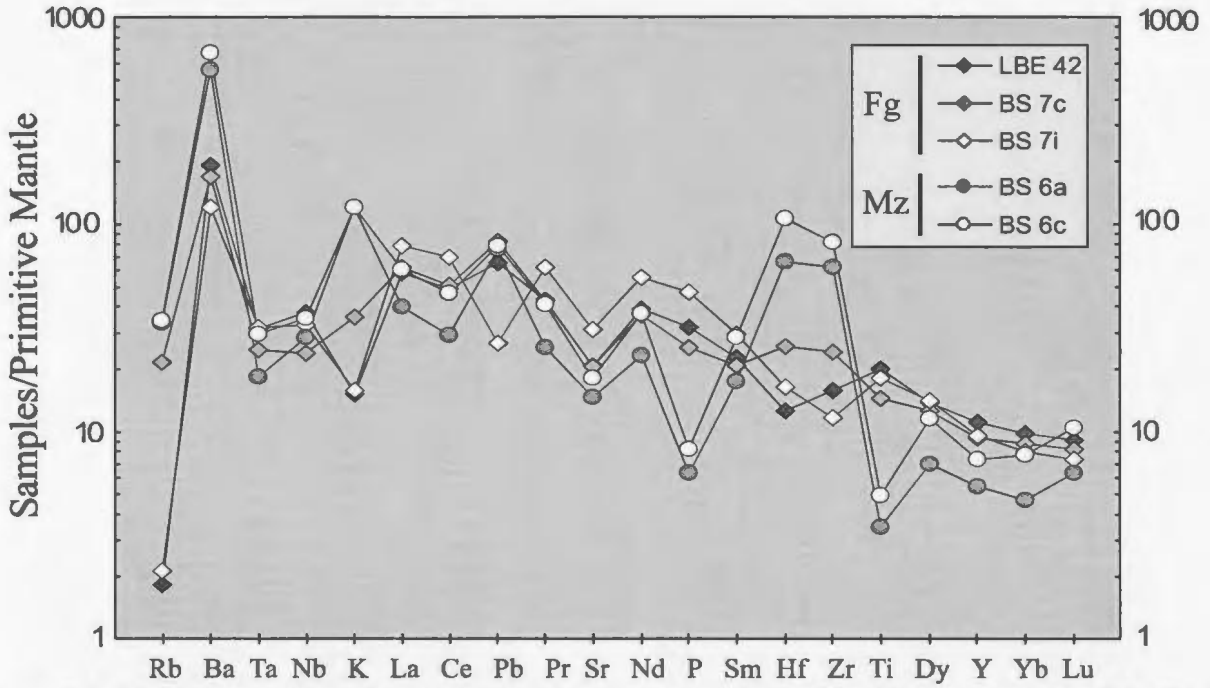

Figure 3-8. Multi-element plot of trace-element values for outer ferrogabbroid and monzonite of the Barth Island Ring Complex. Fg is ferrogabbroid; Mz is monzonite.

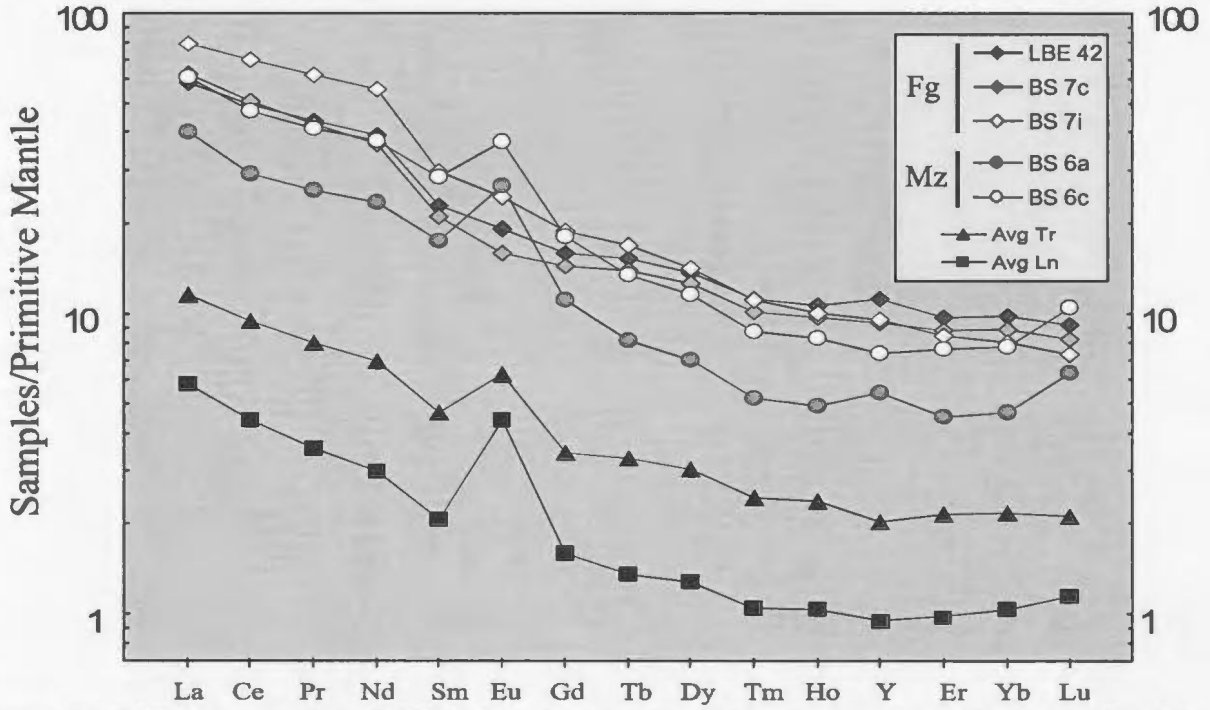

Figure 3-9. Multi-element plot of REE values for troctolite and norite samples of the Barth Island Ring Complex. Abbreviations as in fig. 3-8.

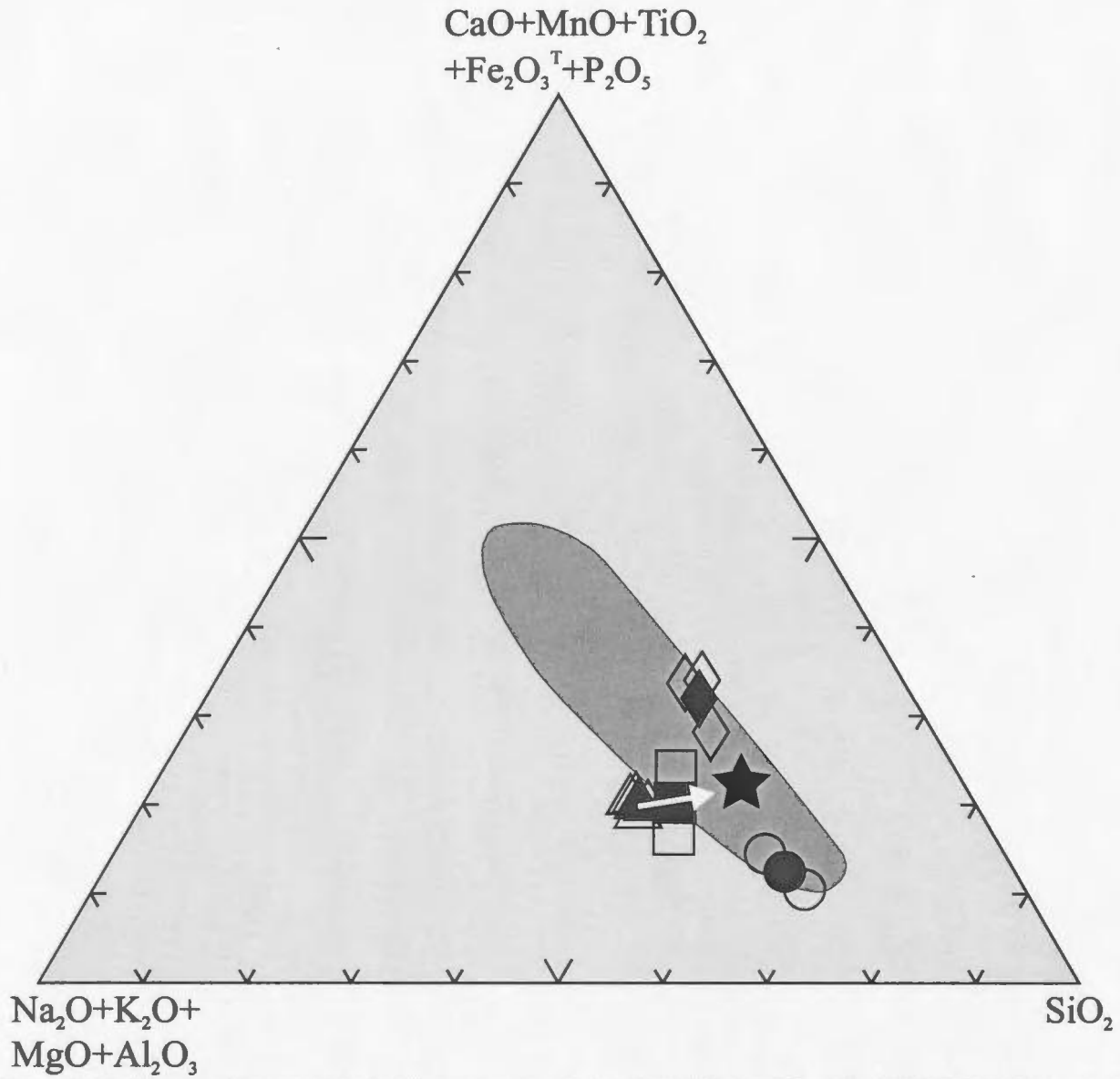

Figure 3-10. Ternary diagram showing the approximate two-liquid field of Roedder (1951) from the system fayalite-leucite-silica (dark area). The average ferrogabbroid and monzonite of the Barth Island Ring Complex lie at the edges of the field. The white arrow shows the apparent path of evolution of the troctolitic rocks through norite; the average combined composition of ferrogabbroid and monzonite (the star, assuming one-to-one proportions) lies in the path of the trend. Symbols as in fig. 3-2. Modified from Philpotts (1990), pp. 253 and 308; his figs. 13-17 and 14-22, respectively.

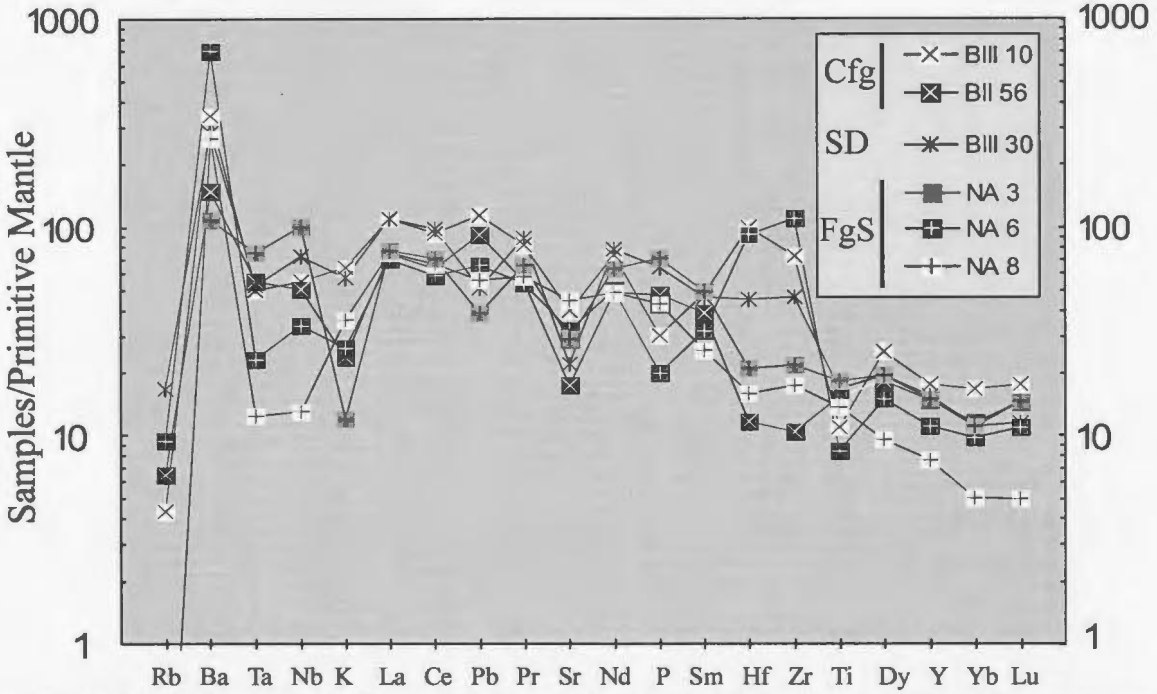

Figure 3-11. Multi-element plot for central ferrogabbroid of the Barth Island Ring Complex, and for ferrogabbroid dykes and sheets. Rb for sample NA 8 is below the LOD for this element. See legend at upper right for symbols. Cfg is central ferrogabbroid; SD is the Satorsoakulluk Dyke; FgS is two ferrogabbroid sheets and one ferrogabbroid dyke.

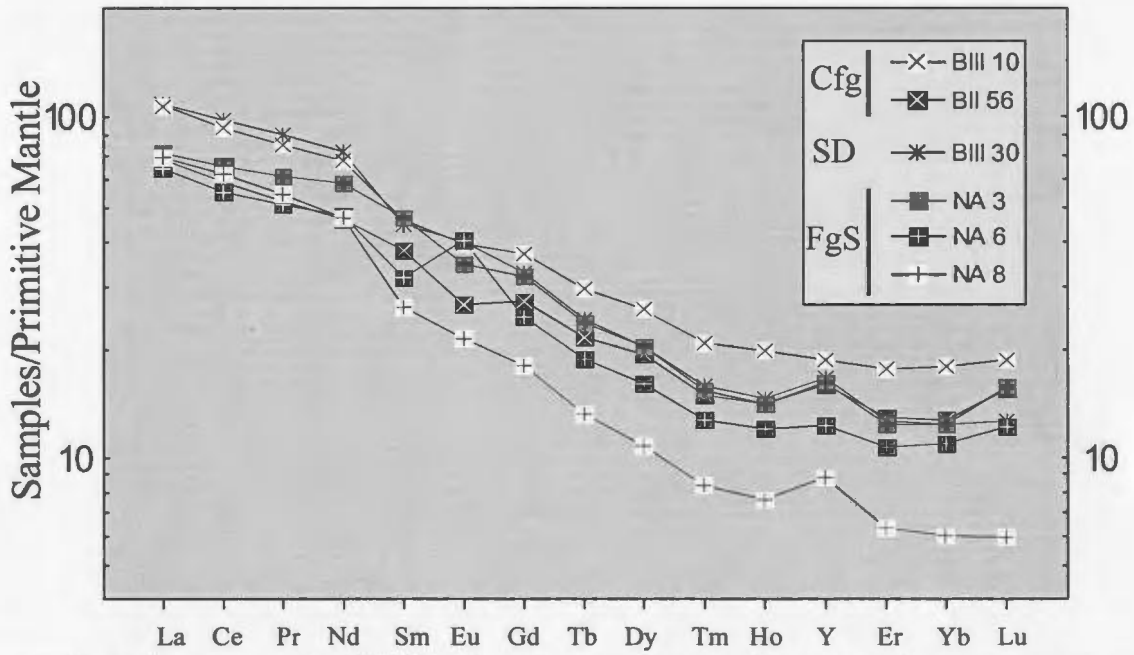

Figure 3-12. Multi-element plot of REE values for central ferrogabbroid and ferrogabbroid sheets and dykes. Abbreviations as in fig. 3-11.

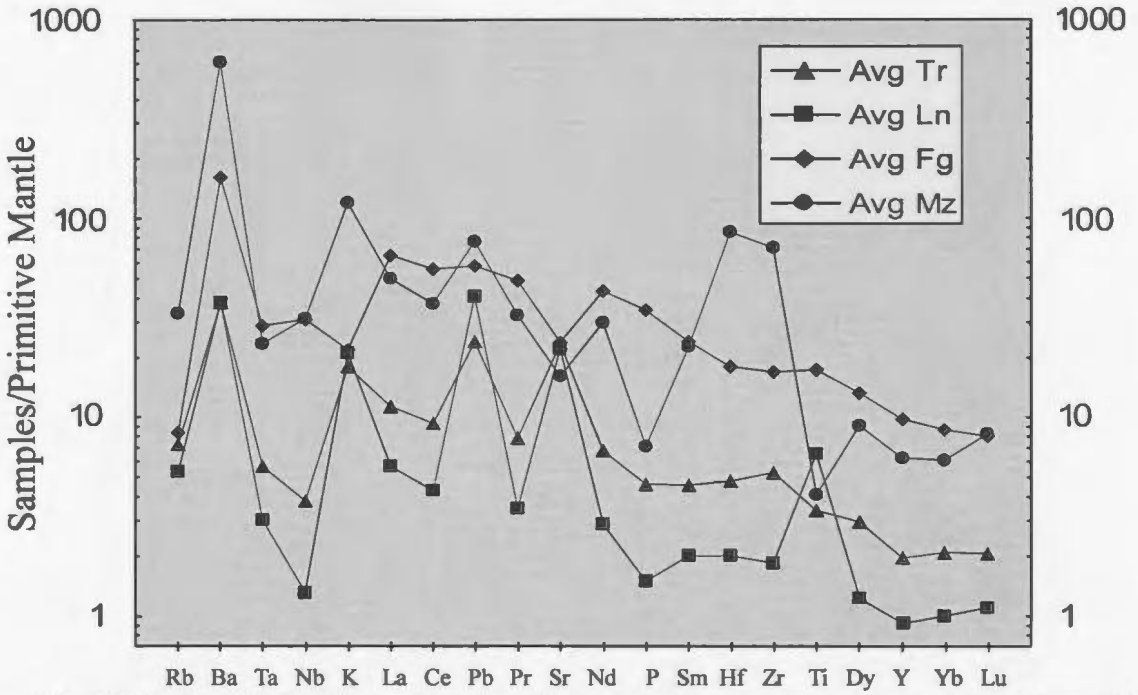

Figure 3-13. Multi-element plot of average values for troctolite, norite, monzonite, and outer ferrogabbroid samples from the Barth Island Ring Complex.

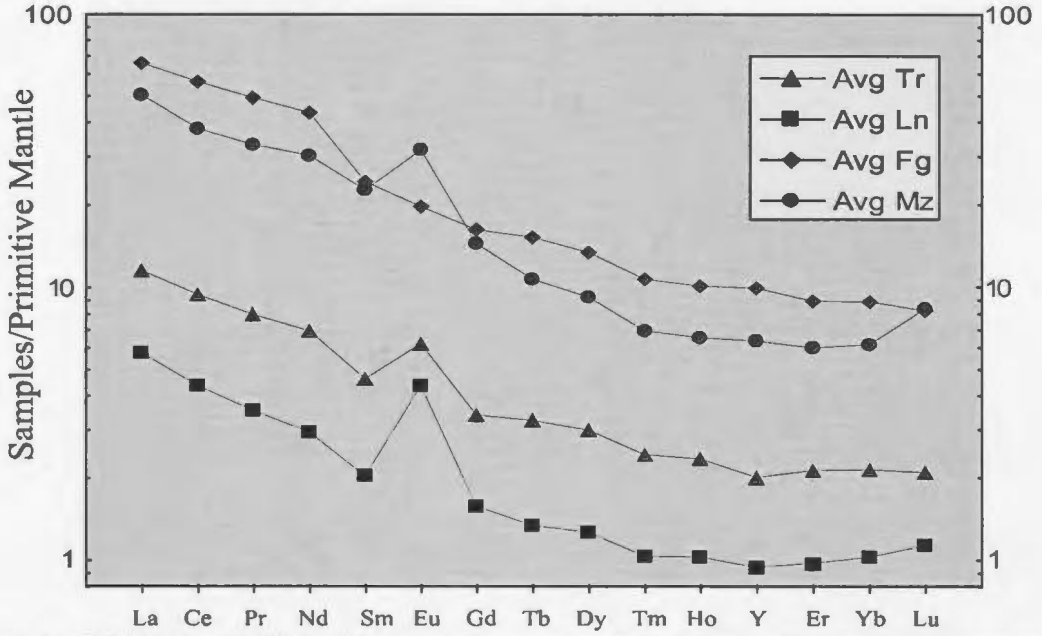

Figure 3-14. Multi-element REE plot showing average values for troctolite, norite, monzonite, and outer ferrogabbroid of the Barth Island Ring Complex.

Chapter 4 U-Pb Geochronology

4.1 Introduction

The establishment of an absolute chronology enables comparisons between geographically disparate rocks, and may resolve ages of contiguous rocks where relative age based on field relations is ambiguous. Such resolution is particularly important in the Nain Batholith (NB), where the genesis and fundamental relations of a group of well-recognized rock types are much debated.

The Barth Island Ring Complex contains four distinct rock types (leuconorite, monzonite, ferrogabbroid, and troctolite), which were previously inferred to have been differentiation products of a single body of mafic magma (de Waard, 1976). The present study has found that the ring complex is not derived from a single body of magma. The contact relationships within the Barth Island Ring Complex indicate that the monzonite and ferrogabbroid are derived from contemporaneous, but probably distinct, magmas (section 2.6.1); that the troctolite is probably older than the other members of the ring complex; and that the leuconorite is the youngest member of the ring complex.

In a previous study (Hamilton, 1997), it was claimed that monzonite and troctolite are comingled at one location along their contact south of Nain Bay (fig. 4-1, point A). However, I found that the contact relations at this location are ambiguous, and therefore give no evidence of the relative ages of the two rock types. Other *prima facie* evidence for the relative timing of the troctolite with respect to the monzonite and ferrogabbroid of the

Barth Island Ring Complex suggests that the monzonite is younger than the troctolite (section 2.9.3); the troctolite and norite appear to have been part of a separate magmatic event. U-Pb dating of zircon and baddeleyite was carried out to clarify this issue.

4.1.1 Previous work

The outer ferrogabbroid and monzonite of the Barth Island Ring Complex were dated, using sensitive high-mass resolution ion microprobe (SHRIMP) U-Pb techniques on zircon, by Hamilton *et al.* (1994) and Hamilton (1997) respectively. The ferrogabbroid sample used by Hamilton *et al.* (1994) was taken from the west end of Barth Island (point B, fig. 4-1), and the monzonite sample used by Hamilton (1997) was obtained near the contact with the southern margin of the troctolite (point A, fig. 4-1)[1]. The monzonite age is 1320 ± 1.5 Ma; the ferrogabbroid was originally reported as 1322 ± 2 Ma, but has been revised to 1321 ± 1 Ma (Hamilton, 2002, pers. comm.). The agreement within error is consistent with the observed field relationships; the ages support the conclusion of monzonite-ferrogabbroid contemporaneity.

4.1.2 Sample selection

The unit of ferrogabbroid dated by Hamilton *et al.* (1994) from the west end of Barth Island has no exposed contact with the ferrogabbroid on either the south or north sides of Nain Bay. It was decided that another ferrogabbroid sample should be subject to

[1]This sample was acquired at the site where Hamilton inferred that monzonite and troctolite are comingled.

age determination because such an age determination would provide clear evidence in support of establishing (or dismissing) a temporal link between ferrogabbroid on Barth Island and the south side of Nain Bay. As noted, an absolute age for the ferrogabbroid also provides an age for the monzonite.

The location of the sample dated is shown in fig. 4-1 (BS 9d). The ferrogabbroid is a complex rock type, having a wide range of textures and some heterogeneity in mineral assemblage. Multiple layers, defined by grain size, texture, and mineral assemblage, of various thickness and extent, are present everywhere (section 2.4). The location of sample BS 9d was chosen to maximize distance from the monzonite, reducing the likelihood of contamination. Thin section analysis of sample 9d, however, has shown that it may be a monzonite-ferrogabbroid hybrid.

Because some disagreement exists about the relative age of the troctolite (Ryan, 2001; Hamilton, 2002, pers. comm.) it was decided that the troctolite should be the subject of an absolute age determination. Two samples of the troctolite were dated; the locations of these samples are shown in fig. 4-1. One sample of leuconorite (BS 4a) was also the subject of absolute age determination.

4.1.3 Grain morphology

The ferrogabbroid sample had two populations of zircon: small, light pink, needle-like grains that have abundant inclusions of apatite grains, and a second group of yellow-pink prismatic fragments (plate 4-1). Grains were picked from each population for

dating. Care was taken to pick grains from the needle-like population that did not contain inclusions of apatite.

One troctolite sample (BS 8b) contained two U-rich minerals, baddeleyite and zircon, both of which were used for U-Pb age determination. The troctolite zircon grains are generally clear pale yellow fragments that show no crystal faces, though some subhedral grains have been found (plate 4-2). Baddeleyite from sample BS 8b are small (ca. 0.05 to 0.1 mm), thin, honey brown flakes (plate 4-2, inset). The second sample, BS 8e, was thought to contain only baddeleyite, but was later found to have zircon (Hinchey, 2004, pers. comm.). Only the baddeleyite were dated. The baddeleyite is generally larger (up to ca. 0.2 mm) than baddeleyite from sample 8b, and occurs as honey brown to deep brown subhedral to euhedral grains and fragments of variable size (plate 4-3). A few large, irregular grains were present.

The leuconorite sample, BS 4a, contains both baddeleyite and zircon, but only zircons were dated. The zircons are primarily pale yellow fragments without crystal faces (plate 4-4), like those in troctolite sample BS 8b; the zircon was observed in a thin section of the sample. These grains occur interstitially, in association with magnetite and biotite. The zircon was analysed by electron microprobe to ensure that it was not a mineral of optical properties similar to zircon, and a positive identification was obtained. Plates 4-5a and 4-5b show backscatter images of the zircon grain, obtained from the electron microprobe. Plates 4-6a and 4-6b are photomicrographs of the same grains in plane polarized light and with crossed polars, respectively.

The morphology of baddeleyite grains from sample BS 4a is similar to those found in sample BS 8b (plate 4-2).

4.2 Preparation and analytical procedures

4.2.1 Initial sample preparation

Samples were scrubbed using a stiff-bristle plastic brush, and crushed to a long radius of less than 4 cm using a hydraulic press. The sample was bagged and taped shut awaiting full preparation[2] of the jaw crusher. When the jaw crusher was fully assembled, a bag was carefully taped underneath to catch the sample. After all the sample had been fed, the bag was removed and again taped shut. A disc mill was utilised for the final crushing stage. A bag was taped underneath this machine to catch the sample, then removed and taped shut again.

The Wilfley table is the first stage of mineral separation. The table uses running water to separate minerals by density. The separates from this process were collected, rinsed at least three times[3] in ethanol, then dried and stored in closed plastic tubs. The light fraction was set aside and remains unused. The heavy fraction was sieved to remove large material, and a magnet was then utilized to remove highly magnetic material. Both the magnetic fraction and nonmagnetic fraction were kept.

---

[2] Preparation of all equipment includes a thorough cleaning using a shop vacuum, a high pressure air hose, and ethyl alcohol. A drum vacuum is run during equipment usage to minimize airborne particulate matter.
[3] I used additional rinses for larger separates.

The nonmagnetic fraction was immersed in methylene iodide. After mixing and settling the sample three times, the part of sample that sank was drained off first, thoroughly rinsed with acetone, and kept for a further magnetic separation process. The less dense fraction was also rinsed, but was set aside and remains unused.

The magnetic separation process was carried out using a Frantz isodynamic magnetic separator. The sample was run at an angle of 10° and 0.5, 1.0, and 1.7 amperes. The amperage was then held at 1.7 A and the angle was successively reduced to 5°, 3°, 1°, and then held at 0°. The troctolite and norite samples were not run at an angle of less than 3°, because the remaining fraction had become too small.

The final separate was examined under a microscope, and suitable grains were hand-picked for morphology, colour, size, and crystal quality. The final grains were abraded (Krogh, 1982), washed with 4N HNO_3 at 120°C, water, and alcohol. The best grains were then chosen for isotopic analysis.

4.2.2 Final sample preparation

Final sample preparation and analyses were carried out by Dr. Marc Poujol. The picked fractions were washed with water, leached at >100°C with 4N nitric acid, and then washed again using acetone. Each wash was accompanied by 10 seconds ultrasonic agitation. Fractions were then weighed (uncertainty 2-10 mcg), and dissolved (at 220°C) in concentrated hydrofluoric and nitric acid over a period of 5 days, using high-P Teflon

bombs or Teflon Savillex containers. The solutions were spiked with a ^{205}Pb-^{235}U tracer solution according to sample weight, expected age, and U concentration. The samples were then redissolved in 3.1N HCl. U and Pb were separated using zircon-modified ion-exchange chemistry (Dubé *et al.*, 1996). Blanks of 1 pg U and 2-12 pg Pb were used during the analysis.

4.2.3 Sample analysis

Analyses were conducted using thermal ionization mass spectrometry (TIMS), on a Finnegan MAT 262 mass spectrometer. U and Pb were loaded in a substrate of trihydrogen phosphate and silica gel, on an outgassed single rhenium filament. U and Pb were measured in static mode on Faraday cups; ^{204}Pb was measured on an ion-counting secondary electron multiplier (SEM), which was calibrated with the Faraday cups. Small fractions, such as ^{205}Pb or ^{207}Pb, were measured by peak jumping on the SEM and were checked against data from the Faraday cups. Emission intensity was monitored, allowing temperature adjustment to maintain stable emission.

The calculation of common Pb was made by subtracting blanks and assuming that the remaining common Pb has Proterozoic composition determined from the model of Stacey and Kramers (1975). Data were reduced using PbDat (Ludwig, 1993). Analytical uncertainties in Table 4-1 are listed at 2 and age determinations were processed using Isoplot/Ex (Ludwig, 2000).

4.3 Results

A total of 8 single zircon grains or small fractions from both types of zircon in the ferrogabbroid sample, BS 9d, were analysed. The abundances of U and Pb are heterogeneous: from 90-415 ppm and 23-109 ppm, respectively (table 4-1). On a concordia diagram (fig. 4-2), they are concordant to slightly discordant (maximum 1.5%) and define a discordia pointing to a well-defined upper intercept age of 1317.2 + 2/- 1.8 Ma (MSWD = 0.61). This result is nearly within error of the age of Hamilton *et al.* (1994) for the Barth Island ferrogabbroid, 1321 ± 1 Ma. It is within error of the monzonite (1320 ± 1.5 Ma) dated by Hamilton (1997). The results are evidence for the contemporaneity of monzonite and ferrogabbroid, which is in any case made plain by the field relations. The results provide a temporal link between ferrogabbroid on Barth Island and similar ferrogabbroid on the south side of Nain Bay, because the difference between the margins of error is small.

The normal discordance of a few of the zircon fractions indicates that there was some Pb loss, which could be due to a thermal disturbance. However, two of the fractions are slightly reversely discordant. This might be caused by an analytical problem, such as incomplete dissolution of the measured zircon or small problems with correction factors. Alternatively, it might be a real quality of the analysed zircon caused by in-grain mobility of radiogenic Pb, which was the explanation used for reversely discordant zircon cores from the Mt. Sones granulite (Williams, 1992). If the observed reverse discordance is a real quality of the zircon, it most likely would result from the measurement of a

zircon fragment, because a whole-grain analysis would measure both depleted and enriched areas of a specific zircon. However, one of the reversely discordant points (Zr 4) is an analysis of a single grain which, on the basis of its morphology, was probably not a fragment. It is therefore considered more likely that reverse discordance exhibited by this grain resulted from some analytical imprecision, although the possibility remains that the abrasion process (Krogh, 1982) removed an exterior depleted in radiogenic Pb.

Of the other reversely discordant analyses, one (Zr 1) is a single grain analysis, and the other (Zr 6) is a multi-grain analysis. The morphology of these zircons was such that they could have been fragments of larger grains. It is therefore possible that some in-grain Pb mobility resulted in the observed reverse discordance. However, the discordance is small (0.1-0.2%), and, because the grain with the most reverse discordance (0.3%) has been interpreted to be the result of analytical error, the simplest interpretation of all the reverse discordance is as the result of analytical imprecision.

Five single grains or small fractions of zircon were dated from leuconorite sample 4a. These zircons are U- and Pb-poor (22-53 ppm and 6-15 ppm, respectively). They plot in a concordant to sub-concordant position (fig. 4-3) and yield a well-defined upper intercept age of 1333.2 ± 3.8 Ma (MSWD = 1.5). The lower intercept is nearly within error of the present day, indicating that the discordance could be due to weathering processes.

Zircon in leuconorite sample 4a are anhedral, interstitial (plate 4-6), and have low U and Pb concentrations, consistent with crystallization from a U-poor parental

magma. Contacts between zircon and other minerals are sharp, indicating that the original morphology of the zircon was not modified subsequent to crystallization. These observations indicate it is unlikely that the zircons are inherited. The age of ca. 1333 Ma is taken as the leuconorite's emplacement age.

The troctolite sample BS 8b has two U-rich minerals, baddeleyite and zircon. Both of these minerals were analysed, with different results for each. Four small fractions of zircons (1-6 grains each) were analysed for leucotroctolite sample 8b. Their U and Pb contents are consistent, ranging from 200-350 ppm and 50-108 ppm, respectively (table 4-1), and, when plotted on a concordia diagram (fig. 4-4a), they are sub-concordant to slightly (5%) discordant. They define a discordia with an upper intercept age of 1331 ± 1.4 Ma, significantly older than the age obtained for the outer ferrogabbroid (and monzonite). The lower intercept age is ca. 0 Ma, indicating the discordance can be interpreted as recent Pb loss, perhaps due to weathering processes.

Five small fractions of baddeleyite were also analysed for sample 8b (table 4-1). These are characterised by high U and Pb contents (305-780 ppm and 64-164 ppm, respectively), higher, on average, than those of the 8b zircon. This finding is contrary to some other reports (see Heaman and LeCheminant, 1993), in which baddeleyite from particular samples have lower U and Pb concentrations than correlative zircon.

In contrast to the 8b zircon, the 8b baddeleyite fractions do not define a simple trend on the concordia diagram (fig. 4-4b). One fraction (BAD 1) is perfectly concordant at 1317 ± 2 Ma, and a second (BAD 2) is 99.9% concordant at 1314 ± 2 Ma,

and the three remaining fractions plot in a scattered way around these two dates. A poorly constrained discordia age of 1318 ± 10 Ma (MSWD = 6.1), obtained by combining the data of all five fractions, is calculated but must be considered tentative. These data are further discussed below.

In order to eliminate the possibility that the first troctolite sample (BS 8b) had somehow been contaminated by zircon during the mineral separation process, a second sample (BS 8e) from the same area was crushed and prepared. Four small fractions of baddeleyite were analysed (table 4-1). They plot in a slightly discordant (maximum 1.5%) position (fig. 4-5), and do not define a simple trend. Two baddeleyite fractions (BAD 1 and BAD 3) display the same $^{207}Pb/^{206}Pb$ date of 1332 Ma (table 4-1), defining an upper intercept age of 1332 ± 2 Ma, within error of the BS 8b zircon ages. The two remaining fractions, BAD 2 and BAD 4, yield younger $^{207}Pb/^{206}Pb$ dates of 1325 Ma and 1318 Ma, respectively (table 4-1).

The presence, in troctolite sample BS 8e, of baddeleyite of coincidental age with the BS 8b zircon is good evidence that there was no contamination of either sample. However, the baddeleyite dates from BS 8e, as with those of BS 8b, indicate some complexity. There are several possibilities which might explain the various dates, and these are discussed in the next section.

4.4 Discussion

Field observations and petrography have been interpreted to suggest the leuconorite is related to the troctolite, as a product of differentiation of the troctolitic magma. If so, the zircon age for the leuconorite, 1333.2 ± 3.8 Ma, confirms the age of the troctolite at ca. 1331 Ma. However, geochemical and isotopic data (chapter 3) could be interpreted to suggest a more complex relationship between the norite and troctolite. Although these data alone may be plausibly explained without contradicting the suggested genetic relationship between the two rocks, the baddeleyite data indicate that the alternative, that the rocks are not genetically related, must be considered.

For instance, the U contents of zircon in the troctolite and norite are different, which could be taken to confirm the hypothesis of a separate parent magma for each. However, the difference in U contents is consistent with the primary mafic mineral in each rock: the size of the U^{4+} ion (Shannon, 1976) is more compatible with the site radii of clinopyroxene (Wood and Blundy, 1997) and orthopyroxene than to that of olivine (Beattie *et al.*, 1991); the U pyroxene/melt partition coefficient should be higher than the corresponding olivine value. The broad exclusion of U from olivine would result in melt enrichment of U and, eventually, higher U contents in the troctolite's zircon, as is observed.

The U data are consistent with the norite and troctolite being related, but the following text still considers explanations for the data which are premised on the two rocks being unrelated. Assuming this premise, there are a few theories which could

explain the discrepancy between the older zircon and baddeleyite ages obtained from the troctolite, and the younger baddeleyite ages.

1. The zircon age is the correct age of emplacement for the troctolite; baddeleyite from sample BS8b formed as the result of metamorphism, perhaps induced by the intrusion of the outer ferrogabbroid.
2. The baddeleyites from sample BS 8b give the emplacement age for the troctolite. The zircon and older baddeleyite are therefore inherited or are products of crystallization at depth.
3. The zircon age is the correct emplacement age for the troctolite; baddeleyite grains from sample BS 8b have lost a fraction of their Pb.

There is a simple test available for the first possibility. The few data available on the formation temperature of baddeleyite from zircon focus on reactions which occur at temperatures upwards of 800°C (Ferry *et al.*, 2002). Petrographic analysis has shown there is no evidence for a metamorphic event of this nature.

The second scenario, that of zircon inheritance, requires consideration of a few lines of argument.

In a study of zircon and baddeleyite found together in gabbroic dykes, Vaasjoki and Sipilä (2001) reasoned that the zircons they found were unlikely to have crystallized from a silica-undersaturated magma, whereas baddeleyite is the characteristic

Zr-bearing mineral of silica undersaturation. The zircons were therefore interpreted by the authors as inherited. Zircon occurrence in low-silica magmas, however, is well documented (Heaman and LeCheminant, 1993; Amelin *et al.*, 1999), so reasoning of the type used by Vaasjoki and Sipilä (2001) is not binding for all situations where zircon and baddeleyite occur together in mafic rocks.

An obvious possible objection to zircon inheritance concerns whether inherited zircon (and baddeleyite) crystals could survive in a troctolitic magma. This seems unreasonable, because zircon saturation in a typical mafic magma occurs 500°C below the liquidus temperature of the troctolite[4]. However, zircon survival in this environment could be ensured if the zircon provided a nucleation site for early crystals of other minerals in the magma, subsequently became armoured by them, and were therefore protected from reaction with the liquid. This is a mechanism invoked to explain inherited zircons in hot granitic magmas (Clemens, 2003)[5]. Strongly resorbed, 'amoeboid' zircon grains in olivine gabbro of the Voisey's Bay Intrusion yielded an age of ca. 1.9 Ga, some 550 m.y. older than the well-constrained age of 1334 Ma from magmatic zircon and baddeleyite (Amelin *et al.*, 1999).

The morphology of zircon from sample BS 8b, however, is similar to that of zircon interpreted by other authors to have formed in mafic intrusions (Heaman and LeCheminant, 1993; Scoates and Chamberlain, 1995). If the grains are inherited, then,

[4]A liquidus temperature of 1317.77°C was calculated for the troctolite using MELTS (Ghiorso and Sack, 1995). This is a rough approximation, because the troctolite is a cumulate rock.
[5]The temperatures of which are still below those of typical mafic magmas.

they may have been inherited from a penecontemporaneous mafic intrusion, parts of which were assimilated or transported as xenoliths by the troctolitic magma. In this case, there are two distinct possibilities which could lead to zircon inheritance. First, some baddeleyite and all zircon might have crystallized in a long-lived staging chamber at lower crustal depths, whereas the rest of the baddeleyite was formed much later upon the final ascent of troctolitic magma. This origin requires crystallization of these minerals at high temperatures and pressures. The other possibility is 'inheritance' of the zircons from already crystalline material, either at depth or during ascent and emplacement. These two possibilities can be reduced by considering the following argument.

Baddeleyite and zircon probably would not be saturated in a mafic magma chamber at lower crustal temperatures and pressures before the magma was mostly solid. Zircon saturation in a typical mafic magma, for example, occurs at temperatures of ca. 750°C (Watson and Harrison, 1983), and Heaman and LeCheminant (1993) report that baddeleyite most commonly crystallizes from the late-stage, fractionated part of mafic melts, along with apatite, zircon, and ilmenite. It is therefore requisite that, if the zircon and older baddeleyite are inherited, they must have been inherited from an already-crystalline body. The argument supporting this is as follows.

Assume that baddeleyite and zircon did form early in the history of a lower crustal staging chamber. Whether armored by early-formed crystals or not, the temperature of a magmatic system would certainly have been above the closure temperature of zircon, estimated to be ca. 900°C (Lee *et al.*, 1997; Cherniak and Watson,

2000). Although there is uncontestable evidence that partial resorption and transport in mafic magmatic systems need not completely reset the U-Pb system of zircons (Amelin *et al.*, 1999), in the Barth Island Ring Complex there would exist a minimum 2 m.y. lag between crystallization of troctolitic zircon and younger baddeleyite. It is therefore requisite that the zircons were isolated from temperatures in excess of their closure temperature for at least part of that time lag. The ambient temperature, then, must have approached the troctolitic magma's solidus, and the two possibilities are therefore reduced to the assimilation or remobilization of already crystalline material. On a theoretical basis, this kind of inheritance is a possibility for the zircon and older baddeleyite of the Barth Island Ring Complex. In the Pearly Gates Anorthosite, a part of the Nain Batholith, such inheritance has been documented by Tettelaar (2004), where that author found a range of ages for zircon in the same sample, and concluded that plagioclase formation must have been occurring for long periods of time at depth.

The third scenario is that the younger baddeleyite experienced an episode of Pb loss. The samples BS 4a, 8b and 8e were all obtained from the surface outcrop and, though they appear to be fresh, low-T Pb loss in baddeleyite has been reported in samples exposed to weathering processes (Heaman and LeCheminant, 1993). If it is a Pb-loss pattern that is shown by the baddeleyite in sample BS 8b (fig. 4-4b), however, it is inconsistent with Pb loss due to contemporary weathering processes. Pb loss from weathering processes would result on the error ellipses for each zircon analysis lying

along a line which had concordia intercepts at the actual igneous age and at 0 Ma, as the BS 8b zircons and two of the BS 8e baddeleyite fractions do.

Instead, the pattern of Pb loss is correlatable with a heating event. As reported above, large baddeleyite grains gave an older age than small grains. This is a result expected of U-Pb systems that have experienced an episode of Pb loss. Most authors, however, report that baddeleyite is more resistant to resetting events (via heating) than is zircon (Heaman and LeCheminant, 1993; Amelin *et al.*, 1999; Wingate, 2001), so it would be surprising if the zircon U-Pb system had remained closed while the baddeleyite U-Pb systems were opened.

4.5 Conclusion

The most plausible scenarios for the genesis of zircon and baddeleyite in the troctolite are either inheritance of zircon or Pb loss in baddeleyite. In the Pb-loss scenario, the troctolite was emplaced and crystallized at 1332 Ma. At least one heating event, perhaps associated the intrusion of the monzonite and ferrogabbroid, occurred at ca. 1317 Ma, resetting some the U-Pb system of some baddeleyite grains. This heating event did not affect zircon. In the inheritance scenario, baddeleyite and zircon crystallized, probably from the late-stage, fractionated part of a mafic intrusion or anorthosite, and were inherited by troctolitic magma of the Barth Island Ring Complex. The partial assimilation of the inherited material may have occurred at depth, or near the level of emplacement.

The petrographic context of the noritic zircon, as grains found in the interstices with the final crystallization products of the norite, is evidence linking it to late-stage formation from the norite, and the dominant grain morphology supports their formation from a mafic magma. The zircon grain morphologies of both troctolite and norite are similar, and they consistently give the same age. This is good evidence for linking their origin to a single event. Furthermore, some baddeleyite grains yielded an age within error of the zircon, and in the only report of xenocrystic baddeleyite in mafic rock, the baddeleyite occurs as inclusions within mantle xenocrysts (Heaman and LeCheminant, 2001). It therefore seems unlikely that the baddeleyite are inherited; instead, the data point to complexities in the U-Pb systems of the baddeleyite grains. Furthermore, most of the analyses plot off the concordia, which probably indicates thermal disturbance of the zircon and baddeleyite U-Pb systems.

The conclusion of this work is that some heating event, perhaps associated with the emplacement of the monzonite and ferrogabbroid, caused Pb loss in the smallest baddeleyite grains. The zircon age of 1331 ± 1.4 obtained for the troctolite is taken as its igneous age, and the norite and troctolite are interpreted to be products of the same magmatic event. The problem of why the zircon U-Pb system remained closed while baddeleyite systems were opened is unexplained, but this would be a problem irrespective of the interpretation imposed on the zircon origin. Alternatively, the undisturbed nature of the zircon may indicate that the baddeleyite U-Pb system, or the processes of baddeleyite formation, are complicated by processes which are as yet unclear.

Table 4-1. U-Pb data (ID-TIMS).

Sample	Run	Char.	wt. (μg)	U (ppm)	Th/U	Pb* (ppm)	C. Pb (pg)
9d (Ofd)	Zr 1	1 YTPr	10	415	0.83	109	3.4
	Zr 2	1 YTPr	5	265	0.71	67	4.7
	Zr 3	1 YTPr	8	218	0.71	55	1.9
	Zr 4	1 YTEl	15	111	0.77	29	2.9
	Zr 5	1 YTPr	4	97	0.46	23	1.8
	Zr 6	3 YTPr	18	131	0.77	34	5.8
	Zr 7	5 YTEl	20	131	0.7	33	4.2
	Zr 8	8 YTEl	40	89	0.82	23	3.9
8b (Tr)	Zr 1	3 TPFt	35	198	0.69	50	13
	Zr 2	2 TPFt	20	295	1.18	81	3.6
	Zr 3	1 TPFt	15	357	1.46	108	12
	Zr 4	6 TPFt	8	200	1.16	56	25
	BAD 1	5	5	584	0.02	124	6
	BAD 2	10	8	780	0.02	164	2.5
	BAD 3	6	6	356	0.02	75	6
	BAD 4	6	6	342	0.02	72	10
	BAD 5	10	10	305	0.02	64	5.7
8e (Tr)	BAD 1	2	40	58	0.03	12	49
	BAD 2	2	42	43	0.03	9	26
	BAD 3	2	41	22	0.04	5	27
	BAD 4	4	70	51	0.02	11	23
4a (N)	Zr 1	2 PTPr	20	42	1.02	11	15
	Zr 2	1 PTPr	30	53	1.32	15	10
	Zr 3	2 PTEl	20	30	1.27	8	14
	Zr 4	4 PTPr	20	22	1.29	6	13
	Zr 5	5 PTPr	30	47	1.03	14	14

Note. For both zircon and baddeleyite, the number indicates the number of grains per fraction; Y=Yellow, P=Pink, T=Translucent, Pr=Prismatic, El=Elongated, Ft=Fragment. Th/U is calculated from $^{208}Pb/^{206}Pb$ ratio and $^{207}Pb/^{206}Pb$ age assuming concordance; common Pb (C. Pb) is equivalent to total common Pb from sample and laboratory sources. $^{206}Pb/^{204}Pb$ ratios have been corrected for fractionation; all the other isotopic ratios have been corrected for spike, fractionation, blank and initial common Pb. This table was constructed by Marc Poujol.

Table 4-1 (cont.). U-Pb data (ID-TIMS).

Sample	Run	$^{206}Pb/^{204}Pb$	$^{206}Pb/^{238}U$	±	$^{207}Pb/^{235}U$	±	$^{207}Pb/^{206}Pb$	±	$^{206}Pb/^{238}U$	$^{207}Pb/^{235}U$	$^{207}Pb/^{206}Pb$	Conc. %
9d (Ofd)	Zr 1	1800	0.2270	1.01	2.6620	1.02	0.08504	0.12	1318	1318	1317	100.2
	Zr 2	826	0.2263	0.54	2.6580	0.84	0.08517	0.71	1315	1317	1319	99.6
	Zr 3	2477	0.2253	0.45	2.6390	0.46	0.08497	0.17	1310	1312	1315	99.6
	Zr 4	900	0.2286	0.26	2.6840	0.27	0.08514	0.16	1327	1324	1319	100.3
	Zr 5	386	0.2276	0.48	2.6770	0.57	0.08529	0.32	1322	1322	1322	100
	Zr 6	464	0.2275	0.28	2.6700	0.29	0.08511	0.15	1321	1320	1318	100.1
	Zr 7	975	0.2255	0.38	2.6480	0.42	0.08515	0.34	1311	1314	1319	99.3
	Zr 8	1367	0.2222	0.49	2.5990	0.52	0.08483	0.24	1294	1300	1312	98.5
8b (Tr)	Zr 1	784	0.2254	0.32	2.6620	0.28	0.08566	0.23	1310	1318	1331	98.5
	Zr 2	2360	0.2169	0.3	2.5630	0.28	0.08571	0.17	1265	1290	1332	95
	Zr 3	668	0.2271	0.3	2.6830	0.26	0.08570	0.23	1319	1324	1331	99.1
	Zr 4	908	0.2265	0.26	2.6750	0.25	0.08566	0.16	1316	1322	1331	98.9
	BAD 1	2848	0.2267	0.21	2.6950	0.2	0.08506	0.12	1317	1317	1317	100
	BAD 2	53031	0.2241	0.18	2.6240	0.19	0.08491	0.06	1304	1307	1313	99.1
	BAD 3	6822	0.2258	0.26	2.6430	0.25	0.08491	0.11	1312	1313	1314	99.9
	BAD 4	3811	0.2256	0.21	2.6490	0.21	0.08516	0.1	1311	1314	1319	99.4
	BAD 5	9139	0.2252	0.18	2.6420	0.18	0.08508	0.07	1310	1313	1317	99.5
8e (Tr)	BAD 1	687	0.2259	0.22	2.6690	0.23	0.08571	0.15	1313	1320	1332	98.5
	BAD 2	968	0.2266	0.17	2.6680	0.2	0.08540	0.08	1317	1320	1325	99.3
	BAD 3	478	0.2268	0.27	2.6810	0.29	0.08571	0.2	1318	1323	1332	98.8
	BAD 4	2544	0.2258	0.2	2.6490	0.21	0.08509	0.08	1313	1315	1318	99.5
4a (N)	Zr 1	320	0.2267	0.43	2.6830	0.49	0.0858	0.24	1317	1324	1334	98.6
	Zr 2	1522	0.2282	2.36	2.6950	2.36	0.0857	0.15	1325	1327	1331	99.5
	Zr 3	420	0.2189	0.81	2.5820	0.83	0.0855	0.21	1276	1296	1328	95.7
	Zr 4	256	0.2311	0.45	2.7410	0.65	0.0860	0.46	1340	1340	1339	100
	Zr 5	471	0.2267	0.26	2.6750	0.34	0.0856	0.25	1317	1322	1329	99

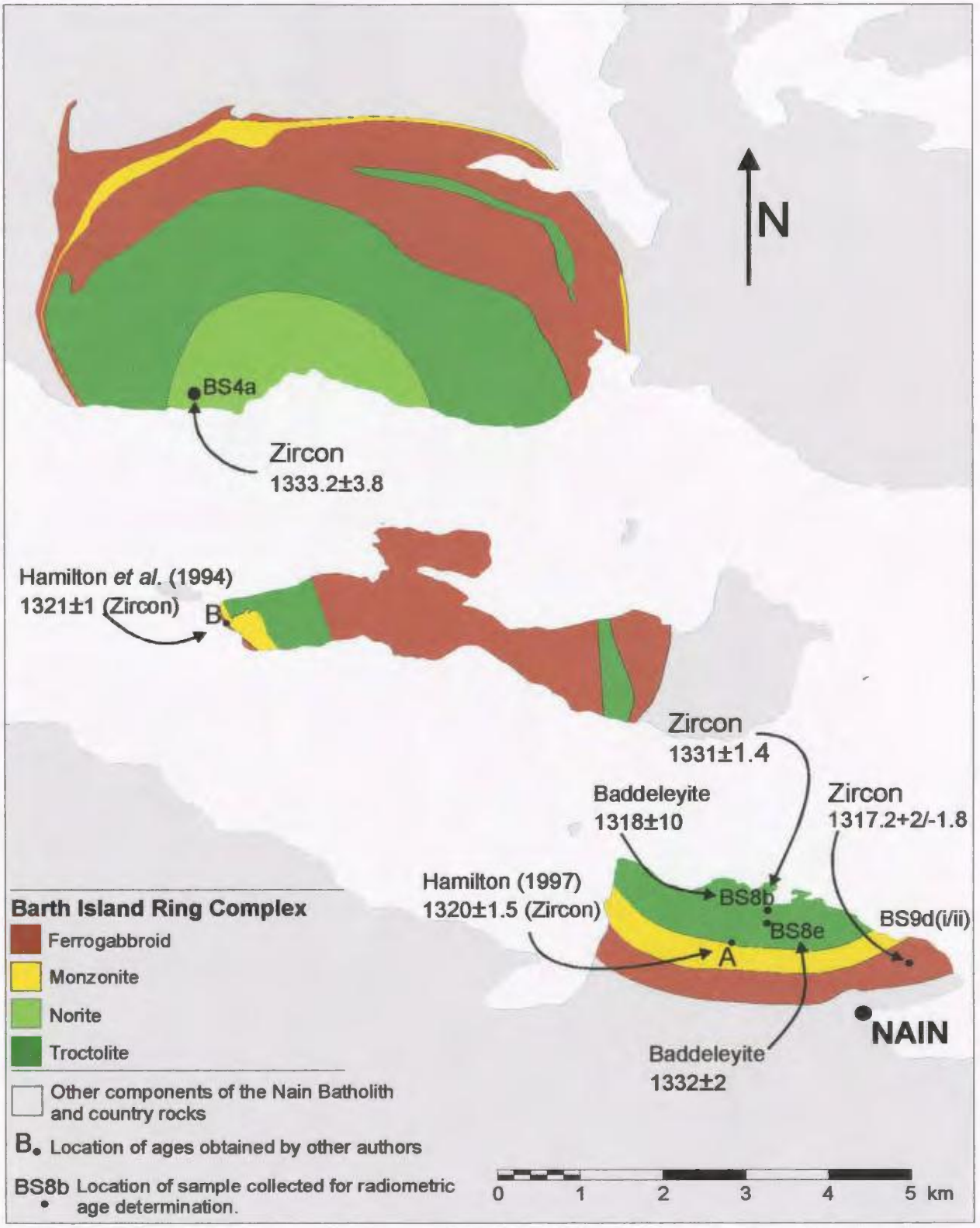

Figure 4-1. Simplified geological map of the Barth Island Ring Complex showing the locations of samples subject to radiometric age determinations. Outer Leuconorite unit

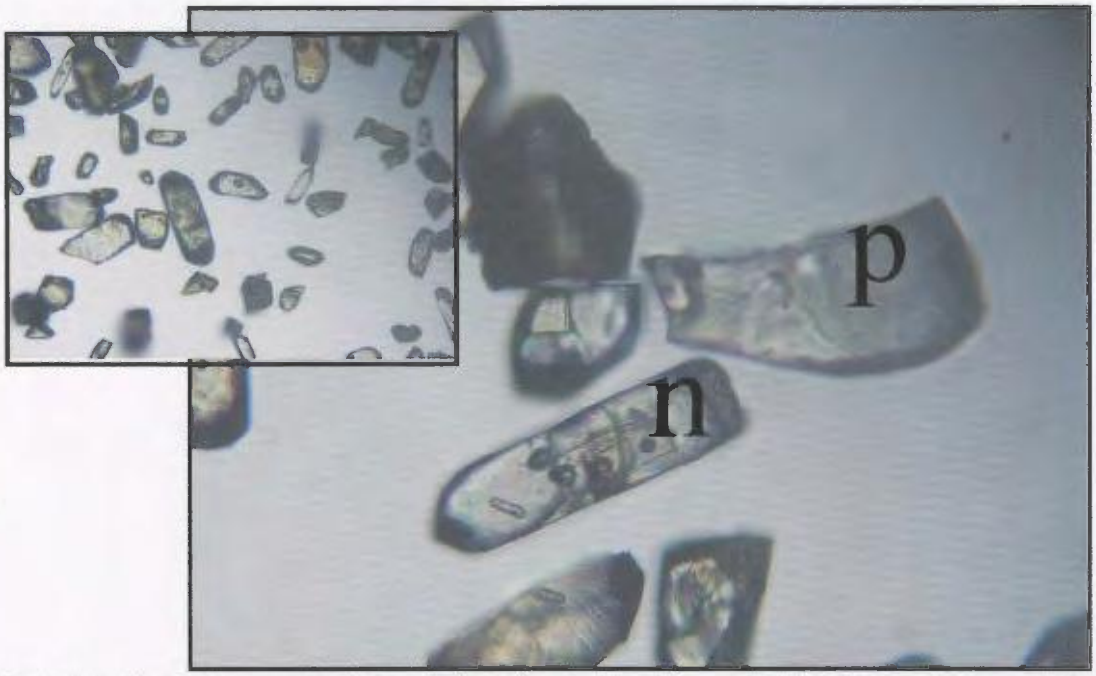

Plate 4-1. Photomicrograph of zircons from ferrogabbroid sample BS 9d(i)/(ii). The populations consists of needles (n) and prismatic fragments (p). The inset is at lower magnification and shows a typical population. Notice the elongate inclusion in the needle; this is apatite. Field of view ca. 0.5 mm; inset field of view 1 mm.

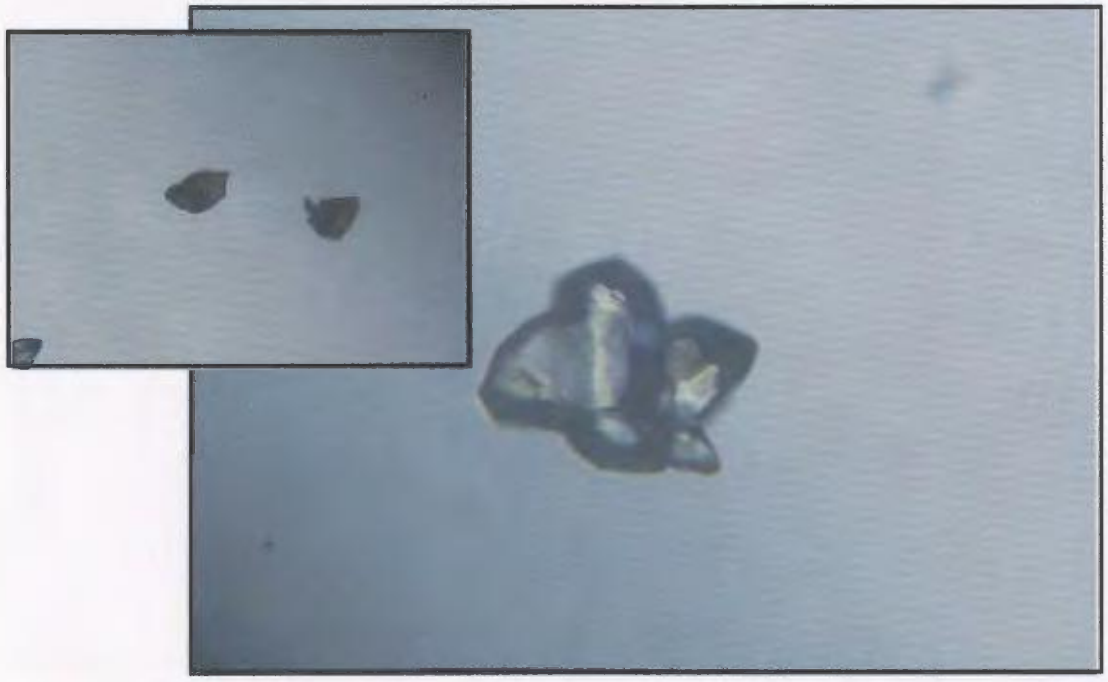

Plate 4-2. Photomicrograph of zircon and baddeleyite (inset) from sample BS 8b. Field of view for both photomicrographs 0.5 mm.

Plate 4-3. Photomicrograph of baddeleyite from troctolite sample BS 8e. Field of view ca. 0.5 mm.

Plate 4-4. Photomicrograph of zircon from leuconorite sample BS 4a. Field of view ca. 0.5 mm.

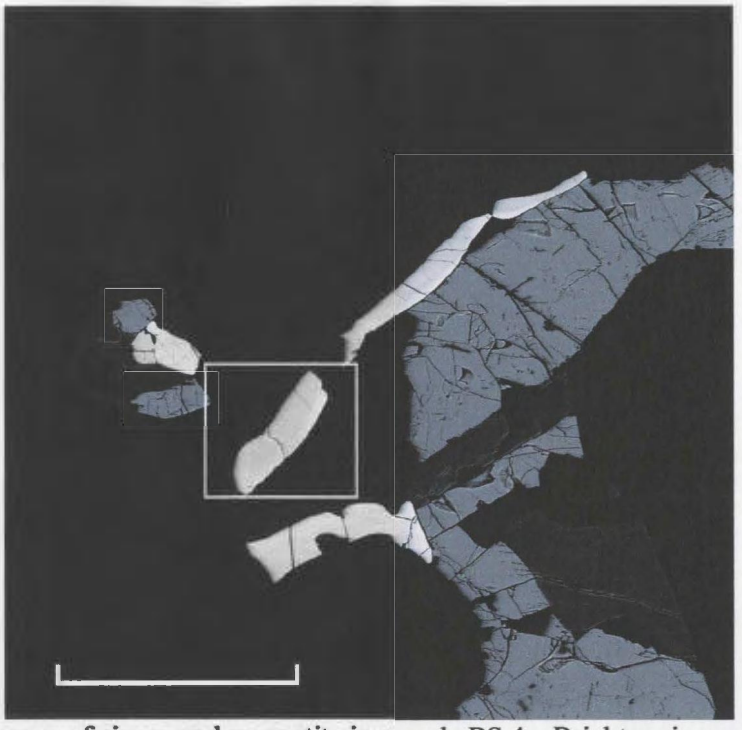

Plate 4-5a. Backscatter image of zircon and magnetite in sample BS 4a. Bright grains are zircon. White box delineates area of plate 4-5b. Scale bar is 500 microns.

Plate 4-5b. Backscatter image of zircon from sample BS 4a. Scale bar is 50 microns.

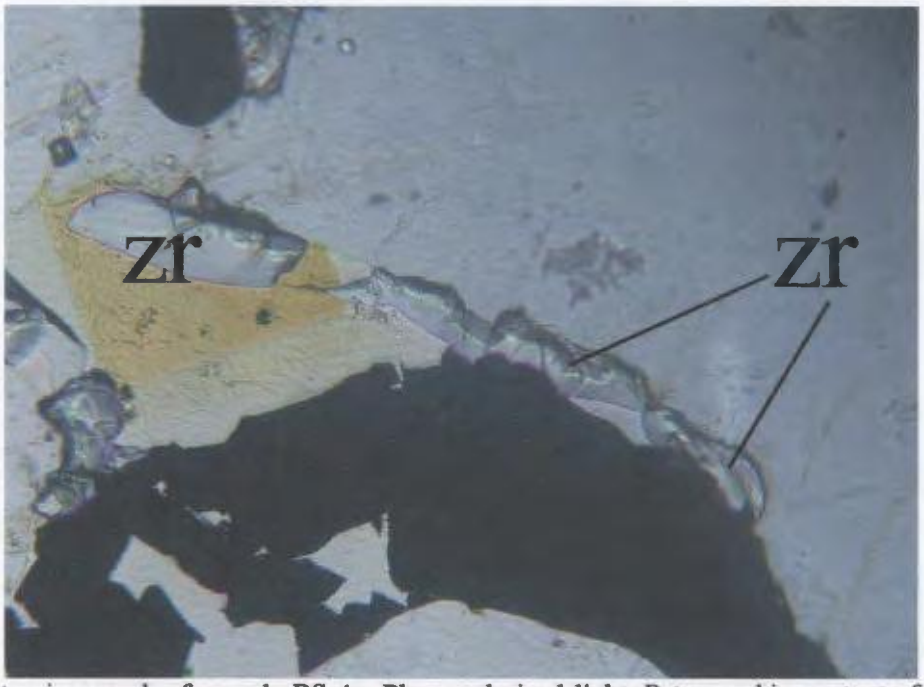

Plate 4-6a. Photomicrograph of sample BS 4a. Plane polarized light. Petrographic context of zircon. The dark mineral is magnetite and the light areas are plagioclase. Field of view ca. 0.5 mm.

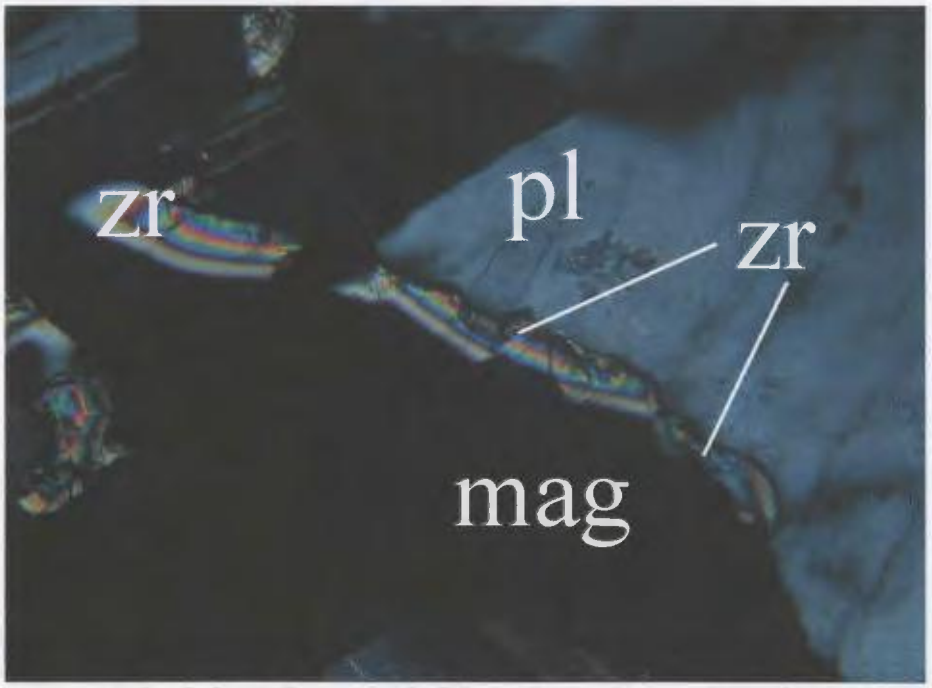

Plate 4-6b. Photomicrograph of zircon from sample BS 4a. Same view as above, but with crossed polars. Note the high birefringence. Field of view ca. 0.5 mm.

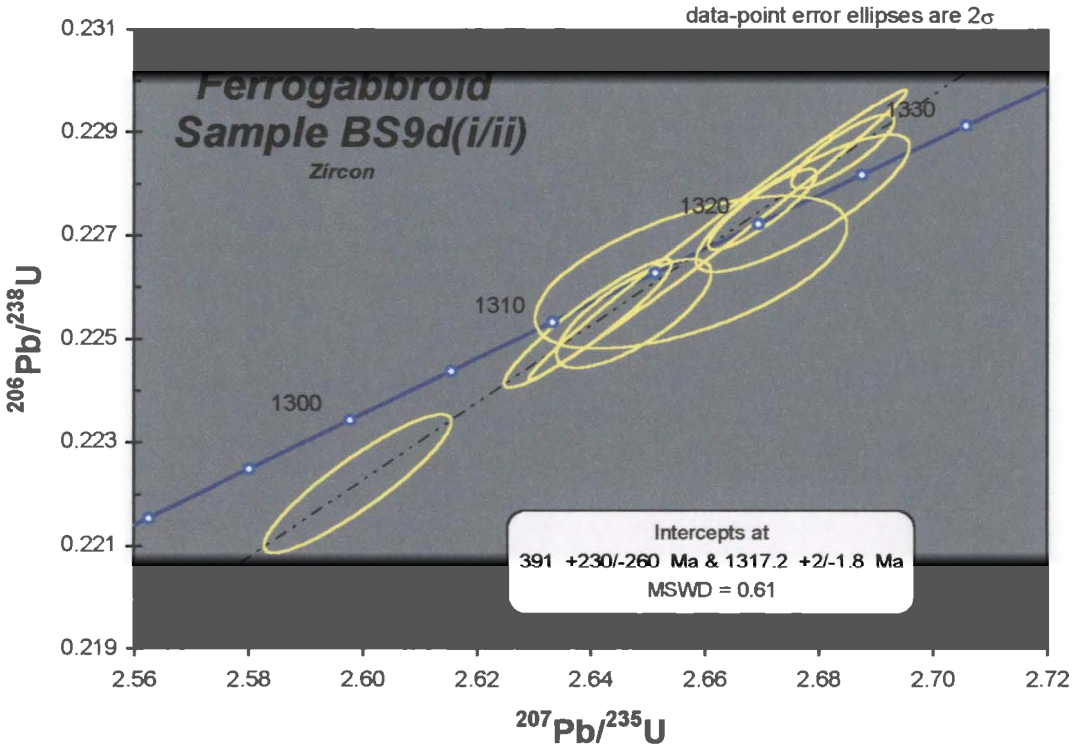

Figure 4-2. Concordia diagram for zircon from ferrogabbroid sample BS 9d(i/ii). Analysis and diagram by M. Poujol.

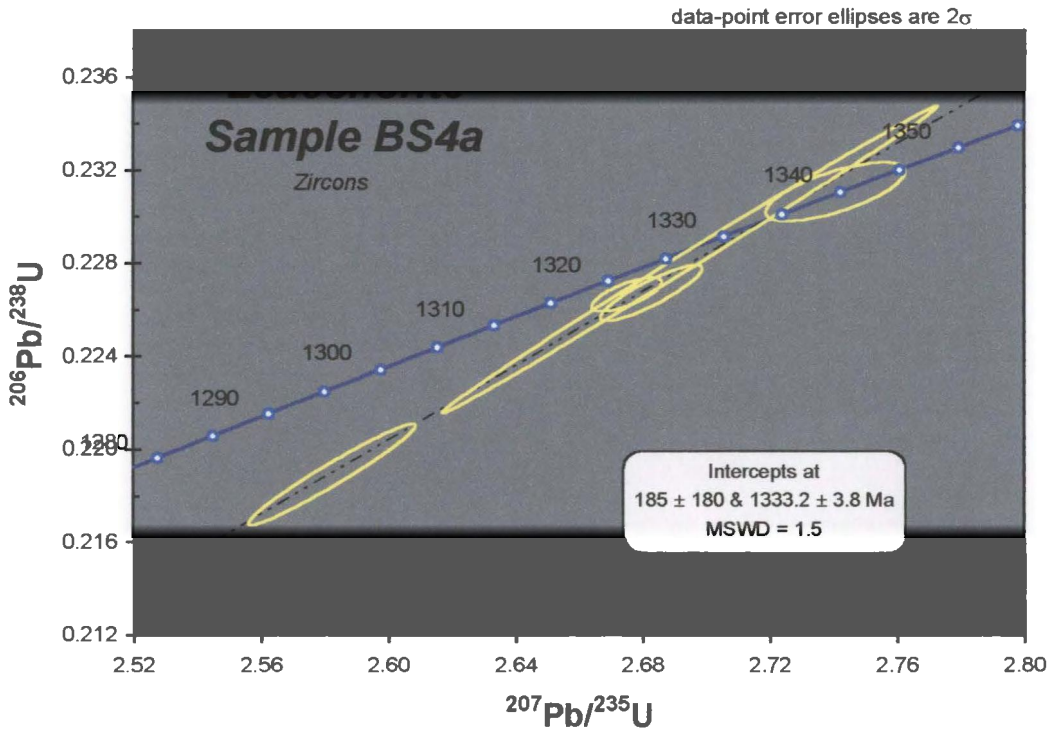

Figure 4-3. Concordia diagram for zircon from leuconorite sample BS 4a. Analysis and diagram by M. Poujol.

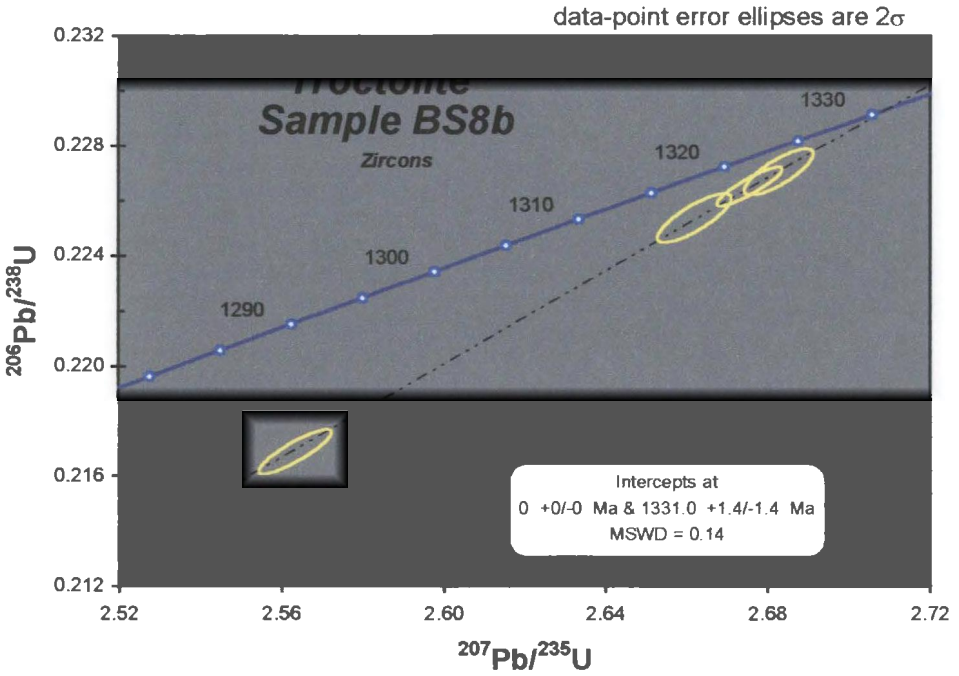

Figure 4-4a. Concordia diagram for zircon from troctolite sample BS 8b. Analysis and diagram by M. Poujol.

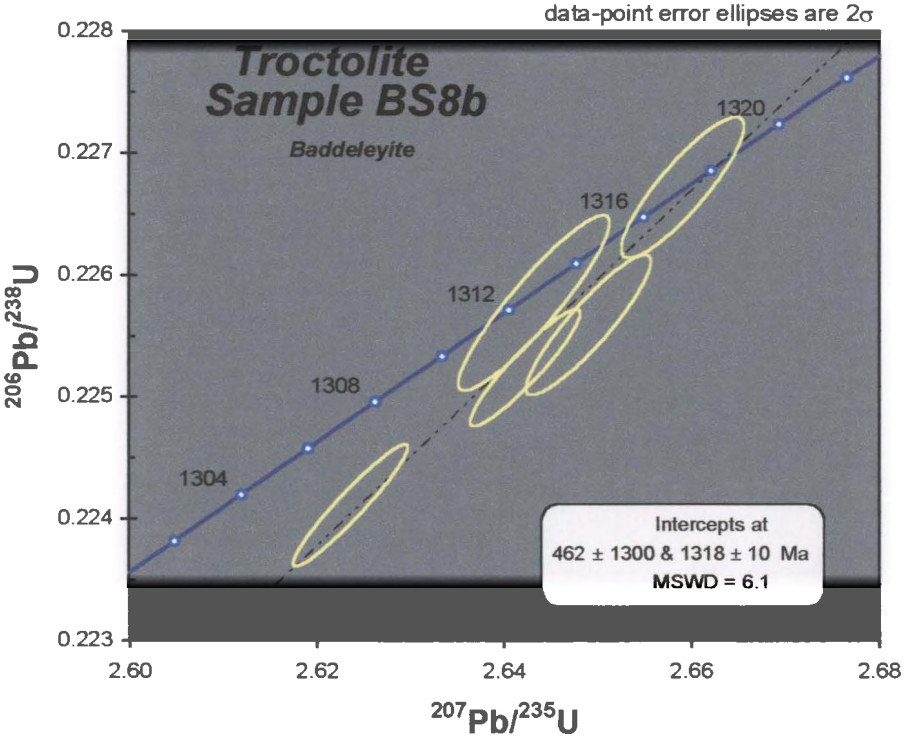

Figure 4-4b. Concordia diagram for baddeleyite from troctolite sample BS 8b. Analysis and diagram by M. Poujol.

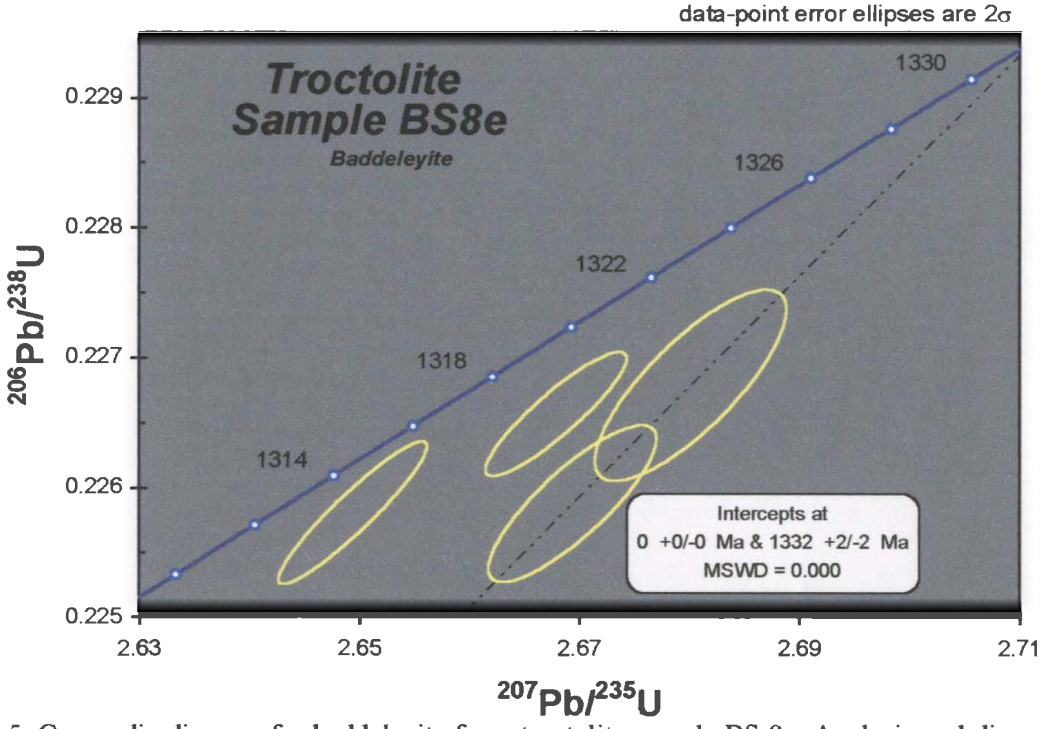

Figure 4-5. Concordia diagram for baddeleyite from troctolite sample BS 8e. Analysis and diagram by M. Poujol.

Chapter 5 Emplacement Model and Conclusions

5.1 Review and reappraisal of previous theories of formation

The Barth Island Ring Complex has previously been interpreted by Rubins (1973), Mulhern (1974), Levendosky (1975), de Waard (1976), and de Waard *et al.* (1976) to represent the result of closed-system differentiation of a single pulse of mafic magma. The anorthosite at the edges of the ring complex was also interpreted to be the result of same differentiation event. The contacts between the various rock types were interpreted to be gradational; this interpretation was founded on field observations and mineral composition analyses. The geological map of de Waard (1976) is shown in fig. 5-1a. Note that the outer leuconorite of the ring complex was included by de Waard (1976) as part of the ferrogabbroid, which de Waard referred to as 'jotunite'.

The more evolved members of the Barth Island Ring Complex, the ferrogabbroid and monzonite (which de Waard referred to as 'adamellite'), are found stratigraphically below the most primitive member of the sequence, the troctolite. This contradicts the typical result of differentiation, which results in the most primitive rock types at or near the base of an intrusion and the evolved products in the upper portion. In order to explain the observed inversion of the sequence, the previous workers (Mulhern, 1974; de Waard *et al.*, 1976; de Waard, 1976) suggested that, prior to final solidification of the Barth Island Ring Complex but after the primary components had been formed, the buoyancy of the monzonite dragged the structure upward, forming a highly deformed body. An

interpretive cross-section of the Barth Island Ring Complex according to the previous theory of formation, accompanied by compositional data of de Waard *et al.* (1976) is given in fig. 5-1b.

The present study has exposed severe shortcomings in the model of de Waard (1976). For instance, the points labeled A and B on the revised map (fig. 5-2), and on the map and cross-section of de Waard (1976) shown in figs. 5-1a and 5-1b, are at the same geographic locations on each map. De Waard's interpretation of the nature of the Barth Island Ring Complex requires that these points correspond to identical stratigraphic locations. The conclusions of this study and those of de Waard (1976) are in accord in interpreting the inward transition of rock types at point A on figs. 5-1a and 5-2 as gradational. The model of de Waard *et al.* (1976), however, equates the medium to coarse-grained, cumulate-textured leuconorite at point A with the medium to coarse-grained ferrogabbroid and ferrogabbroid-monzonite hybrids found at the troctolite's north boundary (point B, on figs. 5-1a and 5-2). Notice that, on the map of de Waard (1976), the rock defined in the present study as leuconorite is classified as ferrogabbroid (which he called jotunite).

The ferrogabbroid found at B displays a typical relationship with monzonite (for description see section 2.6.1), has primarily anhedral grain morphology, lacks the cumulus textures characteristic of the leuconorite, and has a different mineral assemblage than the leuconorite. It is texturally heterogeneous. Discontinuous layers of monzonite and monzonite-ferrogabbroid hybrid rocks are exposed at various locations along the

contact with troctolite. This contact, between the ferrogabbroid and troctolite, is abrupt and the mineral components and textures of the two rocks are dissimilar. Anastamosing dykes of light-coloured, fine-grained rock are commonly seen to be present at the contact, and throughout the adjoining margin of the troctolite; however, they are absent from ferrogabbroid and monzonitic rock below the contact. The leuconorite at A shares none of these features. Comparison of major and trace element geochemistry of outer ferrogabbroid samples from other locations in the Barth Island Ring Complex with geochemistry of the leuconorite at B has also revealed significant differences, such as more than an order-of-magnitude difference in trace element abundances. Furthermore, zircon U-Pb results (this study, chapter 4) indicate a ca. 13 m.y. difference in the age of the two rocks.

Within the context of the model of de Waard (1976), the only way to explain the differences described above is to invoke removal of intervening stratigraphy, present at A, from B by intensive shearing during deformation of the structure. However, structures corresponding to such a process are absent. Igneous textures (such as euhedral crystals and plagioclase lamination) are well-preserved in the troctolite. Where the texture of the troctolite is indicative of recrystallization, structures indicative of the dynamic processes associated with intense shearing are absent. Textures that would likely have been eradicated during an intense process of shearing (such as subophitic textures) are found in ferrogabbroid at other locations along the troctolite's northern contact.

Therefore, there is no evidence of deformation and recrystallization of the kind that would be required to produce the folded structure proposed by de Waard (1976) (fig. 5-1b).

With regard to the field relationships, the findings of the present study are generally in accord with the findings of Ryan (2000, 2001), who performed reconaissance investigation of the Barth Island Ring Complex. Ryan concluded that the theory of formation of the Barth Island Ring Complex put forward by de Waard (1976) needed to be reassessed, and suggested that the troctolite was not comagmatic with the ferrogabbroid and monzonite. It was also concluded that the latter two rock types were approximately contemporaneous, and that the monzonite had been emplaced before the ferrogabbroid. Ryan (2000) suggested that the troctolite was older than the ferrogabbroid and monzonite. However, this interpretation was discarded in Ryan (2001), and the troctolite was re-interpreted to be younger than, but broadly contemporaneous with, the ferrogabbroid and monzonite. An interpretive cross-section of this model, which I constructed for the purpose of illustration, is presented in fig. 5-3. It must be emphasized that the details of this model are a product of work completed during the course of this thesis, and cannot be ascribed to Ryan (2001).

In the model presented in fig. 5-3, the monzonite and ferrogabbroid magmas intruded as a ring dyke, separating the country rock in the centre of the ring from the rocks at the outside. The central block subsided, creating the necessary space for the intruding magmas. Its continued subsidence created space for the troctolitic magma,

which intruded before all the contents of the magma chamber were completely solidified. In this model, the troctolite must be bounded by a fault at its southern margin; this fault implies the presence of shear structures in the monzonite that correspond with the movement along the fault, but these structures were not observed. It is therefore necessary to invoke removal of these structures by the troctolitic magma during its emplacement.

In this model, the troctolite would have intruded before the monzonite and ferrogabbroid magmas were completely solidified, because monzonite dykes emanate from the monzonite into the troctolite, at the troctolite's southern margin. The ductile state of the ferrogabbroid and monzonite in the chamber during the intrusion of the troctolite could explain the lack of cross-cutting contacts between the troctolite and either of the ferrogabbroid and monzonite. For instance, a largely ductile-state body of monzonite could be deformed by the intrusion of troctolitic magma, instead of being cross-cut. However, because the removal of shear structures in the monzonite by the troctolitic magma is invoked above, it is not clear why the foliations in the monzonite would not locally cross-cut by the troctolite. Furthermore, there is no evidence of mingling along the contact between troctolite and monzonite or troctolite and ferrogabbroid, which might be expected if they were contemporaneous.

There are other objections to this mechanism of formation. For instance, a magma chamber which has formed by cauldron subsidence should have walls that are nearly vertical. The orientation of contacts between rocks of the Barth Island Ring Complex and outlying rocks, particularly along the northern boundary of the ring complex, dip inward

at angles of between 50° and 80°, and the contacts of the troctolite with the other rocks of the ring complex are also not vertical.

5.2 A preferred emplacement model

The proximity of outer ferrogabbroid, monzonite, and troctolite of the Barth Island Ring Complex suggests that they may have been emplaced through the same conduit system. Exploitation of the same conduit by the various magmas may be facilitated by the existence of preexisting structures or weaknesses (anisotropies) in the crust. The shear zone in country rock found at the western edge of the Barth Island Ring Complex, for example, could provide a planar zone of weakness. The field relationships, which indicate the ferrogabbroid and monzonite were emplaced contemporaneously, also support their magmas having a shared conduit.

The geochronological data obtained during the present study indicate that the troctolite and norite were intruded some 13 m.y. before the ferrogabbroid and monzonite. An interpretive cross-section illustrating the result of this model is presented in fig. 5-4. The model illustrated in fig. 5-4 interprets the emplacement of the troctolite as a cone sheet. The troctolitic magma spread out at the level of emplacement, started to crystallize, and developed relatively steep, inward-dipping layering at its margins. The remaining troctolite magma then differentiated, and possibly interacted with other lithologies, to produce the norite. Intrusion of the monzonite occurred some 13 m.y. later, and was

followed by the ferrogabbroid. The intrusion of these latter magmas exploited the same cone-shaped fracture, and therefore occurred around the margins of the intrusion. The outer leuconorite was emplaced later than the ferrogabbroid and monzonite, again both at the margins of the suite, and for the most part, concordantly with pre-existing structures in the ferrogabbroid. As related in section 2.2.1, the outer leuconorite was observed to locally cross-cut the ferrogabbroid.

Depending on the minimum dip and minimum annular width of the cone sheet, space for the troctolite could have been made by subsidence. For instance, if the cone sheet dipped at 60° and had a minimum thickness of 400 m, 800 m of space for the chamber could be made by subsidence before the wide section of the cone jammed the conduit.

The apparent emplacement of ferrogabbroid and monzonite at the margins of the troctolite is a problematic aspect of the Barth Island Ring Complex: there are few indisputable instances of the troctolite being cross-cut by either the monzonite or the ferrogabbroid. It could be argued that the isolated body of troctolite in the northeastern corner of the ring complex is similar to the main body of troctolite, and that this body was split off the main body of troctolite during the intrusion of the ferrogabbroid and monzonite. Also, the lack of any fine-grained troctolitic rocks that could be considered 'chills' may also be evidence of removal of such rocks during the intrusion of the monzonite and ferrogabbroid. These features would be consistent with the interpretation given above.

However, these examples rest on negative evidence, and are therefore not compelling. In any case, they do not address the most pressing aspect of the problem, which is that structures in the ferrogabbroid and monzonite have preferentially paralleled the pre-existing layering and magmatic foliation of the troctolite in most localities over the exposed area of the ring complex.

The physical properties of the monzonite could partly explain the lack of cross-cutting contacts. If the monzonite intruded as a viscous, crystal-rich mass, it may have preferentially exploited planes of weakness at the troctolite margin. The hotter, less viscous ferrogabbroid magma would have intruded into a chamber filled with highly polymerized, cooler monzonite. However, the weight of this explanation rests on the existence of pre-existing anisotropies in the crust, and it is the existence of such anisotropies that must be appealed to for explanation of the lack of cross-cutting relationships in the Barth Island Ring Complex.

5.3 Magmatic histories and possible genetic associations: summary

Based on field and petrographic evidence, the troctolite and norite are interpreted to be related differentiation products of mafic magma. New U-Pb chronological data from zircon and baddeleyite places the solidification of these rocks at ca. 1332 Ma. Baddeleyite data conflict with this age, suggesting a younger age of emplacement. However, all these data are presented in combination with petrographic evidence supporting the formation of

zircon late in the magmatic history of the norite. Furthermore, whole rock and mineralogical major element chemical evidence from this study and others (Mulhern, 1974; de Waard *et al.*, 1976; de Waard, 1976) supports a genetic link between the norite and troctolite, and the trace element signatures of these two rock types are also similar, although the norite has lower abundances of most trace elements. The baddeleyite are therefore interpreted to have a complicated history, perhaps involving Pb loss or complicated mechanisms of formation. The pattern of relative depletion and enrichment of trace elements in the norite, as compared to the troctolite, could have been caused by lower modal abundances of accessory minerals, or could suggest assimilation, by the norite, of some contaminant, such as anorthosite.

Field observations support the contemporaneity of the magmas which produced the outer ferrogabbroid and monzonite, and suggest that the monzonite was at the level of emplacement before the ferrogabbroid, in accord with the conclusions of Ryan (2000, 2001). Field evidence also indicates that the monzonite was largely crystalline at the time of the emplacement of the ferrogabbroid, although large amounts of mingling and some mixing did take place. U-Pb geochronological data from zircon, obtained both in this study and in previous studies (Hamilton *et al.*, 1994; Hamilton, 1997) indicate that the ferrogabbroid and monzonite crystallized at ca. 1319 Ma.

The texture of the ferrogabbroid indicates that it is probably not a cumulate. However, wide variations across the ring complex in phase proportions and textures cast doubt on the possibility of inferring a single liquid composition. It is probable that the

ferrogabbroid is the result of multiple pulses of heterogeneously contaminated magma, a conclusion supported by the presence of diverse exotic crystals or rocks in several distinct layers. Trace element and Nd isotopic data for typical samples of outer ferrogabbroid have revealed similar heterogeneity and cast further doubt on the possibility of precisely and accurately characterizing a magma parental to the ferrogabbroid. The trace element chemistry of the central ferrogabbroid, and other ferrogabbroic rocks intruded into country rock at the margins of the Barth Island Ring Complex, has shown that other ferrogabbroid in the same geographic area have similar heterogeneities. The rocks do have some similarities, such as the presence of a negative Sr anomaly.

The ferrodiorites (ferrogabbroids) of the Nain Batholith have been suggested to be formed from magmas residual to the crystallization of anorthosites, that in turn fractionated from a mafic magma (Emslie *et al.*, 1994). The crystallization of large amounts of plagioclase from a typical mafic magma should leave a residual magma with negative Pb, Sr, and Eu anomalies, since these elements are preferentially included in plagioclase. The trace element geochemistry of the outer ferrogabbroids of the Barth Island Ring Complex does not have all the features of such residual liquids. In particular, negative Eu anomalies are absent. The outer ferrogabbroid samples do invariably have negative Sr anomalies, but the monzonite samples, which are unlikely to be a residual product of crystallization of anorthosites, also have negative Sr anomalies. This introduces an alternative plausible explanation for the Sr anomalies in the ferrogabbroid, (one that is linked to the monzonite) other than that proposed by Emslie *et al.* (1994), and

it is concluded to be unlikely that the ferrogabbroids in this study were produced from magmas residual to the crystallization of anorthosite.

The major element composition of the outer ferrogabbroid is similar to the composition of rocks interpreted to be the result of differentiation of mafic magmas (Wager and Deer, 1939; McBirney and Naslund, 1990; Jang *et al.*, 2001); therefore the ferrogabbroid may have evolved from mafic magma. It is also possible that the ferrogabbroid and monzonite are conjugate immiscible liquids. However, this study has found no convincing reason to prefer this explanation of their origin. It is clear that, if the latter hypothesis is correct, the parent magma for these two rock types did not become immiscible at the level of emplacement, because field relationships indicate that the monzonite was emplaced before the ferrogabbroid.

Whether the monzonite and outer ferrogabbroid are derived from conjugate liquids or not, their contemporaneity and geographic proximity indicate that the magmas that produced these rocks could have been stratified together in a chamber at depth. The density measurements (appendix 4) indicate that the monzonitic magma would have been stably stratified atop the more-dense ferrogabbroid magma.

The mineral assemblages and textures of the monzonite are typical of granitic rocks (Shelley, 1993, pp. 29-31, 228-238), and geochemical data support the interpretation of the monzonite as a feldspar cumulate rock. The overall trace element abundances of the monzonite and ferrogabbroid are similar, although the monzonite has highly elevated K and Zr, much lower P and Ti, and more elevated La/Yb than the

ferrogabbroids. The monzonite samples also have a positive Eu anomaly and an upturned Er-Yb-Lu segment, which are absent in the ferrogabbroid samples. Some of these differences can be attributed to the respective modal compositions of each rock type.

The proximity of the major rock types of the Barth Island Ring Complex may be taken to implicate similar sources in their formation. If the same sources are involved in the formation of the troctolite and ferrogabbroid-monzonite, ϵ_{Nd} values which were obtained for typical samples of each major rock type show that the the degree of influence of these sources varies by rock type. The troctolite has somewhat negative ϵ_{Nd}, whereas the monzonite and ferrogabbroid have relatively more negative ϵ_{Nd} values which overlap with each other.

In the context of the two-component scheme described by Emslie *et al.* (1994), the one component being a mantle-derived, mafic magma with weakly negative ϵ_{Nd}, and the other component being some crustal source with highly negative ϵ_{Nd}, the troctolite and norite must show some influence from this crustal source. The ferrogabbroid and monzonite must have had comparatively more influence from this source, since they have more negative ϵ_{Nd}. This conclusion is accepted in the present work as a reasonably broad result: the monzonite and ferrogabbroid were derived with significant influence, of similar amount, of a relatively old crustal source.

The troctolite and norite have compositions that might represent derivation from a mantle source with some contamination, particularly in the case of the norite. However, it must be noted that the conclusions of, for instance, Emslie *et al.* (1994) and Rudnick and

Fountain (1995), suggest that a two-component scheme is too simplistic. Emslie *et al.* (1994) predicted the presence of a third component, which they inferred to be mafic intrusive rocks in the lower crust. This third component should have an ϵ_{Nd} value similar to that of the mantle component. The most comprehensive summaries of data on the present composition of the bulk lower crust indicate that it is approximated by mafic granulite, and that lower crustal compositions for any particular location are likely to be heterogeneous (Rudnick and Fountain, 1995). It is therefore possible that the troctolite and norite had significant influence from young, mafic crust.

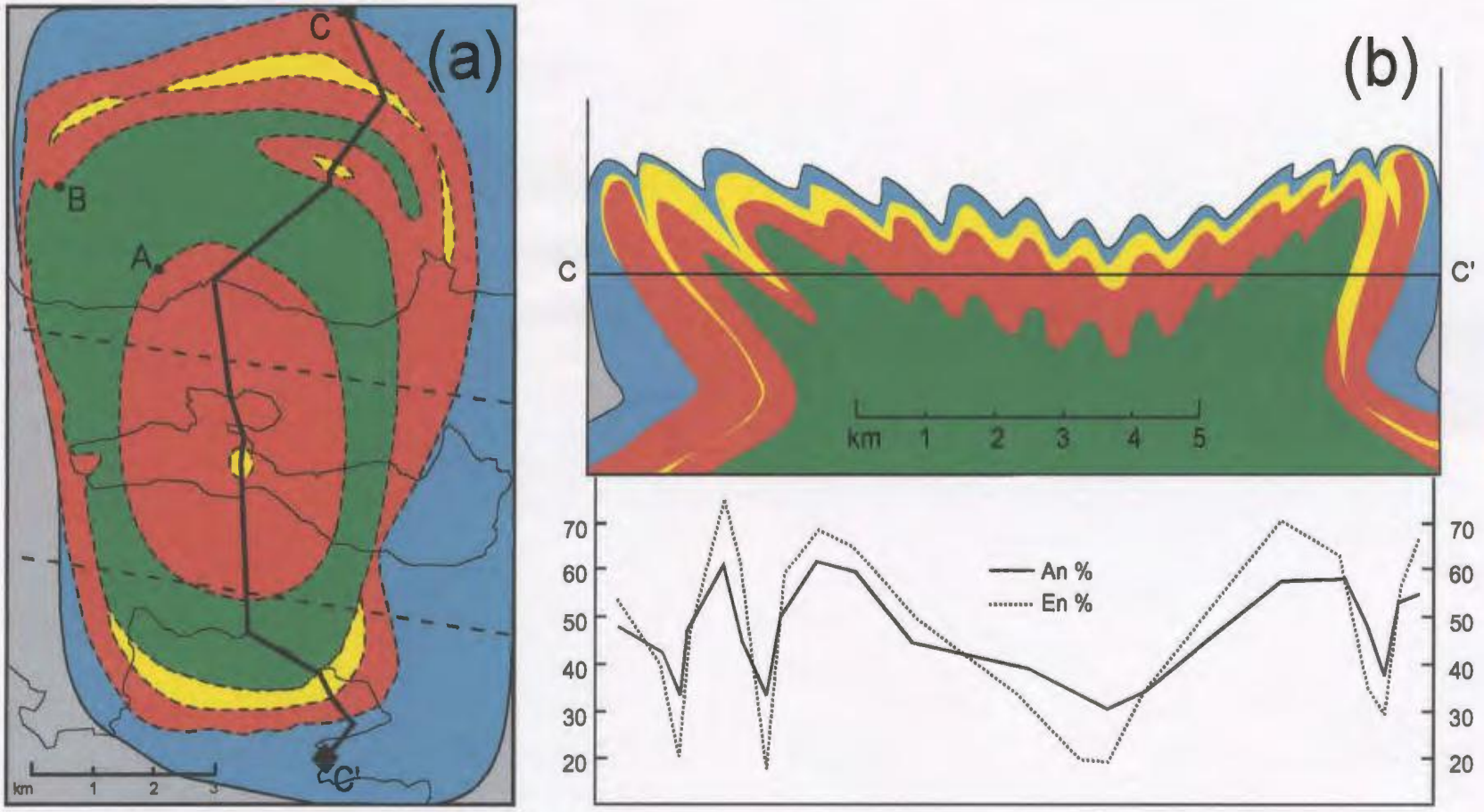

Figure 5.1a. Simplified geological map of the Barth Island Ring Complex after de Waard (1976; fig. 2). Inferred movement along the faults (thin solid lines) has been restored. Green is troctolite, red is ferrogabbroid, yellow is monzonite, turquoise is anorthosite, grey is undivided Nain Batholith. See text for description of points A and B. Location of cross-section from C to C'.

Figure 5.1b. Cross-section and corresponding mineral compositional data for the Barth Island Ring Complex (modified after de Waard, 1976; fig. 4). Rock types as in fig. 5.1a.

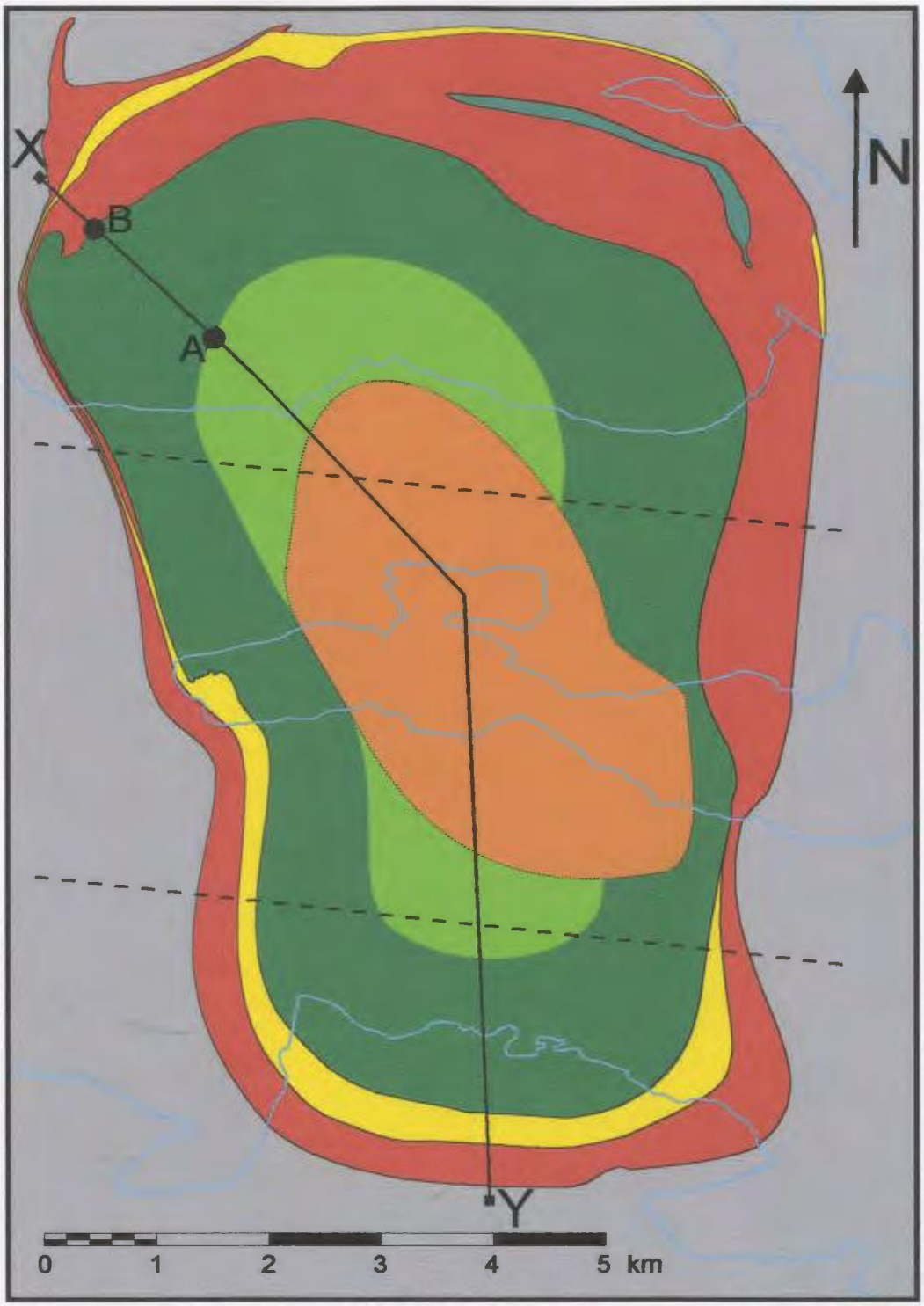

Figure 5-2. Simplified geological map of the Barth Island Ring Complex (this study). Outer leuconorite unit not shown. Inferred movement along the faults (dashed lines) has been restored, in a similar manner to de Waard (1976). Colours indicate the same rocks as in fig. 5-1a except: light green is norite, orange is central ferrogabbroid. Interpretive cross-sections for the line X to Y are given in figs. 5-3 and 5-4. Locations A and B are explained in the text.

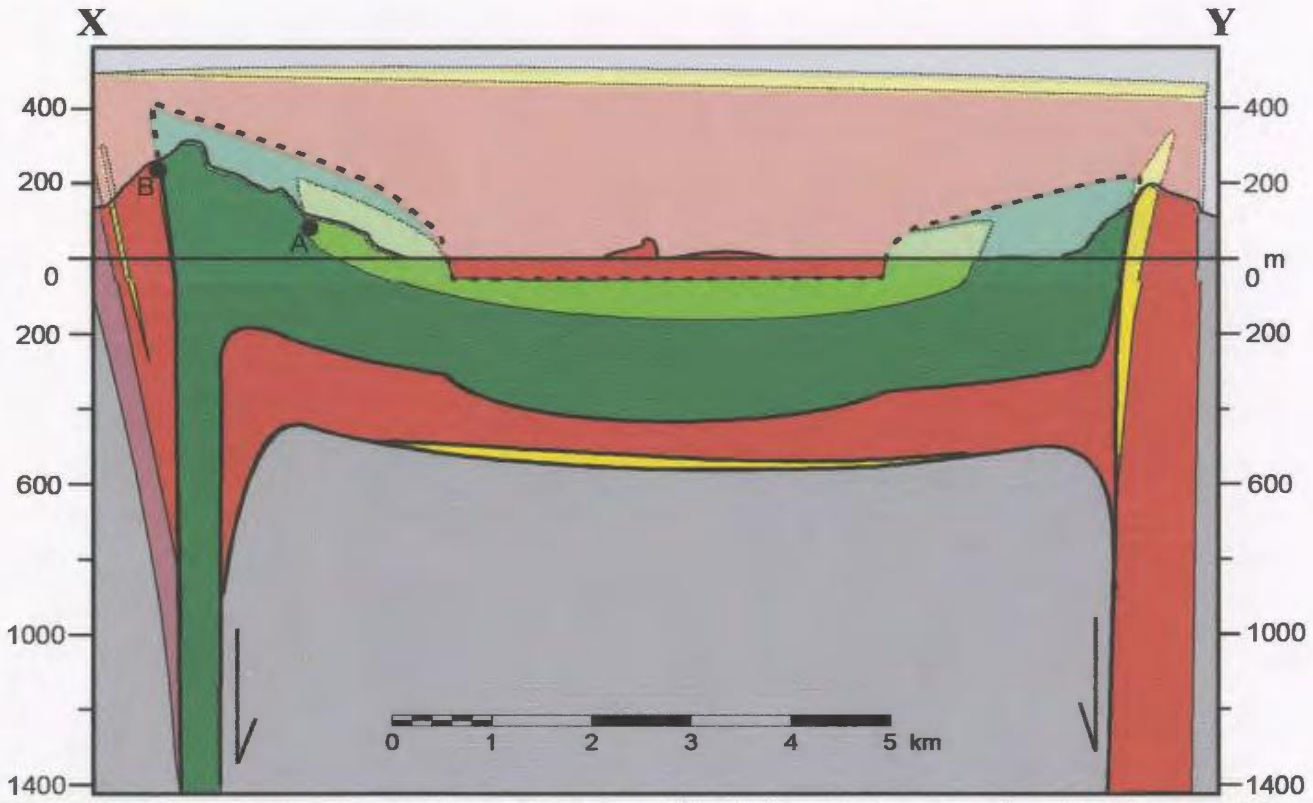

Figure 5-3. Cross-section (X to Y on fig. 5-2) of Barth Island Ring Complex showing a cauldron subsidence model. The thick black lines are faults. In this model, the monzonite intruded as a ring dyke, and was followed by the ferrogabbroid. The magmas disconnect the country rock in the center of the ring from the surrounding country rock. The center acts as a piston, subsiding to make space for the ferrogabbroid and monzonite; further subsidence creates space for the troctolite. In this diagram, the central ferrogabbroid is interpreted to be a roof pendant, related to the outer ferrogabbroid (and is therefore coloured red instead of orange as in fig. 5-2), although there are no exposed contacts between the central ferrogabbroid and other members of the Barth Island Ring Complex. All rocks as in fig. 5-2 except: purple is gneiss. Vertical exaggeration 4:1; dip angles have been adjusted accordingly.

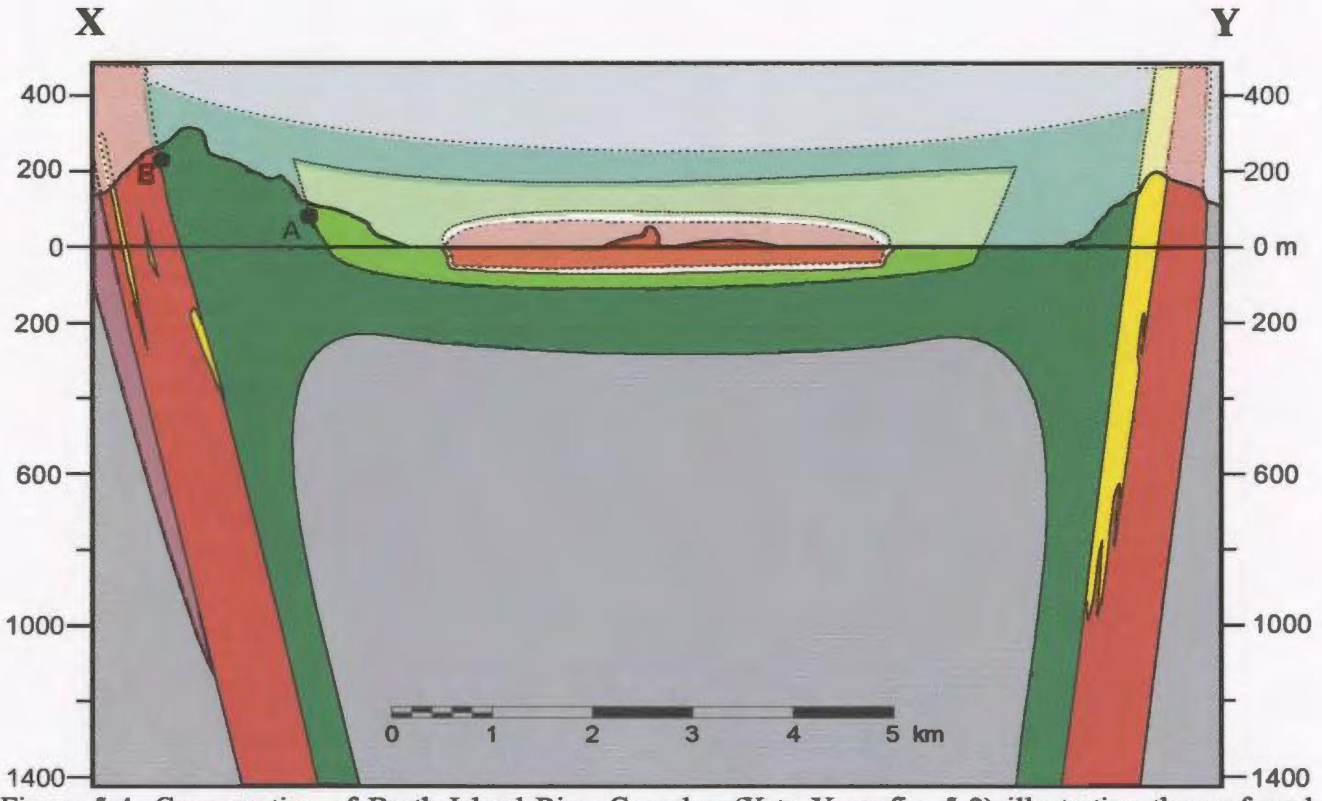

Figure 5-4. Cross-section of Barth Island Ring Complex (X to Y on fig. 5-2) illustrating the preferred emplacement model. In this model, the troctolite formed as a cone sheet, which was connected by a horizontal sheet. The outer ferrogabbroid and monzonite intruded some 13 m.y. later, exploiting the same cone-shaped fracture system. The nature of the relationship of the central ferrogabbroid to the other members of the suite is unknown and so is not interpreted in this diagram. All rocks as in fig. 5-2 except: purple is gneiss. See text for explanation and discussion. Vertical exaggeration 4:1; exaggeration compensated for in dip angles.

References

Amelin, Y., Li, C.S., Naldrett, A.J., 1999. Geochronology of the Voisey's Bay Intrusion, Labrador, Canada, by precise U-Pb dating of coexisting baddeleyite, zircon, and apatite. Lithos **47**, 33-51.

Ashwal, L.D., 1993. Anorthosites. Springer-Verlag, Berlin.

Barnichon, J.D., Havenith, H., Hoffer, B., Charlier, R., Jongmans, D., Duchesne, J.C., 1999. The deformation of the Egersund-Ogna anorthosite massif, south Norway: finite-element modelling of diapirism. Tectonophysics **303**, 109-130.

Beattie, P., 1994. Systematics and energetics of trace-element partitioning between olivine and silicate melts: Implications for the nature of mineral/melt partitioning. Chemical Geology **117**, 57-71.

Beattie, P., Ford, C., Russel, D., 1991. Partition coefficients for olivine-melt and orthopyroxene-melt systems. Contributions to Mineralogy and Petrology **109**, 212-224.

Bédard, J.H., 2001. Parental magmas of the Nain Plutonic Suite anorthosites and mafic cumulates: a trace element modelling approach. Journal of Petrology **141**, 747-771.

Berg, J.H., 1977a. Regional geobarometry in the contact aureoles of the anorthositic Nain Complex, Labrador. Journal of Petrology **18**, 399-430.

Berg, J.H., 1977b. Dry granulite mineral assemblages in the contact aureoles of the Nain Complex, Labrador. Contributions to Mineralogy and Petrology **64**, 33-52.

Blatt, H., Tracy, R.J., 1996. Petrology. W.H. Freeman & Co, New York, 529 p.

Blundy, J., Wood, B., 1994. Prediction of crystal-melt partition coefficients from elastic moduli. Nature **372**, 452-454.

Bowen, N.L., 1913. The melting phenomena of the plagioclase feldspars. American Journal of Science **35**, 577-599.

Bowen, N.L., 1928. The evolution of igneous rocks. Dover, New York, 334 p.

Cherniak, D.J., Watson, E.B., 2000. Pb diffusion in zircon. Chemical Geology **172**, 5-24.

Clemens, J.D., 2003. S-type granitic models - petrogenetic issues, models, and evidence. Earth Science Reviews **61**, 1-18.

Condie, K.C., 1989. Plate Tectonics & Crustal Evolution. Pergamon, Toronto, 476 p.

Cox, K.G., Bell, J.D., Pankhurst, R.J., 1979. The interpretation of igneous rocks. George Allen and Unwin, London, 450 p.

Dempster, T.J., Preston, R.J., Bell, B.R., 1999. The origin of Proterozoic massif-type anorthosites: evidence from interactions between crustal xenoliths and basaltic magma. Journal of the Geological Society **156**, 41-46.

DePaolo, D.J., 1981. Neodymium isotopes in the Colorado Front Range and implications for crust formation and mantle evolution in the Proterozoic. Nature **291**, 193-197.

DePaolo, D.J., 1988. Neodymium isotope geochemistry: an introduction. Springer-Verlag, Berlin, 187 p.

DePaolo, D.J., Perry, F.V., Baldridge, W.S., 1992. Crustal versus mantle sources of granitic magmas: a two-parameter model based on Nd isotopic studies. Transactions of the Royal Society (Edinburgh) Earth Sciences **83**, 439-446.

de Waard, D., 1976. Anorthosite-adamellite-troctolite layering in the Barth Island structure of the Nain complex, Labrador. Lithos **9**, 293-308.

de Waard, D., Hancock, S., 1974. Gabbroic-granodiorite dyke in the Nain anorthosite massif, Labrador. In: The Nain Anorthosite Project, Labrador: Field Report, 1973. Morse, S.A. (ed.). Geology Department, University of Massachusetts, Contribution 11, 71-80.

de Waard, D., Mulhern, K., Merriam, D.F., 1976. Mineral variation in anorthositic, troctolitic, and adamellitic rocks of the Barth Island Layered Structure in the Nain Anorthosite Complex, Labrador. Mathematical Geology **8**, 561-574.

Dickin, A.P., 1995. Radiogenic isotope geology. Cambridge University Press, Cambridge, 452 p.

Dubé, B., Dunning, G.R., Lauziere, K., Roddick, J.C., 1996. New insights into the Appalachian orogen from geology and geochronology along the Cape Ray fault zone southwest Newfoundland. Geological Society of America Bulletin **108**, 101-116.

Duchesne, J.-C., Legeois, J.P., Vander Auwera, J., Longhi, J., 1999. The crystal tongue melting model and the origin of massif anorthosites. Terra Nova **11**, 100-105.

Eby, G.N., 1983. The identification of silicate-liquid immiscibility processes using minor and trace element distributions. In: Augustithis, S.S., The significance of trace elements in solving petrogenetic problems and controversies. Theophrastus Publiscations, Athens, Greece.

Emslie, R.F., 1975. Pyroxene megacrysts from anorthositic rocks: new clues to the sources and evolution of the parent magmas. Canadian Mineralalogist **13**, 138-145.

Emslie, R.F., 1978. Elsonian magmatism in Labrador: age, characteristics and tectonic setting. Canadian Journal of Earth Sciences **15**, 438-453.

Emslie, R.F., 1980. Geology and Petrology of the Harp Lake Complex, Central Labrador: an example of Elsonian Magmatism. Geological Survey of Canada Bulletin **293**, 1-136.

Emslie, R.F., Hamilton, M.A., Theriault, R.J., 1994. Petrogenesis of a Mid-Proterozoic Anorthosite-Mangerite-Charnockite-Granite (AMCG) Complex: Isotopic and Chemical Evidence from the Nain Plutonic Suite. Journal of Geology **102**, 539-558.

Emslie, R.F., Stirling, J.A.R., 1993. Rapakivi and related granitoids of the Nain Plutonic Suite: geochemistry, mineral assemblages and fluid equilibria. Canadian Mineralogist **31**, 821-847.

Ferry, J.M., Newton, R.C., Manning, C.E., 2002. Experimental determination of the equilibria: rutile + magnesite = geikielite + CO_2 and zircon + 2 magnesite = baddeleyite + forsterite + $2CO_2$. American Mineralogist **87**, 1342-1350.

Fram, M.S., Longhi, J., 1992. Phase eqilibria of dykes associated with Proterozoic anorthosite complexes. American Mineralogist **77,** 605-616.

Funck, T., Louden, K.E., Reid, I.D., 2000. Wide-angle seismic imaging of a Mesoproterozoic anorthosite complex: The Nain Plutonic Suite in Labrador, Canada. Journal of Geophysical Research **105**, No. B11, 25693-25707.

Furlong, C., 2004. The Composition, Structure, and Emplacement Mechanisms of the Satorsoakulluk Dike, Nain Plutonic Suite, Labrador, and Relevance to Voisey's Bay-type Mineral Deposits. Unpublished Honours Thesis, Memorial University.

Ghiorso, M.S., Sack, R.O., 1985. Chemical mass transfer in magmatic processes IV. A revised and internally consistent thermodynamic model for the interpolation and extrapolation of liquid-solid equilibria in magmatic systems at elevated temperatures and pressures. Contributions to Mineralogy and Petrology **119**, 197-212.

Glazner, A.F., 1994. Foundering of mafic plutons and density stratification of continental crust. Geology **22**, 435-438.

Goddard, C., 2004. Composition, Structure, and Emplacement Mechanism of a Ferrodiorite Cone Sheet: the Satorsoakulluk Dyke, Nain, Labrador. Unpublished Honours Thesis, Memorial University.

Green, T.H., 1969. Experimental fractional crystallization of quartz diorite and its application to the problem of anorthosite origin. Isachsen, Y.W. (ed.), 1969. NY State Museum and Science Service, Memoir 18, 466 p.

Hall, A., 1996. Igneous Petrology. Longman Group Limited, Harlow, 551 p.

Hamilton, M.A., 1997. New U-Pb geochronological results from the Mesoproterozoic Nain Plutonic Suite, Labrador, and implications for the origin and emplacement of massif anorthosites and related rocks. Copena-IGCP 371 Conference, Abstract and Proceedings.

Hamilton, M.A., Emslie, R.F., Roddick, J.S., 1994. Detailed emplacement chronology of basic magmas of the Mid-Proterozoic Nain Plutonic Suite, Labrador: Insights from U-Pb systematics in zircon and baddeleyite. International Conference on Geochronology, Cosmochronology, and Isotope Geology VIII. In: USGS Circular 1107, p.124.

Harley, S.L., 1989. The origins of granulites: a metamorphic perspective. Geological Magazine **126**, 215-247.

Heaman, L.M., LeCheminant, A.N., 1993. Paragenesis and U-Pb systematics of baddeleyite (ZrO_2). Chemical Geology **110**, 95-126.

Heaman, L.M., LeCheminant A.N., 2001. Anomalous U-Pb systematics in mantle-derived baddeleyite xenocrysts from Ile Bizard: evidence for high temperature radon diffusion? Chemical Geology **172**, 77-93.

Hinchey, J., Kerr, A., Wilton, D., 1999. Magmatic sulphide-oxide mineralization in the Nain Hill area (NTS 14C/12), northern Labrador. Newfoundland Department of Mines and Energy, Geological Survey, Current Research Report, 99-1, 183-194.

Hofmann, A.W., 1988. Chemical differentiation of the Earth; the relationship between mantle, continental crust, and oceanic crust. Earth and Planetary Science Letters **90**, no. 3, 297-314.

Hunter, R.H., 1996. Texture Development in Cumulate Rocks. Cawthorn, R.G. (ed.),1996. Layered Intrusions. Elsevier, New York, 531 p.

Isachsen, Y.W. (ed.), 1969. Origin of anorthosite and related rocks. NY State Museum and Science Service, Memoir 18, 466 p.

Jang, Y.D., Naslund, H.R., McBirney, A.R., 2001. The differentiation of the Skaergaard intrusion and the timing of magnetite crystallization: iron enrichment revisited. Earth and Planetary Science Letters **189**, 189-196.

Kilfoil, G.J., 2002. A digital atlas of merged magnetic data from existing airborne surveys, Labrador (NTS 14C,14D, 14E, 14F; 24A). Newfoundland and Labrador Geological Survey, Open File LAB/1370, Version 1.0 (on CD-ROM).

Krogh, T.E., 1982. Improved accuracy of U-Pb ages by the creation of more concordant systems using an air abrasion technique. Geochimica et Cosmochimica Acta **46**, 617-649.

Larsen, L.M., 1979. Distribution of REE and other trace elements between phenocrysts and peralkaline undersaturated magmas, exemplified by rocks from the Gardar igneous province, south Greenland. Lithos **12**, 303-315.

Lee, J.K.W., Williams, I.S., Ellis, D.J., 1997. Pb, U and Th diffusion in natural zircon. Nature **390**, 159-162.

Le Maitre, R.W. (ed.), 2002. Igneous Rocks: A Classification and Glossary of Terms. Cambridge University Press, Cambridge, 236 p.

Levendosky, W.T., 1975. The geology of the Barth layered intrusion, Labrador. Unpublished M. Sc. Thesis, Syracuse University, 73 p.

Longerich, H.P., 1993. Application of a New Treated LiF200 Crystal to X-Ray Fluorescence Analysis of Geological Samples. X-Ray Spectrometry **22**, 114-118.

Longerich, H.P., 1995. Analysis of Pressed Pellets of Geological Samples Using Wavelength-Dispersive X-Ray Fluorescence Spectrometry. X-Ray Spectrometry **24**, 123-126.

Longerich, H.P., Jenner, G.A., Fryer, B.J., Jackson, S.E., 1990. Inductively coupled plasma-mass spectrometric analysis of geological samples: an overview. Chemical Geology **83**, 105-118.

Longhi, J., Fram, M.S., Vander Auwera, J., Montieth, J.N., 1993. Pressure effects, kinetics, and rheology of anorthositic and related magmas. American Mineralogist **78**, 1016-1030.

Longhi, J., Vander Auwera, J., Fram, M.S., Duchesne, J.-C., 1999. Some phase equilibrium constraints on the origin of Proterozoic (massif) anorthosites and related rocks. Journal of Petrology **40**, no. 2, 339-362.

Ludwig, K.R., 1993. A computer program for processing Pb-U-Th isotope data, version 1.24, Denver. United States Geological Survey, Open File Report, 88-542.

Ludwig, K.R., 2000. Isoplot/Ex: A geochronological toolkit for Microsoft Excel. Berkeley Geochronology Center, Berkeley.

McBirney, A.R., 1984. Igneous Petrology. Oxford University Press, Oxford, 509 p.

McBirney, A.R., Naslund, H.R., 1990. The differentiation of the Skaergaard Intrusion: A discussion of Hunter and Sparks (Contrib Mineral Petrol 95: 451-461). Contributions to Mineralogy and Petrology **104**, 235-247.

McDonough, W.F., Sun, S-S., 1995. Composition of the Earth. Chemical Geology **120**, 223-253.

Mueller, R.F., Saxena, S.K., 1977. Chemical petrology. Springer-Verlag, New York, 394 p.

Miller, R.R., Heaman, L.M., Birkett, T.C., 1997. U-Pb zircon age of the Strange Lake peralkaline complex: implications for Mesoproterozoic peralkaline magmatism in north-central Labrador. Precambrian Research **81**, no. 1-2, 67-82.

Morse, S.A., 1972. An alternative model for the anorthositic and associated rocks of the Nain massif, Labrador. Lithos **5**, no. 1, 89-92.

Morse, S.A., 1982. A partisan review of Proterozoic anorthosites. American Mineralogist **67**, 1087-1100.

Mulhern, K., 1974. Petrography and structure of the northern margin of the Barth Layered Structure, Labrador. Unpublished M.Sc. Thesis, Syracuse University, Northampton, 99 p.

Naslund, H.R., 1983. The effect of oxygen fugacity on liquid immiscibility in iron-bearing silicate melts. American Journal of Science **283**, no.10, 1034-1059.

Nesse, W.D., 1991. Introduction to optical mineralogy. Oxford University Press, Oxford, 335 p.

Passchier, C.W., Trouw, R.A.J., 1996. Microtectonics. Springer, Berlin, 289 p.

Philpotts, A.R., 1990. Principles of igneous and metamorphic petrology. Prentice-Hall, Englewood Cliffs NJ, 498 p.

Philpotts, A.R., Carroll, M., 1996. Physical properties of partly melted tholeiitic basalt. Geology **24**, no. 11, 1029-1032.

Roedder, E., 1951. Low temperature liquid immiscibility in the system K_2O-FeO-Al_2O_3-SiO_2. American Mineralogist **36**, 282-286.

Rollinson, H.R., 1993. Using geochemical data: evaluation, presentation, interpretation. Longman, Harlow, 352 p.

Rubins, C.C., 1973. Structural, statigraphic and petrologic relations of rocks south of the Barth Island layered intrusion. Unpublished Ph.D. Thesis, Syracuse University, 100 p.

Rudnick, R.L., Fountain, D.M., 1995. Nature and composition of the continental crust: a lower crustal perspective. Reviews in Geophysics **33**, no. 3, 267-309.

Ryan, B., 2000. Geological investigations in the type locality of the Nain Plutonic Suite (NTS 14C/12). Newfoundland Department of Mines and Energy, Geological Survey, Current Research Report 2000-1, 251-277.

Ryan B, 2001. A provisional subdivision of the Nain Plutonic Suite in its type area, Nain, Labrador (NTS Map Area 14C/12). Newfoundland Department of Mines and Energy, Geological Survey, Current Research Report 2001-1, 127-157.

Ryan, B., James, D., 2003. Unpublished digital map of the Mesoproterozoic Nain Plutonic Suite and surrounding rocks, Labrador, Canada. Newfoundland Department of Mines and Energy, Geological Survey.

Schwartz, J.M., McCallum, I.S., 1998. Minor elements in plagioclase as indicators of subsolidus processes in lunar and terrestrial rocks. Lunar and Planetary Science Conference **29**, Abstract 1952.

Scoates, J.S., Chamberlain, K.R., 1995. Baddeleyite (ZrO_2) and zircon ($ZrSiO_4$) from anorthositic rocks of the Laramie anorthosite complex, Wyoming: Petrologic consequences and U-Pb ages. American Mineralogist **80**, 1317-1327.

Scott, D.J., 1998. An overview of the U-Pb geochronolgy of the Paleoproterozoic Torngat Orogen, Northeastern Canada. Precambrian Research **91**, 91-107.

Shannon, R.D., 1976. Revised effective ionic radii in oxides and fluorides. Acta Crystallographica **32,** Section A, 751-767.

Shelley, D., 1993. Igneous and metamorphic rocks under the microscope: textures, microstructures, and mineral-preferred orientations. Chapman and Hall, London, 445 p.

Smith, V.G., Tiller, W.A., Rutter, J.W., 1955. A mathematical alaysis of solute redistribution during solidification. Canadian Journal of Physics **33**, 723-745.

Stacey, J.S., Kramers, J.D., 1975. Approximation of terrestrial lead isotope evolution by a two stage model. Earth and Planetary Sciences Letters **26**, 207-221.

Stix, J., Gorton, M.P., 1990. Variations in trace element partition coefficients in sanidine in the Cerro Toledo Rhyolite, Jemez Mountains, New Mexico: effects of composition, temperature and volatiles. Geochimica et Cosmochimica Acta **54**, 2697-2708.

Sun, S-S., McDonough, W.F., 1989. Chemical and isotopic systematics of oceanic basalts; implications for mantle composition and processes. In: Magmatism in the ocean basins. Saunders, A.D., Norry, M.J. (eds.). Geological Society Special Publication **42**, 313-345. Geological Society of London, London, 398 p.

Tettelaar, T.A., 2004. Emplacement history of the Pearly Gates Anorthosite Pluton and spatially related Tessiarsuyungoakh Intrusion, and metamorphic petrology of the adjacent Tasiuyak Paragneiss, Northern Labrador.

Vaasjoki, M., Sipilä, P., 2001. U-Pb isotopic determinations on baddeleyite and zircon from the Halti-Ridnitsohkka Intrusion in Finnish Lapland: a further constraint on Caledonide evolution. In: Radiometric age determinations from Finnish Lapland and their

bearing on the timing of Precambrian volcano-sedimentary sequences, Vaasjoki, M. (ed). Geological Survey of Finland, Special Paper 33, 247-253.

Vander Auwera, J., Longhi, J., 1994. Experimental study of a jotunite (hypersthene monzodiorite): Constraints on the parent magma composition and crystallization conditions (P, T, f_{O2}) of the Bjerkreim-Sokndal layered intrusion (Norway). Contributions to Mineralogy and Petrology **118**, 60-78.

Vander Auwera, J., Longhi, J., Duchesne, J.-C., 1997. A Liquid Line of Descent of the Jotunite (Hypersthene Monzodiorite) Suite. Journal of Petrology **39,** no. 3, 441-468.

Voordouw, R.J., 2004. Geology of the Mesoproterozoic anorthosite intrusions in the vicinity of Nain, Labrador. Unpublished Ph.D Thesis, Memorial University.

Wager, L.R., Deer, W.A., 1939. Geological investigations in east Greenland, part III. The petrology of the Skaergaard intrusion, Kangerdlugssuak, east Greenland. Meddelelser om Grønland **105**, no. 4, 1-352.

Watson, E.B., Harrison, T.M., 1983. Zircon saturation revisited: temperature and composition effects in a variety of crustal magma types. Earth and Planetary Science Letters **64**, 295-304.

Wheeler, E.P., 1942. Anorthosite and related rocks about Nain, Labrador. Journal of Geology **50**, 611-642.

Wiebe, R.A., 1979. Anorthositic dikes, southern Nain Complex, Labrador. American Journal of Science **279**, 394-410.

Wiebe, R.A., 1990a. Evidence for unusually feldspathic liquids in the Nain complex, Labrador. American Mineralogist **75**, 1-12.

Wiebe, R.A., 1990b. Dioritic rocks in the Nain complex, Labrador. Schweizer Mineralogie Petrographe Mittelser **70**, 199-208.

Wiebe, R.A., 1992. Proterozoic Anorthosite Complexes. In: Proterozoic Crustal Evolution, Condie, K.C. (ed.). Developments in Precambrian Geology **10**, 215-261.

Wiebe, R.A., 1994. Silicic Magma Chambers as Traps for Basaltic Magmas: The Cadillac Mountain Intrusive Complex, Mount Desert Island, Maine. Journal of Geology **102**, 423-437.

Wiebe, R.A., Blair, K.D., Hawkins, D.P., Sabine, C.P., 2002. Mafic injections, in situ hybridization, and crystal accumulation in the Pyramid Peak granite, California. Geological Society of America Bulletin **114**, no. 7, 909-920.

Wiebe, R.A., Wild, T., 1983. Fractional crystallization and magma mixing in the Tigalak layered intrusion, the Nain anorthosite complex, Labrador. Contributions to Mineralogy and Petrology **84**, 327-344.

Williams, I.S., 1992. Some observations on the use of zircon U-Pb geochronology in the study of granitic rocks. Transactions of the Royal Society of Edinburgh: Earth Sciences **83**, 447-458.

Wingate, M.T.D., 2001. SHRIMP baddeleyite and zircon ages for an Umkondo dolerite sill, Nyanga Mountains, Eastern Zimbabwe. South African Journal of Geology **104**, 13-22.

Wohletz, K., 2003. Magma. Online at: http://geont1.lanl.gov/Wohletz/Heat.htm

Wood, B.J., Blundy, J.D., 1997. A predictive model for rare earth element partitioning between clinopyroxene and anhydrous silicate melt. Contributions to Mineralogy and Petrology **129**, 166-181.

Xue, S., Morse, S.A., 1993. Geochemistry of the Nain massif anorthosite, Labrador: Magma diversity in five intrusions. Geochimica et Cosmochimica Acta **57**, 3925-3948.

Xue, S., Morse, S.A., 1994. Chemical characteristics of plagioclase and pyroxene megacrysts and their significance to the petrogenesis of the Nain Anorthosites. Geochimica et Cosmochimica Acta **58**, 4317-4331.

Yoder, H.S., 1969. Experimental studies bearing on the origin of anorthosite. In: Origin of anorthosite and related rocks. Isachsen, Y.W. (ed.), 1969. NY State Museum and Science Service, Memoir 18, 466 p.

Appendix 1. Modal proportions of selected samples analysed for major and trace elements, determined by thin section analysis

Sample	BS 2d	BI 32	BII 3	BII 1	LBE 42
Rock Type	Troctolite	Troctolite	Norite	Norite	Ferrogabbroid
Plagioclase	65	70	85	60	60
K- feldspar			minor		
Quartz					
Olivine	30	15			
Orthopyroxene	<5	5	10	30	25
Clinopyroxene					5
Biotite	<5	5	<5	<5	
Amphibole					
Magnetite	<5	<5	<5	<10	10
Apatite					
Zircon					
Rutile			acc	acc	

Sample	BS 7c	BS 7i	BS 6a	BS 6c	BII 56
Rock Type	Ferrogabbroid	Ferrogabbroid	Monzonite	Monzonite	Ferrogabbroid
Plagioclase	60	65	60	80	40
K- feldspar	5				10
Quartz			present	present	
Olivine					
Orthopyroxene	25	10	30		25
Clinopyroxene	5	20	minor	<15	<20
Biotite		minor			
Amphibole		minor		minor	
Magnetite	5		<10	5	<10
Apatite	acc	acc	acc	acc	acc
Zircon	acc			acc	acc
Rutile					

Sample	NA 3	NA 6	NA 8
Rock Type	Fg-Mz hybrid	Ferrogabbroid	Ferrogabbroid
Plagioclase	65	85	75
K- feldspar			
Quartz			
Olivine			
Orthopyroxene	<30	10	15
Clinopyroxene			5
Biotite			
Amphibole			
Magnetite	<10	5	5
Apatite	acc		
Zircon		acc	
Rutile			

Appendix 2. Calculation of melt polymerization from major element geochemistry

Table A2-1. Wt% oxides for selected samples of the Barth Island Ring Complex.

	Ferrogabbroid			Monzonite	
	LBE42	BS7c	BS7i	BS6a	BS6c
SiO2	45.870	49.670	44.850	65.830	60.750
TiO2	4.040	2.930	3.670	0.700	0.990
Al2O3	11.810	12.850	12.780	13.160	14.480
Fe2O3	8.135	7.228	7.391	3.467	4.600
FeO	12.725	9.982	12.059	2.953	4.600
MnO	0.270	0.220	0.260	0.080	0.130
MgO	3.890	3.850	4.910	0.430	0.570
CaO	7.590	6.820	9.020	2.730	3.560
Na2O	2.630	3.080	2.790	3.250	3.730
K2O	0.500	1.130	0.320	3.510	3.490
P2O5	0.660	0.530	0.980	0.130	0.170
Total	98.120	98.290	99.030	96.240	97.070

Table A2-2. Atomic proportions are calculated by dividing wt% oxides by the appropriate molecular weight, then mutliplying by the ratio appropriate to each oxide.

SiO2	0.254	0.276	0.249	0.365	0.337
TiO2	0.017	0.012	0.015	0.003	0.004
Al2O3	0.046	0.050	0.050	0.052	0.057
Fe2O3	0.020	0.018	0.019	0.009	0.012
FeO	0.089	0.069	0.084	0.021	0.032
MnO	0.002	0.002	0.002	0.001	0.001
MgO	0.048	0.048	0.061	0.005	0.007
CaO	0.068	0.061	0.080	0.024	0.032
Na2O	0.028	0.033	0.030	0.035	0.040
K2O	0.004	0.008	0.002	0.025	0.025
P2O5	0.001	0.001	0.002	0.000	0.000

Table A2-3. Calculation of NBO and T proceeds after Eby (1983).

T	0.318	0.338	0.314	0.428	0.406
NBO	18.729	18.647	18.743	18.288	18.376
NBO/T	58.96	55.13	59.64	42.73	45.26
avg NBO/T		57.91		44	
NBO/T (Mz)			0.76		
NBO/T (Fg)					

Appendix 3. Calculation of anomalous behaviour for selected trace elements.

		Pb (Ce,Pr)	Sr (Pr,Nd)	P (Pr,Sm)	Eu (Sm,Gd)	Zr (Nd,Dy)	Ti (Sm,Dy)
BS 8G	Tr	2.63	3.35	0.77	1.62	1.21	1.03
BS 2D	Tr	2.92	3.78	0.92	1.56	1.23	0.91
BS 8C	Tr	4.85	4.16	0.73	1.88	1.09	0.97
BI 32	Tr	1.7	2.19	0.7	1.35	1.17	0.84
BII 3	N	9.2	6.68	0.69	2.39	0.93	2.11
BII 1	N	12.03	7.21	0.42	2.49	1.04	6.46
LBE 42	OFg	1.41	0.51	1.02	1.01	0.68	1.14
BS 7C	OFg	1.79	0.52	0.86	0.92	1.13	0.9
BS 7I	OFg	0.41	0.53	1.11	1.04	0.41	0.89
BS 6A	Mz	2.77	0.6	0.3	1.91	4.86	0.31
BS 6C	Mz	1.8	0.46	0.24	1.64	3.95	0.27
BIII 10	CFg	1.29	0.51	0.48	0.96	1.68	0.31
BII 56	CFg	1.56	0.34	1.03	0.81	0.35	0.57
BIII 30	SD	0.55	0.27	0.99	1.05	1.18	0.56
NA 3	FgSh	0.57	0.45	1.25	0.88	0.62	0.59
NA 6	F/MSh	1.16	0.62	0.48	1.51	4.03	0.39
NA 8	FgD	0.9	0.85	1.12	0.99	0.81	0.88
Avg Tr		2.81	3.19	0.77	1.57	1.18	0.93
Avg Ln		10.39	6.9	0.57	2.44	0.98	4.11
Avg Fg		1.11	0.52	1.01	0.99	0.71	0.97
Avg Mz		2.18	0.52	0.26	1.74	4.3	0.29
Avg Fg/Mz		1.54	0.52	0.54	1.35	2.18	0.66

Note. Calculation of anomalies proceeds as described in the text. Anomalous behaviour is calculated for the element at the top of each column using bracketed elements in the same respective column. Abundances are calculated using abundances normalized to the primitive mantle of McDonough and Sun (1995). Rock name abbreviations as in table 3-1.

Appendix 4. Density measurements of typical samples of the rocks of the Barth Island Ring Complex.

A4.1 Method

The samples were weighed using a digital scale. The samples were then suspended, using light gauge fishing line, from a balance. The suspended sample was completely immersed in water. The balance was then equilibrated such that the mass of the immersed sample was known. Each sample remained in the water until no change in density was observed, normally for a few minutes, to allow for air pockets or cracks to become filled with water. The masses of weights used for equilibration were measured using the digital scale. The temperature of the water was measured prior to scale equilibration, so that the density of the water was known. The relevant values were then used to determine the density of the sample, according to the equation

$$(1)\ (M_R/M_{RW})/((M_R/M_{RW}) - 1) \cdot p_W$$

where M_R is the mass of the rock, M_{RW} is the mass of the rock after immersion in water, and p_W is the density of the water for that particular measurement.

A4.2 Results

Sample	Rock type	Sample mass	Immersed mass	Water density	Water T (C)	Rock density
LBE 10	Outer Fg	1489.3	1011.6	0.99898	15.8	3.114
LBE 14	Outer Fg	969.7	653.2	0.99833	19.4	3.061
BII 52	Outer Fg	1024.6	672.8	0.99886	16.5	2.909
BIII 3	Outer Fg	812.8	542.4	0.99802	20.9	3.000
BIII 4	Outer Fg	1624.9	1085.2	0.99827	19.7	3.003
BIII 6	Outer Fg	1532.5	1027.2	0.99870	17.4	3.029
BS 7b	Outer Fg	1183.9	802.3	0.99829	19.6	3.094
BS 7d	Outer Fg	1063	700.9	0.99777	22	2.929
BS 7d (2)	Outer Fg	649.11	429.9	0.99829	19.6	2.953
BS 7g	Outer Fg	891.5	601.5	0.99814	20.3	3.068
BS 9c	Outer Fg	1200.9	804.9	0.99859	18.1	3.028

A4.2 Results (cont.)

Sample	Rock type	Sample mass	Immersed mass	Water density	Water T (C)	Rock density
BS 9f(*ii*)	Outer Fg	1101.6	717.1	0.99863	17.8	2.861
BS 9h(*i*)	Outer Fg	1971.6	1319	0.99831	19.5	3.012
BS 9h(*ii*)	Outer Fg	611.02	408.7	0.99827	19.7	3.012
Avg	Outer Fg					3.005
BIII 7	Central Fg	1182.7	781.9	0.99876	17.1	2.947
BIII 13	Central Fg	995.3	656.4	0.99808	20.6	2.931
BIII 10a	Central Fg	769.03	516.6	0.99793	21.3	3.040
Avg	Central Fg					2.973
LBE 5	Fg	2705.5	1845.7	0.99780	21.9	3.140
LBE 6	OLn	3519.1	2346.5	0.99786	21.6	2.995
BII 20	Tr	1543.7	703.8	0.99821	20	3.110
BII 45	Tr	1393	924.6	0.99788	21.5	2.968
BS 2c	Tr	1155.4	767.6	0.99740	23.6	2.972
BS 2b	Tr	824.9	546.5	0.99740	23.6	2.955
BS 3a	Tr	1377.2	910.2	0.99735	23.8	2.941
BS 3b	Tr	1104	729.5	0.99740	23.7	2.940
BS 3d	Tr	1100.5	726.1	0.99737	23.7	2.932
BII 11	Tr	954.9	629.2	0.99737	23.7	2.924
BII 19	Tr	1417.4	917.8	0.99735	23.8	2.83
BII 49	Tr	1312.8	856.3	0.99730	24	2.868
Avg	Tr					2.944
BS 1b	N	1116.6	718.4	0.99735	23.8	2.797
BS 6e	Mz	867.3	545.4	0.99816	20.4	2.689
BII 32	Mz	1157	750.4	0.99788	21.5	2.84
NBS 4a	Mz	966.5	610.9	0.99730	24	2.711
NBS 4b	Mz	1402	884.3	0.99730	24	2.701
BII 64	Mz	1402.6	888.5	0.99831	19.5	2.720
NBS 20	Mz	1667.7	1060.7	0.99829	19.6	2.740
Avg	Mz					2.733

Note. Rock masses given in grams. All densities given in grams per cubic centimeter. Temperature of water is given in degrees Celsius. Rock abbreviations are as follows: Fg is ferrogabbroid, Tr is troctolite, Mz is monzonite, N is norite, OLn is outer leuconorite. Sample LBE 5 may be related to outer ferrogabbroid of the Barth Island Ring Complex.